UNIVERSITY OF CALIFORNIA,

IRVINE

Ground Motion Simulation Validation for building design and response assessment

DISSERTATION

submitted in partial satisfaction of the requirements
for the degree of

DOCTOR OF PHILOSOPHY

in Civil Engineering

By

Peng Zhong

Dissertation Committee:
Associate Professor Farzin Zareian, Chair
Professor Lizhi Sun
Dr Sanaz Rezaeian

2016

DEDICATION

To

My family

TABLE OF CONTENTS

Page

List of Tables

Page

List of Figures

Page

Acknowledgments

First and foremost, I would like to thank my advisor, Professor Farzin Zareian, for his support without reservation. It was such an honor to work with him for more than seven years. Apart from sharing his substantial knowledge with me, he offered me unlimited trust and encouragement to build my confidence and overcome any kinds of research problems. He was a role model of hard working and perseverance. He was a life-time mentor, his advice on both research as well as on my life have been priceless. All in all, all I am or can be, I owe to him.

I would also like to thank my committee members, Professor Lizhi Sun and Dr Sanaz Rezaeian, for their insightful comments and feedback. Thanks also to Professor Zhaoxia Yu and Professor Xiaogang Gao for being a part of my qualifying exam committees and providing knowledgeable research discussions.

Thanks especially to Dr Sanaz Rezaeian for patiently explaining her simulation method and using her raw model to develop the validation metrics in Chapter 3. I am grateful for the experience of working and publishing papers together with Professor Carmine Galasso, Professor Iunio Iervolino, Dr Robert Graves and Dr Stephen Hartzell. Their insightful vision and professional attitude taught me a lot. Thanks to everyone in Southern California Earthquake Center (SCEC) Ground Motion Simulation Validation (GMSV) group for providing data and valuable discussion for my research, particularly Dr Nico Luco, Philip Maechling, Professor Greg Deierlein, Professor Jack Baker, Professor Kim Olsen, and Dr Paul Somerville.

I also want to thank to the colleague of Performance Based Earthquake Engineering Lab to share research discussion and joy, including Dr Omid Esmaili, Dr Peyman Kaviani, Dr Roshanak Omrani, Bahareh Mobasher, Marta De Bortoli, Huda Munjy, Pablo Torres, Dr Behzad Zakeri, Yijun Xiang, especially Dr Pierson Jones and Dr Carmine Galasso who taught me hand by hand

when I was rookie. I would also like to thank all of my friends who supported me in writing, and incented me to strive towards my goal, such as Huda Munjy and Yuxiao Wang. I would like to thank all the faculty and staff in department of Civil and Environmental Engineering, especially April Heath.

This research was partially supported by funding from the SCEC. Any opinions, findings, and conclusions expressed in this document are those of the author and do not necessarily reflect the views of the funding sources.

Finally, I would like to thank my parents, Dezhi Zhong and Ping Chen, for their love and my wife, Jing Yu, for motivating me and supporting me unconditionally.

Abstract of the Dissertation

Ground Motion Simulation Validation for building design and response assessment

By

Peng Zhong

Doctor of Philosophy in Civil Engineering

University of California, Irvine, 2016

Professor Farzin Zareian, Chair

Earthquake ground motion records are used as inputs for seismic hazard analysis, development of ground motion prediction equations and nonlinear response history analysis of structures. Real records from past earthquake events have traditionally been recognized as the best representation of seismic input to these analysis. However, our current way of implementing recorded ground motions is poorly constrained and suffers from the paucity of certain condition ground motions, such as the one with short distance and large magnitude. Meanwhile, even though the scaled ground motion is capable of matching the target spectrum, the content of frequency domain and ground motion parameters become unrealistic. With the rapid growth of computational ability and efficiency of computers, simulated ground motion can be an alternative to provide detailed and accurate prediction of earthquake effect. At the same time, simulated ground motions can provide a better representation of the whole ground motion generation process, such as fault rupture, wave propagation phenomena, and site response characterization. Hence, the aforementioned disadvantage of recorded ground motion can be overcame.

Despite ground motion simulations have existed for decades, and the design code, such as ASCE/SEI 7-10 (ASCE, 2010), allow use of simulated ground motions for engineering practice,

engineers still worried about the stability in ground motion simulation process and similarity between response of engineered structures to similar simulated and recorded ground motions. In order to draw simulated ground motions into engineering applications and make them practical, this dissertation is making contribution to address this issue. Simulated ground motions have to be validated and compared with recorded ground motions to prove their equivalence in engineering applications.

This dissertation proposes a simulation validation framework. First step: Identify ground motion waveform parameters that well correlate with response of Multi-Degree of Freedom (MDOF) buildings and bridges. Second step: Develop goodness-of-fit measures and error functions that can describe the difference between simulated and recorded ground motion waveform characteristics and their effect on MDOF systems. Third step: Device the required update to ground motion simulation methods through which better simulations are possible. Forth step: Assess the current state of simulated ground motions for engineering applications.

In general, simulated ground motions are found to be an effective surrogate and replenishment of natural records in engineering applications. However, certain drawbacks are detected, 1) Simulated ground motions are likelihood to mismatch certain ground motion parameters, for example, Arias intensity, duration and so on; 2) Structural behavior resulting from recorded ground motions and simulated ground motions are different. The difference stems from the fact that simulated motions are mostly pulse like motions. Because the simulation methods are still developing, our intent is not ranking or classifying them, but rather to provide feedback to update ground motion simulation techniques such that future simulations are more representative of recorded motions.

CURRICULUM VITAE

PENG ZHONG

Education

Ph.D. University of California at Irvine, 2011
Major: Structural Engineering
Dissertation Title: Ground Motion Simulation Validation for building design and response assessment
Advisor: Farzin Zareian

M.S. University of California at Irvine, 2008
Major: Structural Engineering
Dissertation Title: Sensitivity of building response to variation in integration time step of response history analysis.
Advisor: Farzin Zareian

B.A Guangdong University of Technology, 2004
Major: Civil Engineering

Publications

Journals:

1. Zhong, P. and Zareian, F., (tentatively submitted) Applicability of smulated ground motion waveforms for building-code applications. Earthquake Spectra
2. Zhong, P. Rezaeian, S., Hartzell, S., Munjy,H., and Zareian, F., (tentatively submitted) Sensitivity of engineering demand parameters to evolutionary ground motion intensity and frequency content parameters . Earthquake Engineering & Structural Dynamics
3. Rezaeian, S., Zhong, P., Hartzell, S., and Zareian, F (2015) Validation of simulated earthquake ground motions based on evolution of intensity and frequency content. Bulletin of the Seismological Society of America, 105(6)
4. Galasso, C., Zhong, P., Zareian, F., Iervolino, I. and Graves, R. W. (2013), Validation of ground-motion simulations for historical events using MDoF systems. Earthquake Engineering & Structural Dynamics. doi: 10.1002/eqe.2278
5. Sensitivity of building response to variation in integration time step of response history analysis. (Publisher: ProQuest, UMI Dissertation Publishing (May 4, 2012) ISBN-10: 1248958543 ISBN-13: 978-1248958544)

Conferences:

1. Zhong, P., Esmaili, O. & Zareian F. (2017) Validation of Simulated Ground Motion for Engineering Applications in Loss Estimation. 16th World Conference on Earthquake Engineering

2. Deierlein, G., Zareian, F., Zhong, P. & Bijelic, N. (2015) Engineering Utilization of Earthquake Simulations. 2015 Southern California Earthquake Center Annual Meeting
3. Zhong, P. & Zareian F. (2015) Validation of simulated ground motions for engineering applications. 26th International Union of Geodesy and Geophysics (#IUGG-3654).
4. Zhong, P., Galasso, C., Iervolino, I. & Zareian, F. (2014) Ground motion simulation for building-code nonlinear response history analysis. 2014 Southern California Earthquake Center Annual Meeting
5. Zhong, P. & Zareian, F. (2014). Method of speeding up buildings time history analysis by using appropriate downsampled integration time step. 10th US National Conference on Earthquake Engineer
6. Zareian, F., Zhong, P. & Rezaeian, S. (2014) Validation of Simulated Ground Motions Based on Evolution of Intensity and Frequency Content. 2014 Southern California Earthquake Center Annual Meeting
7. Esmaili, O., Zhong, P., Zareian F & Jones, P. (2014). Improved performance-based seismic assessment of tall buildings by utilizing bayesian statistics. 2014 Los Angeles tall buildings structural design council conference
8. Zareian F., Zhong P. & Iervolino, I. (2013) Validation for Building-Code Nonlinear Response History Analysis. 2013 Southern California Earthquake Center Annual Meeting
9. Zhong, P., Rezaeian, S., & Zareian F (2012) Validation of Simulated Ground Motions using Time Domain Cumulative Statistical Measures. 2012 Pacific Earthquake Engineering Research Center
10. Galasso C, Zhong P, & Zareian F, Engineering Validation of Ground Motion Simulation: Part 1. Tall Buildings, 2012 Southern California Earthquake Center (SCEC) Annual Meeting, Palm Springs, CA, USA, September 9-12 2012.
11. Galasso C., Zhong P. & Zareian F. (2012). A statistical analysis of the response of linear and nonlinear building systems to observed and simulated ground motions for past earthquakes. Seismological Research Letters, 83(2) (Proceedings of the 2012 Seismological Society of America (SSA) Annual Meeting, San Diego, CA, USA, April 17-19 2012).
12. Zareian F., & Zhong P (2010) Ground motion selection and scaling for analysis of the tall building case studies. 2010 Los Angeles tall buildings structural design council conference

Scholarships and Awards

1. Chinese Government Award for Outstanding Self-Financed Students Abroad 2015
   Issuer: China Scholarship Council

2. Liu Huixian Earthquake Engineering Scholarship 2015
   Issuer: the Huixian Earthquake Engineering Foundation (China) and the US-China Earthquake Engineering Foundation (USA)

3. Medhat Haroun Fellowship 2015
   Issuer: University of California, Irvine

4. Chinese-American Engineers and Scientists Association of Southern California scholarship 2015
   Issuer: Chinese-American Engineers and Scientists Association of Southern California

5. International Chinese Transportation Professionals Association scholarship 2011
   Issuer: International Chinese Transportation Professionals Association

6. Scholarships for Outstanding Students 2004-2008
   Issuer: Guangdong University of Technology

CHAPTER 1: INTRODUCTION

1.1 PROBLEM STATEMENT

Recently, simulated ground motions are gaining more attention and are opening their way into engineering applications. Simulated ground motions are now next to recorded motions and spectrally matched ground motions (created by manipulating the frequency content and intensity of recorded ground motions to match a specific response spectrum) for building seismic performance assessment; they are also used for design for target performance. However, there are serious doubts about similarity between simulated and recorded ground motions that causes hesitation among engineers to utilize them in engineering applications. Validating simulated ground motions for such purposes, and updating the simulated methodology, is the topic of this dissertation.

Real records from past earthquake events have traditionally been recognized as the best representation of seismic input to dynamic analyses in geotechnical and structural engineering; see (Bommer, JJ, et. al., 2004) for a review. Recorded ground motion are usually selected and scaled to represent a target seismic hazard. Ground Motion Selection and Modification (GMSM) techniques have been studied by various researchers in the past, for example Naeim et al. (2004), Baker & Cornell (2006), Iervolino et al. (2011), Lin et al. (2013). Although GMSM is the classical method to bring recorded ground motions into seismic assessment and design of engineered structures, however, there are few critical drawbacks to this technique that limits their application. For instance, there is an inconsistency in scaling of ground motion parameters once GMSM is utilized. In other words, once a ground motion is scaled, few of its waveform parameters–such as energy and amplitude–follow the same scaling pattern, however, other waveform parameters–such as strong motion duration and frequency content–do not scale

accordingly. Altogether, a scaled ground motion does not well represent another ground motion unless certain conditions are met. Moreover, GMSM cannot reconcile data for large magnitude earthquakes at close distances as well as certain combinations of source, fault type, distance and site characterizes. Lastly, current GMSM methods are incapable of addressing three-dimensional nature of seismic input.

These shortcoming have led researchers to work on ground motion simulation techniques (e.g., Graves and Pitarka, 2010; Rezaeian and Der Kiureghian, 2011; Hartzell et al., 2011). Given the advances in the understanding of fault rupture process, wave propagation phenomena, and site response characterization, simulated ground motions appear to be one of the viable and attractive alternatives to the very limited amount of recorded ground motions. The recently released ASCE Standard ASCE/SEI 7-10 explicitly states that, in performing nonlinear dynamic analysis, "where the required number of appropriate recorded ground motion records are not available, appropriate simulated ground motion shall be used to make up the total number required."

In spite of the fact that design codes such as ASCE/SEI 7-10 (ASCE, 2010) allow use of simulated ground motions for engineering practice, such motions still fall out of favor with engineers. In essence, engineers look for stability in ground motion simulation process and similarity between response of engineered structures to similar simulated and recorded ground motions. In order to draw simulated ground motions into engineering applications and make them practical, simulated ground motions have to be validated and compared with recorded ground motions to prove their equivalence in engineering applications. Early work in ground motion simulation validation goes back to Zareian & Rahnama (1996), and recently Zareian & Jones (2010); Star et al., 2011; Seyhan et al., 2012; Galasso et al., 2012 and Galasso et al., 2013.

This dissertation is continuation of the previous work and tries to address where and how simulated ground motion can be utilized in engineering practice. At the same time, the research presented here will be utilized for updating ground motion simulation techniques such that future simulations are more representative of recorded motions.

1.2 LITERATURE REVIEW

1.2.1 Ground Motion Simulation Theory

Traditionally, ground motion recordings form past earthquake events have been selected and modified (GMSM) to meet certain requirement such as target spectrum, magnitude, distance, mechanism and site characteristics, to substitute ground motions that may happen in future earthquakes. Although the database of recorded motions has increased by thousands during recent earthquakes, there is a shortage of records for large magnitude earthquakes at short distances, as well as records that sample specific combinations for source, path and site characteristics. Moreover, simulated ground motions can provide a better representation of the whole ground motion generation process, such as fault rupture, wave propagation phenomena, and site response characterization. The aforementioned advantage of simulated ground motion can overcome the shortage of recorded ground and curtail the use of GMSM methods. With the rapid growth of computational ability and efficiency of computers, simulated ground motion can be an alternative to provide detailed and accurate prediction of earthquake effect.

Early work in simulating ground motions goes back to P.C.Jennings et al (1968) where artificial acceleration are simulated by a random process with a prescribed power spectral density, multiplied by envelope function, which is capable of modifying intensity at the two end of real motion acceleration. As the fault rupture is studied and better understood, Hartzell (1978) proposed a method of modeling earthquake strong ground motions, which takes advantage of aftershocks

associated with a large earthquake as Green's functions. The earthquake motions are simulated by summing up point sources distributed over the fault surface, whose response is evaluated by ground motion of the correlated aftershock. After that, the stochastic representation of source and path effects are brought into the simulation methodology (Boore, 1983). In 1994, a full deterministic simulation method called composite source model is developed by (Zeng et al, 1994). This full waveform green function's approach randomly puts subevents with a power-law distribution of sizes onto the fault. And each subevent propagates a displacement pulse at a time determined by a constant rupture velocity radiating from the hypocenter. After all these years, a large amount of simulators make remarkable contribution and refinement to their simulation methodologies. Unfortunately, the progress is hindered by the limited direct observational measurements, especially the one which is related to high frequency motion propagation.

Currently, by taking advantage of available information in fault rupture behavior including source and wave propagation effects, ground motion simulation based on a hybrid (deterministic and stochastic) approach has been established (i.e., broadband ground motion simulation). For instance, Graves and Pitarka (2010) developed a hybrid broadband (0-10 Hz) ground motion simulation methodology which combines a physics-based deterministic approach at low frequency ($f \leq 1$ Hz; i.e., $T \geq 1$s) with a semistochastic approach at high frequency ($f > 1$ Hz; i.e., $T < 1$s). The low and high frequency waveforms are computed separately and then combined to produce a single time history through a matching filter. At frequencies below 1 Hz, the methodology contains a theoretically rigorous representation of fault rupture and wave propagation effects and attempts to reproduce recorded ground motion waveforms and amplitudes. At frequencies above 1 Hz, waveforms are simulated using a stochastic representation of source radiation combined with a simplified theoretical representation of wave propagation and scattering effects. The use of

different simulation approaches for the different frequency bands results from the seismological observation that source radiation and wave propagation effects tend to become stochastic at frequencies of about 1 Hz and higher, primarily reflecting the relative lack of knowledge about these phenomena's details at higher frequencies. For both short and long periods, the effect of relatively shallow site conditions, as represented by shear wave velocity in the upper 30 m (Vs30) is accounted for using Campbell and Bozorgnia's (2008) empirical site amplification model.

In this study, the aforementioned ground motion simulation method is chosen as primary method for the validation exercise. Meanwhile, five popular ground motion simulation methods are added to assure the body of research accomplished here is comprehensive:

1) Zeng, Anderson and Yu (1994) Composite source Model (CSM): By taking advantage of the convolution with synthetic Green's functions, CSM simulation method is able to describe the kinematic earthquake source time function and simulate strong ground motions. All input simulated parameters, such as fault mechanism, dimension and slip, R_{max} and so on, have some kinship with physical basis. CSM method hypothesize the source slip function can be simulated by randomly distributed subevents on fault. And the power-law distribution are used to define the relationship between number of subevents and their radius. Each subevent radiates a displacement pulse with the shape of a Brune's pulse in the far field, determined by a constant rupture velocity propagating from the hypocenter.
2) Olsen and Mayhew (2010): This simulation method generate broadband (0-10 Hz) synthetic ground-motions by combining low-frequency 3D finite-difference synthetics with a high-frequency scattered wave-field. Deterministic techniques for waveform computations at low frequencies (up to about 1 Hz) in 3D Earth model are well developed,

accounting for the complicated physical part in the rupture process. Meanwhile, methods for high-frequency (1–10 Hz) ground-motion simulations are based on empirical-stochastic approaches and do not consider the physics of seismic scattering due to small-scale heterogeneous earth structure or include 3D wave-propagation effects. The multiple shear-to-shear backscattering theory is used to obtain high-frequency seismogram by applying a rupture-specific convolution operator to the scattering Green's function. These signals are then reconciled with the low frequency deterministic waveforms to optimize the fitness of amplitude and phase spectra around the target intersection frequency.

3) Hartzell, Harmsen, Frankel and Larsen (1999): This simulation creates broadband time history of ground motion. In low frequencies (<1 Hz), a kinematic-fault model and 3D finite-difference code are used to propagate energy through a realistic 3D velocity model, where as in high frequencies (>1 Hz), by taking advantage of scattering effects, composite fault model with a fractal subevent size distribution is used.
4) Liu, Archuleta and Hartzell (2006): This simulation calculates broadband time series ground motion by using correlated source parameters. A finite-difference method (<1 Hz) and a frequency-wavenumber method (>1 Hz) are used in 3D and 1D velocity structure respectively. And the signal are combined by using matched filtering at crossover frequency of 1Hz. The correlated random distributions for slip amplitude, rupture velocity, and rise time are included in modeling. To produce accurate result of high-frequency amplitudes and durations, the 1D simulation are adjusted with a randomized, frequency-dependent radiation pattern. And 1D nonlinear propagation code and generic velocity structure are used to further correct for site effect.

5) Frankel (1995): In order to predict prospective earthquake in specific sites, this simulation is generated by summing and filtering recordings of adjacent small earthquakes. The asperity rupture model is used, and root mean square (rms) stress drop is constant with moment. Each simulation add up the seismogram of one aftershock with time delays suitable to propagating rupture and incorporates directivity and site response. The simulation scales the spectrum in accordance with a constant stress drop.

1.2.2 Current Goodness of Fit Measures

In order to create confidence for engineering applications of simulated ground motions, these motions should first be validated against available strong ground motion data. Ground motion simulation validation is the substantiation that simulated ground motions are sufficiently accurate in predicting system behavior. In general, once the simulators establish their ground motion simulation methods, they will provide simplest comparisons between simulated ground motions and recorded ground motion in term of PGA, PGV and others intensity measurements. With the consideration of site-specific geologic conditions, simulations are finalized at the site level.

Most of researchers focus on validation at this type of motions, showed in part two of Figure 1.1. According to our literature review, the Spectral Acceleration, Fourier Spectrum Amplitude, Peak Ground Velocity, Peak Ground Acceleration and their durations were chosen to measure the goodness of fit between simulated ground motions and recorded ground motions (Hartzell et al., 1999). Anderson (Anderson et al., 2004), brought in the energy concept, such as Arias Intensity and Energy integral, as well as cross correlation to compared simulated ground motions with recorded ground motions. Meanwhile, he designed a score system to rank the fitness of simulation. In 2006, the misfit criteria based on the time-frequency representation of seismograms by using wavelet transform has been developed and numerically tested. This criteria included time-

frequency envelope and phase misfits, time-dependent envelope and phase misfits, frequency-dependent envelope and phase misfits, and single-valued envelope and phase misfits (Kristekova et al., 2006). In 2010, IE Ratio (the ratio between inelastic and elastic response spectra), the spectral acceleration at 16 individual periods used by recent NGA relations (SA16) and up to 10 different metrics have been considered, and eventually a goodness of fit algorithm was developed to evaluate and rank the simulated ground motions(Olsen et al., 2006).

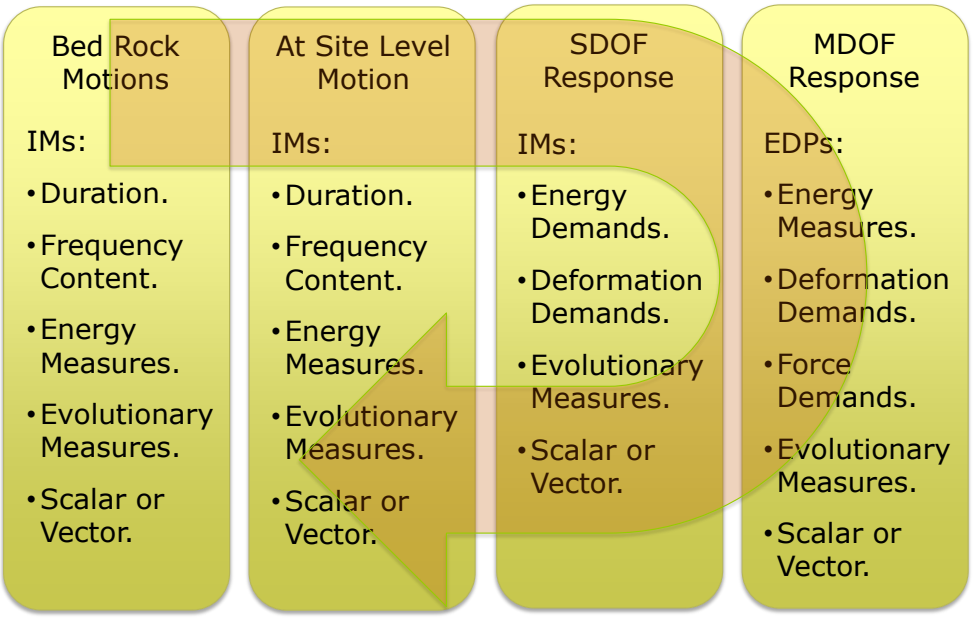

Figure 1.1. Ground motion simulation validation scheme.

Ground motion validation methods and tools described so far are merely conducted at the waveform level. In order to bring validation one step closer to engineering application, researchers (e.g. Bazzurro, et. al., 2004; Galasso et. al., 2012) have addressed validating simulated GMs by looking at their nonlinear response in the domain of single degree of freedom (SDOF) systems. In particular, Galasso et al (2012) formally compared the seismic demands of SDOF to simulated and recorded ground motions by investigating a wide range of SDOF systems and seismic events. Results show, using formal statistical hypothesis tests, that in most cases the differences found are

not significant, increasing the confidence in the use of simulated motions for engineering applications.

1.3 HYPOTHESIS AND PROPOSED RESEARCH PLAN

We hypothesis that a ground motion simulation method can generate acceptable simulated ground motions for engineering application if there is a good fit between certain waveform parameters (i.e., intensity measures) of the simulations and similar naturally recorded ground motions. To this aim, the objectives of this research is fourfold:

1. Identify ground motion waveform parameters that well correlate with response of Multi-Degree of Freedom (MDOF) buildings and bridges.
2. Develop goodness-of-fit measures and error functions that can describe the difference between simulated and recorded ground motion waveform characteristics and their effect on MDOF systems.
3. Device the required update to ground motion simulation methods through which better simulations are possible.
4. Assess the current state of simulated ground motions for engineering applications.

In essence, the research effort conducted under this dissertation will cover the path outlined with the arrow shown in Figure 1.1. As shown in this figure, validation in various domains are highly correlated. As we discussed earlier, various intensity measures have been used to assess the closeness between simulated and recorded motions. A synthetic ground motion may accurately represent a single intensity measure, while misrepresenting other characteristics of the waveform. Hence, further research is necessary to develop a comprehensive metric to validate synthetic ground motions. In this research, instead of intensity measures at single points in time

or frequency, we consider the entire evolution of intensity and frequency content of ground motion over the whole duration. These two criteria are important in engineering applications because they control the response of the structure; many intensity measures that are known to have strong effects on structural responses such as total energy, predominant frequency, or duration can be extracted from these criteria.

The following chapters show our progress in achieving the goals outlined above. In particular, Chapter 2, 3, and 4 address objectives 1, 2, and 4. Future research is needed to accomplish objective 3 of the proposed research.

This chapter has been published as journal paper:

Galasso, C., Zhong, P., Zareian, F., Iervolino, I. and Graves, R. W. (2013), Validation of ground-motion simulations for historical events using MDoF systems. Earthquake Engng. Struct. Dyn., 42: 1395–1412. doi: 10.1002/eqe.2278

CHAPTER 2: VALIDATION OF HISTORICAL EVENT FOR TALL BUILDING RESPONSE ASSESSMENT

Ground motion simulation validation is assessing how well the waveform of synthetic ground motion can be simulated and whether it is capable of representing recorded ground motion. Instead of comparing the characteristics of ground motion itself, we take a step forward and try to understand whether simulated ground motions are comparable to real records in terms of their building response in the domain. In this way, engineers have a better vision to understand the difference between simulated ground motions and recorded ground motions. And this kind of validation can objectively convince engineers of using simulated ground motions.

2.1 LITERATURE REIVEW FOR VALIDATION IN STRUCTURE RESPONSE

Lots of studies have been conducted in simplest structure model: single degree of freedom. Such investigation is a proxy for assessing the similarity of damage potential of simulated and recorded motions for many real structural types. Similarly, Bazzurro, Sjoberg, and Luco (2004) have examined engineering validation in terms of elastic and inelastic SDOF structural response to seven suites of synthetic records that emulate the real ground motions recorded at 20 stations located within 20km from the Northridge fault rupture. The results show that six out of seven simulation methods appear to be biased, especially in the short period range, both in the linear elastic and in the nonlinear post-elastic regimes.

Few years later, Galasso et al., (2012) provides a statistical comparison between seismic demands of single degree of freedom (SDOF) systems subjected to past events using simulations and actual recordings. A number of SDOF systems are selected, considering: (1) 16 oscillation periods between 0.1s

and 6s; (2) elastic case and four nonlinearity levels, from mildly inelastic to severely inelastic systems; and (3) two hysteretic behaviors, namely, non-degrading/non-evolutionary and degrading/evolutionary. As a preliminary, demand spectra are derived in terms of peak and cyclic response, as well as their statistics for four historical earthquakes: 1979 M_w 6.5 Imperial Valley, 1989 M_w 6.8 Loma Prieta, 1992 M_w 7.2 Landers, and 1994 M_w 6.7 Northridge.

Galasso's research shows that both elastic and inelastic demands to simulated and recorded motions are generally similar. However, for some structural systems, the inelastic response to simulated accelerograms may produce median demands that differ from those obtained using corresponding recorded motions. The magnitude of such differences depends on the SDOF period and the nonlinearity level and, to a lesser extent, on the hysteretic model used. In the case of peak response, these discrepancies are likely due to differences in the spectral shape, while the differences in terms of cyclic response can be explained by some integral parameters of ground motion (i.e., duration-related). Moreover, the intra-event standard deviation values of structural demands calculated from the simulations are generally lower than those given by recorded ground motions, especially at short periods. Assessment of the results using formal statistical hypothesis tests indicates that in most cases the differences found are not significant, increasing the confidence in the use of simulated motions for engineering applications. Even though obtained based on limited sets of ground motion records, are in good agreement with previous similar studies, e.g. Bazzurro et al, 2004.

2.2 VALIDATION IN MULTIPLE DEGREE OF FREEDOM MODELS

This validation aims at taking a step forward and trying to understand if simulated ground motions are comparable to real records in assessing the seismic behavior of MDOF structural systems where higher modes may substantially contribute to the total response. For such structural systems, whose fundamental period can be long, the traditional SDOF spectral analyses may significantly underestimate local structural deformation. Furthermore, the displacement response

obtained from spectral ordinates can only provide an overall measure of lateral deformation of the structure and do not take into account concentration of demand in certain stories that may occur in actual buildings, especially for building response corresponding to the pulse-like ground motions. Higher modes of vibration also contribute significantly to the acceleration demands in buildings—a response parameter that recent studies show significant to nonstructural damage and monetary loss.

This part of validation addresses the issue of engineering validation of Graves and Pitarka's (2010) hybrid broadband ground motion simulation methodology with respect to some well-recorded historical events and considering the response of multiple degrees of freedom (MDOF) systems. Herein, validation encompasses detailed assessment of how similar is, for a given event, the seismic response due to comparable hybrid broadband simulated records and real records. In the first part of this validation, in order to investigate the dynamic response of a wide range of buildings, MDOF structures are modeled as elastic continuum systems consisting of a combination of a flexural cantilever beam coupled with a shear cantilever beam. A number of such continuum systems are selected including the following: (1) 16 oscillation periods between 0.1 and 6 s; (2) three shear to flexural deformation ratios to represent respectively shear-wall structures, dual systems, and moment-resisting frames; and (3) two stiffness distributions along the height of the systems, that is, uniform and linear. Demand spectra in terms of generalized maximum interstory drift ratio (IDR) and peak floor acceleration (PFA) are derived using simulations and actual recordings for four historical earthquakes, namely, the 1979 Mw 6.5 Imperial Valley earthquake, 1989 Mw 6.8 Loma Prieta earthquake, 1992 Mw 7.2 Landers earthquake, and 1994 Mw 6.7 Northridge earthquake. In the second part, for two nonlinear case study structures, the IDR and PFA distributions over the height and their statistics, are obtained and compared for both recorded

and simulated time histories. These structures are steel moment frames designed for high seismic hazard, 20-story high-rise and 6-story low-rise buildings. The results highlight the similarities and differences between simulated and real records in terms of median and intra-event standard deviation of logs of seismic demands for MDOF building systems. This general agreement, in a broad range of moderate and long periods, may provide confidence in the use of the simulation methodology for engineering applications, whereas the discrepancies, statistically significant only at short periods, may help in addressing improvements in generation of synthetic records.

2.2.1 Description of Synthetic and Real Ground Motion Datasets

Graves and Pitarka developed and validated (in terms of elastic spectral ordinates) a hybrid broadband (0–10 Hz) ground motion simulation methodology that uses simple kinematic representation of slip distribution and rupture velocity on the fault surface. For the validation process addressed in this part, four historical earthquakes, modeled by using the technique described in chapter 1, are used: 1979 Mw 6.5 Imperial Valley, 1989 Mw 6.8 Loma Prieta, 1992 Mw 7.2 Landers, and 1994 Mw 6.7 Northridge. The earthquake-specific input parameters used in the simulation process are seismic moment, overall fault dimensions and geometry, hypocenter location, and a smoothed representation of the final slip distribution. All other required source parameters (e.g., rupture propagation time, rise time, slip function, and fine-scale slip heterogeneity) are simulated using the scaling relations presented in (Graves et al 2010). Furthermore, the methodology provides a framework to generate rupture descriptions for future earthquakes, as demonstrated in (Graves et al 2011).

For each earthquake simulation, the model region covers a wide area surrounding the fault including many strong motion recording sites available in the Next Generation Attenuation database (http://peer. berkeley.edu/peer_ground_motion_database): 33 for Imperial Valley, 71 for

Loma Prieta, 23 for Landers, and 133 for Northridge earthquake. Only a limited number of these sites are used here, that is, those with a usable bandwidth of the real records exceeding 0.1 s–8 s, yielding a total of 126 sites (Figure 2.1), while the analysis and results presented refer to structures with fundamental periods less than 6 s. With this approach, it is possible to cover a realistic range of initial linear elastic fundamental vibration periods.

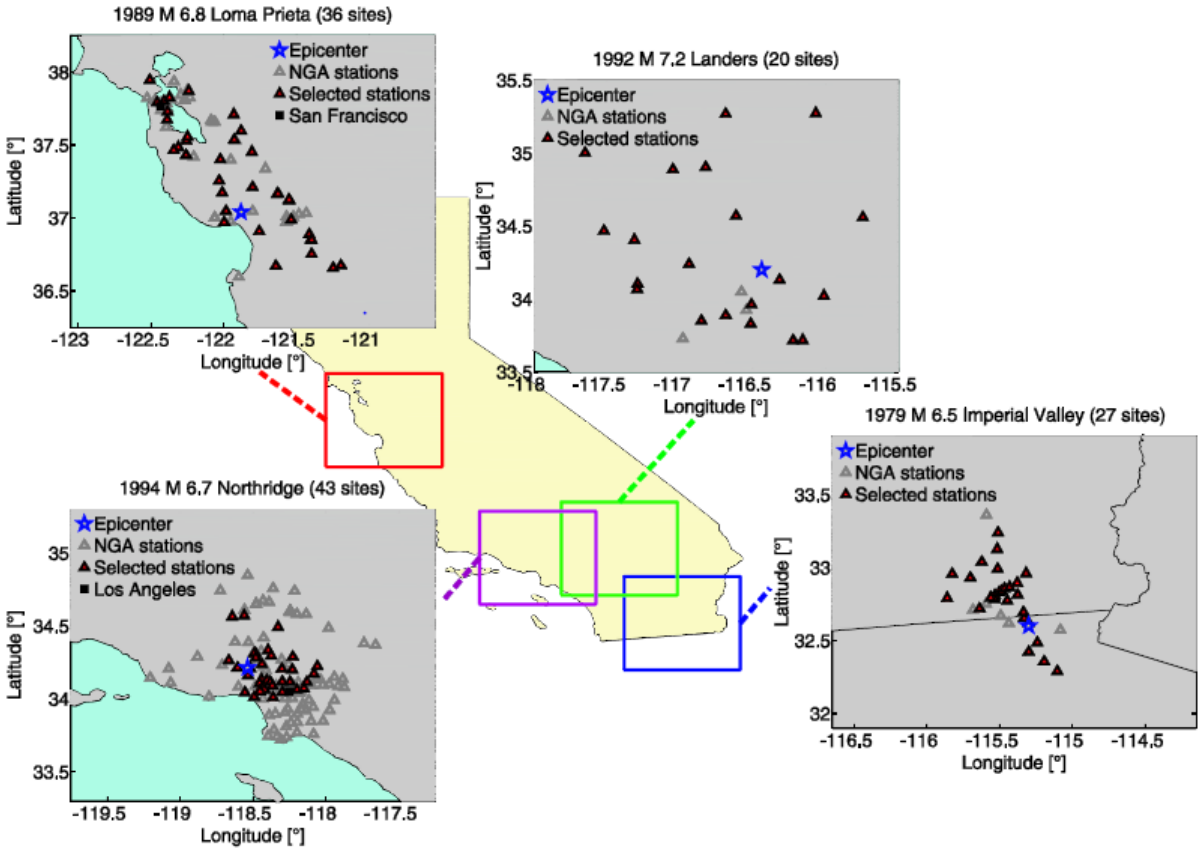

Figure 2. 1. Maps of the considered earthquakes. The star is the epicenter and the grey triangles are recording stations of the NGA database for which the simulations are available. The red triangles are recording stations considered in this study. San Francisco and Los Angeles are also indicated on the map (black squares).

2.2.2. Validation for Generalized Linear MDOF Systems

The conceptual model used in the first part of this study is schematically shown in Figure 2.2. It consists of a flexural cantilever beam and a shear cantilever beam deforming in bending and

shear configurations, respectively (Miranda 1999). The two beams are assumed to be connected by an infinite number of axially rigid members that transmit horizontal forces; thus, the flexural and shear cantilevers in the combined system undergo the same lateral deformation at all heights. Floor mass and lateral stiffness are assumed to remain constant along the height of the building, although modifications for non-uniform mass and stiffness distribution over the height of the building have been proposed and are considered in the following.

Previous studies have provided closed form solutions for the fourth-order partial differential equation describing the combined shear and flexural beams for: (1) lateral static loading to approximate the maximum roof and interstory drift demands of first-mode dominated structures (Miranda 1999); (2) computing the approximate dynamic structural behavior (in terms of lateral displacements and peak floor accelerations) by using up to the first three modes of vibration (Miranda 2005); (3) estimating generalized drift spectrum (Miranda 2006). Evaluation of the results presented in the aforementioned studies indicates that this analysis tool provides relatively good result not only in terms of peak values of response parameters but also, in most cases, for response history results.

The power of the conceptual MDOF system described here is in its simplicity; in fact, mode shapes, modal participation factors, and the ratio of the period of vibration of higher modes to the fundamental period are fully defined by only three parameters: T_1,ξ, andα, namely, the fundamental period, the critical damping ratio at the first mode of vibration, and the lateral shear to flexural stiffness ratio (Miranda 2006). In particular, Equation (2.1) givesα, where H is the total height of the building, GA is the shear stiffness of the shear beam and EI is the flexural stiffness of the flexural beam.

$$\alpha = H\sqrt{\frac{GA}{EI}} \tag{2.1}$$

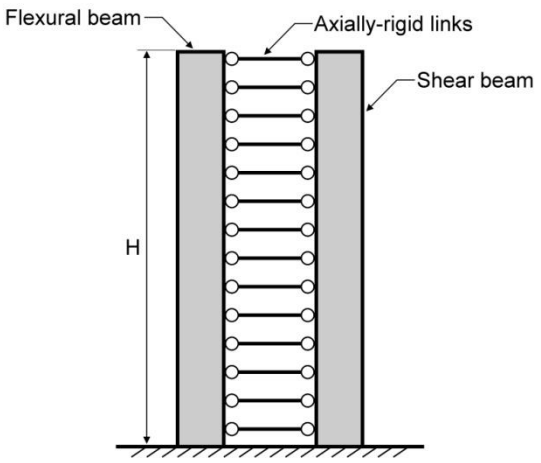

Figure 2. 2. Simplified model used in generalized interstory drift spectrum

The dimensionless parameter α controls the degree of participation of flexural and shear deformations in the total deformation of the simplified model. Miranda and Reyes that lateral deflected shapes of buildings, whose lateral resisting system consists only of structural walls, can usually be approximated by α between 0 and 2. The same study indicates that for buildings with dual lateral resisting systems consisting of a combination of moment-resisting frames and shear walls or a combination of moment-resisting frames and braced frames, values of α are typically between 1.5 and 6. For buildings whose lateral resisting system consists only of moment-resisting frames, values of α are typically between 5 and 20.

As an example, the curves in Figure 2.3a show the normalized fundamental modal shapes and corresponding interstory drift as a function of the nondimensional height $z = x/H$ for three considered α values (i.e., 0.1, 8 and 30; these values are used in the rest of the study). In extreme cases when the structure behaves as a flexural cantilever beam ($\alpha = 0.1$) or in the buildings where lateral shear deformations dominate over lateral flexural deformations ($\alpha = 30$), the maximum IDR occurs at the top or near the ground story, respectively (assuming that the structural behavior is

dominated by the first mode of vibration). Figure 2.3b shows the relationship between the fundamental period of buildings and second mode period. Note that in the case of α = 0.1, for structures with fundamental period less than 6s, the second mode period is less than 1s, which is in the semistochastic part of the hybrid broadband simulation. In the other two cases (i.e., α = 8 & 30), this happens only for structure with a fundamental period less than about 3s. This confirms the importance of considering the higher modes effect in comparing the seismic demands to simulated and recorded ground motions, beyond the simple validation in terms of elastic spectral ordinates at the fundamental period of the structure.

Note that, while assuming the mass to remain constant along the height of buildings is reasonable in most cases, the building's lateral stiffness does not remain constant along the height except for low rise buildings (e.g., less than three stories). Miranda and Taghavi provided expressions to compute the dynamic characteristic of non-uniform buildings, although they concluded that in many cases, using the dynamic characteristics of uniform models could provide reasonable approximations to the dynamic characteristics of non-uniform models. In the simplified model used in this study, the base of the model has been assumed to be fixed; foundation flexibility and torsional deformations are neglected.

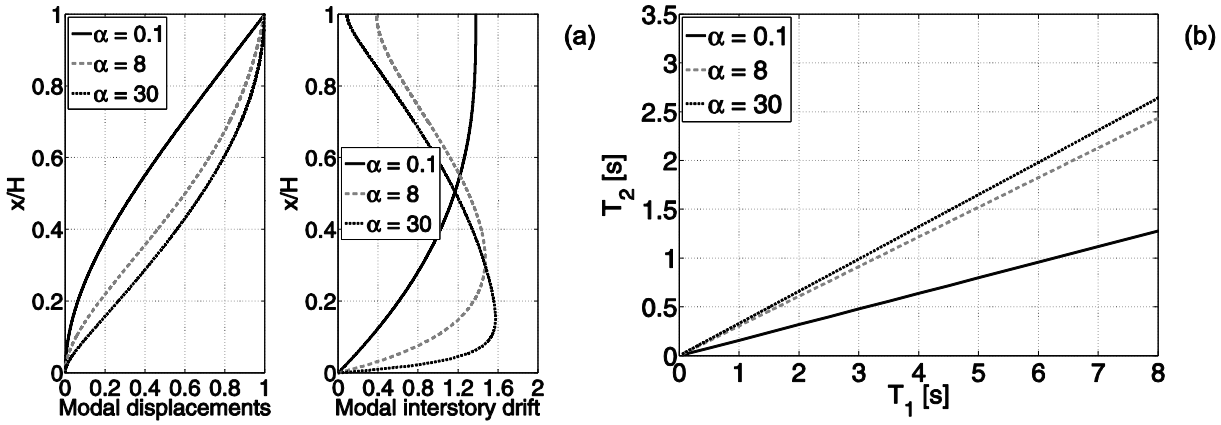

Figure 2. 3. (a) Dependence of lateral deformation (in terms of modal displacement and modal interstory drift) on α for the first mode. (b) Dependence of second mode period (T2) on first mode period (T1) for different α values.

2.2.2.1 Description of the considered systems and demand measures

In order to study the dynamic response of a wide range of buildings, a number of simplified continuum systems are selected including: (1) sixteen (fundamental) oscillation periods, simply T_1 hereafter, between 0.1s and 6s; (2) three shear to flexural deformation ratios, α, to represent respectively shear walls structures (α = 0.1), dual systems (α = 8), and moment-resisting frames (α = 30); (3) two stiffness distributions along the height of the systems; i.e., uniform and linear. In the latter case, the ratio of the lateral stiffness at the top of the structure to the lateral stiffness at the base is assumed equal to 0.25. The period range is sampled with a 0.1s step from 0.1s to 0.5s, with a step of 0.25s between 0.5s and 1s, with a step of 0.5s between 1s and 5s, and with a step of 1s between 5s and 6s.

It is general belief that the Engineering Demand Parameter (EDP) that is best correlated with seismic damage is the peak interstory drift ratio, defined as the difference in lateral displacements between two consecutive floors normalized by the interstory height. Similarly, damage to contents and many nonstructural components are primarily related to peak floor acceleration and to floor acceleration spectra (to follow).

The generalized demand spectra in terms of maximum IDR, MIDR (i.e., the maximum time-peak rotation $\theta(z,t)$ over the height of the building), is derived as shown in Equation 2.2. For a given fundamental period of vibration, the total height of the model is computed using the relationship (in metric units) suggested for steel moment-resisting frames in ASCE 7-210, Equation 2.3. To derive the system demands, some approximations were taken: (1) uniform distribution of mass along the height of the building, (2) equal damping ratios of 5% for all modes; (3) only the first six modes of vibration is considered so that the sum of their effective modal masses contains more than 90% of the system total mass.

$$MIDR = \max_{\forall t,z} |\theta(z,t)| \tag{2.2}$$

$$T = 0.0724H^{0.8} \rightarrow H = \sqrt[0.8]{\frac{T}{0.0724}} \tag{2.3}$$

2.2.2.2 Results and discussions

A direct comparison of response statistics is appropriate because the simulated datasets were developed to match exactly the same earthquakes and site conditions (i.e., at the same stations) of the real recordings. Ground motion pairs (recorded and simulated) selected for each earthquake are used as input for the seismic analysis of the MDOFs discussed in the previous section; a total of about 24,000 analyses are performed. Only horizontal components of ground motions (i.e., north-south, NS, and east-west, EW) are used, while the vertical component is neglected. The spectral responses for the two horizontal components at each station is computed and then combined into an "average" spectral response by using the geometric mean.

For each earthquake, the median value of the MIDR (i.e., the exponential of the mean of the natural log of the MIDR across all the available stations) for simulated records divided by the

corresponding median value for the recorded dataset is computed and plotted across the considered period range (for different values of α). A ratio above unity, if statistically significant, means systematic overestimation (i.e., bias) of the response by simulation and below unity means underestimation. More specifically, a deviation above unity of the considered ratio, indicates that the synthetic records in that dataset tend to produce, on average, systematically more intense seismic demands in terms of MIDR than those by real records. Conversely, deviations below unity indicate that the simulated records tend to be, on average, more benign, in terms of MIDR, than those in nature.

In order to provide a measure of inherent variability in the simulations compared to that of real ground motions, the ratio of standard deviation of MIDR (in terms of the natural log of the data) for recorded and simulated ground motions was plotted as a function of MDOF fundamental period and α. A line above unity means relatively more record-to-record variability produced by synthetic ground motions whereas the opposite is true for a line below unity.

2.2.2.2.1 Comparison between statistical measures of generalized MIDR spectra

In general, the generalized MIDR spectra from simulated waveforms agree reasonably well with those from the observations. The median value of the MIDR for the simulated records ($MIDR_{sim}$) divided by the median value of the MIDR for the recorded dataset ($MIDR_{rec}$) is plotted across the period range of 0.1s to 6s in Figure 2.4a for the three considered α values for the Imperial Valley earthquake. Similarly, Figure 2.4b shows, for the same event, the ratio of the standard deviation of MIDR (log of the data) for synthetic ground motions divided by the standard deviation of MIDR (log of the data) for recorded ground motions. Figure 2.4 refers to uniform stiffness distribution along the height of the systems. Figures 2.5-2.7 are developed in the same fashion as Figure 2.4, however, for Loma Prieta, Landers and Northridge respectively. Results for the case

of linear stiffness distribution along the height of the systems are not shown to save space and similar observations can be drawn for this case.

Based on the simplified model introduced in the previous sections, bias (i.e., the departure of the considered ratios from unity) in the elastic response of conceptual MDOF systems is earthquake-, period- and slightly α-dependent. Deviations seem to be concentrated in the zone of semi-stochastic simulation (at very short periods) and around 2s. The observed differences at given periods are likely due to systematic differences in the average shape around those periods of the linear response spectra generated by synthetic and by real ground motions (to follow). For Loma Prieta and Northridge, both characterized by buried ruptures, the comparisons in Figure 2.5 and Figure 2.7 produces very similar results; Imperial Valley and Landers are both surface events with similar results.

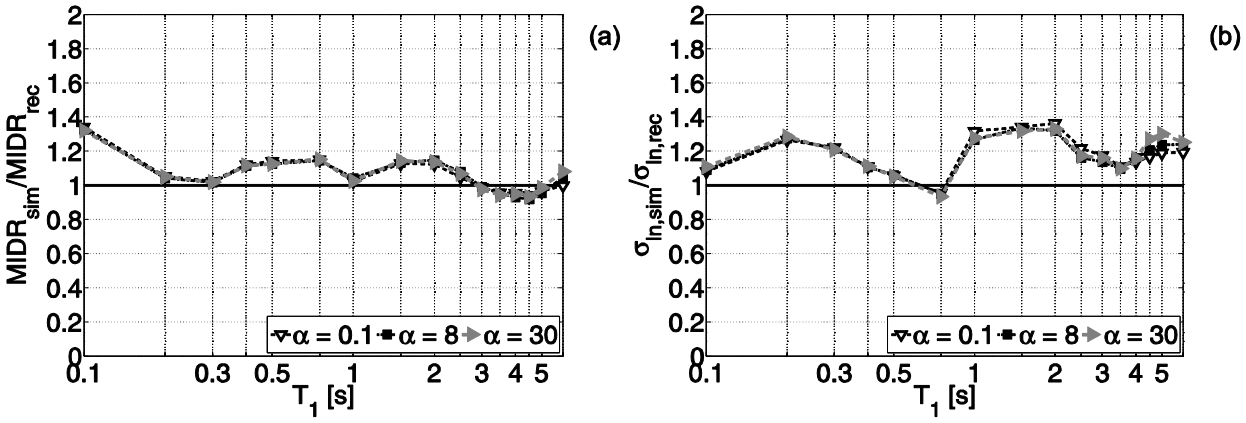

Figure 2. 4. Ratios of the medians (a) and standard deviations (b) of the generalized MIDR spectra for simulated ground motions to the corresponding quantity computed for the recorded ground motions for the Imperial Valley earthquake.

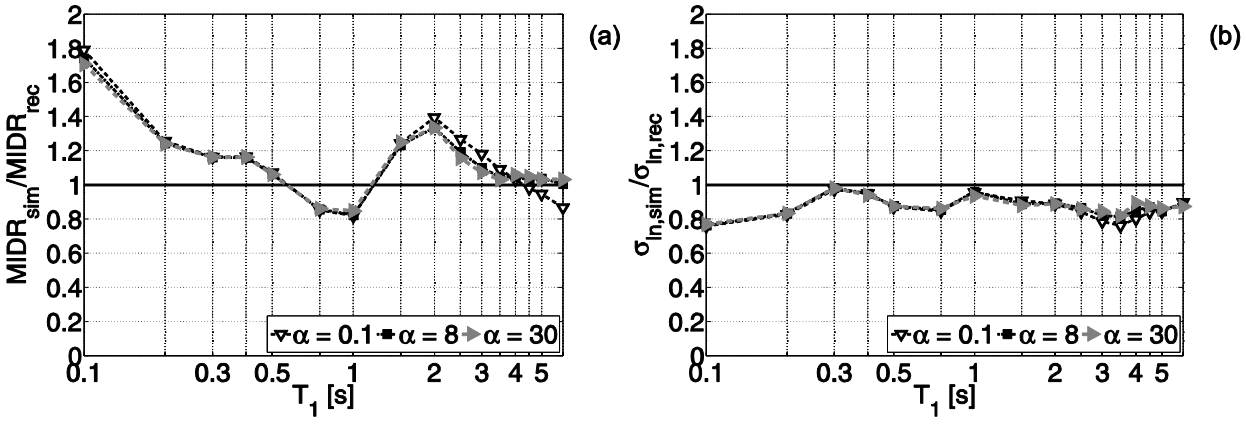

Figure 2. 5. Ratios of the medians (a) and standard deviations (b) of the generalized MIDR spectra for simulated ground motions to the corresponding quantity computed for the recorded ground motions for the Loma Prieta earthquake.

Except for one out of four historical events studied here, i.e. Imperial Valley, the standard deviations of the generalized MIDR spectra of the real records are generally larger compared to the simulated ground motions, particularly at the shorter periods. This trend of relatively low intra-event variability in the simulations, especially at short periods, has been noted previously in (Star et al 2011). Seyhan et al. have recently proposed a revision to the simulation approach that incorporates greater stochastic variability in the high frequency portion to address this issue, although this revision has not yet been applied to the simulations considered in the current analysis. From a practical standpoint, if an engineer seeks to design a new structure or assess the performance of an existing one, the use of simulated records that tend to generate less variable response would underestimate the likelihood of extreme response values.

In the case of the Imperial Valley event, the standard deviation of the response to simulated records is larger than that to recorded ones across the entire period range (the considered ratio is almost constant and above the unity). At long periods, this can be attributed to the presence in the simulated dataset of ground motions featuring strong coherent velocity pulses (Graves et al 2010) and then large elastic response. The reason for this increased variability is that the deterministic

approach can create strong spatial variability in the near fault ground motions due to the characteristics of the rupture and also the 3D geology (if that is included). This is not only limited to strong coherent pulses in the forward rupture direction, but also includes less coherent motions in the neutral or backward directivity direction. In addition, at low frequencies, the deterministic simulations are also much more sensitive to the distribution of slip on the fault. Due to the nature of the randomness in the stochastic approach, all these features tend to be homogenized (e.g., the stochastic approach uses an averaged radiation pattern for all sites), and thus the spatial variability in the near fault region is generally diminished relative to the deterministic approach and to the recorded ground motions. However, in the case of Imperial Valley, the relative complexity of the regional velocity structures where this event occurred and, probably, some inadequacies in the velocity model used in the simulation (and the assumed inelastic attenuation function) result in large variability of the response due to simulated ground motions also at short periods.

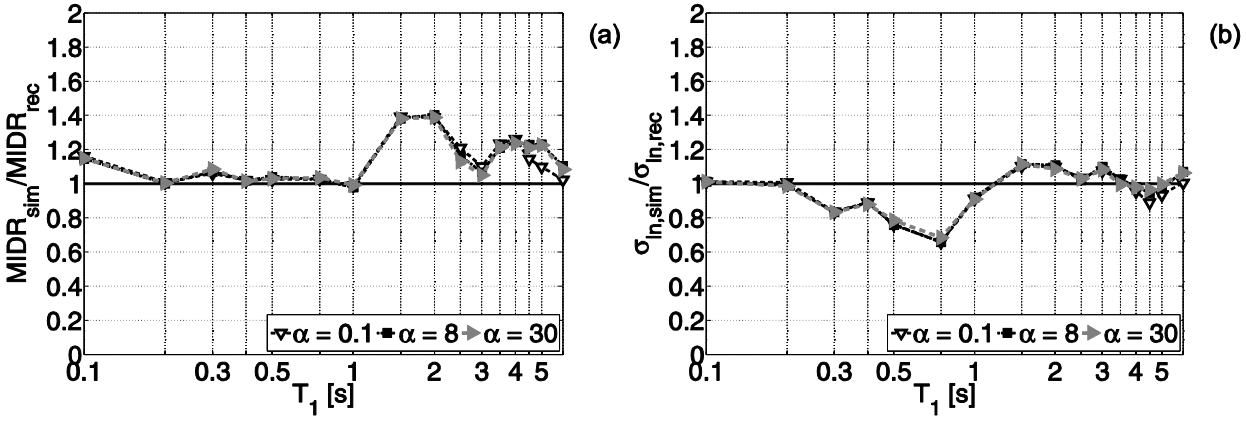

Figure 2. 6. Ratios of the medians (a) and standard deviations (b) of the generalized MIDR spectra for simulated ground motions to the corresponding quantity computed for the recorded ground motions for the Landers earthquake.

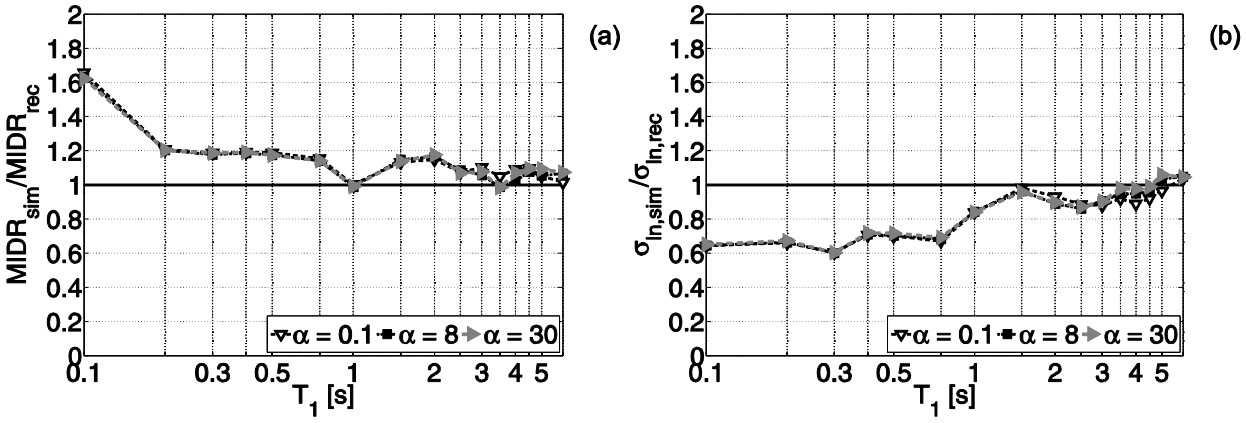

Figure 2. 7. Ratios of the medians (a) and standard deviations (b) of the generalized MIDR spectra for simulated ground motions to the corresponding quantity computed for the recorded ground motions for the Northridge earthquake.

2.2.2.2.2 Comparison in terms of floor acceleration spectra

In this section, focus is made on acceleration demands of two case study tall buildings subjected to simulated and recorded ground motions. In particular, floor acceleration spectra for four different locations along the height are obtained and plotted in terms of ratio between median of structural response to simulated and recorded ground motions. Floor accelerations spectra allow the estimation of accelerations demands at different frequencies. This information is useful, for example, for acceleration-sensitive non-structural components (characterized by a weight smaller than the weight of the building) for which the peak floor acceleration is not enough.

The first structure (SF48) is a pyramidal-shape 257m tall building in San Francisco, built in 1972; its lateral resisting system consists of interior and exterior steel moment-resisting frames. It was shaken by the 1989 Loma Prieta earthquake. The second structure considered (LA52), built in 1990, is in Los Angeles and has 52 stories above ground; it has a square floor plan and the lateral resisting system, in both directions, consists of concentrically braced steel frames at the core with outrigger moment-resisting frames in the exterior. This structure was hit by several earthquakes, including the 1994 Northridge event.

Table 2.1. Buildings and events used in this study

ID	Location	Stories	Earthquake	Ep. Dist.	Comp.	T_1 [s]	α	ξ
SF48	San Francisco	48	Loma Prieta	97km	NS	3.57	25.0	1.2
					EW	3.70	25.0	1.5
LA52	Los Angeles	52	Northridge	31km	NS	5.90	9.8	1.0
					EW	6.20	6.0	1.5

Both structures are instrumented, allowing the estimation of the parameters that are needed in each direction to perform the simplified analysis, see (Reinoso et al 2005) for details. The parameters used for each of the buildings are listed in the last three columns of Table 2.1 (the damping ratio of all modes is assumed to be the same in order to reduce the number of parameters required to fully define the simplified model to three); also in this case six modes for each direction of the motions are considered for both structures. For both buildings, despite some important reductions in lateral stiffness that exist as height increases (especially for the SF48 building), Reinoso and Miranda showed that the simplified model is able to capture very well the variation of seismic demands along the height derived from recorded data. Given the different properties of the two buildings in each horizontal direction, separate comparisons for each component of ground motion (i.e., north-south, NS, and east-west, EW) are performed.

The median value of floor accelerations for the simulated records (acc_{sim}) divided by the median value of floor accelerations for the recorded dataset (acc_{rec}) is plotted across the period range of 0.1s to 8s in Figure 2.12a for the SF48 building subjected to the Loma Prieta event, and in Figure 2.12b for the LA52 building shaken by the Northridge earthquake. In both plots, four different locations along the height of the building, expressed in terms of nondimensional height z, are considered, i.e., 25%, 50%, 75% and the roof. The considered ratios seem to be slightly dependent on the z values in all the period range and on the ground motion component. The results in Figure 2.12 confirm the results found in terms of MIDR for the Loma Prieta and Northridge earthquakes (Figure 2.5 and 2.7 respectively): simulated ground motions tend to significantly

overestimate the accelerations demands in the short periods part of the spectra. In the moderate to long period range, simulation matches well the acceleration demands produced by recorded ground motions and the bias is close to zero for a wide period range. Also in this case, it is evident that the simple validation of ground motion simulations by using elastic spectral ordinates may not suffice.

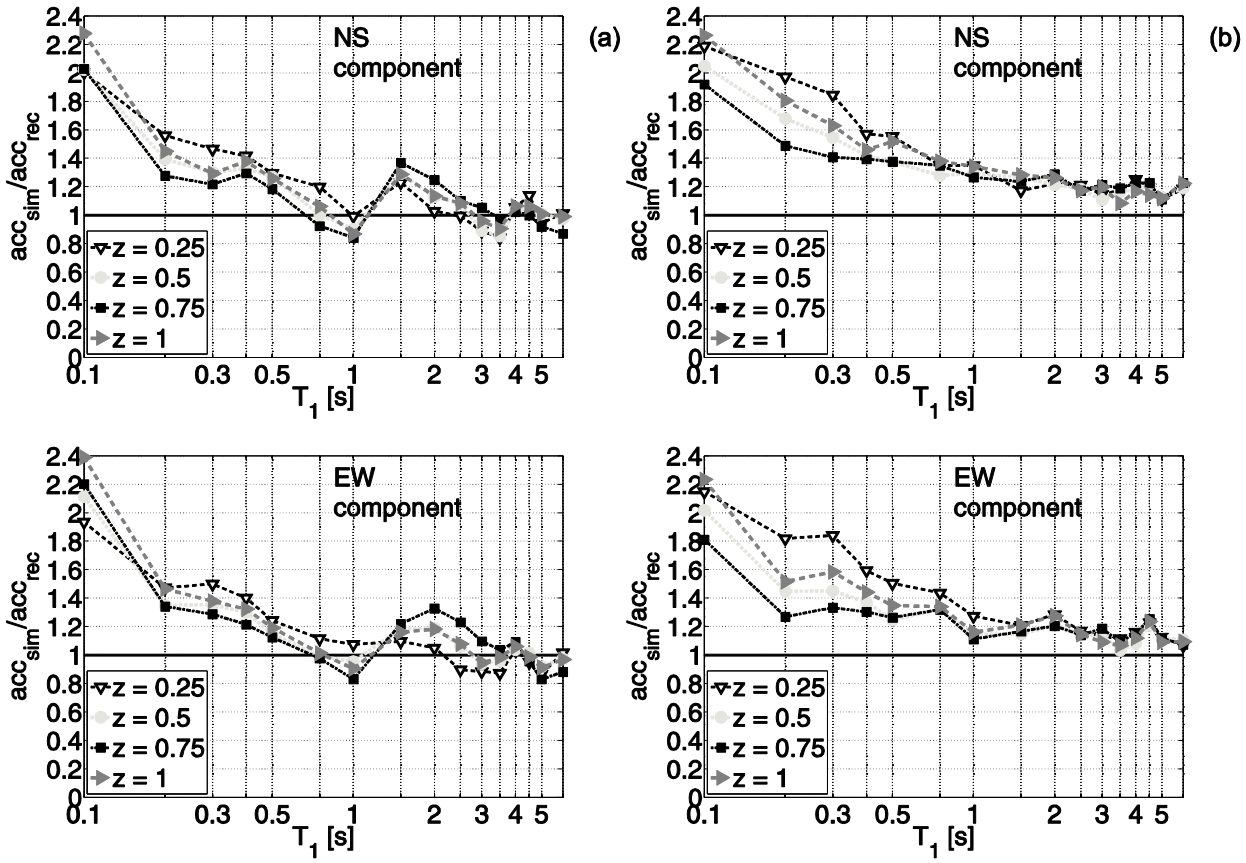

Figure 2. 8. Ratios of the medians of the floor accelerations spectra for simulated ground motions to the corresponding quantity computed for the recorded ground motions for the (a) SF48 buildings and (b) LA52 building.

2.2.2.3 Hypothesis tests

Parametric hypothesis tests are performed to quantitatively assess the statistical significance of the results found in terms of median response (for each oscillation period, each α value, and each earthquake) to recorded and simulated ground motions. The intention is to asses if the ratios

presented in the previous section differ systematically from unity. Hypothesis tests are performed assuming a lognormal distribution for both EDPs, i.e., MIDR and PFA. This distribution assumption is checked with the Shapiro-Wilk test and could not be rejected at the 95% significance level.

Taking the same validation approach in Iervolino et al 2010, the hypothesis is whether the median MIDR (and the median PFA) for simulated ground motions is equal (i.e., null hypothesis) or not (i.e., alternate hypothesis) to those from recorded ground motions. To this aim, a two tails Aspin-Welch is considered. The test statistic employed is reported in Equation 2.4, in which z_x and z_y are the sample means, s_x and s_y are the sample standard deviations and m and n are the sample sizes (in this case always equal for each earthquake). The test statistic, under the null hypothesis, has a Student t-distribution with the number of degrees if freedom given by Satterthwaite's approximation.

$$t = \frac{z_x - z_y}{\sqrt{\frac{s_x^2}{n}} + \sqrt{\frac{s_y^2}{m}}} \tag{2.4}$$

A F-test (Mood et al 1974) for normally distributed data, has been performed in terms of comparison between variances (in logs terms), for the two datasets (recorded and simulated) corresponding to each earthquake; in this case, for each structural system, the null hypothesis is that the variance of structural response (i.e., MIDR and PFA) for simulated ground motions is equal to the variance from recorded ground motions.

Hypothesis tests results for MIDR spectra are summarized in Figure 2.9. To draw conclusions, percentage of hypothesis tests rejections assuming a 95% significance level (i.e., choosing a I-type risk, α_I equal to 0.05) are shown in Figures 2.9 for each pair (T, α). In computing

these percentages, all the earthquakes and structural models are considered together, yielding a total of 8 cases. Based on Figure 2.9, tests have shown a statistical significance of the bias of simulated record in terms of MIDR ratio only for very short period structures and around 2s for all the considered α levels. These results confirm the considerations based on the visual inspection of Figures 2.4-2.7.

Similarly, tests have shown a statistical significance of the bias of simulated record in terms of PFA. This significance goes up to period of 0.5s in the case of SF48 building and up to 1.0s in the case of LA52 building, confirming that the derived conclusions on bases using visual inspection of Figure 2.8.

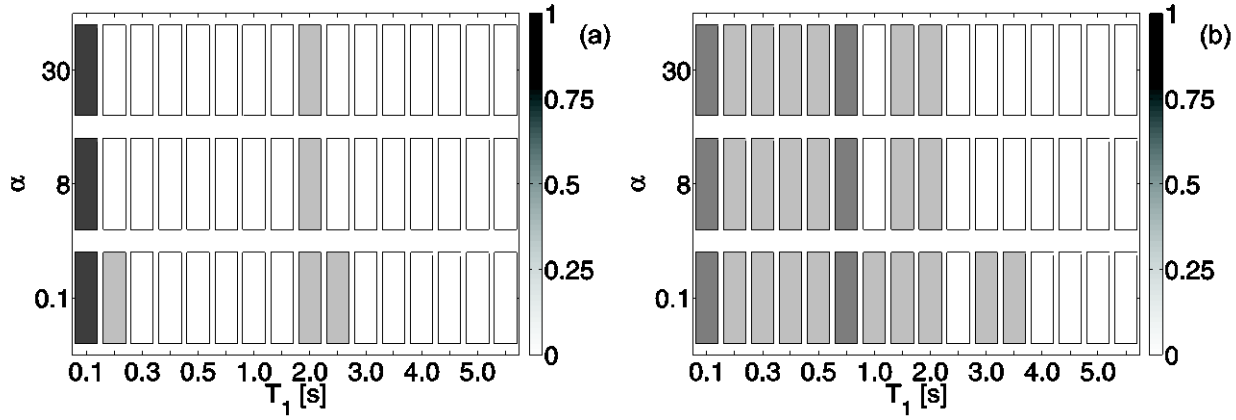

Figure 2. 9. Percentage of hypothesis test rejections ($\alpha I = 0.05$) for MIDR; (a) equality of medians and (b) equality of variances.

To investigate the possible sources of the found differences in the short periods range, for each of the four events considered in this study, the median value of the elastic displacement spectral ordinates for the simulated records divided by the median of that parameter for the recorded dataset is computed and plotted across the considered period range in Figure 2.9. From inspecting the graphs in Figure 2.10, it is clear that not only the median spectral amplitudes, but also the spectral shapes for simulated ground motions can be different from the median response spectrum of real recordings. In fact, any trend across the periods in the median ratios shown in

Figure 2.10 that departs from a horizontal line, suggests that the elastic spectra generated by the synthetic model have, on average, a different shape than those produce by nature. The difference in spectral shape is large especially for Loma Prieta and Landers events, for a wide range of periods. These differences in terms of spectral shape have an influence on the multi-mode response of the considered systems. In fact, given the contribution of higher modes, the displacement and acceleration demands of an MDOF system (i.e., MIDR and PFA), is dependent on the frequency content of the record in a fairy large bandwidth, including smaller periods, and not only in the neighborhood of the first period of vibration. Therefore, even if hypothesis tests do not confirm the differences in spectral amplitudes to be statistically significant, the differences in spectral shape leads to statistical significant differences in terms of MIDR and PFA, confirming the need for an engineering validation beyond the simple elastic SDOF analysis.

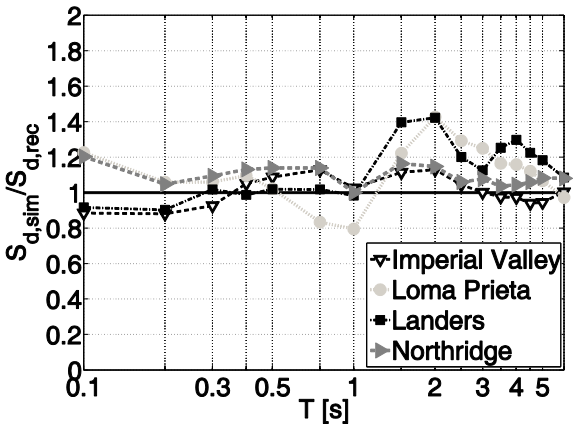

Figure 2. 10. Ratios of the medians of the elastic displacement spectra for simulated ground motions to the corresponding quantity computed for the recorded ground motions.

2.2.2.4 Sensitivity of Ground Motion Simulations to Source-To-Site Distance and Site Conditions

In this section a closer look at the influence of source-to-site distance, and site conditions, on the ratios of the medians and standard deviations of the generalized MIDR spectra for simulated and recorded ground motions is presented. Specifically, the considered variables are the closest

distance to the fault, *D* (in km), and the shear wave velocity in the upper 30 m, $V_{S,30}$.

2.2.2.4.1 Effect of distance to the source

Two subsets of the recording stations for the Northridge earthquake representing two different distance ranges, i.e., D ≤ 20km (with 20 ground motions), and D > 20km (with 23 ground motions), are assembled. Northridge earthquake was selected because it is characterized by the largest number of stations. Figure 2.11a shows the ratio of the median spectrum in terms of MIDR from the simulated ground motions to the median spectrum (again in terms of MIDR) from the recorded ground motions for each subset (as a function of the period and α); similarly, Figure 2.11b shows the ratio of the standard deviations of the data in terms of MIDR from the simulated ground motions to the standard deviation of the data (again in terms of MIDR) from the recorded ground motions for each subset.

Figure 2.11 refers to systems with uniform stiffness distribution along the height (results for the other cases, not presented for the sake of brevity, confirm these findings). For the range of distances considered in this study (5km < D < 52km), ratios of the medians do not significantly change when computed from ground motions ensembles representative of different distance ranges for all the considered systems. Conversely, looking at the ratios of standard deviations for simulated and recorded ground motions, moderate and long period ordinates are significantly influenced by the distance range. In particular, the standard deviation of response to simulated records is larger than that of recorded ones across the period range 1s-6s. As discussed for the MIDR spectra of the Imperial Valley event (Figure 2.4), sensitivity of standard deviation of response to distance can be attributed to the presence of near fault effects (e.g., strong coherent velocity pulses) in the simulated dataset. To confirm this, it is worth to note that the Imperial Valley dataset features a total of 27 ground motions all within 21km from the associated fault.

Addressing near fault effects is the topic of current research; however, it is difficult to precisely quantify and/or calibrate these effects due to the scarcity of near-field recordings of moderate and large earthquakes. Insights from dynamic rupture simulations (Schmedes et al 2010) have the potential to provide additional constraints on the characteristics of the rupture process used in the simulations. However, it is evident that strong directivity effects in the simulations require more study.

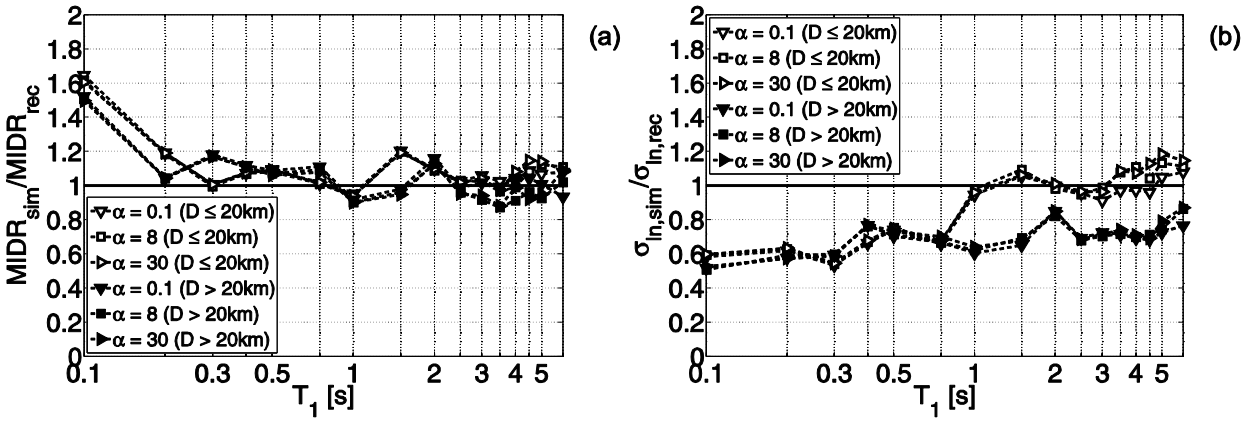

Figure 2. 11. Effect of distance on the ratios of the medians (a) and standard deviations (b) of the generalized MIDR spectra for simulated ground motions to the corresponding quantity computed for the recorded ground motions (Northridge earthquake, systems with uniform stiffness distribution along the height).

2.2.2.4.2 Effect of site class

Two subsets of 16 and 27 ground motions representing two different $V_{S,30}$ ranges (in m/s), i.e., $V_{S,30} < 400$m/s and $V_{S,30} \geq 400$m/s, are assembled from the datasets corresponding to the Northridge earthquake. Figure 2.12a shows the ratio of the median spectrum in terms of MIDR from the simulated ground motions to the median spectrum (again in terms of MIDR) from the recorded ground motions for each subset (as a function of the period); similarly, Figure 2.12b shows the ratio of the standard deviations of the data in terms of MIDR from the simulated ground motions to the standard deviation of the data (again in terms of MIDR) from the recorded ground motions for each subset (also in this case we refer to the systems with uniform stiffness distribution

along the height). It can be seen that, for the range of $V_{S,30}$ considered in this study, ratios of the medians and standard deviations do not significantly change when computed from ground motions ensembles representative of different $V_{S,30}$ ranges for all the considered period and α values.

2.2.3. Validation of Simulated Ground Motions Using Nonlinear MDOF Building Systems

The results presented in the previous sections shed light on the importance of considering the contribution of higher modes in the engineering validation of hybrid broadband ground motions. However, the generalized MIDR analysis inherits some of the limitations and assumptions of modal analysis, such as assuming a linear elastic behavior. To alleviate this limitation two nonlinear case study structures were considered. In particular, moderate and long period structures where both the comparisons presented in the previous sections in terms of spectral ordinates and generalized MIDR and floor acceleration spectra have not shown statistically significant differences of the seismic demands to simulated and recorded ground motions, are of interest. To investigate whether this conclusion holds in the case on inelastic response, a 6- and a 20-storey buildings with perimeter SMFs and designed for high seismic risk under the 1994 UBC are considered here. These structures are selected due to the prevalence of this building type in the Los Angeles region, although, they are not necessarily representative of all SMFs. The 6- and the 20-storey structures are denoted as U6 and U20, respectively. Details for the design of the structure can be found in (Hall 1997).

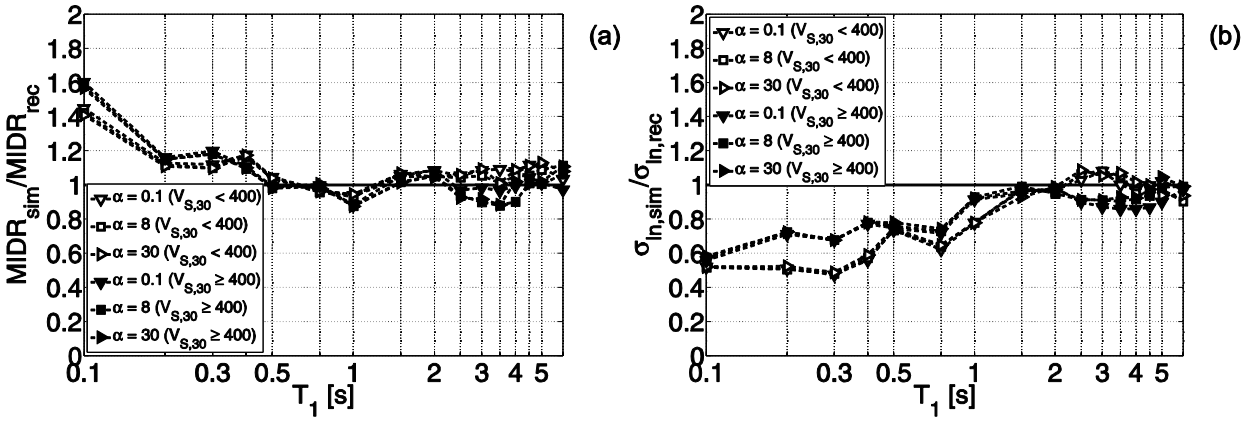

Figure 2. 12. Effect of Vs30 on the ratios of the medians (a) and standard deviations (b) of the generalized MIDR spectra for simulated ground motions to the corresponding quantity computed for the recorded ground motions (Northridge earthquake, systems with uniform stiffness distribution along the height).

2.2.3.1 Description of the structures and analytic models

The finite element models of the considered structures is constructed, using the Open System for Earthquake Engineering Simulation (OpenSees) software (http://opensees.berkeley.edu/). In total, eight models are produced, with four variations on each of the two base structures. Two variations for the beam connection type are used, a brittle pre-Northridge connection and a ductile post-Northridge connection, denoted as 'preNR' and 'postNR', respectively. Additionally, two variations on the modeling strategy are implemented, a bare frame model, and a more robust model that consists of the bare frame model in all respects with addition of the gravity frame, denoted as '+GFL', as well as the slab contribution, denoted as '+MFS'. In the following we will discuss the results for the (postNR + GFL + MFS) case; results for other buildings variations are not shown to save space and similar observations can be drawn for these cases. The diaphragm of the structure is assumed to be rigid. Soil–structure–foundation interaction is not considered in the model and the basement walls are not modeled; column bases are fixed. Lumped plasticity models are employed and attempted to consider all significant contributions to the strength and stiffness of the structures as well as the cyclic deterioration of components. P-delta effects are included in the

analysis and 2.5% viscous damping is used in all modes of vibration. Further details can be found in (Jones et al 2010).

Figure 2.13 shows the schematic configuration of the 6- and 20-storey moment frames. The structural components are elastic beam elements with plastic hinges at their ends and elastic column elements with P–M plastic hinges at their ends.

Table 2.2 Buildings periods.

	Period (in direction of MF only)	
Structure name	**T_1 [s]**	**T_2 [s]**
U20 (postNR + GFL + MFS)	3.683	1.265
U6 (postNR + GFL + MFS)	1.937	0.657

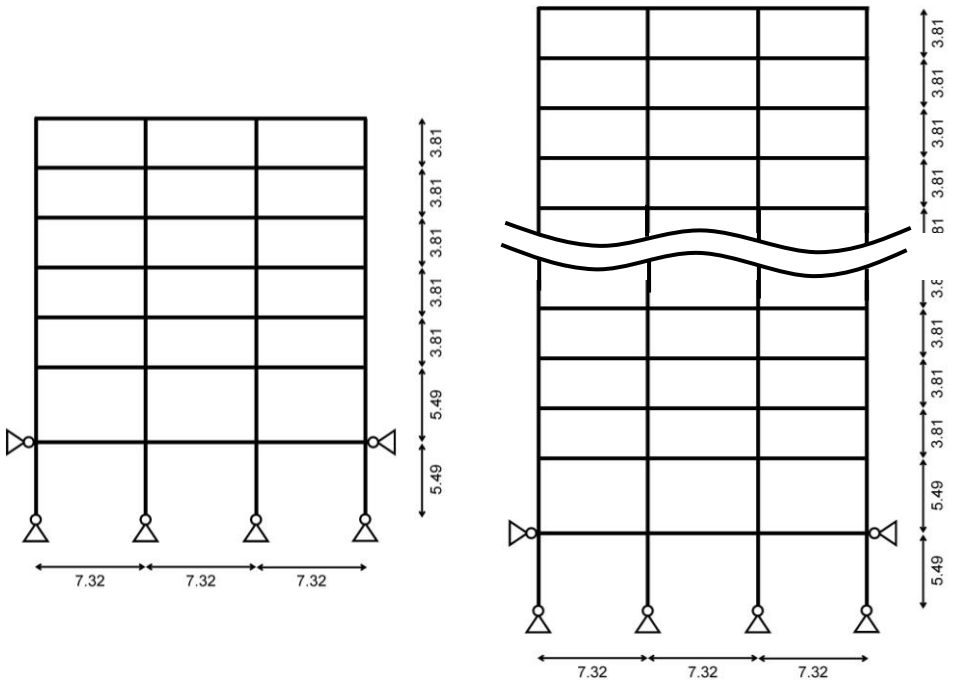

Figure 2. 13. Elevations of the individual moment frames from the U20 and U6 structures.

The geometries and spring properties of these components are varied according to the properties of the frames they represent. In particular, the moment frame connection type, whether

pre- or post-Northridge, is considered in the plastic hinges of the moment frame beams. When the slab effect is modeled (+MFS), strength capacity of beam plastic hinges are increased. For models that included the gravity frame (+GFL), partially restrained rotation hinges are employed at the beam–column connections of gravity frame members. The effect of axial loading on column bending strength is incorporated in the models through P-M interaction. Table 2.2 shows the first and second mode period of the structural systems used in this study. Further information on modeling aspects of the 6-storey and 20-storey frames can be found in (Jones et al 2010). Although three-dimensional models of the structures are built, the analysis is essentially two-dimensional in that the ground motions are applied along the building's transverse axis, parallel to the moment frames.

2.2.3.2 Results and discussions

The model region for each event covers a wide area surrounding the fault, including many strong motion recording sites, in a large range of distances. In an effort to analyze structural response in the nonlinear range, only a limited number of these sites are used here in performing NLDA. To this aim, for each building, the value of the MIDR for each simulated record divided by the value of the MIDR for the corresponding recorded waveform (at the same station) is computed and plotted as a function of the ratio of the recorded spectral acceleration at the first period of the structure, $S_{a,rec}\left(T_1\right)$, divided by yield base shear coefficient γ. The latter is the ratio between the base shear at yielding point to the seismic weight of the structure. The base shear at yielding point is obtained from a pushover analysis performed with the load pattern described in ASCE 7-10 and the displacement control strategy; Figure 2.14.

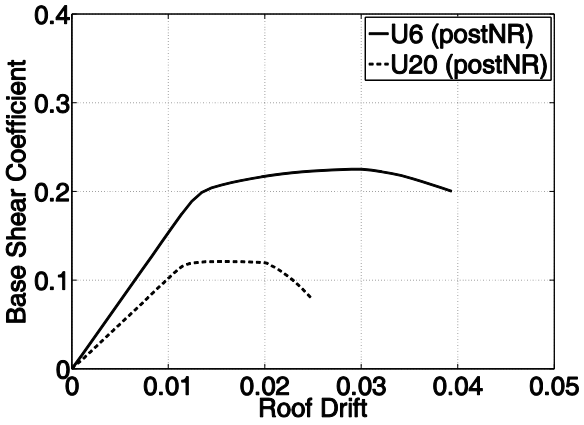

Figure 2. 14. Pushover curves of the structures used in this study.

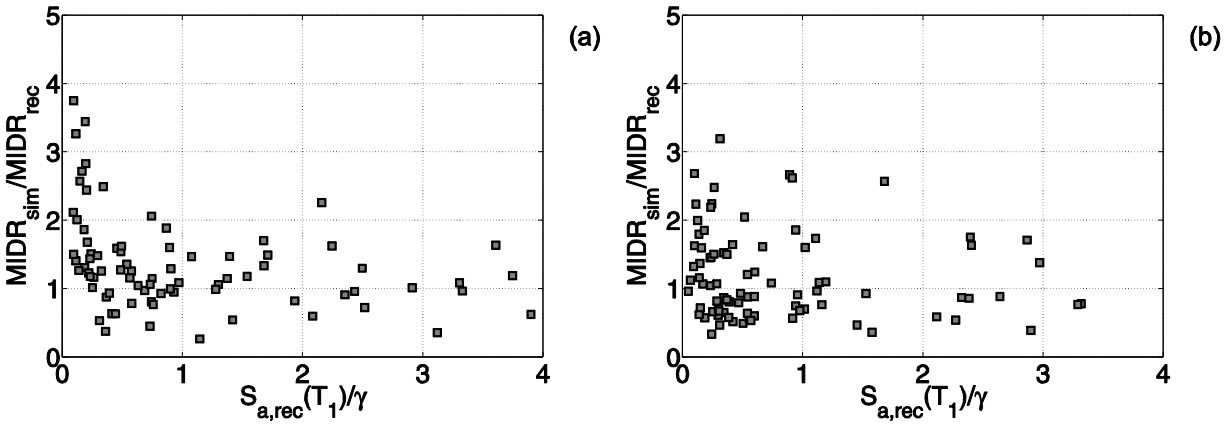

Figure 2. 15. Ratios of the individual MIDR values for simulated ground motions to the corresponding quantity computed for the recorded ground motions as a function of $S_{a,rec}(T_1)/\gamma$ for (a) U6 and (b) U20.

Figure 2.15a refers to the U6 (postNR + GFL + MFS) building and Northridge event, while Figure 2.15b refers to the U20 (postNR + GFL + MFS) building (same event). This event has been selected because it is characterized by the largest number of stations; results for the other events are not shown to save space and similar observations can be drawn for these cases. One can assume that ground motions characterized by $S_{a,rec}(T_1)/\gamma$ larger than unity has forced the structure into inelastic response.

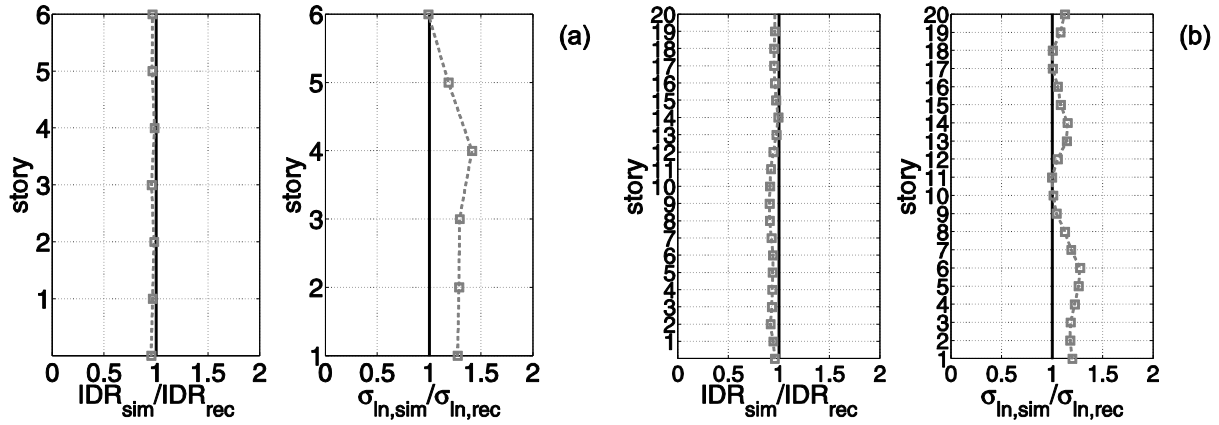

Figure 2. 16. Ratios of the medians and standard deviations of IDR profiles for simulated GMs to the corresponding quantities computed for the recorded GMs for (a) U6 and (b) U20.

For a subset of ground motions with $S_{a,rec}(T_1)/\gamma \geq 1.0$, the median value of the time-peak IDR at a story level for the simulated records (IDR_{sim}) divided by the median value of IDR for the recorded dataset (IDR_{rec}) is plotted over the height of the building in Figure 2.16a (U6) and Figure 2.16b (U20). In the same figure, the ratio of the standard deviation of IDR (log of the data) for synthetic ground motions divided by the standard deviation of IDR (log of the data) for recorded ground motions is also plotted along the height of the building. In general, the median IDR profiles due to the simulated waveforms agree reasonably well with those due to the recorded ground motions. In particular, for the U6 building subjected to the Northridge earthquake, the comparison between the median profiles for recorded and simulated ground motions (Figure 2.16a) exhibit a technically zero bias along the height. Also for the U20 building subjected to the Northridge earthquake, the bias is close to zero along the height (Figure 2.16b). These results are confirmed in terms of PFA (Figure 2.17), with a negligible bias along the height in terms of median response.

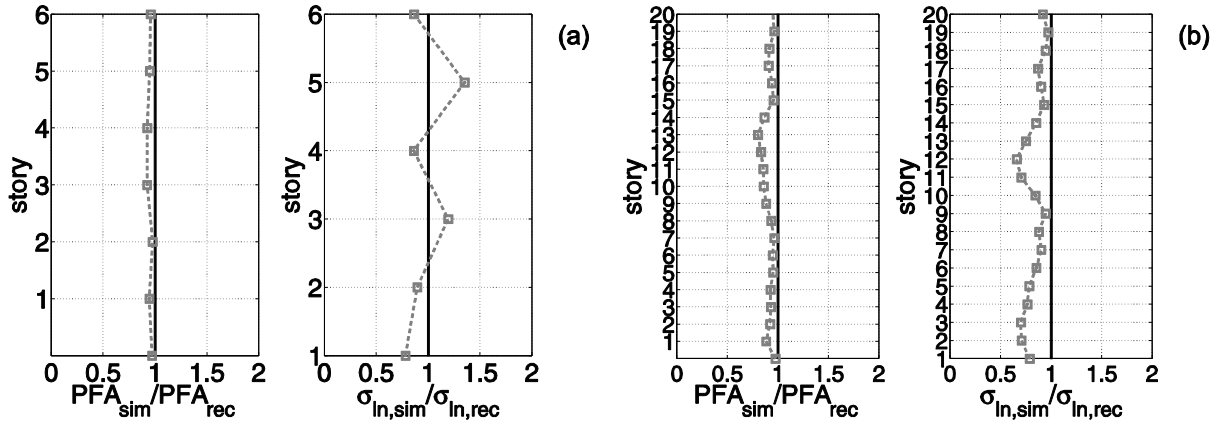

Figure 2. 17. Ratios of the medians and standard deviations of PFA profiles for simulated ground motions to the corresponding quantities computed for the recorded ground motions for (a) U6 and (b) U20.

Figure 2.16 shows that the standard deviations of the IDR profiles produced by the simulated records are generally larger compared to those from the recorded ground motions. This result is consistent with the finding of Section 2.2.3.4.1 for the elastic response. In fact, the ground motions for which the ratio $S_{a,rec}(T_1)/\gamma$ is larger than unity are those characterized by the short source-to-site distances and then, potentially, affected by forward directivity effects. However, hypothesis tests do not confirm these differences to be statistically significant, for both buildings and considered EDP.

The favorable comparisons shown for these two buildings lend support to the predictive capabilities of the simulation methodology. However, it is to stress on the fact that observations and conclusions made here are based on the limited set of building models used in this study and further research is required to make definitive conclusions.

2.3. CONCLUSIONS

In recent years, significant progress has been made in modeling and simulation of broadband ground motions suitable for both design and assessment of structures. The first part of this validation investigated whether a state-of-the-art simulation technique produces generalized

interstory drift and peak floor acceleration spectra that are statistically distinguishable from those created by real records. The spectra are computed for elastic MDOF systems with period ranging from 0.1s to 6s and for different earthquake resistant systems. The investigation is done by means of simulations for four historical earthquake recorded at several stations located at various distances from the fault rupture, i.e., 1979 M_w 6.5 Imperial Valley earthquake, 1989 M_w 6.8 Loma Prieta earthquake, 1992 M_w 7.2 Landers earthquake and 1994 M_w 6.7 Northridge earthquake. Results show that structural response estimated by using simulated records generally matches the response obtained using recorded motions. However, differences exist between median estimate of seismic demand obtained by using real records and that obtained by simulations, especially in the short periods part of the spectra, where the simulation is semistochastic. The observed differences are due to systematic differences in the average shape around those periods of the elastic response spectra generated by synthetic and by real ground motions. Moreover, the record-to-record variability of seismic demands produced by simulated and recorded ground motions may be different, especially in the short period range.

Using two case study structures, nonlinear interstory drift ratio and peak floor acceleration distributions over building height was studied; statistics are obtained and compared for both recorded and simulated time histories. These structures are steel moment frames designed for high seismic risk, a 20-storey high-rise and a 6-storey low-rise buildings, similar to many steel moment frames structures in Los Angeles. Results of this analysis show that simulation matches well the inelastic demands produced by recorded ground motions, at least for the cases made here.

Hypothesis tests are carried out with the aim of assessing quantitatively how significant the estimated biases can be. Tests have shown a statistical significance of the bias of simulated record in terms of maximum interstory drift ratio and peak floor acceleration only in the elastic case for

short period structures.

Finally, it is worth to remark that, while the study is mostly addressed to the engineering community, it may also provide insight for the simulations of earthquake records for engineering application.

This chapter has been published as journal paper:

Rezaeian, S., Zhong, P., Hartzell, S., and Zareian, F., (2015) Validation of simulated earthquake ground motions based on evolution of intensity and frequency content. Bulletin of the Seismological Society of America, 105(6)

CHAPTER 3: VALIDATION OF SIMULATED GROUND MOTIONS BASED ON EVOLUTION OF INTENSITY AND FREQUENCY CONTENT

Given the results of the previous validation in structures response, it is required to take a step back and look into the fundamental differences between waveforms from simulations and recordings of historic events. Studying waveforms, in contrast with scrutinizing SDOF and MDOF responses, would provide us with the opportunity to understand the "true" differences between ground motion simulations and recordings and not the differences between the "effects" of such motions on structural systems. This paper provides the means to address the cause of differences between response of SDOF (and MDOF) systems to simulated and recorded motions of historic events. A few other studies have considered goodness-of-fit (GOF) measures that are based on characteristics of the waveform (e.g., Kristekova et al., 2006; Olsen and Mayhew, 2010). These GOFs are usually based on commonly used intensity measures (e.g., peak ground response or Fourier amplitudes) and shaking duration of motion. A new ground motion simulation validation methodology is introduced in which three validation metrics are examined that characterize the evolution of intensity (and by extension duration) and frequency content over time. Each metric is a function of time. These time varying properties of earthquake ground motions are important in engineering applications because they influence linear and nonlinear structural responses.

In the following, the three validation metrics characterizing the goodness of fit of simulated motions to recorded motions are introduced. The error between simulated and recorded motions is quantified using a single number that represents the average error over the entire duration of

motion. A few key parameters that control the intensity and shape of each metric (each metric is a function of time) are then suggested for simplification of the proposed methodology and comparison to other validation approaches. The validation methodology is then outlined using an example simulation from the 1994 Northridge earthquake. Finally, an example application of the proposed validation methodology is presented to examine the relative closeness of four different simulation methods to observations from the Northridge earthquake. The results of this study can be used in two ways. First, to provide quantifiable metrics through which ground motion validation can be accomplished for historic events. Second, validation against historic events demonstrates the advantages and shortcoming of simulation models and provides feedback to seismologists.

3.1 GOODNESS-OF-FIT CRITERIA

In order to be useful in engineering applications, simulated motions must first be statistically validated against available strong ground motion data. Selection of an ideal validation metric is difficult because different engineering applications are interested in different characteristics of ground motions. For example, while a match to the elastic response spectrum might be satisfactory for developing simulation-based ground motion prediction equations, it is not an indication of the suitability for use in inelastic response history analysis. Various intensity measures have been used in practice to assess the fit of simulations to recorded motions; these include peak ground responses (i.e., acceleration, PGA; velocity, PGV; and displacement, PGD), Fourier or response spectral amplitudes, measures of total energy (i.e., integrals of the squared acceleration or velocity), or various measures of shaking duration. A synthetic ground motion may accurately represent a certain intensity measure, while misrepresenting other characteristics of the wave-form. In this chapter, instead of intensity measures at single points in time or frequency, we consider the entire evolution of intensity and frequency content of ground motion over time. These two criteria are

important in engineering applications because they control the response of the structure; many intensity measures that are known to have strong effects on structural responses such as total energy, predominant frequency, or duration can be extracted from these criteria. Furthermore, development and implementation of validation methodologies requires collaboration between ground motion modelers and engineering users. The criteria under consideration provide feedback to seismologists on where their simulations deviate from reality even if they match recorded motions in terms of select few intensity measures.

The evolution of intensity and frequency content of a ground motion can be represented by quantifiable statistical characteristics of the time-series that were used by Rezaeian and Der Kiureghian (2008 and 2010). Rezaeian and Der Kiureghian (2008 and 2010) represented earthquake ground motions as stochastic processes that are nonstationary in both time and frequency domains. Nonstationarity in the time domain refers to the variation of intensity with time, while nonstationarity in the frequency domain refers to the variation of frequency content with time. Both of which are fundamental characteristics of earthquake ground motions and are important factors in controlling linear and nonlinear structural responses. The statistical characteristics of a stochastic process that represent the intensity, frequency content, and their time-variation can be numerically estimated for any given time-series; they can be compared for any given pair of recorded and simulated motions. The three statistical characteristics under consideration are the cumulative standard deviation of the acceleration time-series, the cumulative number of zero-level up-crossings, and the cumulative number of negative maxima and positive minima. While the first metric controls the evolving intensity of the process, the second and third together control the frequency content of the process. Each metric is briefly described in the following, for more details refer to Rezaeian and Der Kiureghian (2008 and 2010).

3.1.1 Validation Metric 1: Evolution of Intensity

In the time domain, a ground motion can be characterized by its evolving intensity. The evolution of intensity over time also defines the duration of motion. The intensity of a zero-mean Gaussian stochastic process can be completely characterized by its time-varying standard deviation. Taking advantage of the same concept, for an acceleration time-series $a(t)$, we represent the evolution of intensity in time t by $E_a(t) = \int_0^t a^2(\tau)d\tau$, where $0 \leq t \leq t_n$ and t_n represents the total duration of motion. The Gaussian assumption is not a disadvantage here because nonstationarity in the frequency domain is separable from the nonstationarity in the time domain (see Rezaeian and Der Kiureghian, 2008) and is accounted for later in metrics 2 and 3. Figure 3.1a shows the evolution of intensity, i.e., *validation metric 1*, for a target recorded motion (component 090 of the 1994 Northridge earthquake recorded at the LA-116th Street station) and the same quantity for a simulated motion (according to Rezaeian and Der Kiureghian, 2010).

This metric, which has previously been used in literature for different purposes (e.g., Yeh and Wen, 1990), has the advantage of being a relatively smooth function (as opposed to acceleration time-series, Fourier amplitude spectra, response spectra, etc.), making it suitable for easy and accurate comparison between two or more ground motion time-series without the need for any artificial smoothing. Preliminary studies of many recorded motions show that the amplitude and shape of metric 1 depends on the type of ground motion. For example, near-fault ground motions in general show a shorter "rise-time" (5 to 20 s range in Figure 3.1a) than far field motions. Ground motions recorded at subduction zones such as the 2011 Tohoku earthquake show a much larger total energy (relevant to the amplitude at around 40 s in Figure 3.1a) compared to ground motions recorded in shallow crustal earthquakes. Furthermore, the shape of the example metric 1 in Figure 3.1a is typical of earthquake ground motions; starts at zero, slowly builds up as

low intensity but high frequency P-waves arrive, quickly rises in a short duration of time as the high intensity S-waves arrive during the strong shaking phase, and finally levels out to a constant value that is proportional to the total energy of the ground motion.

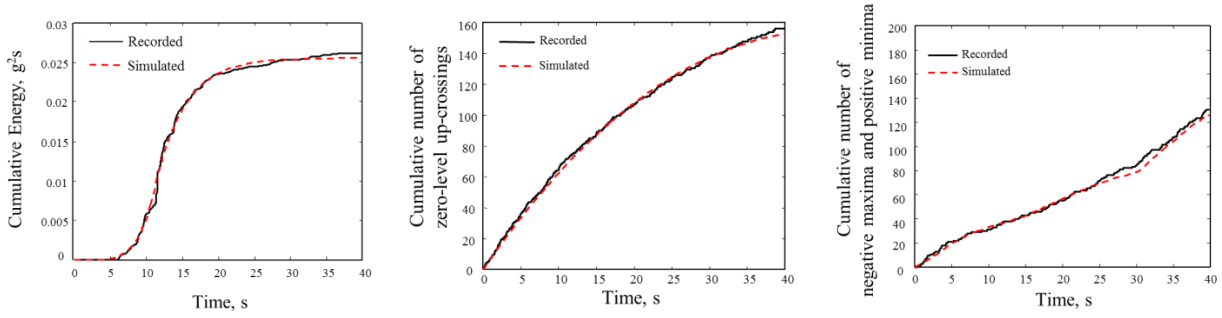

(a) (b) (c)

Figure 3. 1. Validation metrics for an example simulated and recorded earthquake ground motion

ry functions of time and frequency: a constant function, a sine function, and a white-noise process. Figures 3.2b shows Metric 1 for these signals. As seen in Figure 3.2b, the white noise and constant function have similar trends due similarity between a constant function and square of a white noise--the trend of the single sine wave is different.

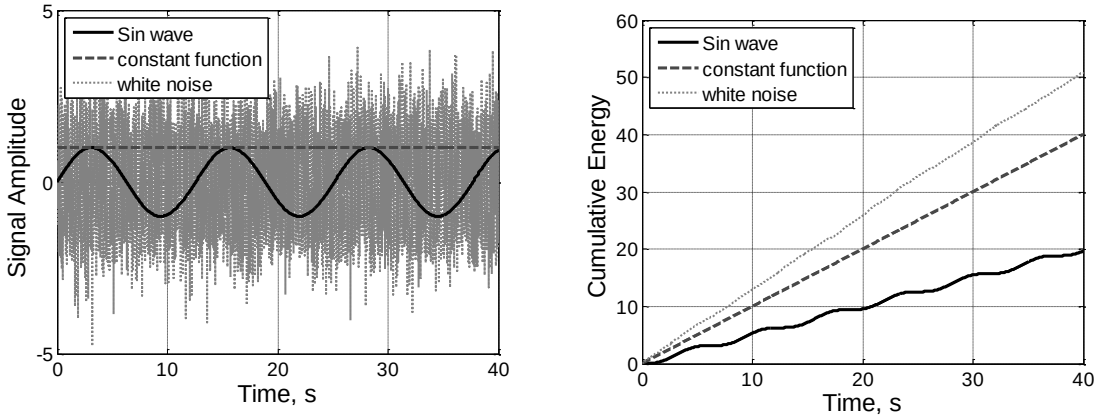

(a) (b)

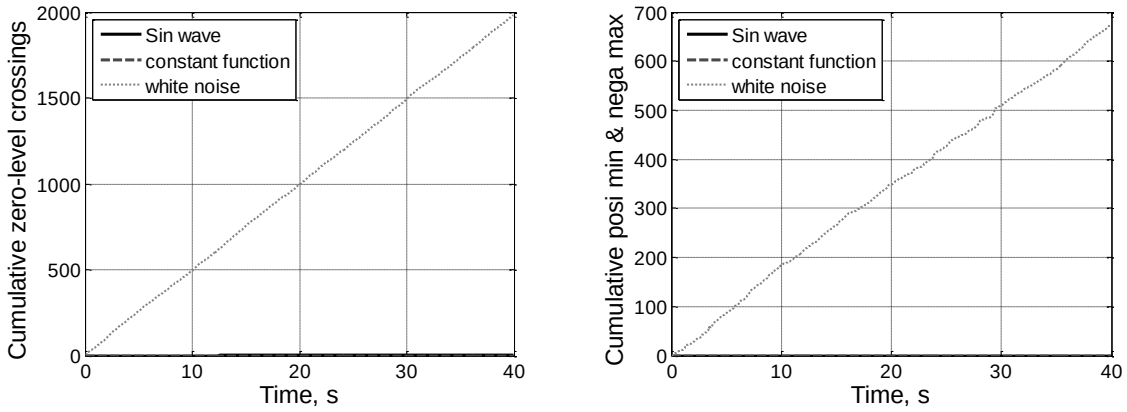

(c) (d)

Figure 3. 2. Validation metrics for stationary signals

3.1.2 Validation Metric 2 and 3: Frequency Content

In the frequency domain, a ground motion process can be characterized by its evolving frequency content. In particular, the frequency content may be characterized in terms of a predominant frequency and a measure of the bandwidth as they change in time. As a surrogate for the predominant frequency of the process, we employ the mean zero-level up-crossing rate, i.e., the mean number of times per unit time that the process crosses the level zero from below. For a zero-mean Gaussian process, analytical solutions are available (Lutes and Sarkani, 2004), but unlike a Gaussian process earthquake ground motions are nonstationary in frequency. For a given time-series, this measure can be estimated numerically by simply counting the zero-crossings in time. Figure 3.1b shows the cumulative number of zero-level up-crossings, i.e., *validation metric 2*, for the same recorded and simulated motions as in Figure 3.1a. In this plot, the rate of up-crossings (i.e., the slope of the curve) decays with time, indicating that the predominant frequency of the ground acceleration decreases with time. Examining many recorded ground motions reveals that this decay is linear in time, suggesting a linear change in the predominant frequency of recorded ground motions. For earthquake ground motions, validation Metric 2 typically follows a

parabolic function. Metric 2 is shown in Figures 3.2c for non-earthquake signals. In Figure 3.2c, because of a large amount of high frequency in white noise, signal passing zero happens all the time, and sin wave signal has few zero-crossing, whereas constant function doesn't have, hence, we can see white noise signal has dominant trend.

To characterize the time-varying bandwidth of the process, we use the mean rate of negative maxima and positive minima as a surrogate. In a zero-mean narrowband process, almost all maxima are positive and almost all minima are negative (e.g., a harmonic excitation). With increasing bandwidth, the rate of occurrence of negative maxima and positive minima increases. Thus, by determining the rate of negative maxima and positive minima, a time-varying measure of bandwidth can be developed. Similar to metric 2, an analytical expression of this rate can be derived for a zero-mean Gaussian process in terms of the well-known distribution of local peaks (Lutes and Sarkani, 2004). For a nonstationary earthquake time-series, this measure can be numerically calculated by simply counting the negative maxima and positive minima in time. Figure 3.1c shows an example of the cumulative count of negative maxima and positive minima, i.e., *validation metric 3*, for the recorded and simulated motions of Figure 3.1a.

Observe that the bandwidth of the motion as measured in terms of the rate of negative maxima and positive minima (slope of the curve), is higher during the initial and final segments of the motion (initial 8 s and final 10 s in Figure 3.1c) relative to the middle segment (between 8 s to 30 s in Figure 3.1c). Examining many recorded motions show that bandwidth remains more or less constant during the strong shaking phase of the excitation (the middle segment). This phenomenon, as suggested by Rezaeian and Der Kiureghian (2008), may be attributed to the arrival and mixing of seismic waves (P-waves, S-waves, and surface-waves). Metric 3 is shown in Figures 3.2d for non-earthquake signals.

3.1.3 Quantification of Error

The three proposed validation metrics are plotted as shown in Figures 3.1-3.2 for any given simulation and by examining their shapes one can indicate if the evolution of intensity and frequency content in the simulation is close to reality. Unlike most other validation techniques, these metrics are not limited to ground motion intensities at single points in time or in frequency. Evolution of intensity and frequency are important to structures especially if nonlinear analyses are undertaken or if intensity at multiple points in time and/or frequency is of interest; as it is the case in more realistic analysis techniques. As previously mentioned, a significant advantage of the proposed metrics is their smoothness and ease of visual compression between recorded and simulated motions. For validation of a few simulations or for the benefit of model developers, the visual comparison approach is recommended. However, for mass validation of many simulation methodologies for many earthquakes, a quantifiable error measure is convenient.

A two component error vector, denoted as $E_{ij}(\epsilon_{ij}, \upsilon_{ij})$ where $i = 1, 2, 3$ and i represents the number associate with each metric, is defined here to summaries the difference between the j^{th} simulated and a recorded motion. ϵ_{ij} is quantified as the normalized absolute area between validation metric i for the j^{th} simulated and recorded ground motion–see Eq. 1. υ_{ij} is quantified as shown in Eq. 2, which is the ratio of the algebraic summation of areas between i^{th} validation metric for the j^{th} simulated and recorded ground motion and summation of same absolute value of same areas. Within these equations, $m_{ij,rec}(t)$ and $m_{ij,siml}(t)$ respectively represent validation metric i for the j^{th} recorded and simulated ground motions.

$$\epsilon_{ij} = \frac{\int_0^{t_n} |m_{ij,rec}(t) - m_{ij,siml}(t)| dt}{\int_0^{t_n} m_{ij,rec}(t) dt} \qquad i = 1,2,3 \tag{3.1}$$

$$\upsilon_{ij} = \frac{\int_0^{t_n} \left(m_{ij,rec}(t) - m_{ij,siml}(t)\right) dt}{\int_0^{t_n} |m_{ij,rec}(t) - m_{ij,siml}(t)| dt} \qquad i = 1,2,3 \tag{3.2}$$

In essence, the proposed error vector is versatile tool of quantifying the difference of a metric between a recorded and corresponding simulated ground motion. Description of few principle cases can help further understanding of the proposed error vector (see Figure 3.3): 1) $E_{ij}(0, a) \wedge a \in \mathbb{R}$ shows a case in which the j^{th} simulated and recorded ground motion have no difference in the i^{th} metric, 2) $E_{ij}(b, \pm 1) \wedge b \in \mathbb{R}$ corresponds to a case that i^{th} metric follows the same trend in the j^{th} ground motion recording and simulation with a shift in between, ultimately, 3) $E_{ij}(c, 0) \wedge c \in \mathbb{R}$ represents a case at which the recording and simulation have different trends with no shift in the considered metric.

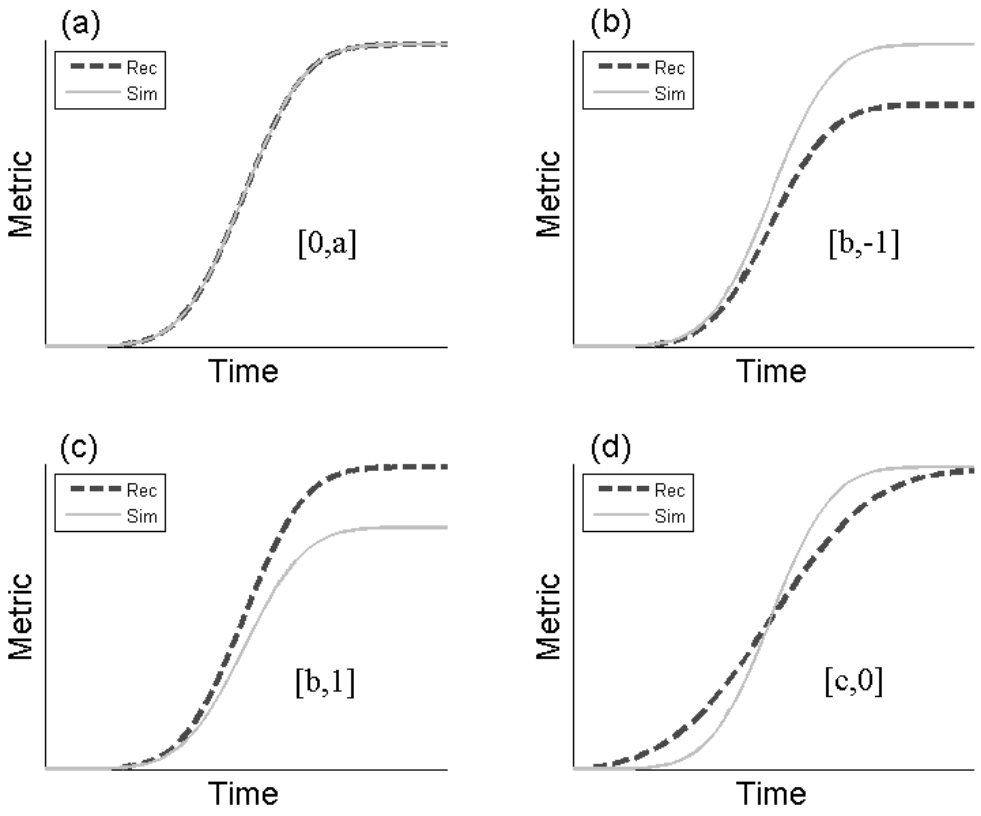

Figure 3. 3. Principle cases of the proposed error vector: a) simulated and recorded ground motion have no difference in a metric, b and c) similar shapes between the metrics but with a shift where the amplitude of the metric for the simulated motion always overestimates or always underestimates that of the recorded motion, and d) recording and simulation have different shapes with no shift.

3.1.4 Key Parameters

In addition to the three validation metrics introduced in the previous section, we look at a few key parameters that can be extracted from the three metrics and control their main shape. Arias intensity, I_a, duration of motion, D_{5-95}, and time at the middle of strong shaking, t_{mid} can be extracted from validation metric 1 and can be used to represent the evolution of intensity in time. Arias intensity is estimated by the value of metric 1 at t_n, I_a, and is representative of the total energy. Duration, D_{5-95}, is measured as the time between instances when 5% and 95% levels of I_a are reached. t_{mid}, as suggested in Rezaeian and Der Kiureghian, is estimated as the time when

45% of I_a is reached.

Another key parameter that we investigate in this paper is the ratio of I_a/D_{5-95} (first proposed in Dashti et al. 2009) as this parameter controls the rate of energy accumulation and has significant impact on many structural and geotechnical responses.

Mid-Frequency, ω_{mid}, and rate of change of frequency, ω', are parameters extracted from metric 2 and control the predominant frequency of the motion. Predominant frequency can be estimated from the slope of metric 2. We fit a parabola to this metric, and then differentiate it to obtain the predominant frequency as a linear function of time. The line is represented by two parameters: ω_{mid}, which is calculated at t_{mid}, and ω', which is the slope of the line.

In summary, we have six key parameters that can be used for simplification as proxies to evaluate the fit of validation metrics. These simple key parameters will be discussed in the following sections in addition to the three time-dependent validation metrics. The first two, I_a and D_{5-95}, can be used for comparisons to other validation studies that consider Arias intensity and duration of motion.

3.2 PROPOSED VALIDATION METHODOLOGY

Given a pair of simulated and recorded ground motion time-series, one can generate the proposed validation metrics and examine the fit by visual inspection as well as calculating the errors presented in Equations 3.1 and 3.2. Furthermore, the key parameters proposed in the previous section can be extracted from validation metrics 1 and 2 and compared for the simulated and recorded ground motion. However, because we are working in the time domain and the validation metrics depend on the discretization of signals, first the simulated and recorded ground motion time-series must be compatible in their discretization steps and initial excitation times. In

this section, we use an example simulation from Graves and Pitarka (2010) to demonstrate the time sampling, indication of a starting point in time, and calculation of validation metrics. Methodology introduction can be found in chapter 1.

3.2.1 Time Sampling

It is common for the time discretization of a simulation to be different from the corresponding recorded motion. In such cases, the finer discretization should be adjusted to that of the coarser motion. In signal processing, down-sampling is the process of reducing the sampling rate of a signal by preserving every n^{th} data point and deleting the points in between. n is the down-sampling factor, which is usually an integer or a rational fraction greater than unity. For example, if a signal at 100 Hz is down-sampled to 50 Hz, the time step is increased from 0.005 s to 0.01 s and the signal is down-sampled by a factor of $n = 2$. However, one should be careful to maintain the Shannon-Nyquist sampling theorem criterion so that the resulting signal does not have aliasing. According to the Shannon-Nyquist theorem, when sampling a signal and increasing the time step, the sampling frequency must be greater than twice the bandwidth of the input signal in order to be able to reconstruct the original perfectly from the sampled version. If this theorem is not satisfied, then aliasing (i.e., overlap of frequencies) occurs and causes different signals to become indistinguishable. As a result, some information on amplitudes at certain frequencies may be lost, which changes the characteristics of the ground motion signal. To ensure that the down-sampling of a simulated ground motion is done properly, we use a low-pass filter as an anti-aliasing filter to reduce the bandwidth of the signal before it is down-sampled. This process is called decimation and the low pass filter is used to eliminate useless frequency which may cause aliasing. Figure 4a shows an example of a simulated and a recorded ground motion. For more information, see Zhong (2010).

3.2.2 Synchronization of Recorded and Simulated Motions for Validation

Recorded and simulated ground motions, at a single recording station, usually have different total duration and starting time (see Figure 3.4 as an example). For recorded motions, start of recording is trigged by certain acceleration amplitude, usually caused by P-wave arrival; hence, the recorded motion may miss some pre-event buffer. There is no easy way to tell exactly when natural recordings start with respect to the event origin time. In contrast, simulated motions do not miss the pre-event buffer. The simulated motions all start at 0 s, which is the event origin time. One can observe the time-shift in the original recorded and simulated traces of Figure 3.4a. The challenging question is how to synchronize (i.e., how far shift the motions horizontally) to assure that the strong shaking parts of the simulated and recorded motions are compatible in time.

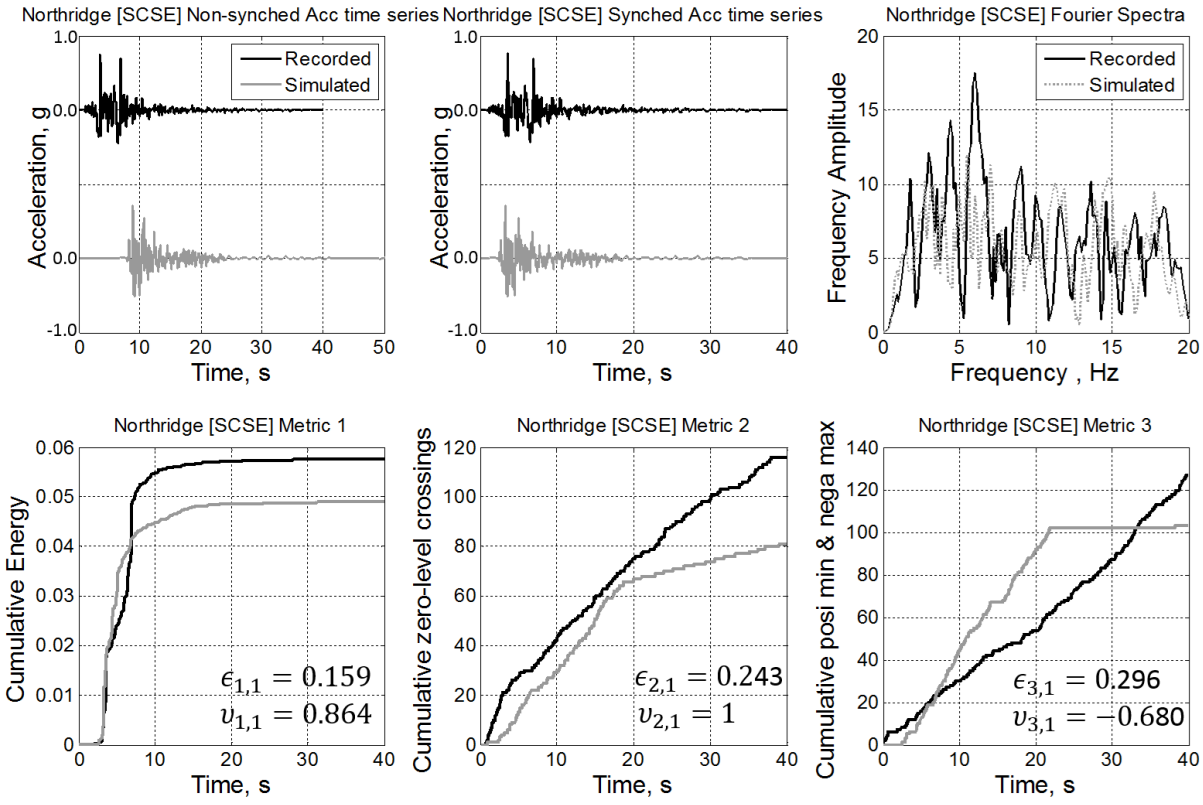

Figure 3. 4. Illustration of proposed Validation metrics

Simulated motions typically (always in the case of five simulation sets we have looked at) have a longer duration than the corresponding recorded motions. We truncate the simulated motions to have the same length as the recorded motion by selecting the part from the original simulated motion that is most similar to the corresponding recorded motion. We have considered various measures of "similarity". These include: using cross-correlation of acceleration time-series, using cross-correlation of velocity time-series, using a certain percentage of cumulative energy, and using a certain percentage of cumulative absolute velocity (CAV). For more detail on each method see Zhong (2010).

Cross-correlation coefficient of acceleration time-series reflects the similarity of the two signals; however, it lacks comparison of the two signals amplitudes. Our observations show that in many cases, simulated and recorded motions have a high cross-correlation coefficient in the low amplitude parts of the two signals that are usually at the tail end of the original simulated motions. Additionally, the final selected part of the simulated motion should at least have 90% Arias Intensity of the original simulated motion. The procedure using cross-correlation of velocity is similar, except that the acceleration has to be integrated into velocity first. Acceleration time-series is a strong signal with a large amount of high frequency; on the other hand, velocity time-series is a much smoother signal. Our observations show that although using cross-correlation of velocity time-series can provide a decent outcome, the common cross-correlation coefficients are around 0.5, which is not a convincing high enough value to prove similarities between two signals.

Even though simulated ground motions are much longer compared to their corresponding recordings, there is very little energy in the beginning and the end of these signals. Therefore, matching certain amount of energy between simulated and recorded ground motion can be a decent approach.

Cumulative Energy at any given time $0 \leq t \leq t_n$ is defined as$E_a(t) = \int_0^t a^2(\tau)d\tau$, where $a(\tau)$ is is the acceleration of ground motion. Detailed procedure is as follows:

1) Calculate the total cumulative Energy for recorded ground motion (E_{total}), mark down the amount of 5 percentage of total cumulative Energy ($E_{5\%}$) and find the corresponding data point which owns $E_{5\%}$ in recorded motion.
2) Find the data point in simulated ground motion which has the same amount energy as $E_{5\%}$.
3) Shift two signals by making those two data point overlapped, and truncate the simulated ground motion based on the length of recorded ground motion.

None of the proposed methods for synchronizing simulated and recorded motions are not perfect. The optimum method will be adopted based on engineering judgment and number of successful applications (or least number unreasonable synchronizations). Method 1, using cross-correlation in acceleration time series, provides satisfactory results; however, the low cross-correlation coefficient between two signals makes it hard to declare significant similarities between two signals. This is mainly due to existence of high frequency signals in acceleration time series. In method 2, even though using cross-correlation in velocity time series is able to provide a higher cross-correlation coefficient, the results are not as good as they should be once one looks back into the synchronized acceleration time series. Method 3, comparing certain percentage of cumulative energy at the beginning of the simulated motion, may result in acceptable synchronization; however, the choice of matching percentage of energy is arbitrary. Matching a 1% cumulative energy is too small to ignore pre-event shaking's energy, and 50% is too large. In method 4, even though CAV is an energy equivalent term, the results are not as good as the one in method 3.

In conclusion, Method 1 and Method 3 are acceptable methods for synchronizing a simulated

and recorded motion. Method 3 is considered as the optimum method. One example of using this method is shown in Figure 3.4. Not only simulated motions are truncated into same length as recorded motions, but also they are shifted into synchronized status.

3.3 EXAMPLE APPLICATION FOR NORTHRIDGE EARTHQUAKE

As an example of assessing the fit of a simulation model to a historic earthquake with many records, we calculated the error vector proposed earlier for each validation metric using 121 recorded motions from the 1994 Northridge earthquake and their simulations by Graves and Pitarka (2010).

3. 3.1 Summary of Errors

Figure 3.5 shows the average and shape errors for metric 1, assessing the evolution of intensity, plotted against distance and V_{S30}. The vertical axis shows $\epsilon_{i,j}$ represented by circles above the horizontal line, and $\nu_{i,j}$ represented by triangles below the horizontal line. Given that a large number of triangles are on ±1, we can argue that the overall shape of metric 1 (i.e., accumulation rate of intensity) is similar for simulated and recorded motions. A large number of $\nu_{1,j}$ fall on −1, indicating that simulated motions overestimate the total input energy into a structure compared to recorded motions. We can also observe a slight increase in $\epsilon_{1,j}$ as the epicentral distance increases, but there is no trend in the errors with V_{S30}.

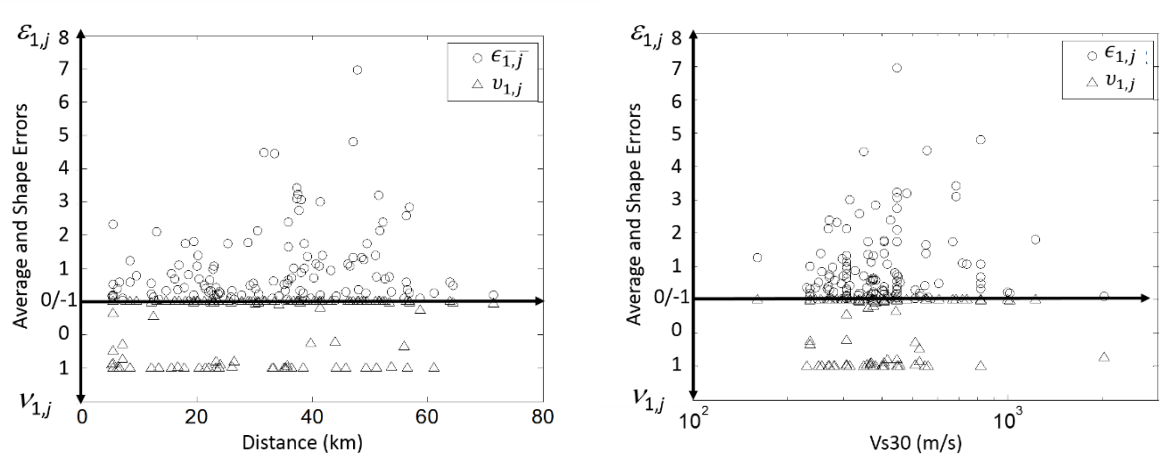

Figure 3. 5. Metric 1 error plotted against distance and V_{S30} for 121 Northridge simulations by Graves and Pitarka (2010).

Figure 3.6 shows the average and shape errors for metric 2, assessing the evolution of frequency, plotted against distance and V_{S30}. Given that the majority of triangles, $\nu_{2,j}$, are on +1, we can argue that the simulated motions' cumulative zero-level up-crossings, the slope of which represents predominant frequency, have similar shapes to recorded motions but underestimate their amplitudes. As illustrated in this figure, there is no obvious dependence between error and epicentral distance or V_{S30}. Further investigations of the evolution of metric 2 show that simulated and recorded ground motions follow a close trend up to the end of the strong shaking phase (see the lower middle plot in Figure 3.4 as a typical case).

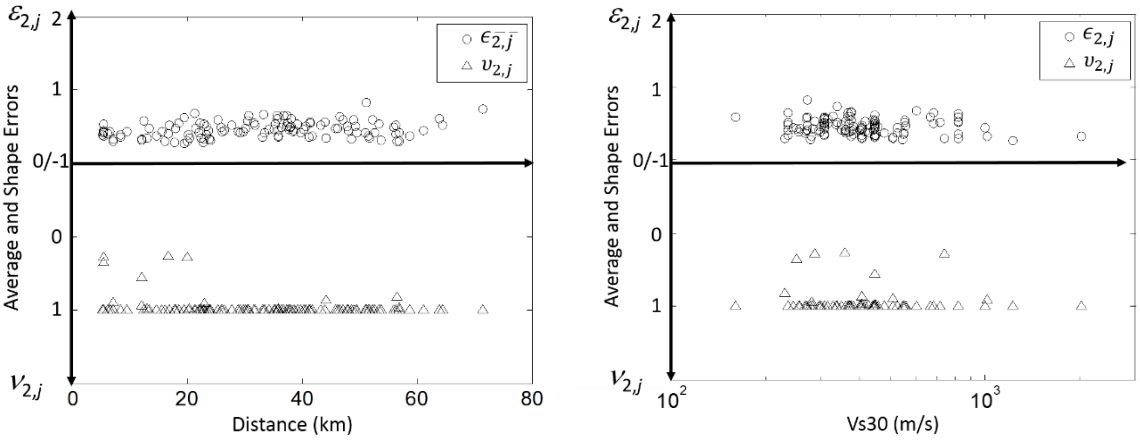

Figure 3. 6. Metric 2 error plotted against distance and V_{S30} for 121 Northridge simulations by Graves and Pitarka (2010).

Finally, Figure 3.7 shows the average and shape errors for metric 3, assessing the evolution of bandwidth, plotted against distance and V_{S30}. The variation of errors shows that the differences between simulated and recorded ground motions in terms of bandwidth are significant. In general, simulated ground motions have a larger bandwidth during the strong shaking phase (see lower right part of Figure 3.4). This trend is uniform across epicentral distances and different soil types.

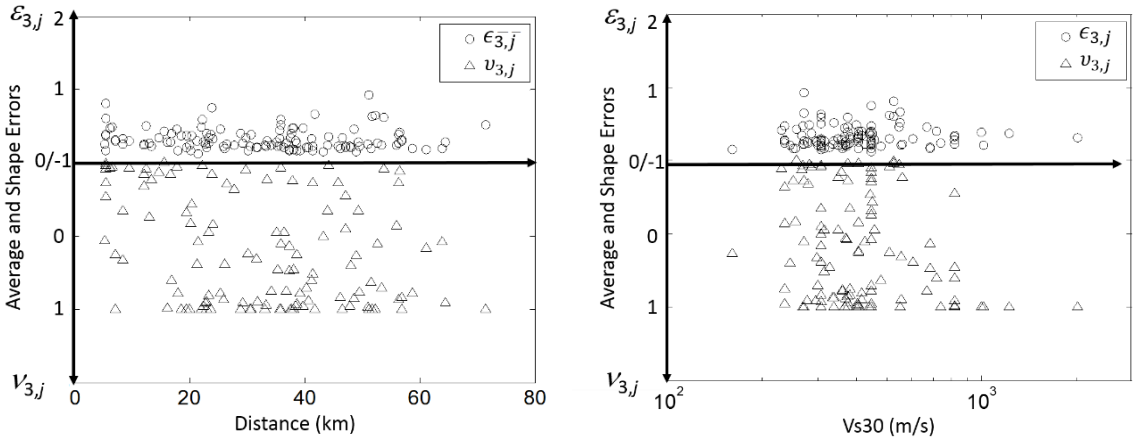

Figure 3. 7. Metric 3 error plotted against distance and V_{S30} for 121 Northridge simulations by Graves and Pitarka (2010).

3. 3.2 Summary of Key Parameters

The six scalar parameters that were introduced previously and control the shapes of validation metrics 1 and 2 are calculated and plotted for the collection of recorded and simulated motions for the Northridge earthquake. Their box plots are shown in Figure 3.8. We can see that in general, simulations overestimate the Arias intensity. Variability in the significant duration of simulated motions is much lower than the variability in recorded motions. The simulated values for the parameter I_a/D_{5-95} , representing the rate of input intensity, and t_{mid}, representing the middle of strong shaking, are overall in good agreement with recordings. And finally, we can see that the simulations overestimate the frequency at the middle of strong shaking, but the rate of frequency decay is faster (more negative numbers for ω'). In addition to estimating the median value for each

parameter, these box plots give the model developers an idea of the spread of each parameter and whether the variability is well represented in the models compared to recorded ground motions. Finally, an interesting observation is shown in Figure 3.9, where the ratio of significant duration for simulated motions to recorded motions is plotted against distance. We can see that in this particular simulation method, simulated and natural recordings have a mismatch in strong shaking duration in the near-field and far-field regions. In the near-field region, simulated motions have longer significant duration compared to natural recordings. This trend is reversed in the far-field regions; other distance dependent trends have been observed for this method, e.g., Seyhan et al. (2013).

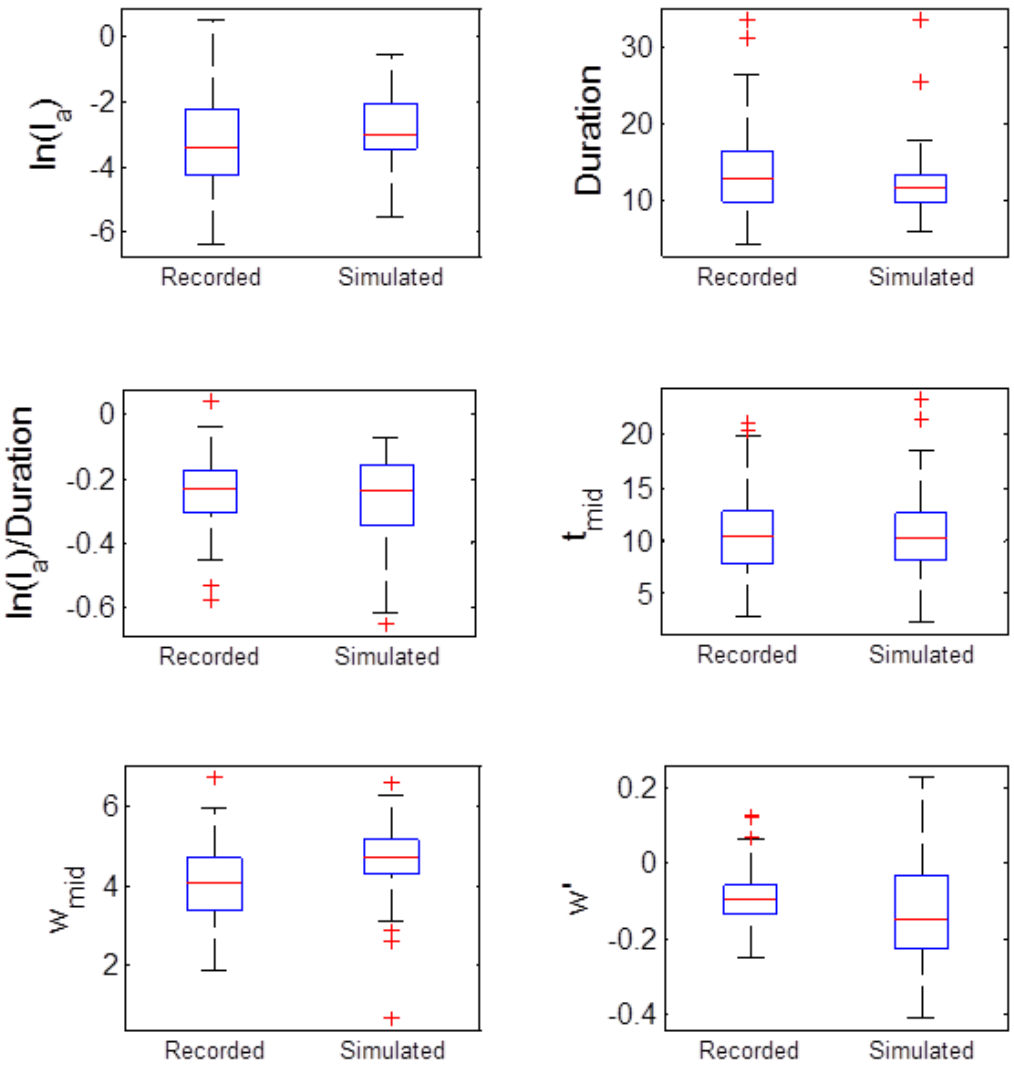

Figure 3. 8. Box plots of key parameters for 121 records from the 1994 Northridge earthquake.

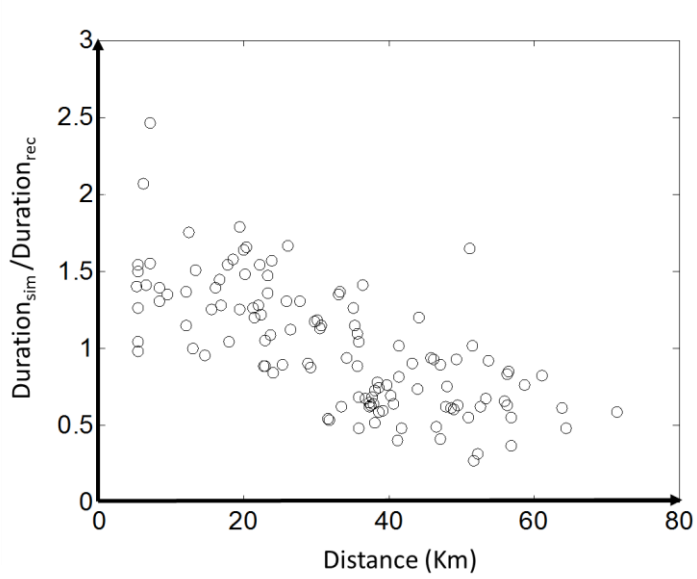

Figure 3. 9. Ratio of significant duration for simulation versus recorded motions plotted against distance.

3. 4 CONCLUSIONS

We propose a new validation methodology to assess the validity of simulated ground motions using three time-dependent validation metrics that characterize the evolution of intensity and frequency content of waveforms. Simulated ground motions are validated against records of historical events. These time-varying properties of earthquake ground motions are important in engineering applications because they can be expected to influence linear and nonlinear responses of structural and geotechnical systems. Because these metrics are smooth functions of time, they allow for visual comparison between the characteristics of recorded and simulated motions, and can provide easily interpretable feedback to the model developers. The difference in each metric between simulated and recorded motions is quantified using an error vector that represents the average error over the entire duration of motion. We also introduce a few key parameters that are extracted from the first two validation metrics. These parameters represent the total intensity, significant duration of motion, time at the middle of strong shaking phase, rate of input energy, frequency at the time of strong shaking, and rate of change of frequency in time. The three

validation metrics and six key parameters were calculated for example simulated and recorded pairs of motions from the 1994 Northridge earthquake. The proposed methodology can benefit both engineers and seismologists.

CHAPTER 4: APPLICABILITY OF SIMULATED GROUND MOTION WAVEFORMS FOR BUILDING-CODE APPLICATIONS

4.1 INTRODUCTION

In recent years, simulated ground motions have been gaining attention, specifically in terms of engineering applications. Simulated ground motions are now considered to be viable options along with recorded and spectrally matched ground motions (created by manipulating the frequency content and intensity of recorded ground motions to match a specific response spectrum) for building seismic performance assessment; they are also used in design for target performance. However, there are serious doubts regarding the accuracy of simulated ground motions in terms of their representation of recorded motions. This leads to hesitation among engineers when it comes to utilizing simulated ground motions in engineering applications. Validating simulated ground motions for such purposes and updating the simulated methodology is the topic of this paper.

Real records from past earthquake events have traditionally been recognized as the best representation of seismic input for dynamic analyses in geotechnical and structural engineering; see (Bommer, JJ, et. al., 2004) for a review. Traditionally, ground motion records from previous earthquake events have been selected and modified (Ground Motion Selection and Modification, GMSM) to meet certain requirements, in order to represent ground motions that may happen in future earthquakes. These requirements include target spectrum, magnitude, distance, mechanism and site characteristics. Although the database of recorded motions has increased by thousands in recent years, there is a shortage of records for large magnitude earthquakes at short distances, as well as records that sample specific combinations for source, path and site characteristics. These shortcoming have led researchers to develop ground motion

simulation techniques (e.g., Graves and Pitarka, 2010; Zeng et al, 1994; Mai et al., 2010). Given the advances in the understanding of fault rupture processes, wave propagation phenomena, and site response characterization, simulated ground motions appear to be one of the viable and attractive alternatives to the very limited amount of recorded ground motions. With advancing computational ability and advanced computer efficiency, implementing simulated ground motions is an alternative to provide detailed and accurate predictions of earthquake effects on structures.

In spite of the fact that design codes such as ASCE/SEI 7-10 (ASCE, 2010) allow the use of simulated ground motions for engineering practice, "where the required number of appropriate recorded ground motion records are not available, appropriate simulated ground motion shall be used to make up the total number required.", such motions still fall out of favor with engineers For instance, although the database of recorded motions has increased by thousands during recent earthquakes, there is a shortage of records for large magnitude earthquakes at short distances, as well as records that sample specific combinations for source, path and site characteristics. In this case, simulated ground motions can be substituted and implemented in the selection database to achieve the required number. In essence, engineers look for stability in the ground motion simulation process and similarities between the response of engineered structures to similar simulated and recorded ground motions. In order to include simulated ground motions in engineering applications in a practical manner, simulated ground motions must be validated and compared with recorded ground motions to prove their equivalence in engineering applications. Early work in ground motion simulation validation can be seen in the following references. Zareian & Jones., 2010; Star et al., 2011; Galasso et al., 2012; Galasso et al., 2013; Burks & Baker., 2014 and Rezaeian et al., 2015.

In this part of the research, a ground motion simulation validation technique is proposed to demonstrate how simulated and recorded ground motions will result in similar building response parameters used for structural design. Ground motion simulation validation verifies how well the simulators are capable of generating the synthetic motions, and checks if these artificial motions can produce accurate building response compared with recorded ground motions. In other words, this technique looks into the similarities between building response obtained from suites of simulated and recorded ground motions conditioned that these suits of ground motions are selected using the code based ground motion selection and scaling （ASEC/SEI 7-10）. A structural system consisting of a steel moment resisting frame is used to demonstrate this approach. The engineering demand parameter of interest is the maximum interstory drift ratio. The difference between the demands from simulated and recorded motions will be compared using Student's t-test for respective engineering demand parameter distributions. Preliminary results show that the structural behavior resulting from recorded ground motions and simulated ground motions are statistically significantly different in short structures. The sets of simulated ground motions clearly overestimate the response compared to the recorded motions. The difference stems from the fact that ground motion simulation models are more likely to generate pulse-like ground motions, which tend to create larger displacement of building response. The higher number of pulse-like motions in the population of simulated motions results in a larger number of pulse-like motions in the selected sets, and therefore, imposes higher seismic demands on structures compared to sets derived from natural recordings. Whereas the results in high structures are comparable, because the GMSM selection range is relatively longer for high structures with large natural periods. The long selection range helps eliminating the selection of pulse-like ground motions. In order to make simulated motions practical for engineering application, an updated GMSM technique is proposed

to elongate the selecting range to avoid choosing abnormal pulse-like ground motions.

4.2 DESCPRTION OF GROUND MOTIONS AND MODELS

4.2.1 Description of Synthetic Ground Motions Datasets

Broadband Platform simulations (BBP, Version 13.5) of five events are used: 1994 Northridge, 1989 Loma Prieta, 1987 Whittier, 1992 Landers, and 1986 North Palm Springs, which give a total of 380 ground motions. In BBP, the modules including rupture generation, low- and high-frequency seismogram synthesis, non-linear site effects, and visualization are developed to generate different types of synthetic motions based on user requirements. Three different methods of ground motion simulations: GP (Graves and Pitarka, 2010), CSM method (Zeng et al., 1994) and SDSU method (Mai et al., 2010) are validated in this research.

The GP simulation method is a hybrid broadband simulation method. It combines a physics-based deterministic approach at a low frequency ($f \leq 1$ Hz; i.e., $T \geq 1$s) with a semistochastic approach at a high frequency ($f > 1$ Hz; i.e., $T < 1$s). The low and high frequency waveforms are computed separately and then combined to produce a single time history through a matching filter. At frequencies below 1 Hz, the methodology contains a theoretically rigorous representation of fault rupture and wave propagation effects and attempts to reproduce recorded ground motion waveforms and amplitudes. At frequencies above 1 Hz, waveforms are simulated using a stochastic representation of source radiation combined with a simplified theoretical representation of wave propagation and scattering effects. The use of different simulation approaches for the different frequency bands results from the seismological observation that source radiation and wave propagation effects tend to become stochastic at frequencies of about 1 Hz and higher, primarily reflecting the relative lack of knowledge about these phenomena's details at higher frequencies.

By taking advantage of the convolution with synthetic Green's functions, CSM simulation method (composite source model) is able to describe the kinematic earthquake source time function and simulate strong ground motions. All input simulated parameters, such as fault mechanism, dimension and slip, R_{max} and so on, have some kinship with physical basis. CSM method hypothesize the source slip function can be simulated by randomly distributed subevents on fault. And the power-law distribution are used to define the relationship between number of subevents and their radius. Each subevent radiates a displacement pulse with the shape of a Brune's pulse in the far field, determined by a constant rupture velocity propagating from the hypocenter.

The SDSU simulation method generate broadband (0-10 Hz) synthetic ground-motions by combining low-frequency 3D finite-difference synthetics with a high-frequency scattered wave-field. Deterministic techniques for waveform computations at low frequencies (up to about 1 Hz) in 3D Earth model are well developed, accounting for the complicated physical part in the rupture process. Meanwhile, methods for high-frequency (1–10 Hz) ground-motion simulations are based on empirical-stochastic approaches and do not consider the physics of seismic scattering due to small-scale heterogeneous earth structure or include 3D wave-propagation effects. The multiple shear-to-shear backscattering theory is used to obtain high-frequency seismogram by applying a rupture-specific convolution operator to the scattering Green's function. These signals are then reconciled with the low frequency deterministic waveforms to optimize the fitness of amplitude and phase spectra around the target intersection frequency.

All ground motion simulations are conducted for *Vs30* of 863 m/s. In the simulated database, 50 realizations for each event in each simulation mothed were generated. Because of the effects of varying random seed number, which represents different slip distribution cases, ground motions in each source realization differ from one another. Further details on how this simulation method

is implemented in BBP can be found in Graves and Pitarka., 2015, Anderson., 2015 and Olsen et al., 2015.

4.2.2 Description of Steel Moment Resisting Frame Models

In this study, we used two steel moment resisting frame (SMRF) model that was designed based on ASCE/SEI 7-02 (ASCE, 2005) and ANSI/AISC 341-05 (AISC, 2005). Figure 4.1 schematically illustrates the low-rise 4-story and high-rise 20-story SMRF and theirs member sizes. The considered frame has three bays, each with a width of 20 feet. Each story height is 13 feet with the exception of the first story with a height of 15 feet. The fundamental period of the building is 1.52s and 4.07s respectively in long side. Since the SMRF is identical in two horizontal directions, the periods in both directions are similar. Structural models are prepared for Open System for Earthquake Engineering Simulation structural analysis software (OpenSees) (http://opensees.berkeley.edu/). The columns and beams in the moment frames are modeled with elements that utilize fiber sections with W shapes. The assumed yield stress of steel is 50 ksi with a hardening ratio of 1%. Rayleigh damping of 2.5% is considered in the first and third modes of vibration. Every floor is designed to have a rigid diaphragm. Readers are referred to (NIST, 2010) for further information regarding SMRF modeling. The 4-story SMRF is subjected to sets of ground motions that were selected and scaled from the recorded and simulated ground motion population. The maximum interstory drift ratios of the building responses caused by these two sets of motions have been compared. Further information can be found in (Zareian and Kanvide, 2012).

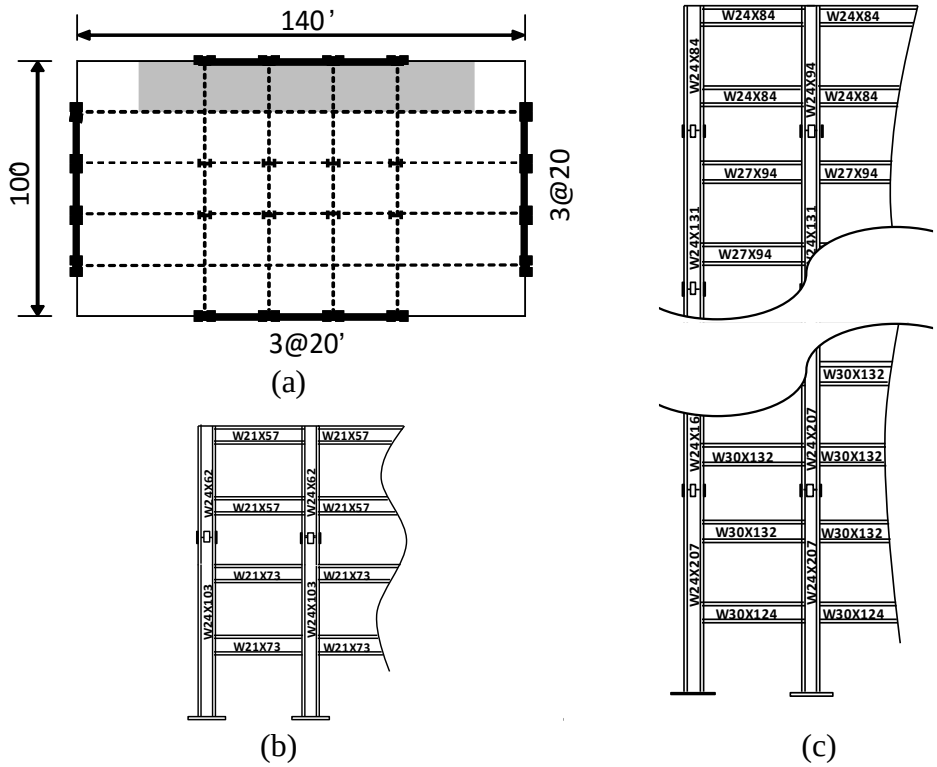

Figure 4. 1. Elevation (a), plan view of 4-story (b) and plan view of 20-story (c) of steel moment frame model

4.3.1 Approach of Ground Motion Selection and Modification Validation Framework

In general, the behavior of building structures caused by simulated and recorded ground motions are compared, in the condition that both sets of ground motions already match the same target spectrum. For validation of simulated ground motions, a set of recorded and simulated ground motions will be independently selected given a code defined target spectrum and a set of rules for ground motion selection and scaling. The design code applied in this research is ASCE/SEI 7-10 (ASCE, 2010). As the aforementioned code states, the ground motions shall be scaled such that the average value of the 5 percent damped response spectra for the suite of motions is not less than the design response spectrum for the site for periods ranging from $0.2T$ to $1.5T$ where T is the fundamental period of the structure in the fundamental mode for the direction of response being analyzed. Then, the maximum interstory drift ratio is compared as the engineering

demand parameter of building response. The difference between demands from simulated and recorded motion sets will be compared using Student's t-test to determine if the difference between the two engineering demand parameter distributions is statistically significant or not .

4.3.1.1 Hypothesis test for comparing building responses

In this research, parametric hypothesis tests are performed to quantitatively assess the statistical significance of the results found in terms of median response of recorded and simulated ground motions. The intention is to asses if the differences in the building response are simply because of stochastic randomness correlated with the limited number of sample sizes or from an intrinsic defect of simulation methodology. The mean maximum interstory drift ratio is the engineering parameter used to validate whether or not simulated ground motions are able to produce the same results as recorded ground motions. The Null hypothesis is defined as follows:

$$mean(MIDR_{rec}) - mean(MIDR_{sim}) = 0 \tag{4.1}$$

Where $MIDR_{rec}$ and $MIDR_{sim}$ are the maximum interstory drift ratios obtained from building response caused by recorded and simulated ground motions respectively. This null hypothesis declares the true difference for those two groups of data is zero, which demonstrate this acceptable difference we obtain by using recorded and simulated ground motions is only due to randomness caused by limited sample size. Meanwhile, this null hypothesis can be rejected if the difference between these two data means exceed the threshold value. 95% significance level are considered, the derived student t-test can be expressed as follows:

$$mean(MIDR_{rec}) - \lambda \sqrt{\frac{\overline{X_{rec}} - \overline{X_{sim}}}{\frac{S_{rec}^2}{n_{rec}} + \frac{S_{sim}^2}{n_{sim}}}} < \text{mean}(MIDR_{sim}) < mean(MIDR_{rec}) + \lambda \sqrt{\frac{\overline{X_{rec}} - \overline{X_{sim}}}{\frac{S_{rec}^2}{n_{rec}} + \frac{S_{sim}^2}{n_{sim}}}} \tag{4.2}$$

When the number of ground motions is 40, λ equals 1.992; whereas, λ is 2.145 for 7 ground

motions. If the mean value falls outside of the abovementioned range, the null hypothesis is rejected, which means the difference between simulated and recorded ground motions is statistically significant and inherent defect exists in the simulation method.

4.4 VALIDATION OF A GROUND MOTION SIMULATION METHOD FOR ENGINEERING APPLICATION

4.4.1 Application of Ground Motions Selection and Modification Method

The ASCE 7-10 (ASCE, 2010) method for ground motion selection and scaling is implemented. In this approach, the target spectrum for the location of a building is obtained using conventional probabilistic seismic hazard analysis (Kramer, 1996). For this study, the target spectrum was found for a site in downtown Los Angeles for one hazard level: Design Based Earthquake (DBE) that is comparable with a 475 year average return period. The aim is to find the ground motions whose response spectrums best match the target spectrum within the $0.2T_1$ and $1.5T_1$ range, where T_1 is the fundamental period of the building.

Two alternatives are considered to investigate if the results of this study are sensitive to the GMSM method and the size of the ground motion sets. The Conditional Mean Spectrum (CMS) (Baker, 2011) is used as the target for GMSM, instead of the Uniform Hazard Spectrum (UHS); 40 sets of ground motions are developed instead of 7 and nonlinear response history analyses is repeated.

To ensure that an acceptable estimate of median building response for each ground motion category, one out of 50 realization in simulated database is randomly selected using code defined ground motion selection and scaling procedures. The procedures for simulated and recorded ground motions including the establishment of the GMSM database to building response observations are similar. In both cases, the GMSM technique is implemented to select and scale

certain number of ground motions, which best match the target spectrum. Then the selected ground motions are applied into the aforementioned structure model and observe the building response. The only difference is the step of choosing the database. In simulated ground motions, because of different slip distribution cases, 50 realizations of 380 ground motions including 5 earthquake events (Northridge, Loma Prieta, Whittier, Landers and North Palm Springs) are generated with each simulation method. Each realization should be treated equally, because each realization (random slip distribution case) is not necessarily better than the others. The new realization event is randomly selected and mixed up to be composed. In this research, the new realization consists of 25th realization of Loma Prieta, 3rd realization of Landers, 15th realization of Northridge, 48th realization of North Palm Spring and 38th realization of Whittier. In recorded ground motions, database are naturally obtained from the PEER NGA database. And each recorded ground motion is consistently one-to-one paired with the previous simulated ground motion in the identical station and same event.

4.4.2 Results of Comparing Building Response Measures for GP Simulation Method in 4-Story Steel Moment Resisting Frame

4.4.2.1 Case of uniform hazard spectrum

The code based validation process explained above has been exercised on the aforementioned 4-story steel moment resisting frame (SMRF) in UHS target spectrums with DBE hazard levels to illustrate how the code based validation process may work. And only GP simulated ground motions are applied and presented for illustration in this session, for the rest of simulated method validation in different structures within two distinct target spectra are summarized and presented in following session.

Once the conventional ASCE 7-10 ground motion selection and scaling method is implemented, even though both recorded and simulated spectrums are good matching with target

spectrum in the selecting range, the general observation is that simulated ground motions overestimate the deformation response of the building structure. The good match between the average spectra for each set of ground motions and the target spectrum is presented. Figure 4.2(a) shows the average spectra of simulated and the one of recorded ground motions scaled to the UHS at DBE hazard level for the 4-story SMRF. The black dash-dot line indicates the target spectrum while the black solid line and red solid line represent the recorded sets and the simulated sets, respectively. Corresponding sets of recorded ground motions are selected among the best of seven motions whose spectra match the target spectrum. For Figure 4.2(a), both spectra of recorded GMs and simulated GMs are good matches with the target spectrum from 0.3s to 2.3s, which is in the GMSM selection range.

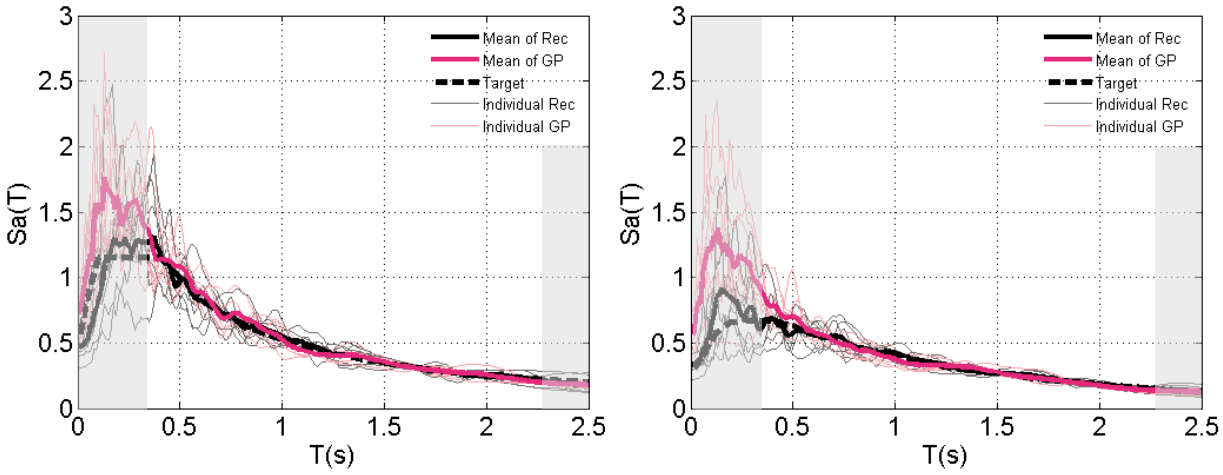

(a) (b)

Figure 4. 2. Average spectra of selected and scaled ground motion sets to DBE level with target spectrum of Uniform Hazard Spectrum (a) and Conditional Mean Spectrum (b), 7 per set.

Figure 4.3(a) shows the difference between the average response of the 4-story SMRF to sets of simulated and recorded ground motions, all of which are selected and scaled to match the UHS target spectrum at DBE hazard level. It is evident from this figure that set of simulated ground motions clearly overestimates the response compared to recorded motions, which exceeds up to

25%. And the simulated set falls out the boundaries of the rejection region derived based on Eq 4.2. This suggests that the difference in response between recorded GMs and simulated GMs is statistically significant at a 5% level. As Figure 4.3(a) shows, overestimations caused by simulated motions occur along the height of SMRF, and floors one to three are statistically significant. Meanwhile, we can see around three out of seven of the building responses caused by simulated motions are the major issue contributing to this significant overestimation. The rest act similar to that of the recorded motions.

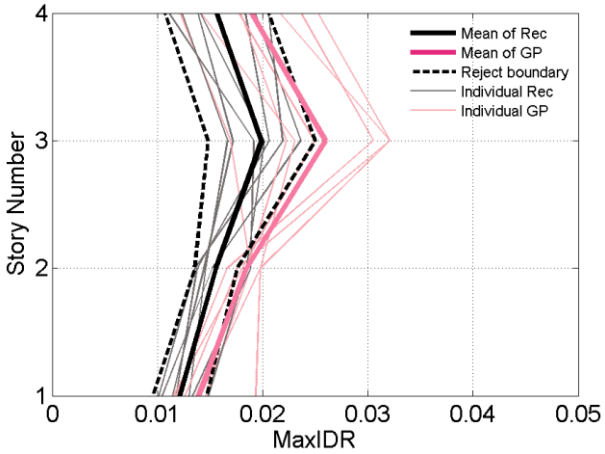

(a)

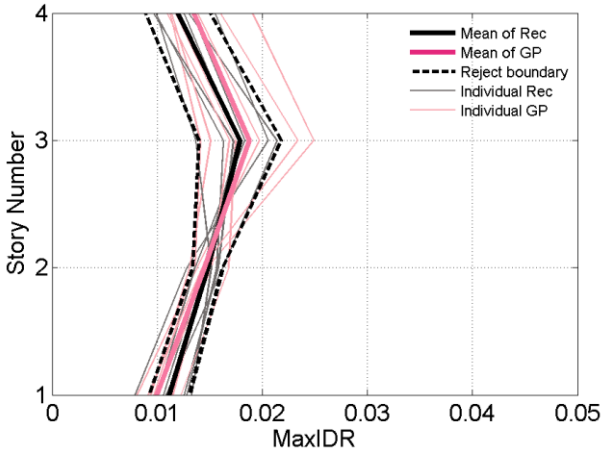

(d)

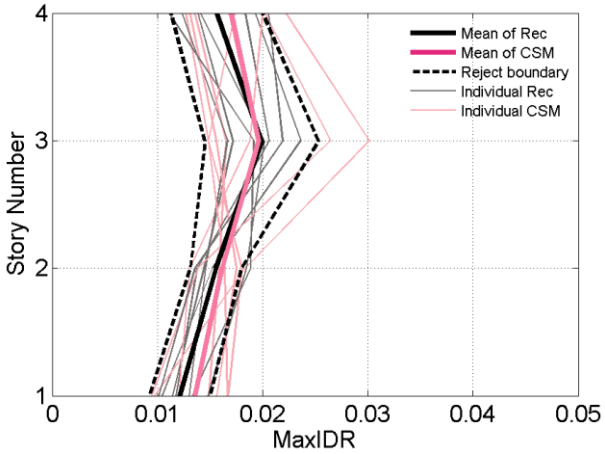

(b)

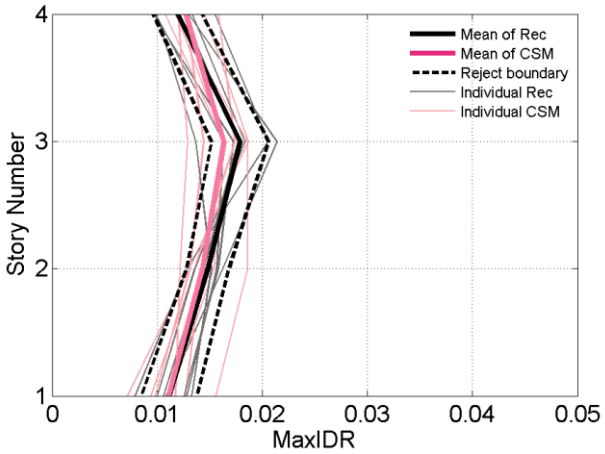

(e)

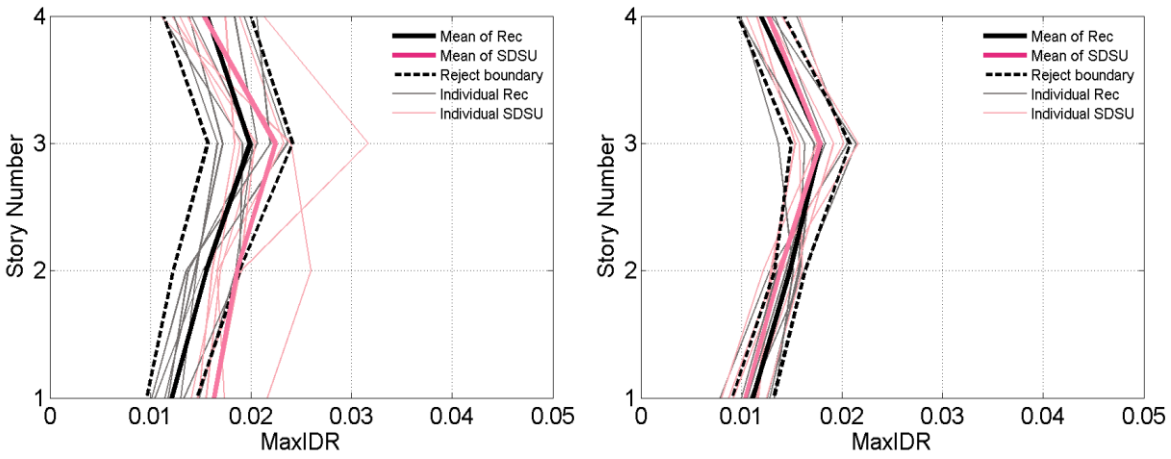

(c) (f)

Figure 4. 3. Average maximum interstory drift ratio of the 4-story SMRF at DBE level with Uniform Hazard Spectrum for GP (a), CSM(b), SDSU(c) simulated GMs and Conditional Mean Spectrum for GP (d), CSM(e), SDSU(f) simulated GMs (7 per set)

The aforementioned differences may have come from the difference between the ground motion waveform characteristics. Figure 4.4(a) shows scatter plots (Baker 2007) of pulse PGV ratio vs Pulse energy ratio for set of simulated ground motions compared with the one of recorded motions. The solid circles represent recorded motions and the open circles describe simulated motions. In this 4D plot, not only are the x and y axes showing the Energy ratio and PGV ratio, but also the size and the color of each circle indicates the total energy and maximum peak ground velocity of each ground motion, respectively. After regression analysis (Baker 2007), the criteria to identify pulse-like ground motions is as follows: any circle above the double red line indicates that that motion does not have pulse characteristics, whereas circles below the double red line are determined as 100 percent pulse-like ground motions, and the area between the red lines are considered as pulse characteristics ambiguous zone. Figure 4.4(a) shows that the simulated record set has more quantity of pulse-like motions compared to the set of recorded motions, even though both sets match a target spectrum. According to pulse effects found by (Krawinkler et al 2005), the pulses, whose periods are smaller or close to structure periods, are easily propagated along the

height of a building and create high deformation demand in the upper floors, whereas, the energy of larger period pulses are concentrated in the lower floors resulting in high displacement at the base of the structure. Hence, pulse-like ground motions tend to create larger building response demand compared to regular ground motions. Meanwhile, when ground motions are classified as pulse-like, the simulated motions have a larger total energy than recorded motions, which can be considered another explanation as to why the interstory drift ratios are overestimated in the aforementioned result.

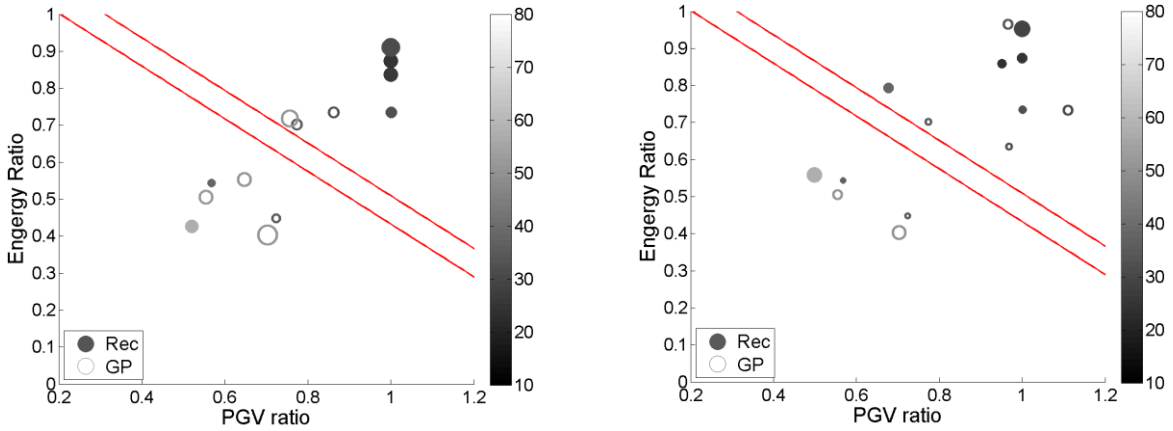

(a) (b)

Figure 4. 4. Scatter plot of energy ratio vs. PGV ratio indicating the pulse-like nature of ground motions in selected sets for case of Uniform Hazard Spectrum (a) and Conditional Mean Spectrum

This investigation shows that the population of simulated ground motions used as a database for ground motion selection and modification did have a larger number of wave pulses as compared to naturally recorded ground motions. The histogram of pulse index (Baker 2007) for naturally recorded ground motions and the GP simulations is illustrated in Figure 4.5. This normalized histogram is a straightforward way to demonstrate that a larger number of pulse-like ground motions exist in the simulated database compared with the recorded one. The pulse index of a ground motion record shows the relative dominance of pulse-like characteristics in that ground motion; a ground motion record is characterized as "pulse-like" if the pulse index is larger than

0.85, however, ground motion records with pulse index larger than 0.15 have shown to include some level of "pulse-like" behavior and non-pulse like ground motions would be determined if the index is smaller than 0.15. As shown in Figure 4.5 ground motion GP simulation models are more likely to generate pulse-like ground motions. The reason why more pulse-like ground motions exist in selected motions for the simulated case is because the GMSM database of simulated motions consists of a larger amount of pulse-like ground motions. Hence, the higher number of pulse-like motions in the population of simulated motions results in a higher chance to select them, and therefore, imposes higher seismic demands on structures compared to sets derived from natural recordings.

Due to the small amount of ground motions used in this procedure, only seven, one question arises which is if the disparity of building response caused by recorded and simulated ground motions is sensitive to the number of ground motions applied in this procedure. With increasing number of ground motions in GMSM procedure up to 40, another repetitive test is conducted to validate the simulated ground motions. In Figure 4.6(a), the overestimation induced by simulated ground motions is still captured. Even though the maximum difference of the mean between the two sets is reduced to a 10% difference, this difference is still statistically significant at a 5% level.

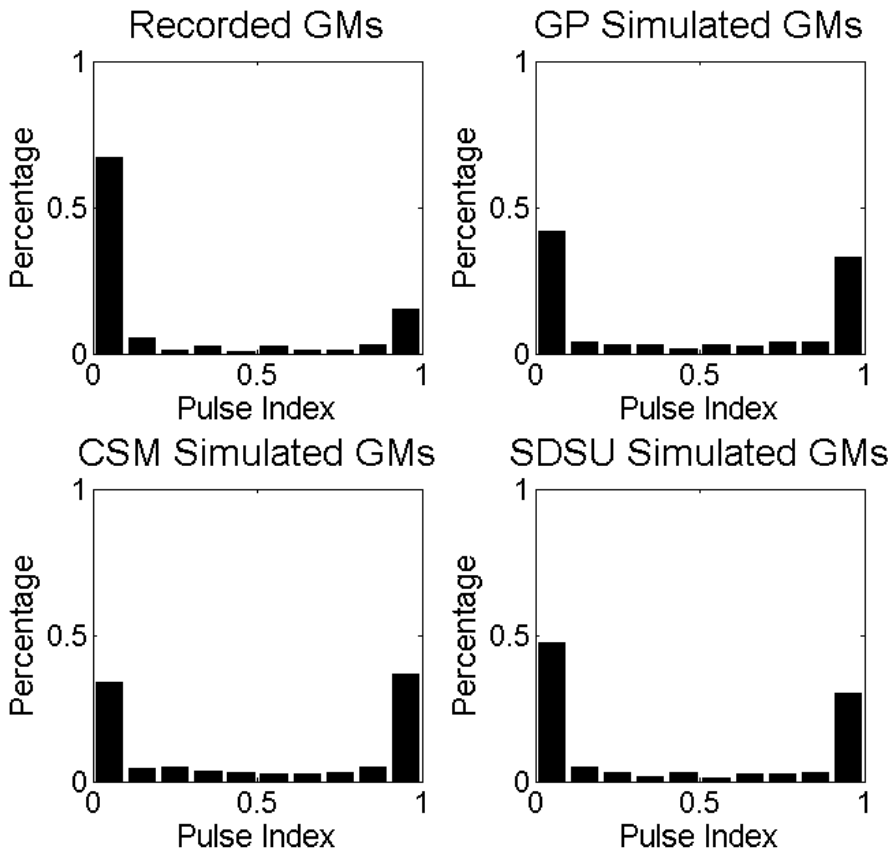

Figure 4. 5. Histogram of pulse index of ground motions in population

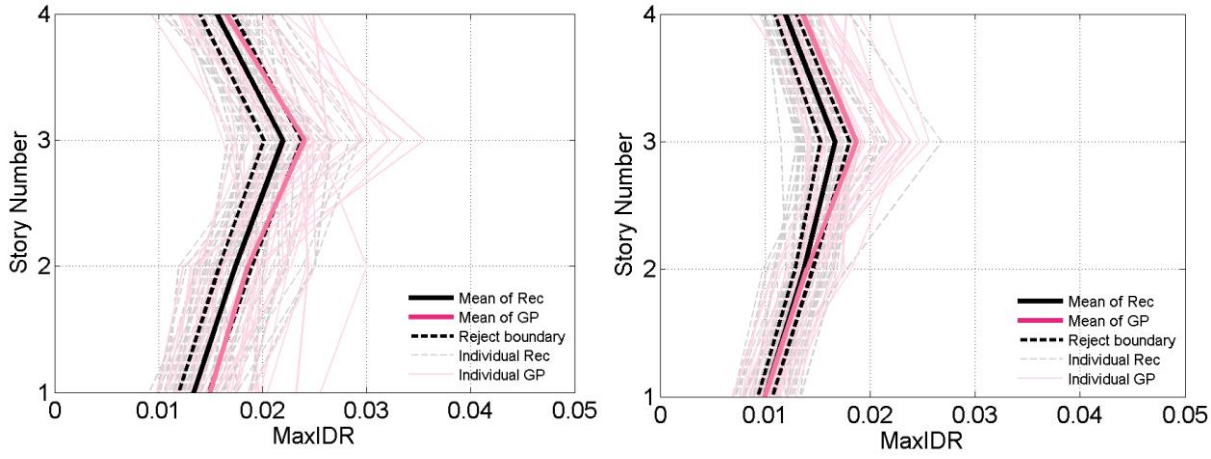

(a) **(b)**

Figure 4. 6. Average maximum interstory drift ratio of the 4-story SMRF at DBE level with target spectrum of Uniform Hazard Spectrum (a) and Conditional Mena Spectrum (b) (40 per set)

Another alternative target spectrum, Conditional Mean Spectrum (CMS), was investigated here in order to verify if the pulse problem would affect the building response in different situations. Figure 4.2(b) shows that the spectrums of recorded GMs and simulated GMs greatly match the CMS target spectrum. However, as Figure 4.3(d) indicates, even though some overestimation can be found in responses of simulated GMs, the level of difference is much smaller, is not statistically significant.

Research studies look into the quality and quantity of pulse in these selected ground motions and compared to the UHS exercise, Figure 4.4(b) shows simulated motions contains less pulse-like ground motions and their ground motion energy is not as high as the one in UHS case, when the CMS is used as the target spectrum. Hence, the expended view of spectrums is investigated and illustrated in Figure 4.7. Both of the spectrums highly match their own target spectrum in the GMSM selecting range (0.2T to 1.5T), however, an obvious difference can be captured in the rest of the range (above 1.5T) in the zoomed view. In the UHS case, Figure 4.7(a) shows, there is a huge gap between recorded and simulated ground motions outside of the selecting range (above 1.5T), whereas in the CMS case, Figure 4.7(b) indicates, the difference of both motions is marginal. Somerville, 2005 indicated that pulse-like ground motions will create a higher demand in the spectrum of the specific area (hump shape) corresponding to the period of pulse. Figure 4.8 shows how pulse affects spectrum shape by comparing cases including and extracting pulse using one pulse-like ground motion with a pulse period of 6.82s. Because the shape of CMS target spectrum is relatively steeper than the one of UHS target spectrum, this may lead to less priority to select pulse-like ground motions, which contain the “hump” shape for larger periods, with the CMS target spectrum.

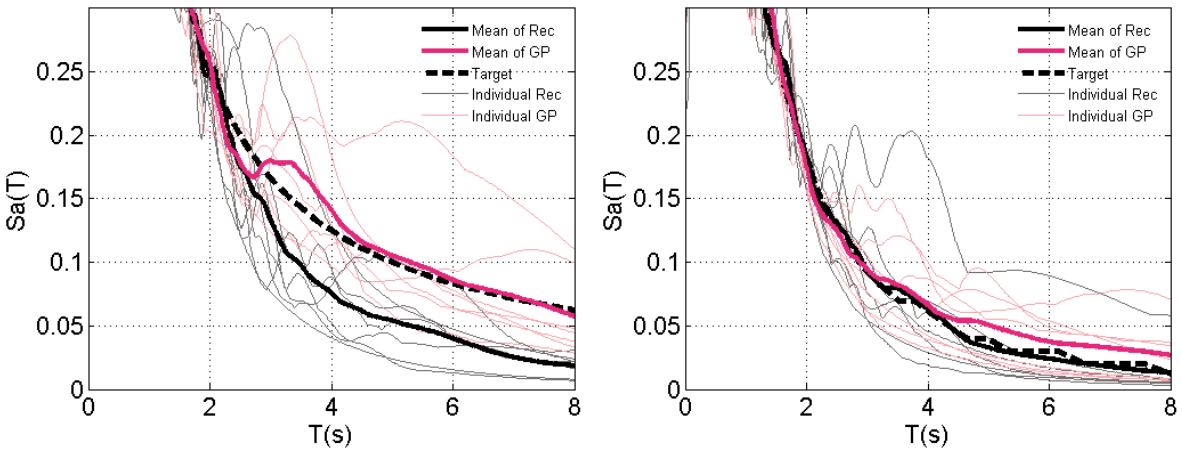

Figure 4. 7. Average spectra of selected and scaled ground motion set, 7 per set, to the DBE with UHS (a) and CMS (b) target spectrum for the 4-story SMRF in zoomed scale.

In consideration that each set consists of 7 motions and the uncertainty in estimation of mean response is large, we have considered increasing the number of ground motions up to 40 as UHS case does, to ascertain that our observations are less biased. However, once we increase the number of selected ground motions from 7 to 40, the pulse-like ground motions are still be chosen in the later order. This is because the simulated database contains too many ground motions with pulse, and a larger number in the database results in a higher chance to select them. Figure 4.6(b) shows that the building response caused by synthetic motions still tend to significantly overestimate.

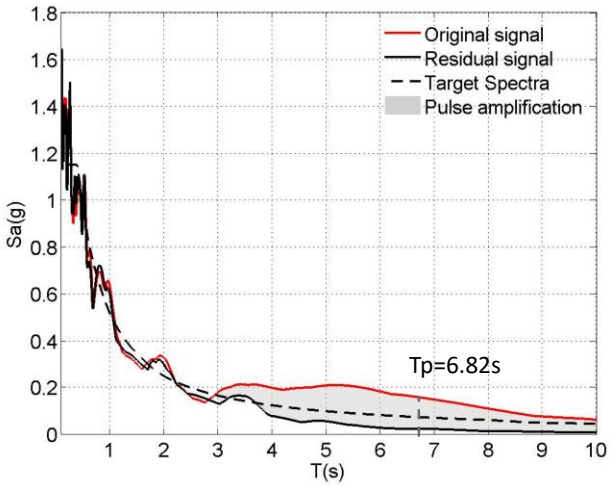

Figure 4. 8. Response spectra of pulse-like ground motions before and after pulse extraction.

4.4.3 Results of Comparing Building Response Measures for All Cases

As Figure 4.4 and Figure 4.9 indicate, all the significant difference happen in low structures, which is 4-story steel moment frames, whereas the result of simulated ground motions match well with the one caused by natural records in high structures. It is because the range of GMSM is much longer in tall building, whose natural period is large. In order to match well with the target spectrum, the long selecting range for the high structures can contribute to the elimination of the pulse like ground motion with large periods, which abnormally exist a lot in database of GP and SDSU illustrated in Figure 4.10. Results for the rest scenarios are summarized in Appendix B.

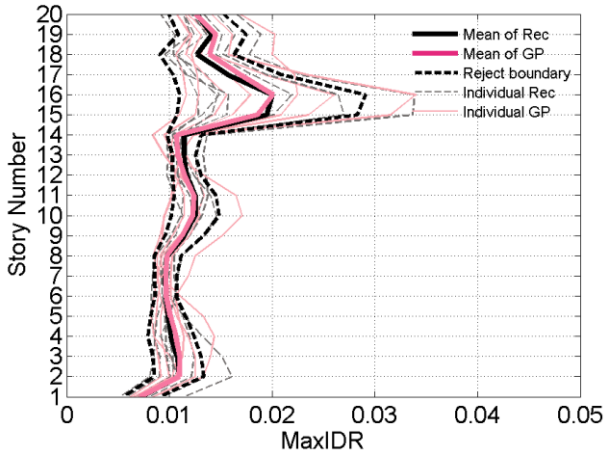

(a)

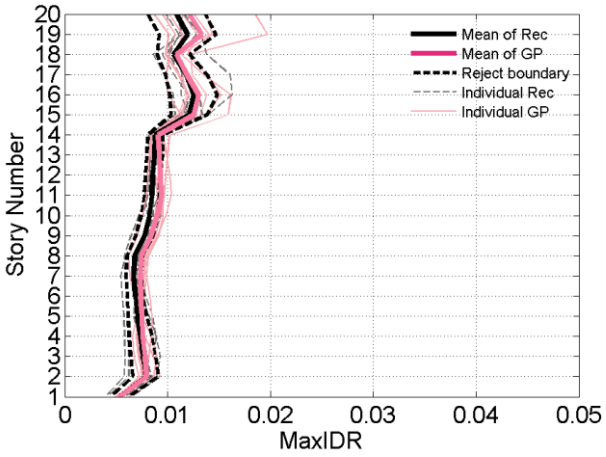

(d)

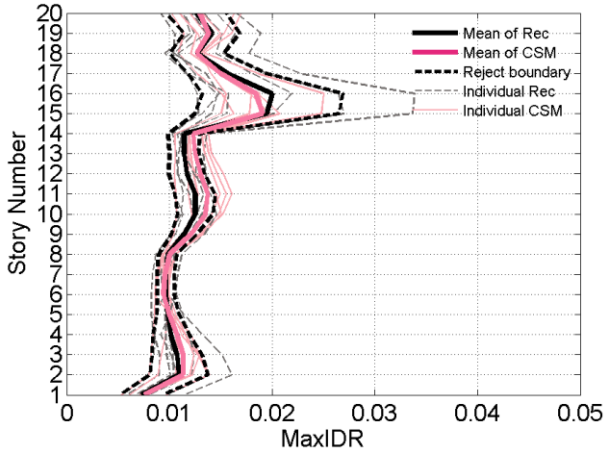

(b)

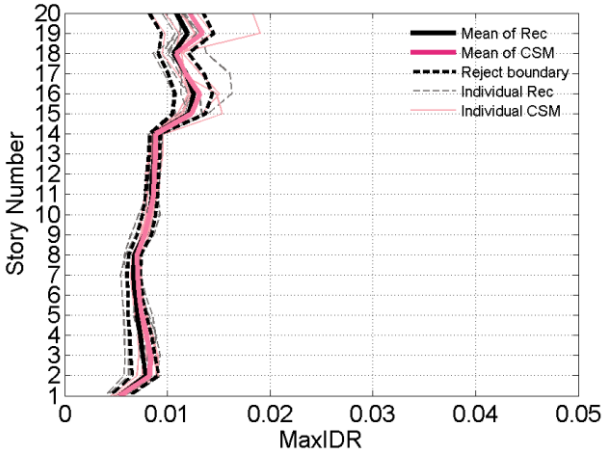

(e)

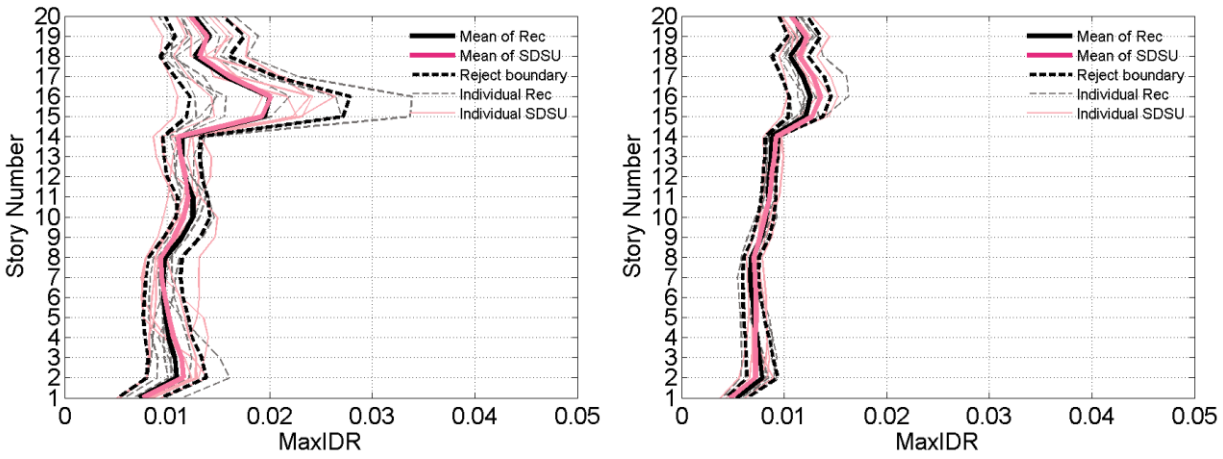

Figure 4. 9. Average maximum interstory drift ratio of the 20-story SMRF at DBE level with Uniform Hazard Spectrum for GP (a), CSM (b), SDSU (c) simulated GMs and Conditional Mean Spectrum for GP (d), CSM (e), SDSU (f) simulated GMs (7 per set)

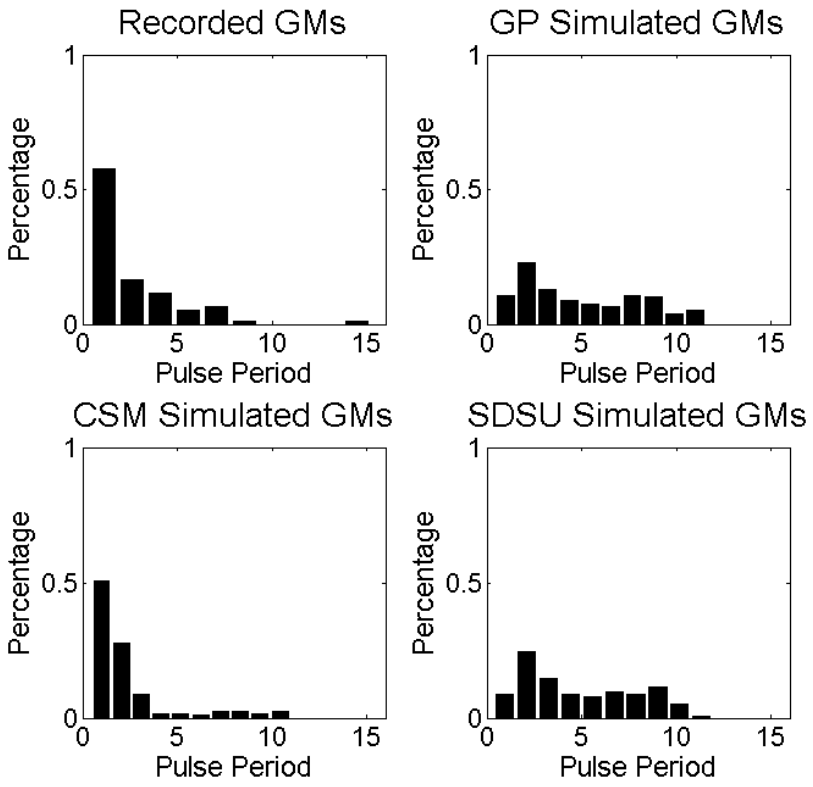

Figure 4. 10. Historgram of pulse period of ground motions in population

4.5 PROPOSED GROUND MOTIONS SELECTION AND MODIFICATION TECHNIQUE FRO SIMULATED GROUND MOTIONS APPLICATION

The aforementioned results indicate the simulated ground motions are easily overestimating the prediction of building response compared with the one caused by nature recordings. And the reason leads to it is because simulation database contains a large amount of pulse-like ground motions, which tend to create larger structure response demand. One additional exercise was conducted to illustrate the effect of pulse-like ground motions. All the pulse-like ground motions are excluded in both ground motion databases with UHS target spectrum. The validation method was executed again, to prove that the large amount of pulse characteristics causes the largest difference in building response. In Figure 4.11, the maximum IDR caused by recorded and simulated ground motions without pulse-like ground motions are almost overlapped on each other within rejection boundary, which prove that simulated ground motions are capable of predicting the building behavior as recorded ground motions do.

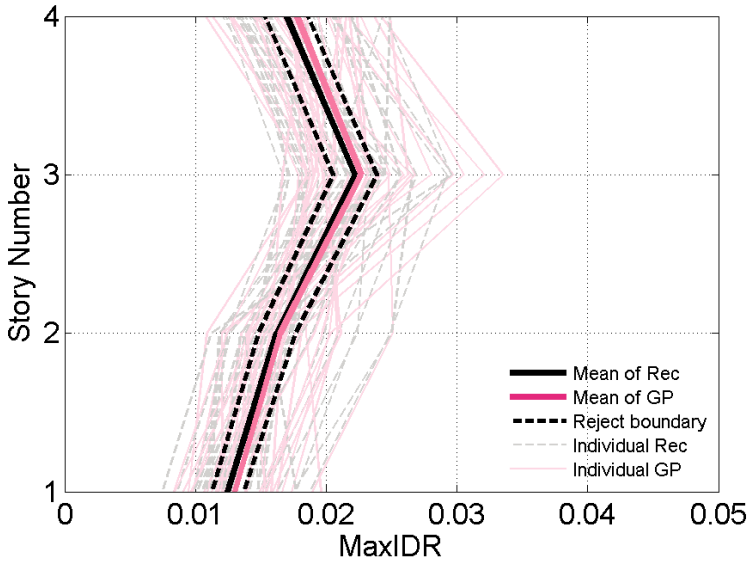

Figure 4. 11. Average maximum interstory drift ratio of the 4-story SMRF at DBE level with Uniform Hazard Spectrum for first realization data without pulse-like ground motions (40 per set)

Accordingly, if the abnormal characteristic of pulse can be eliminated, simulated ground motions can be the substitute of nature earthquake hazard for engineering applications in a practical manner. An updated ground motions selection and modification technique is proposed for making the simulated ground motions usable for engineers. According to the aforementioned explanation, pulse-like ground motions have unique spectrum shape in the way of uplifting spectral acceleration (hump shape) in the corresponding pulse period area, illustrated in Figure 4.8. By increasing the GMSM selecting range, the pulse-like ground motions can be relatively excluded. Because the hump shape of pulse-like ground motion mismatches the smooth target spectrum, and the GMSM technique gives low priority to select these pulse-like ground motions. The original GMSM selecting range is 0.2T to 1.5T, whereas 0.3s to 2.3s for the building whose fundamental period is 1.51s. This range is too narrow to exclude the pulse-like ground motions with periods above 2.3s. Since the hump shape of periods above 2.3s is out of the range, and these pulse-like ground motions are considered as good matching with the target spectrum in these short range. Hence, the updated GMSM technique is proposed to elongate the selecting range up to 4T, which is 6s in this case, to select ground motions with UHS target spectrum for time history analysis. Result is illustrated in Figure 4.12, observation can be seen that the overestimation caused by simulated ground motions is much less severe, and the difference between these two groups of data is not statistically significant. Compared with Figure 4.6(a), one phenomenon can be captured is that the displacement demand in high story become smaller. It is because pulse-like ground motions with small periods tend to propagate along the structure and create higher deformation in upper story, and they are excluded in this updated technique. In synthetic motions, elongating the GMSM selecting range is able to select good quality ground motions to represent nature recording. However, the accurate selecting range can be varied by different types of simulations, and future

study is needed.

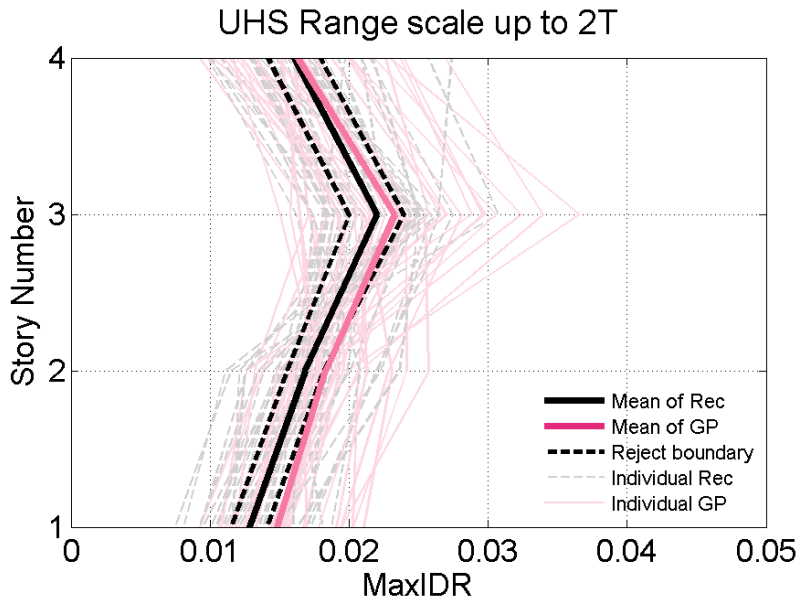

(a)

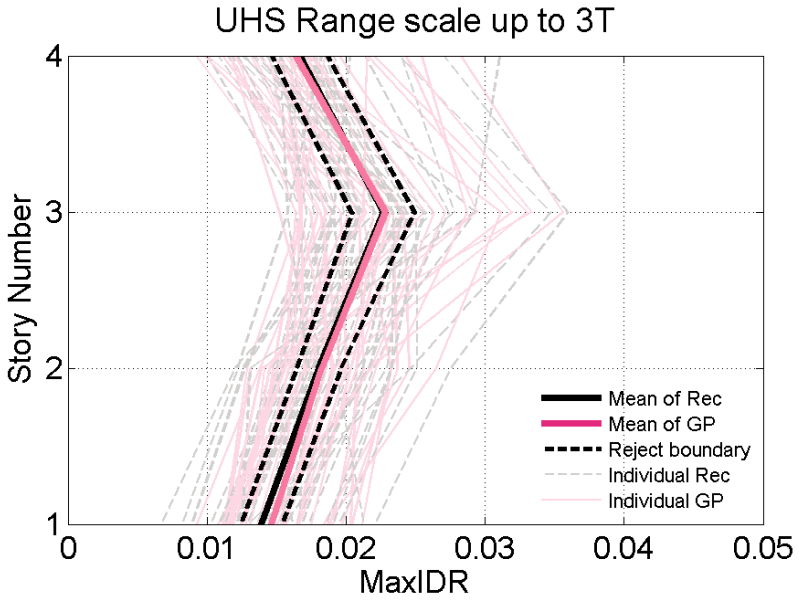

(b)

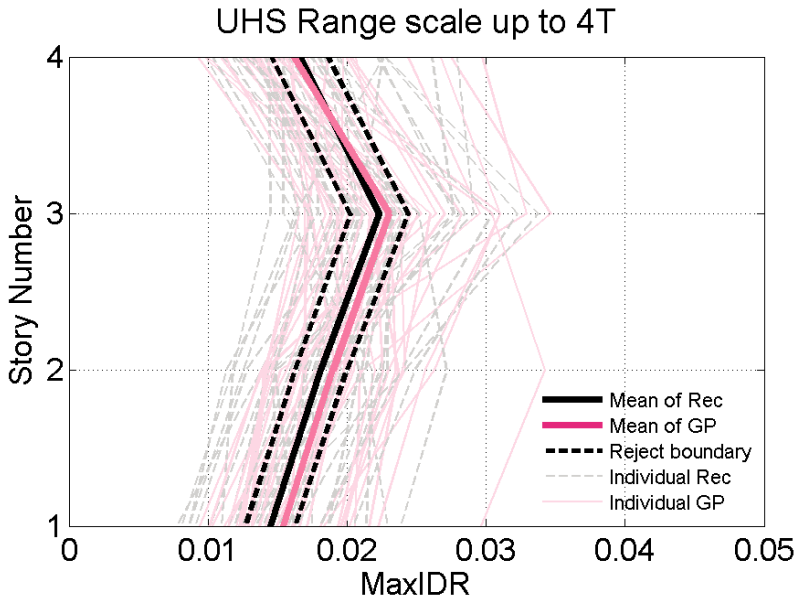

(c)

Figure 4. 12. Average maximum interstory drift ratio of the 4-story SMRF at DBE level with Uniform Hazard Spectrum for first realization data with implementing technique of proposed increasing selection range up to 2T (a), 3T (b) and 4T(c) (40 per set)

4.6 CONCLUSIONS

This study focuses on the validation of broadband simulation for use by structural engineers as input for seismic hazard analysis. The structural analysis procedure applied in this research implements the ASCE7-10 ground motions selection and modification procedure. Simulated ground motions are allowed to be used if a sufficient number of records cannot be found.

An example for a site in downtown Los Angeles for one hazard level was presented: Design Based Earthquake (DBE) that is comparable with a 475 year average return period with two target spectrums: Uniform Hazard Spectrum(UHS) and Conditional Mean Spectrum(CMS) in different number of selected GMs: 7 and 40. And we focus on maximum interstory drift ratio as engineering demand parameter of building response. The difference between demands from simulated and recorded motion sets were compared using Student's t-test between engineering demand parameters at the 5% level. Results show that the structural behavior resulting from recorded

ground motions and simulated ground motions are statistically significantly different in short structures. The sets of simulated ground motions clearly overestimate the response compared to the recorded motions. The difference stems from the fact that ground motion simulation models are more likely to generate pulse-like ground motions, which tend to create larger displacement of building response. The higher number of pulse-like motions in the population of simulated motions results in a larger number of pulse-like motions in the selected sets, and therefore, imposes higher seismic demands on structures compared to sets derived from natural recordings. Whereas tall buildings produce reasonable result for simulated and recorded motions. It is because pulse-like ground motions tend to contain hump shape corresponding to the period of pulse in response spectrum. And larger natural periods in tall buildings bring about long selecting range (0.2T-1.5T), which is able to eliminated pulse-like motions efficiently through the GMSM procedure.

In conclusion, hybrid broadband simulations and recordings with comparable spectra were selected, both of which satisfied building code criteria and fitted for the same target spectrum. These were inputted into 3D steel moment resisting frame structural models. It was found that the structural performance is distinct and statistically significance, where the sets of simulated ground motions clearly overestimate the response compared to the recorded motions. The difference stems from the fact that ground motion simulation models are more likely to generate pulse-like ground motions, which tend to create larger displacement of building response. The higher number of pulse-like motions in the population of simulated motions results in a larger number of pulse-like motions in the selected sets, and therefore, imposes higher seismic demands on structures compared to sets derived from natural recordings. Different target spectrums have unique spectrum shapes, and it may change the order of priority in the selection of pulse-like ground motions. However, as the number of desired selected motions increases, it is inevitable not to select pulse-

like ground motions through the GMSM procedure guided by code. An updated GMSM technique is proposed to elongate the selecting range to avoid choosing abnormal pulse-like ground motions. And the results indicate that with this updated GMSM technique, the simulated ground motions can be the substitute of nature earthquake hazard for engineering applications in a practical manner. Future study is needed to determine the accurate range for elongation.

CHAPTER 5: SENSITIVITY OF ENGINEERING DEMAND PARAMETERS TO EVOLUTIONARY GROUND MOTION INTENSITY AND FREQUENCY CONTENT PARAMETERS

5.1 INTRODUCTION

Over the years, vast improvements in computer technology, along with increasing knowledge in geophysics has led to major advancements in the development of simulated ground motions and widespread popularity in engineering applications. With these developments, simulated ground motions are now considered up to par with recorded motions and spectrally matched ground motions (created by manipulating the frequency content and intensity of recorded ground motions to match a specific response spectrum) in terms of the seismic performance assessment for buildings (Jones and Zareian, 2013); they are also used in designing for target performance, such as ASCE/SEI 7-10(ASCE, 2010). However, serious doubts regarding the accuracy of simulated ground motions exist which cause hesitation amongst engineers to utilize them in engineering practice. In order to incorporate simulated ground motions into engineering applications in a practical sense, they must be validated and compared with recorded ground motions to prove their equivalence

Much efforts have been made to validate simulated ground motions. Rezaeian et al., 2015 developed three validation metrics to evaluate the evolution of intensity and frequency content of ground motions and assess the sufficiency of ground motion simulation models to generate waveforms that represent real motions. Lynne and Baker., 2014 validate simulated ground motions by using simple proxies for the response of engineered systems, including correlation of ε across a range of periods, ratio of maximum to median response across orientations, and the ratio of inelastic to elastic displacement. Instead of a one-to-one validation for a historical event, Afshari and Stewart, 2016 developed a ground motion prediction equations (GMPE) for

the median and standard deviation of the significant duration of earthquake ground motions from shallow crustal earthquakes. Other than validating at the waveform level, engineers are concerned with the similarities of structural response for real and simulated ground motions. Galasso et al., 2012 and 2013 used four historical events (1979 Mw 6.5 Imperial Valley earthquake, 1989 Mw 6.8 Loma Prieta earthquake, 1992 Mw 7.2 Landers earthquake, and 1994 Mw 6.7 Northridge earthquake) to compare the median and standard deviation of seismic response caused by simulated ground motions and recorded ground motions in select SDOF and MDOF systems.

Given the results of validation in terms of waveform and structural response, this research takes a step forward to analyze the effect of a waveform parameter as an engineering demand parameter (EDP). This research bridges the gap between ground motion simulators and engineers and provides an enhanced understanding of the topic. With the knowledge of the relationship between waveform parameters and EDPs, it can be understood that simulators need to pay greater attention to the characteristics of waveform and their effect on the accuracy of predicted structural response.

Four scalar key parameters are considered, which include Arias Intensity (I_a), Duration (D_{5-95}), Mid-Frequency (ω_{mid}), and rate of change of frequency (ω'); detailed definitions can be found in Chapter 3. The effect of these scalar parameters on structural response, in terms of the engineering demand parameter is investigated. By adopting the result from correlation analysis (Rezaeian and Der Kiureghian, 2010), the marginal probability distribution of each parameter conditioned on other three parameters are derived. Synthetic ground motions, using a fully nonstationary stochastic model, (Rezaeian and Der Kiureghian, 2010) are generated for the given scalar key parameters. A sensitivity study on the effect of scalar key parameters on

EDPs is conducted. Groups of synthetic ground motions with one varying parameter and three conditioned parameters are simulated and applied to multiple structures, hence, conclusions may be drawn regarding how individually these four scalar parameters impact the building response in term of EDPs.

Firstly, the proposed sensitivity study is conducted for 77 SDOF systems, including both elastic and inelastic systems, deterioration and non-deterioration systems, three strength reduction factors from 2 to 6 and periods from 0.1s to 4s. The main observation is that building response is highly sensitive to Arias Intensity. The effect of the ω_{mid} on the EDP is observable in nonlinear structures. Duration and rate of change of frequency have little impact on the EDP. A case study using synthetic ground motions for the Northridge earthquake generated by four simulation methods is conducted on the aforementioned SDOF systems and the significance of Arias Intensity is verified. Thirdly, four steel moment frames (SMF) are considered and the maximum interstory drift ratio (IDR) distribution over the height are obtained. Similar trends of effects of scalar key parameters on EDPs are detected. This process, in considering a broad range of periods and structural systems, may provide confidence in drawing conclusions on how these evolutionary ground motion intensity and frequency content parameters impact engineering demand parameters.

5.2 DERIVATION OF CONDITIONAL PROBABILITY DISTRIBUTION

In Chapter 3, we defined and explained how these four scalar key parameters are obtained: Arias Intensity (I_a), Duration (D_{5-95}), Frequency at mid-time (ω_{mid}), and rate of change of frequency (ω'). Rezaeian and Der Kiureghian, 2010 have done statistical analysis on these four scalar parameters. A database of ground motions is built, consisting of a subset of Pacific Earthquake Engineering Research Center: Next Generation Attenuation (PEER NGA) and a subset of

Campell-Bozorgnia NGA (Campbell and Bozorgnia, 2008). The database consists of 31 pairs of horizontal components from 12 earthquakes with strike-slip fault types, and 72 pairs of horizontal components from 7 earthquakes with reverse faults. For each ground motion, one set of these four parameters are identified and statistical characteristics, such as minimum and maximum, mean and standard deviation, and the fitting distribution for the data are generated. Rezaeian and Der Kiureghian, 2010 assign probability distributions to each parameter. The maximum likelihood method is used to verify the optimal distribution fitting. Numerical summaries of the data are provided in Table 5.1.

Table 5.1: Summary statistical data of scalar parameters
Data source: Rezaeian and Der Kiureghian (2010)

Parameter	Minimum	Maximum	Sample Mean	Sample Standard Deviation	Fitted Distribution
I_a(s.g)	0.000275	2.07	0.0468	0.164	Lognormal
$D_{5\text{-}95}$ (S)	5.37	41.29	17.25	9.31	Beta
$\omega_{\text{mid}}/2\pi$ (Hz)	1.31	21.6	5.87	3.11	Gamma
$\omega'/2\pi$ (Hz/s)	-1.502	0.406	-0.089	0.185	Two-sided Truncated Exponential

In order to satisfy the normality assumption of the conditional probability distribution, the fitted distribution of each parameter was transformed to the standard normal space according to Equation (5.1), where i represents the order the of parameter, $F_{\theta_i}(\theta_i)$ denotes the marginal cumulative distribution function fitted to the data of the corresponding parameter, Φ^{-1} indicates the inverse of the standard normal cumulative distribution function and, ν_i and θ_i represent the random variables in the standard normal distribution and the original fitting distribution, respectively.

$$\nu_i = \Phi^{-1}\left[F_{\theta_i}(\theta_i)\right] \qquad i = 1,2,3,4 \tag{5.1}$$

After the transformation, the correlation coefficients between the jointly normal variables ν_i

are calculated and listed in Table 5.2.

Table 5.2: Sample correlation coefficients between the transformed model parameters
Data source: Rezaeian and Der Kiureghian (2010)

	υ_1	υ_2	υ_3	υ_4
υ_1	1	-0.36	-0.15	0.13
υ_2	-0.36	1	-0.13	-0.16
υ_3	-0.15	-0.13	1	-0.2
υ_4	0.13	-0.16	-0.2	1

According to Eaton, 1983, the mean and standard deviation of the conditional probability distribution for a multivariable normal distribution can be derived using Equation 5.2 and Equation 5.3. In this case, , **X** is the $Z = \begin{bmatrix} Y \\ X \end{bmatrix}$ subvector of three parameters with constant value, **Y** is the subvector indicating one parameter of the demand conditional probability distribution, μ_1 is the mean of subvector **Y**, μ_2 indicates the mean of subvector **X**, and $\boldsymbol{\Sigma}_z$ is the covariance matrix for these four scalar parameters, $\boldsymbol{\Sigma}_{11}$, $\boldsymbol{\Sigma}_{12}$, $\boldsymbol{\Sigma}_{21}$, and $\boldsymbol{\Sigma}_{22}$ are its partitions.

$$\mu = \mu_1 + \Sigma_{12}\,\Sigma_{22}^{-1}(X - \mu_2) \tag{5.2}$$

$$\Sigma = \Sigma_{11} - \Sigma_{12}\Sigma_{22}^{-1}\Sigma_{21} \tag{5.3}$$

With the proposed method, the conditional probability distribution of one single parameter conditioned on other parameters equal to the central value is obtained. One hundred realizations from this newly developed conditional probability distribution are generated. Given these scalar key parameters, synthetic ground motions are generated using Rezaeian and Der Kiureghian, 2010. The response of a linear filter with scalar parameters subjected to a white-noise process is normalized by its standard deviation and is multiplied by a deterministic time-modulating function to obtain the corresponding simulated ground motions. Hence, 100 corresponding synthetic ground motions are generated for the sensitivity study in each scalar parameter. The advantage here is that

the effect of each parameter is isolated from other parameters.

5.3 DESCRIPTION OF SIMULATION AND STRUCTURE

The proposed sensitivity study is conducted on a total of 77 SDOF systems, modeled using the Open System for Earthquake Engineering Simulation structural analysis software (OpenSees) (http://opensees.berkeley.edu/). The combination of variation is included using three parameters:

- SDOF fundamental period (T): this study considers 11 oscillation periods between 0.1s and 4s. The period range is sampled with a 0.1s, 0.2s, 0.5s, 0.7s, and a step of 0.5s between 1s and 4s.
- Strength reduction factors (R): this parameter is the ratio of the GM elastic demand to the SDOF system's yield strength; R is varied in order to describe elastic/inelastic structural behavior. To ensure the comprehensiveness, we consider from elastic, to mildly inelastic (R = 2), moderate inelastic (R = 4) and severely inelastic structures (R = 6). In order to achieve constant value in R for structure and applied ground motion, the yield strength of SDOF is varied. The spectral displacement is obtained for each ground motion record and $F_{y\ is}$ equal to the base shear associated with that spectral displacement divided by the desired value of R.
- Backbone curves: this study considers two backbone curves: one with strain hardening (denoted as non-deteriorating), and another with softening behavior (denoted as deteriorating). The non-deterioration backbone curve has a bilinear elastic-plastic behavior with positive strain-hardening of 10%, whereas the deteriorating backbone curve has a softening ratio of −5%. A Rayleigh damping with coefficient corresponding to 5% is used

and kept constant throughout the time history analyses. `Steel01` is the material used in Opensees. The backbone curves for these two cases are illustrated in Figure 5.1.

In this sensitivity study, two engineering demand parameters (EDPs) are considered for the SDOF systems: spectral displacement (S_d) for an elastic structure, and maximum inelastic displacement ($\Delta_{inelastic}$).

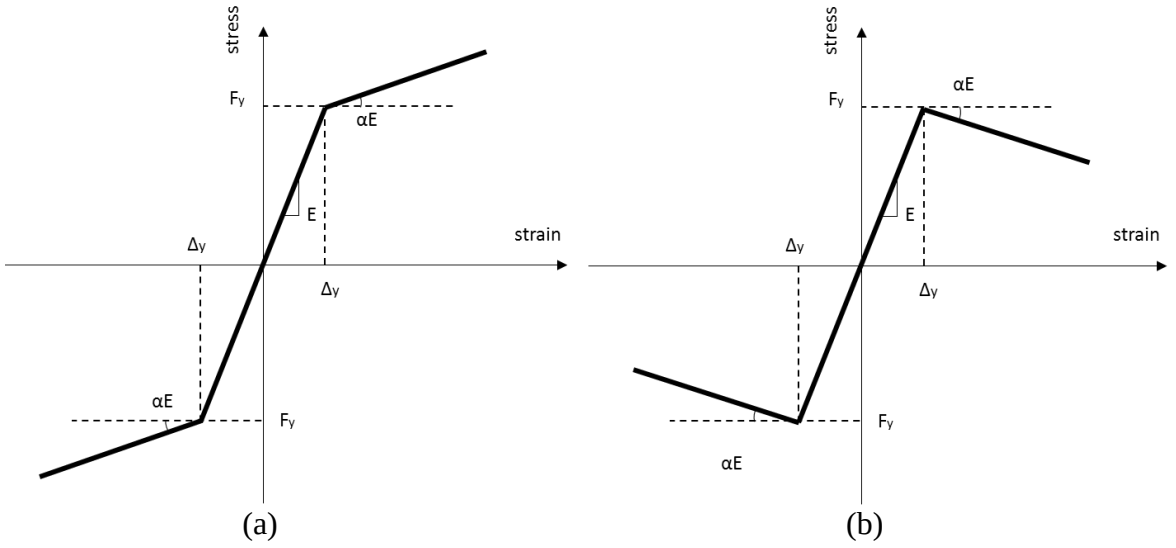

Figure 5. 1. Backbone curve of non-deterioration material (a) and deterioration material (b)

For the case study, four inelastic steel moment frames (SMFs), designed based on ASCE/SEI 7-02(ASCE, 2005) and ANSI/AISC 341-05 (AISC, 2005), are used. The number of stories considered are 4, 8, 12 and 20, and the fundamental periods of the buildings are 1.52s, 2.11s, 2.87s and 4.07s, respectively. Detailed descriptions of these inelastic SMFs can be found in Chapter 4.

The proposed sensitivity study is conducted on a total of 77 SDOF systems, which represent a combination of the aforementioned variations. The synthetic ground motions used are part of the nonstationary stochastic model developed by Rezaeian and Der Kiureghian, 2010. This is described, in detail, in section 5.2.

For the case study, the synthetic ground motions are from four types of simulation methods,

Hart (Hartzell et al., 1999), Artf (Frankel, 1995), Pliu (Liu et al., 2006), and Zeng (Zeng et al., 1996). These four simulators generate the synthetic ground motions for the 1994 Northridge event in 42 stations consisting of 32 soil stations and 10 rock stations.

5.4 RESULT AND DISCUSSION

5.4.1 Sensitivity SDOF System Response to Variation in Scalar Parameters

The effects of the four scalar parameters on EDPs are investigated via SDOF systems. The sensitivity study of each parameter consists of 100 synthetic ground motions, in which the investigated parameter includes 100 samples derived from the proposed conditional probability distribution and transformation between distributions, while the other three parameters are held at a constant value (the mean value of the considered). All synthetic ground motions were simulated using a fully nonstationary stochastic model and are used as inputs for nonlinear dynamics analysis (NLDA) applied to the 77 SDOF systems. A total of 30,800 NLDAs were performed. Only one horizontal component is applied in each NLDA. The spectral displacement (S_d) in an elastic SDOF and maximum inelastic displacement ($\Delta_{inelastic}$) in an inelastic SDOF are computed. In this section, the results of elastic SDOF and inelastic SDOF system (R=2) with positive hardening ratio are presented. The rest of results for other inelastic SDOF systems share the same trend and are illustrated in Appendix B.

The sensitivity range of Arias Intensity considered is from 0.0012 g.s to 0.7155 g.s. As shown in Figure 5.2 and Figure 5.3, there is a clear trend that EDP in SDOF systems with wide range period is highly correlated with Arias Intensity. This phenomenon can be captured in an elastic SDOF as well as inelastic SDOF. Structures with larger periods are more sensitive to Arias Intensity. Along with this, structures with smaller periods exhibit less dispersion compared to SDOFs with larger periods. A conclusion can be drawn that the response of a SDOF structure is highly sensitive to Arias Intensity.

The range of variation in duration is between 5.4s and 35.9s. As shown in Figure 5.4 and Figure 5.5, the effect of duration on an elastic EDP is insignificant in most cases. Only response of inelastic systems with short periods is duration sensitive. This is because duration is conditioned on the same volume of Arias Intensity; ground motions with a short duration tend to have large peak amplitude in acceleration and velocity, this type of motion is inclined to push structures to yield and create large displacement demands within inelastic structures. SDOF systems with short periods are sensitive to ground motions with high frequency, hence, the descending trend in EDP can be observed in short period SDOFs. Moreover, as Chapter 4 indicates, the mismatch of duration may lead to the generation of pulse-like ground motions, which tends to create high displacement demands for buildings. All in all, duration is an important parameter for ground motion simulation validation.

The range of the sensitivity study for ω_{mid} is from 1.16Hz to 9.09Hz. EDP of elastic systems is not sensitive to ω_{mid}, however, as shown in Figure 5.7, the response of inelastic systems is sensitive to ω_{mid} and depends on the natural frequency of the structure. A ground motion with ω_{mid} close to the natural frequency of the structure will cause the structure to experience resonance and yield, creating large displacements in inelastic structures. The selected region for ω' is from -0.64Hz to 0.18Hz. EDPs are sensitive to the negative slope of the frequency. Ground motions with a negative slope of frequency indicate that there is a significant change in the rate of change of frequency. High frequency dominates the first half of the time series, and low frequency dominates the rest of the time history. With significantly less excitation in the rear half part of motions, this type of ground motion may lead the structure acts as its natural frequency and create larger demand of response.

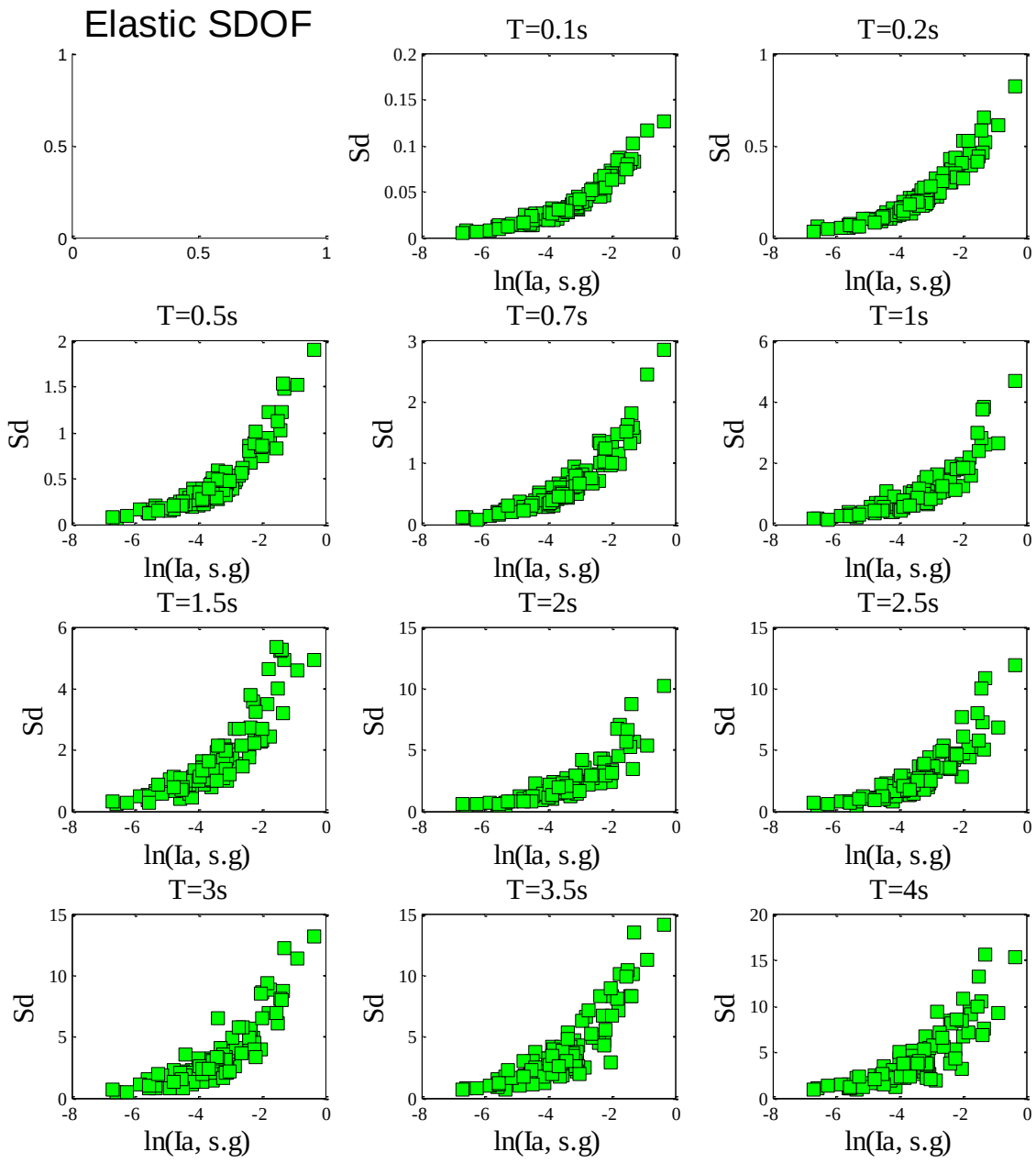

Figure 5.2. Effect of arias intensity on engineering demand parameter in term of spectral displacement for elastic SDOF, period from 0.1s to 4s.

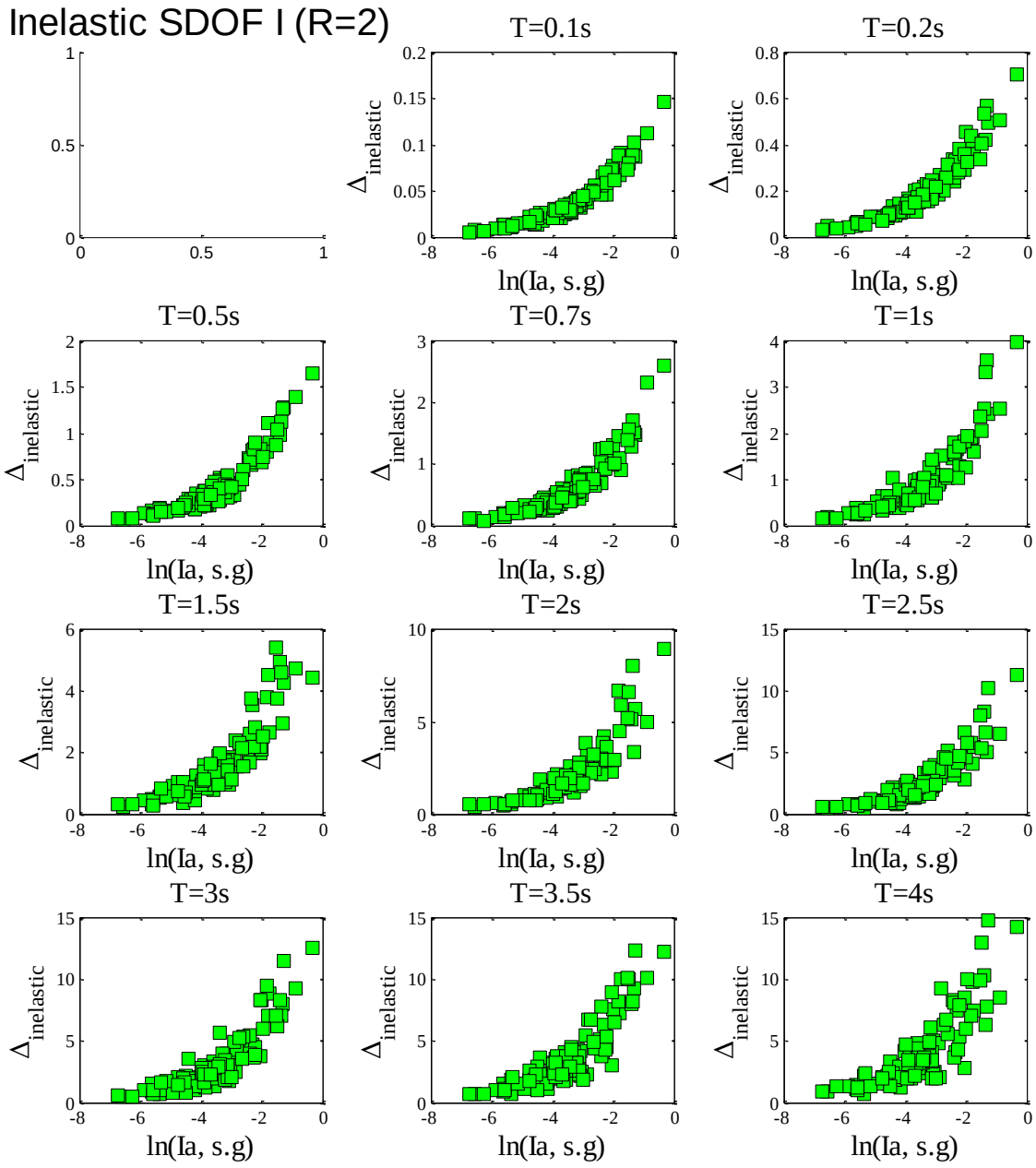

Figure 5. 3. Effect of arias intensity on engineering demand parameter in term of maximum inelastic displacement for non-deterioration inelastic SDOF, period from 0.1s to 4s with strength reduction factor, R=2, and positive strain-hardening, α=0.10.

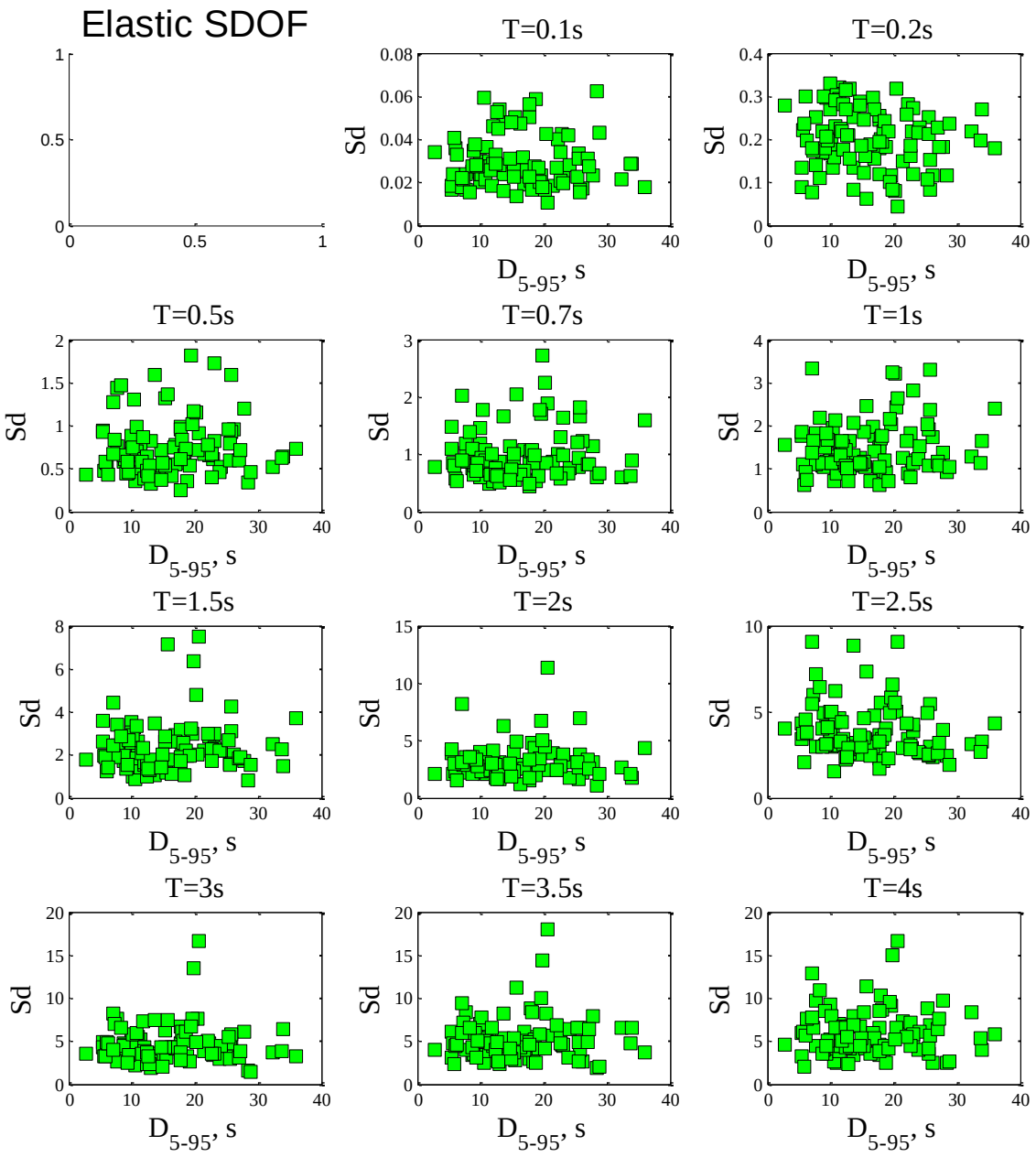

Figure 5. 4. Effect of duration on engineering demand parameter in term of spectral displacement for elastic SDOF, period from 0.1s to 4s.

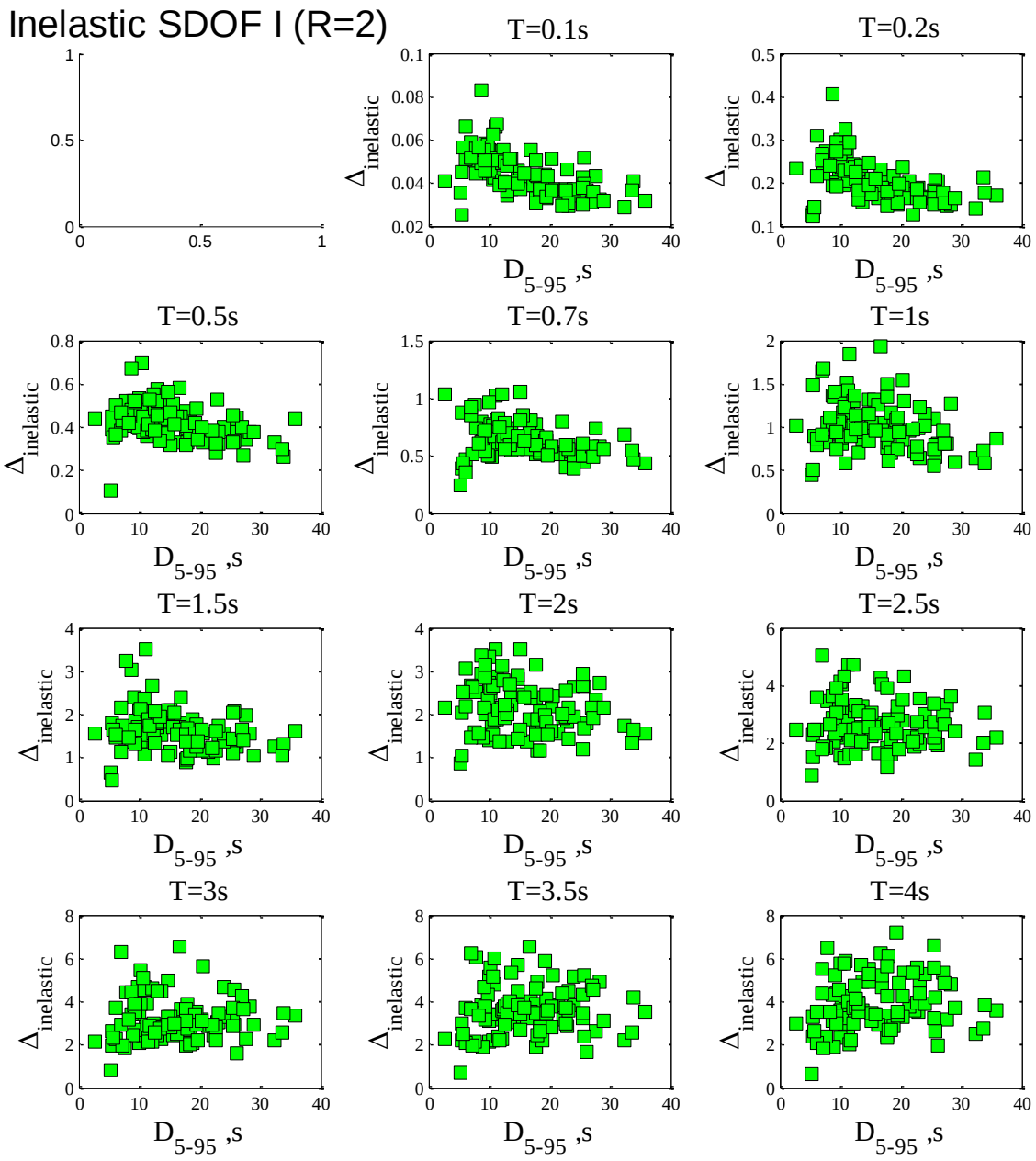

Figure 5. 5. Effect of duration on engineering demand parameter in term of maximum inelastic displacement for non-deterioration inelastic SDOF, period from 0.1s to 4s with strength reduction factor, R=2, and positive strain-hardening, α=0.10.

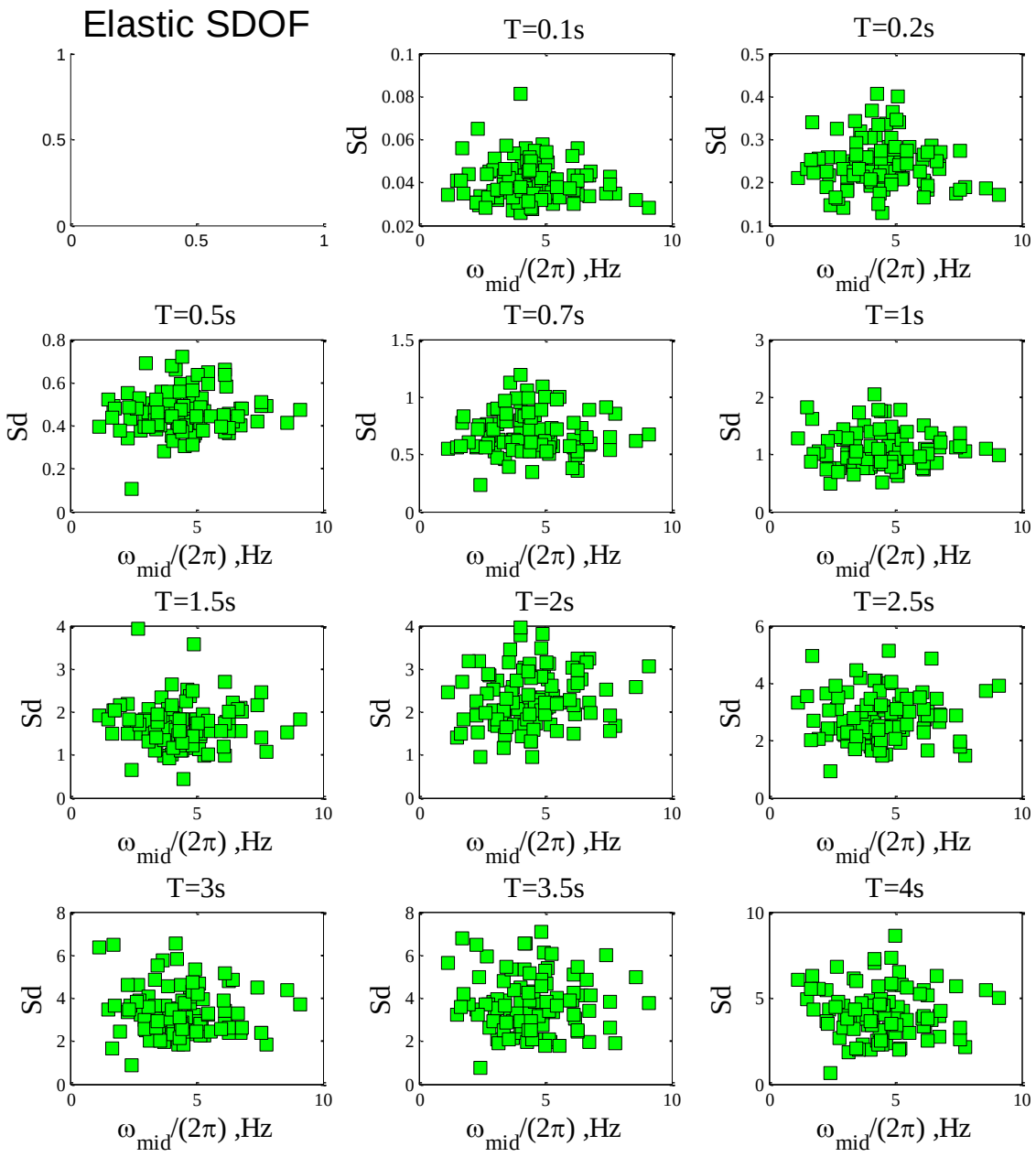

Figure 5. 6. Effect of frequency at mid-time on engineering demand parameter in term of spectral displacement for elastic SDOF, period from 0.1s to 4s.

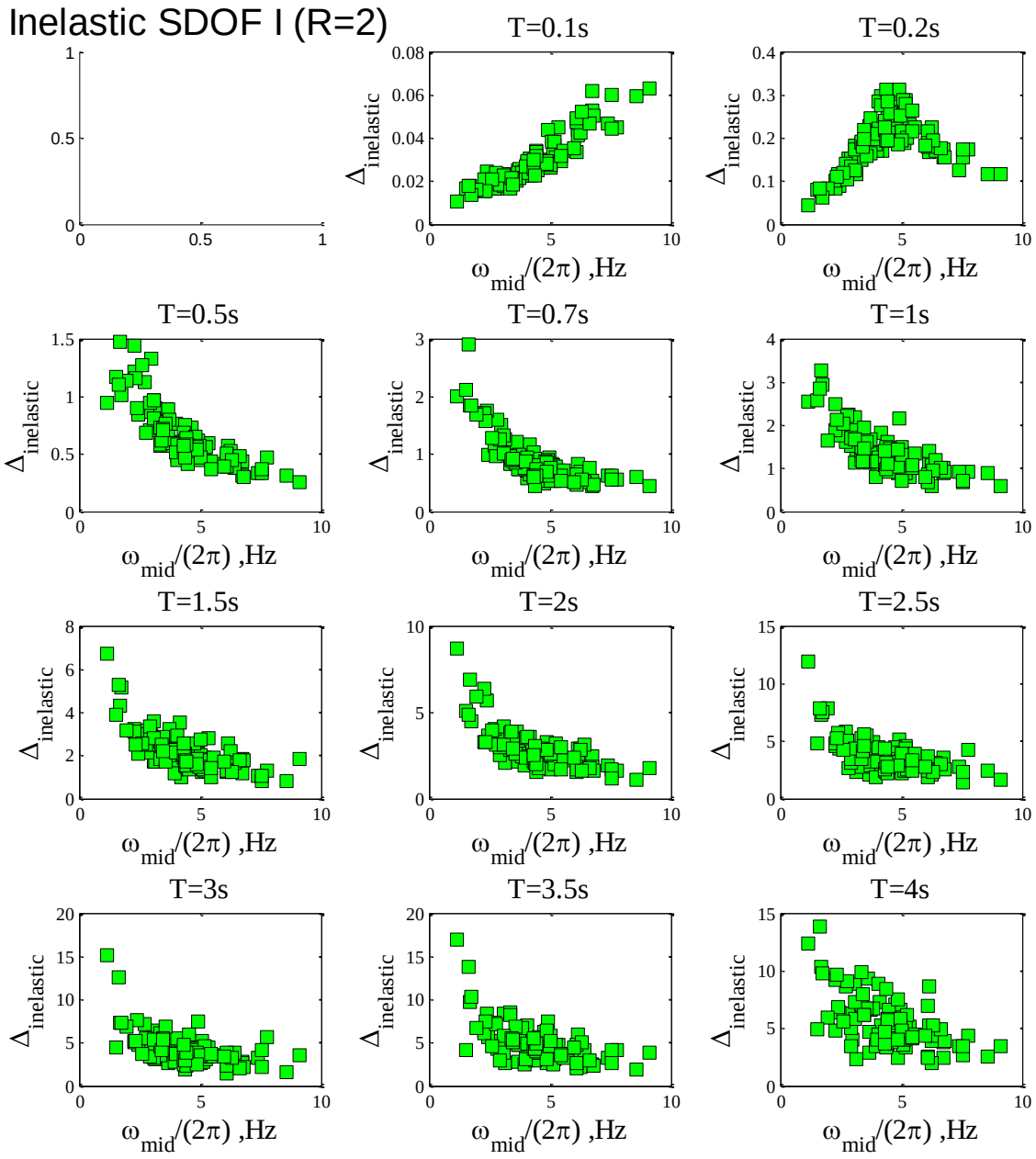

Figure 5. 7. Effect of frequency at mid-time on engineering demand parameter in term of maximum inelastic displacement for non-deterioration inelastic SDOF, period from 0.1s to 4s with strength reduction factor, R=2, and positive strain-hardening, α=0.10.

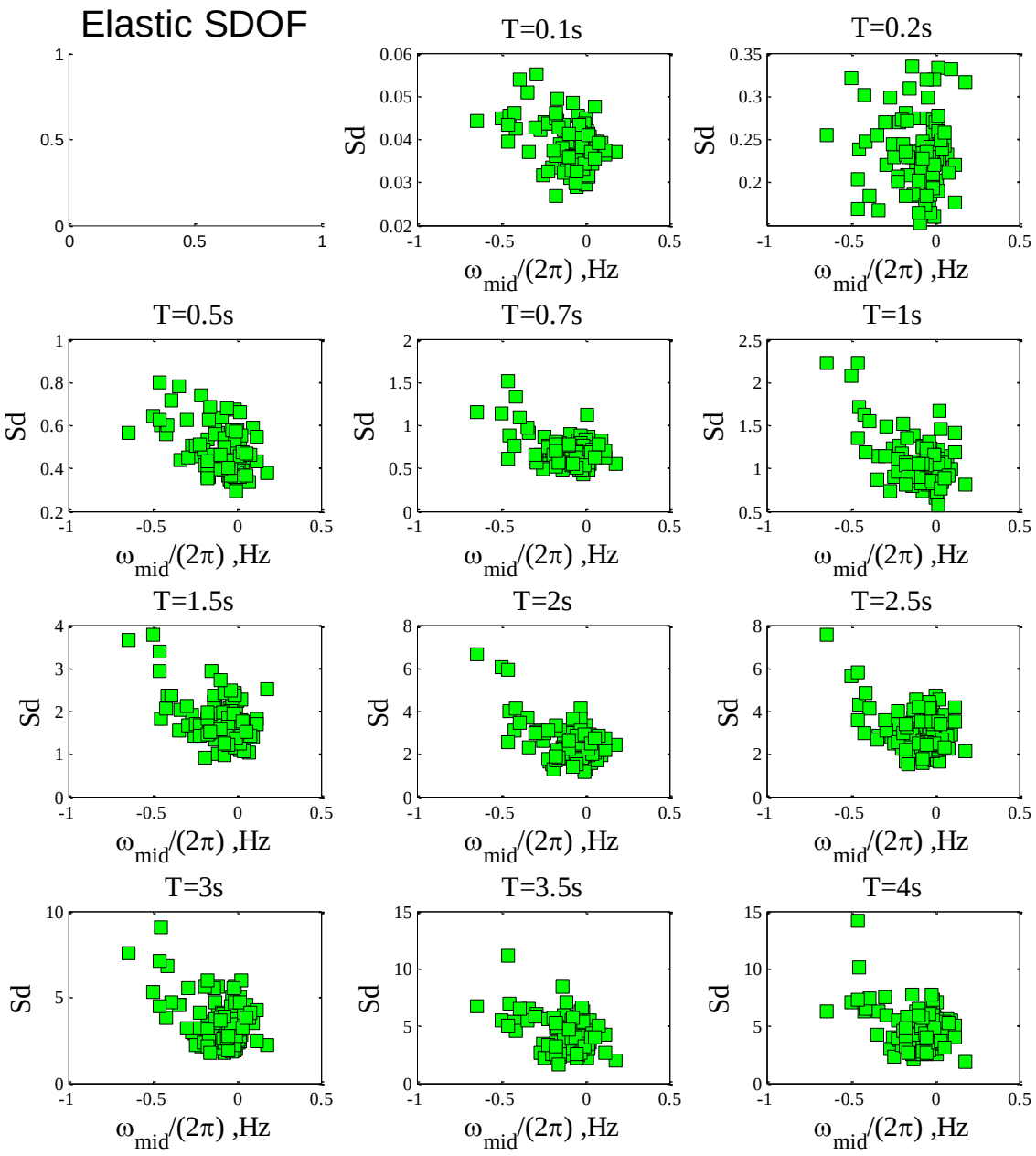

Figure 5. 8. Effect of slope of frequency on engineering demand parameter in term of spectral displacement for elastic SDOF, period from 0.1s to 4s.

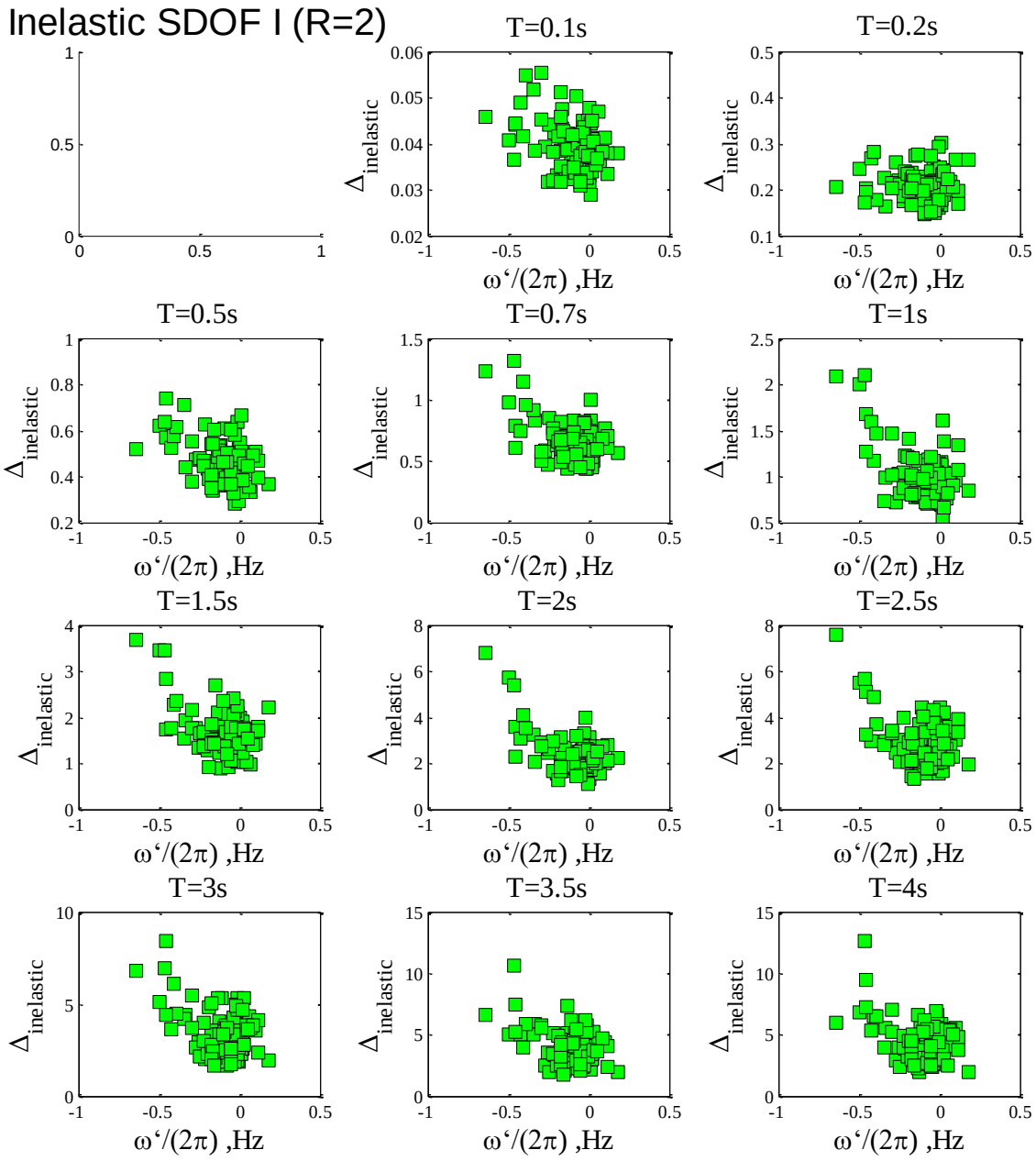

Figure 5. 9. Effect of slope of frequency on engineering demand parameter in term of maximum inelastic displacement for non-deterioration inelastic SDOF, period from 0.1s to 4s with strength reduction factor, R=2, and positive strain-hardening, α=0.10.

5.4.2 Discussion on Response of SDOF System to Simulations of the Northridge Event

To investigate the observations made in the previous section on the importance of scalar parameters in the response of SDOF systems, a case study using four types of simulated ground motions for the Northridge event on SDOF structures is conducted. With the understanding regarding the effect of scalar parameters on EDPs, we try to explain the difference in SDOF response within these four simulations. In each SDOF system, the median value, the exponential of the mean of the natural log of the EDP across all the available stations, for the synthetic records, divided by the median value for the real dataset, is computed and plotted across the period range being considered for different R values. A ratio above unity means the simulations overestimated the response, and the opposite is true if the ratio is smaller than one. For instance, a ratio of the medians of maximum displacement obtained using synthetic and recorded motions larger than one indicates that the synthetic record tends to produce, on average, systematically more damaging spectral displacements than real records. As Figure 5.10 and Figure 5.11 indicate, the results of synthetic ground motions over recorded ground motions are consistent in elastic SDOF as well as inelastic SDOF. The simulation from Hart and Artf tend to have a similar trend, a slight underestimation in low periods, and a small overestimation in large periods. The synthetic ground motions from Pliu overestimate building response in all periods, but the level of overestimation is marginal. The simulation from Zeng creates a significant overestimation in large period structures. By investigating Figure 5.12, we find that the overestimation in SDOF response for Zeng's simulation stems from the over prediction in Arias Intensity. This phenomenon is inconsistent with the result of sensitivity study: structure response is highly sensitive to Arias Intensity.

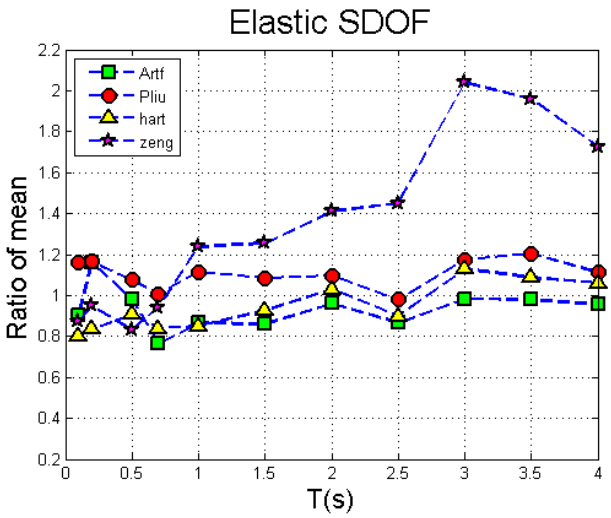

Figure 5. 10. Ratio of medians of the peak elastic displacement for simulated GMs to the corresponding quantity computed for the recorded GMs applied to elastic SDOF for Northridge earthquake.

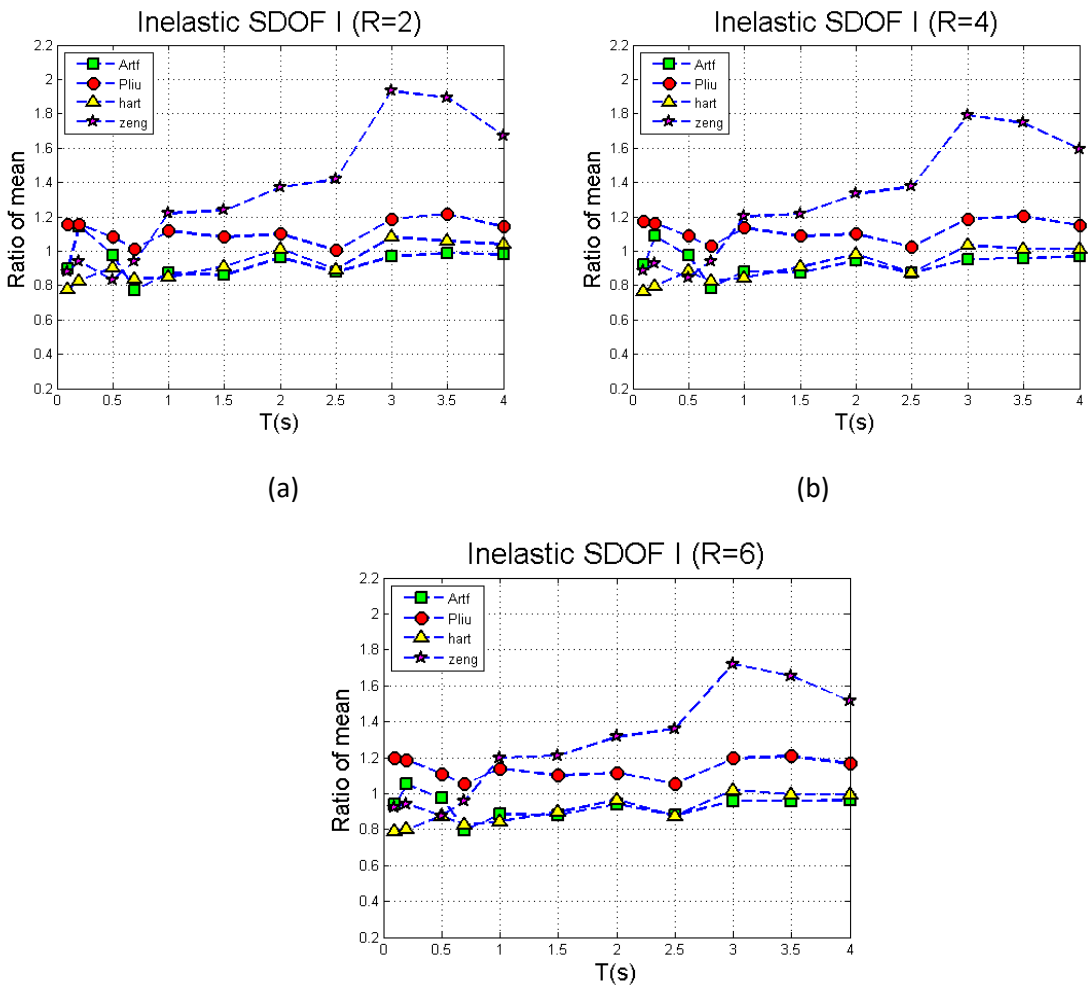

Figure 5. 11. Ratio of medians of the maximum inelastic displacement for simulated GMs to the corresponding quantity computed for the recorded GMs applied to inelastic SDOF with different strength reduction factor R=2 (a), R=4 (b) and R=6 (c) for Northridge earthquake.

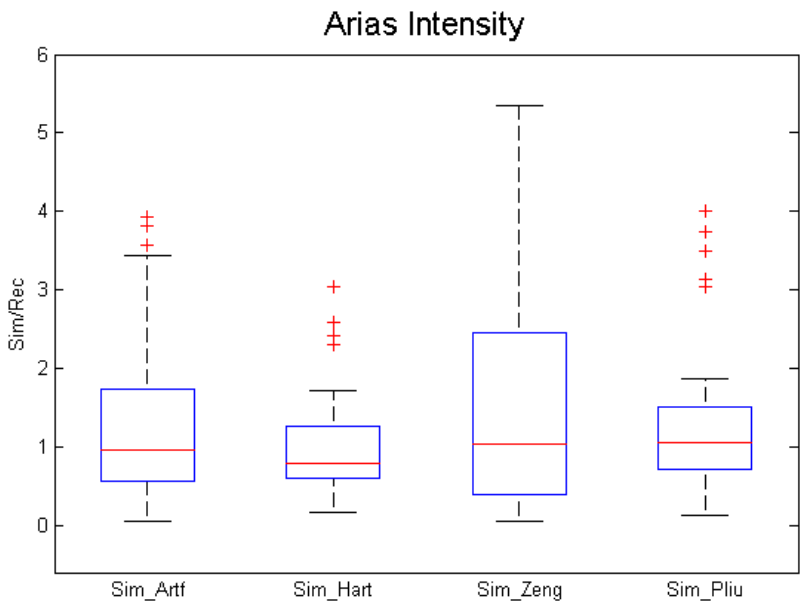

Figure 5. 12. Boxplot of arias intensity ratio for simulated GMs to the corresponding recorded GMs for Northridge earthquake.

5.4.3 Sensitivity MDOF System Response to Variation in Scalar Parameters

The investigation on response of SDOF system to scalar parameters is repeated for a group of steel moment frames including 4, 8, 12 and 20-story. Instead of showing response in each story, the maximum interstory drift ratio in each of the stories along the height of the building (maxIDR) is considered as the engineering demand parameter. Figure 5.13 shows the observed trend in response of 20-story SMF to four scalar parameters; the results are consistent with the ones observed for the SDOF systems. The results for the 4-, 8- and 12-story SMF share the same trend and are presented in Appendix B.

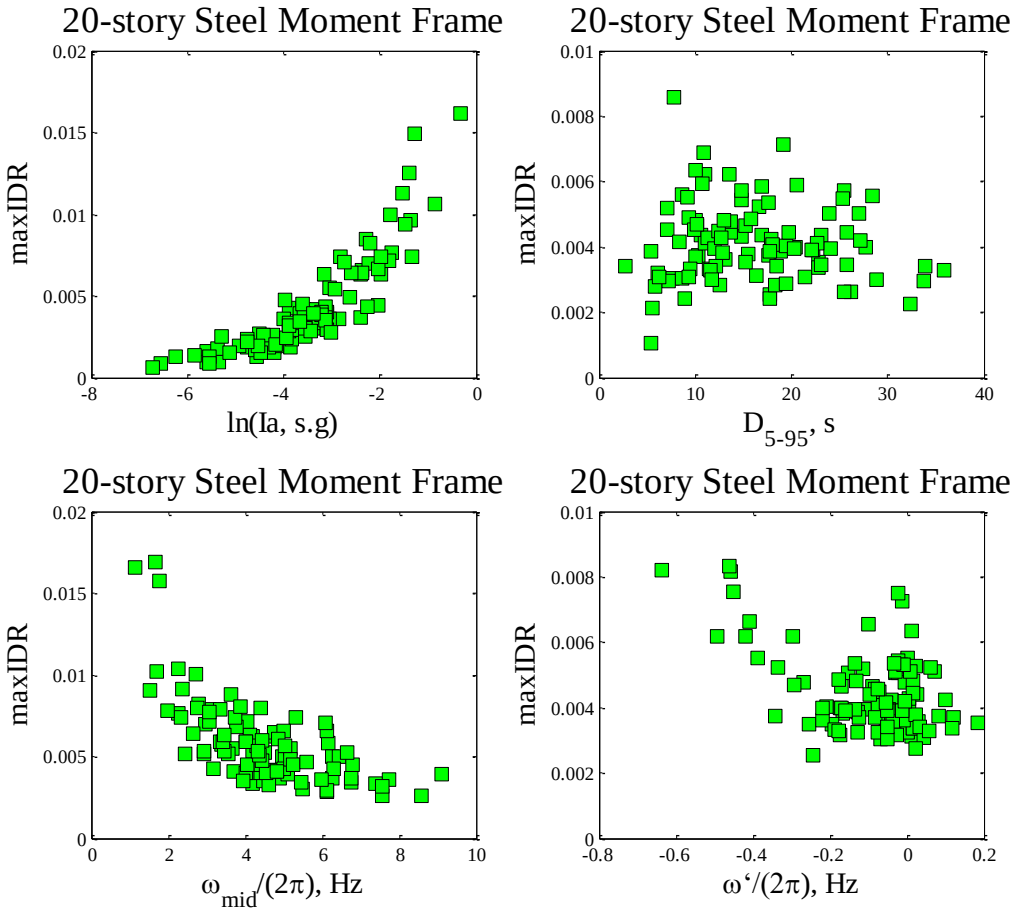

Figure 5. 13. Effect of arias intensity, duration, mid-frequency and slope of frequency on engineering demand parameter in term of maximum interstory drift ratio for 20-story steel moment frame

In the case study considering MDOF systems, the four types of synthetic ground motions for the Northridge earthquake are applied. The ratio of the medians was computed which is the median value of maxIDR for the synthetic records divided by the median value for the real dataset, across the period range of the four SMFs. In Figure 5.14, the ratio of EDPs for the simulation by Hart is slightly below unity, which means that this simulation predicts building response similar to that of the recorded motions (at least in an average). Simulations by Pliu and Artf show a ratio of EDPs that is above unity that indicate overestimation of response; the difference is around 10-20%. Simulations by Zeng create the largest overestimation in response of MDOF systems. Figure 5.15

to Figure 5.18 show the ratio of EDPs from simulation to recorded motion in terms of Arias Intensity vs the ratio of the maxIDR for each simulation method. These plots illustrate how the difference in Arias Intensity will lead to the discrepancy in estimation of maxIDR. In these plots, the two red lines indicate the ratio equal to unity. Compared to other simulations, Hart's simulation tends to have less of a ratio above one in terms of Arias Intensity, which can guarantee less overestimation in building response caused by synthetic ground motions. For Zeng's simulation, the significant overestimation in building response stems from the inaccurate prediction of Arias Intensity, which is obviously off in comparison with the other simulations. Compared with SDOF systems, consistent results for MDOF systems can be found.

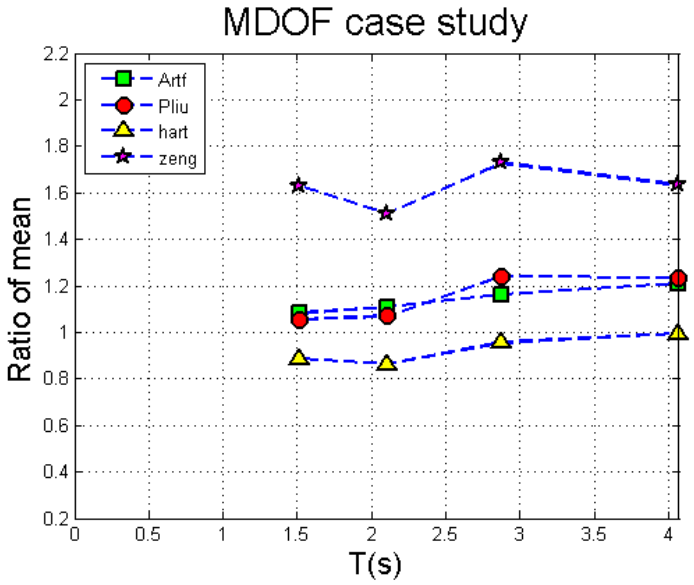

Figure 5. 14. Ratio of medians of the maximum interstory drift ratio for simulated GMs to the corresponding quantity computed for the recorded GMs applied to 4 realistic steel moment frame for Northridge earthquake.

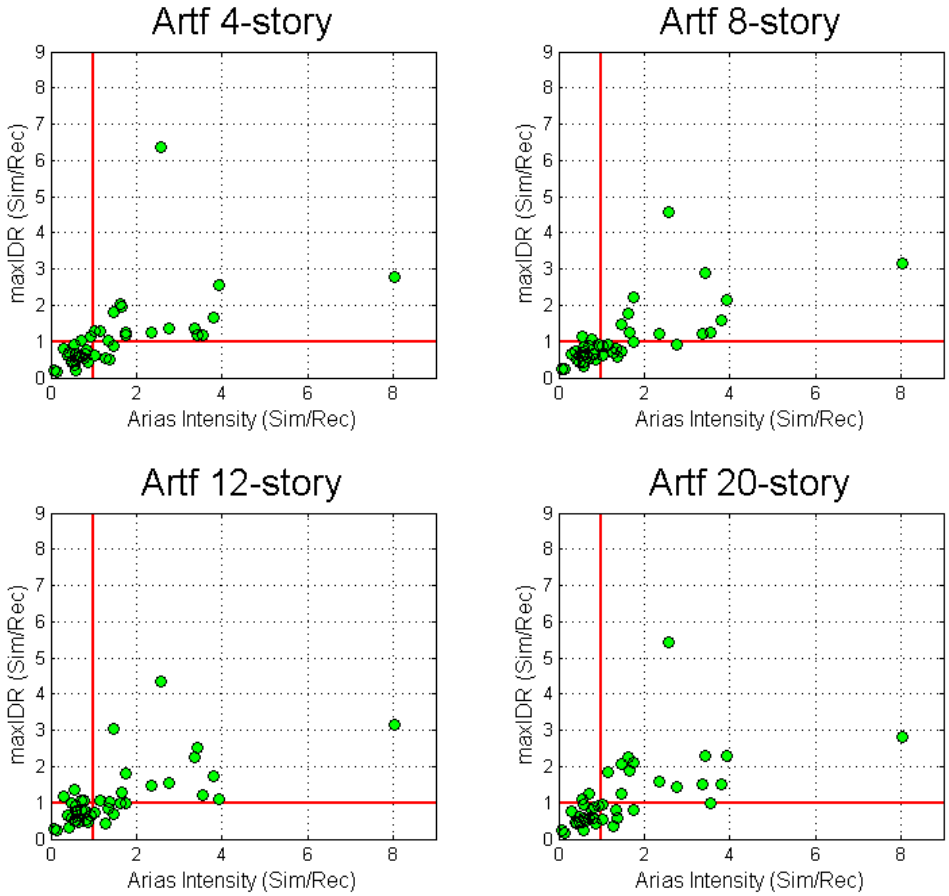

Figure 5. 15. Scatter plots of Arias Intensity vs maximum interstory drift ratio for simulations by Artf.

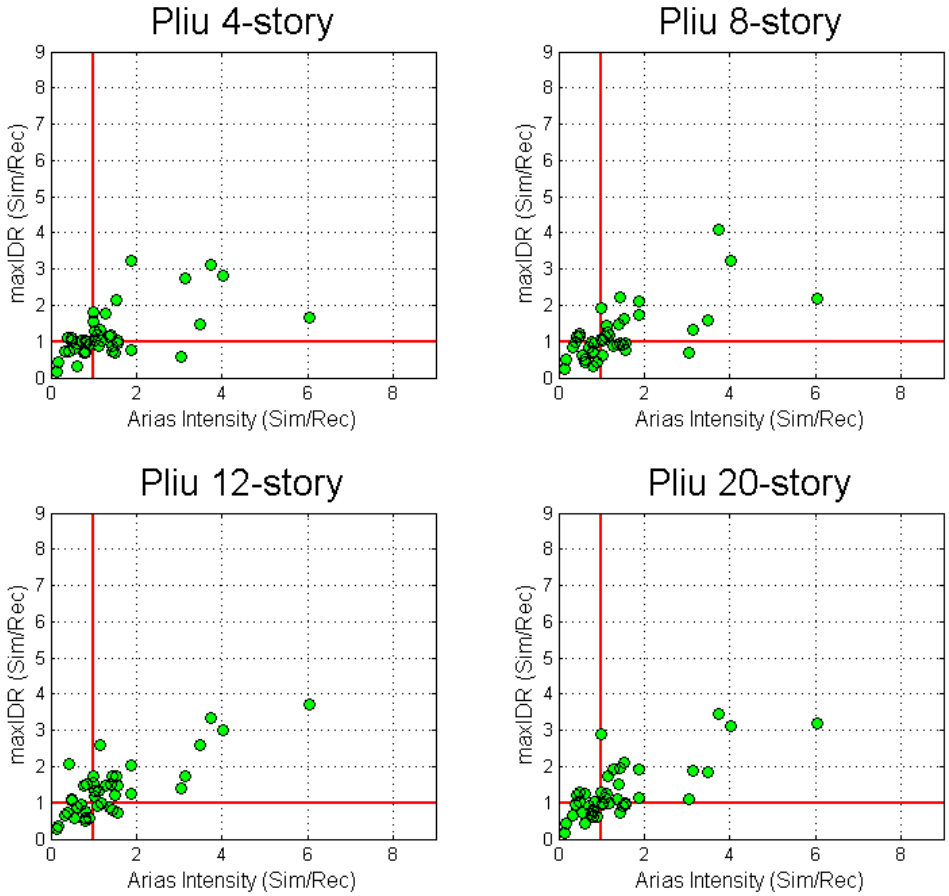

Figure 5. 16. Scatter plots of Arias Intensity vs maximum interstory drift ratio for simulations by Pliu.

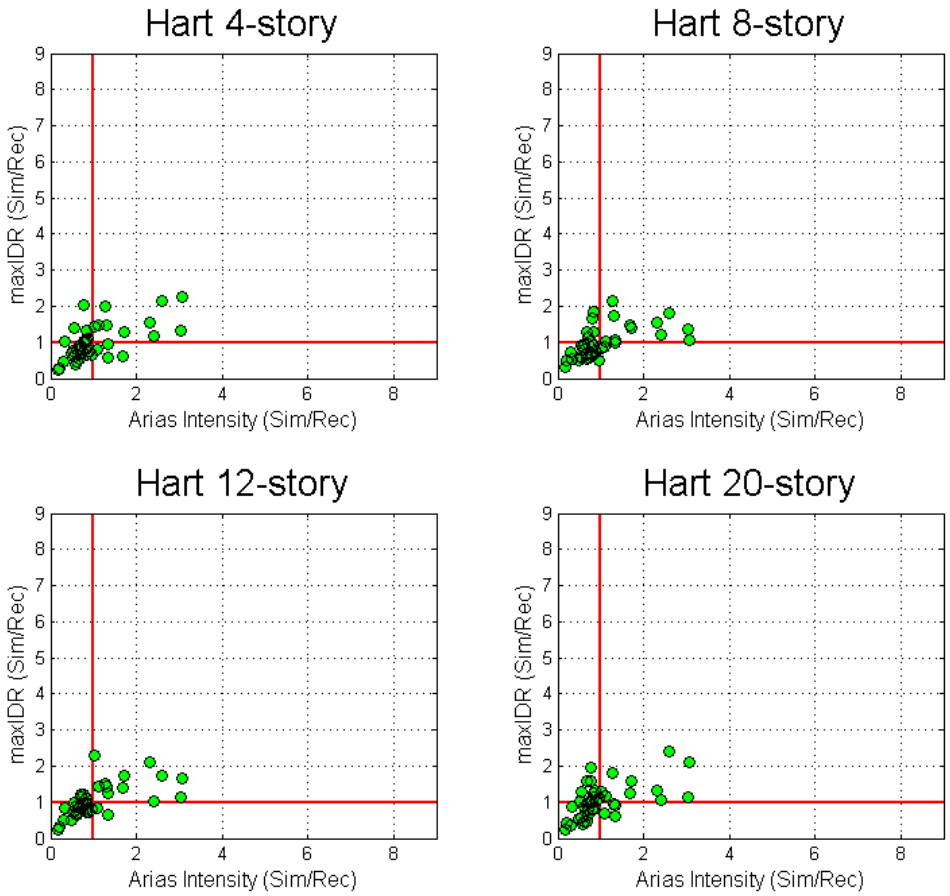

Figure 5. 17. Scatter plots of Arias Intensity vs maximum interstory drift ratio for simulations by Hart.

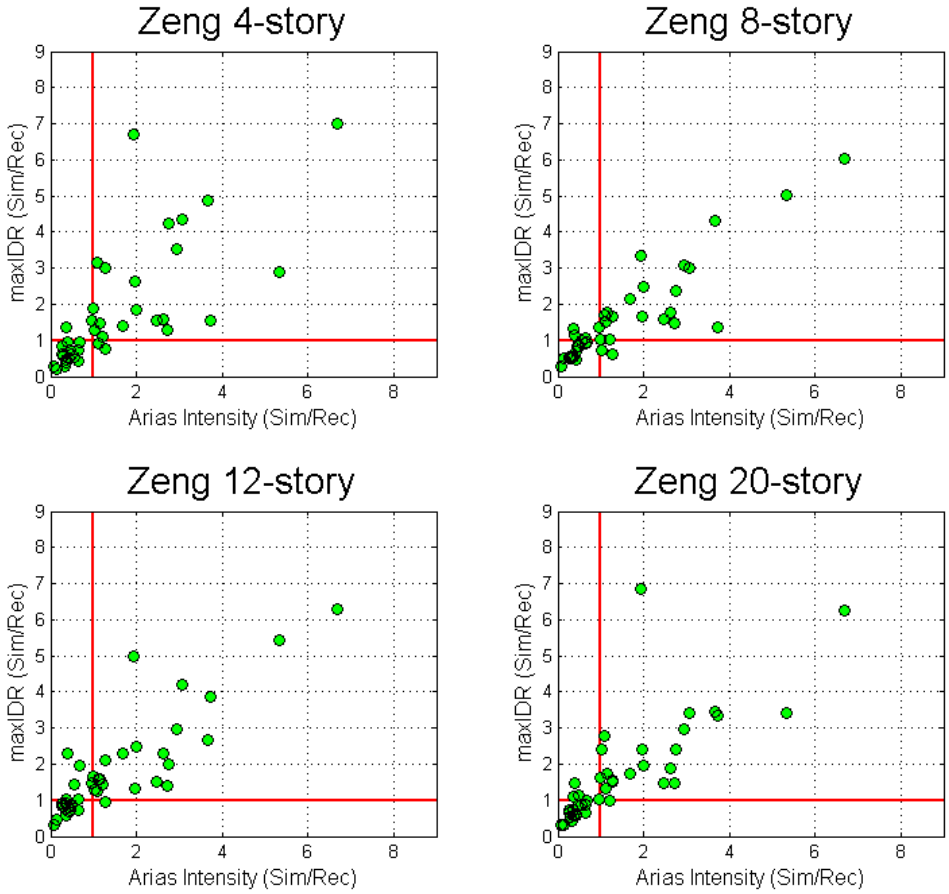

Figure 5. 18. Scatter plots of Arias Intensity vs maximum interstory drift ratio for simulations by Zeng.

5.5 Summary and CONCLUSIONS

Recently, simulated ground motions have been gaining attention, specifically in terms of engineering applications. Simulated ground motions are now considered to be viable options along with recorded ground motions for building seismic performance assessment and design. However, there are serious doubts regarding the accuracy of simulated ground motions in terms of their representation of recorded motions. This leads to limitation of simulated ground motions in engineering applications. Validating simulated ground motions must be conducted to provide engineers with confidence when using them.

In this part of our research we decided to take a step forward and analyze the effect of waveform parameters on engineering demand parameters (EDPs). The intention of this study is to build a bridge between ground motion simulators and engineers in order to enhance simulations.

This study investigates four scalar parameters: Arias Intensity (I_a), Duration (D_{5-95}), Mid-Frequency (ω_{mid}), and rate of change of frequency (ω'), and determines their effect on structural response, in terms of engineering demand parameters. By adopting the result of correlation analysis (Rezaeian and Der Kiureghian, 2010), the marginal probability distribution of a single parameter conditioned on other three parameters are derived. Synthetic ground motions are generated for the given scalar key parameters using fully nonstationary stochastic model,

We investigated the sensitivity of response of a variety of SDOF systems to variation in scalar parameters. The studied SDOF systems include variations in backbone curve, nonlinearity levels, and eleven fundamental periods. Results of this study show that building response is proportional to Arias Intensity. The effect of frequency at mid-time to EDP is sensitive to the natural frequency of the structure. The ground motion with ω_{mid} close to the natural frequency of the structure experiences resonance and is inclined to yield and develop large displacements in inelastic structures. Along with this, duration only shows its effect on inelastic SDOF systems with short periods. Conditioned on the same Arias Intensity, ground motions with a short duration tend to have large amplitudes, which may lead inelastic behavior and exhibit large displacements.

A case study was conducted using synthetic ground motions generated using four simulation methods for SDOF and MDOF systems and the importance of Arias Intensity as a

ground motion simulation validation scalar parameter is verified. Our analysis shows that the simulations made by Zeng tends to create large displacements due to the overestimation of the Arias Intensity. The results in these case study may be used as feedback to seismologists and can assist in updating simulation methods with the intent of making simulated ground motions more practical in engineering applications.

CHAPTER 6: CONCLUSIONS

Earthquake ground motion records are used as inputs for seismic hazard analysis, development of ground motion prediction equations, and nonlinear response history analysis of structures. The natural recordings have certain limitations, such as missing data for large magnitude events at short distances, containing unrealistic frequency content when scaled in GMSM. Given that, simulated ground motions are gaining more attention and can be an effective surrogate to recorded ground motions. Based on different assumption, simulated ground motions can be categorized as stochastic based, physics (deterministic) based, and a hybrid approach. Physics based simulation provides a better representation of the whole ground motion generation process, such as fault rupture, wave propagation phenomena, and site response characterization. Because of their less computation cost, stochastic based simulation is efficient and popular among engineers. With the balance of accuracy and efficiency, hybrid simulation is proposed with deterministic content at low frequency and stochastic content at high frequency.

Despite ground motion simulations advantages, engineers are still worried about the stability in ground motion simulation process and similarity between response of engineered structures to similar simulated and recorded ground motions. In order to draw simulated ground motions into engineering applications and make them practical, this dissertation is concentrated on ground motion simulation validation and application in structural engineering.

Because the simulation methods are still developing, our intent is not on ranking or classifying ground motion simulation methods, but rather to develop ground motion simulation validation framework to provide feedback to simulators to update ground motion simulation techniques such that future simulations are more representative of recorded motions. The simulation validation framework is looks into four steps: 1) identify ground motion waveform

parameters that well correlate with response of Multi-Degree of Freedom (MDOF) buildings and bridges, 2) develop goodness-of-fit measures and error functions that can describe the difference between simulated and recorded ground motion waveform characteristics and their effect on MDOF systems, 3) device the required update to ground motion simulation methods through which better simulations are possible, 4) assess the current state of simulated ground motions for engineering applications.

6.1 GROUND MOTION SIMULATION VALIDATION IN TALL BUILDING RESPONSE ASSESSMENT MAJOR FINDGS

Instead of waveform comparison, engineers are more interested in if synthetic motions can predict the similar result in seismic assessment. The validation tool, the elastic MDOF systems with period ranging from 0.1s and 6s, is proposed. The ratio of median and standard deviations of maxIDR for simulation to the one of natural recording is investigated. Results are able to show if structural response estimated by using simulated records generally matches the response obtained using recorded motions. We use a hybrid broadband simulation simulated by Graves and Pitarka for this validation exercise. Result shows simulation and recorded ground motions generally match in structural response, except in the short periods part of spectra, where the simulation is generated by stochastic calculation. Hypothesis tests are conducted, and statistically significant difference in response is observed in the short periods range. In the second part, two nonlinear SMFs are used as case studies. Nonlinear interstory drift ratio and peak floor acceleration distributions over building height was studied; statistics are obtained and compared for both recorded and simulated time histories. Results of this analysis show that simulation matches well the inelastic demands produced by recorded ground motions, at least for the cases made here.

6.2 GROUND MOTION SIMULATION VALIDATION IN WAVEFORM PARAMETERS

We assess the validity of simulated ground motions using three time-dependent validation metrics that characterize the evolution of intensity and frequency content. Simulated ground motions are validated against records of historic events. These time-varying properties of earthquake ground motions are important in engineering applications because they influence linear and nonlinear structural responses. The difference between each metric for simulated and recorded motions is quantified using a single number that represents the average error over the entire duration of motion. The scalar key parameters extracted from the first two validation metrics are introduced: I_a,D_{5-95}, t_{mid} , I_a/D_{5-95} , ω_{mid} and ω'. These parameters represent the total energy, effective duration of motion, time at the middle of strong shaking phase, rate of input energy, frequency at the time of strong shaking, and rate of change of frequency in time.

The proposed methodology can benefit both engineers and seismologist. In this validation, we presented an application of this validation methodology for four type of simulation methods in Northridge earthquake. The three validation metrics and six key parameters were calculated for an example simulated and recorded set of motions from the 1994 Northridge earthquake.

6.3 GROUND MOTION SIMULATION VALIDATION IN BUILDING-CODE APPLICATIONS

In this part of the research, a ground motion simulation validation technique is proposed to demonstrate how simulated and recorded ground motions will result in similar building response used for structural design. In other words, this technique looks into the similarities between building response obtained from suites of simulated and recorded ground motions conditioned that these suits of ground motions are selected using the code based ground motion selection and

scaling （ASEC/SEI 7-10）. Structural systems consisting of steel moment resisting frames is used to demonstrate this approach. The engineering demand parameter of interest is the maximum interstory drift ratio. Three simulation methods including GP, CSM and SDSU are validated. The difference between the demands from simulated and recorded motions was compared using Student's t-test for respective engineering demand parameter distributions. Results show that the structural behavior resulting from recorded ground motions and simulated ground motions are statistically significantly different. The sets of simulated ground motions clearly overestimate the response compared to the recorded motions. The difference stems from the fact that ground motion simulation models are more likely to generate pulse-like ground motions, which tend to create larger displacement of building response. The higher number of pulse-like motions in the population of simulated motions results in a larger number of pulse-like motions in the selected sets, and therefore, imposes higher seismic demands on structures compared to sets derived from natural recordings. Different target spectrums have unique spectrum shapes, and it may change the order of priority in the selection of pulse-like ground motions. However, as the number of desired selected motions increases, it is inevitable not to select pulse-like ground motions through the GMSM procedure guided by code.

An updated GMSM technique is proposed to elongate the selecting range to avoid choosing abnormal pulse-like ground motions. And the results indicate that with this updated GMSM technique, the simulated ground motions can be the substitute of nature earthquake hazard for engineering applications in a practical manner.

6.4 SENSITIVITY ANALYSIS OF EFFECT OF SCALAR PARAMETERS ON ENGINEERING DEMAND PARAMETERS

Arias Intensity (I_a), Duration (D_{5-95}), Mid-Frequency (ω_{mid}), and rate of change of

frequency (ω'), are investigated to see how they affect structure response in term of EDP. With understanding about the correlation among these parameters, conditional probability distribution of one parameter given other three parameters is derived. The sensitivity study conducted on SDOF systems with different backbones curves, different levels of nonlinearity, and eleven fundamental periods show that building response is highly proportional to Arias Intensity. Effect of the frequency at mid-time on EDP is important for nonlinear systems. Meanwhile, there is no clear trend that duration, rate change of frequency impact the EDPs in the linear domain. A case study with four different simulation method are fulfilled in MDOF systems to prove the aforementioned relationship between scalar parameters and EDPs. This results may be a valuable feedback for seismologists to understand where they should pay attention to rectify, when they generate synthetic ground motions.

6.5 FUTURE WORK

This dissertation proposed a framework for validating ground motion simulations for engineering applications. Further study may be implemented to expand this framework to:

- Utilize other ground motion waveform parameters, for instance, the pulse index and pulse period to assess the validity of simulated ground motions；
- Utilize other engineering demand parameters, such as floor response spectra, cumulative hysteretic energy, and estimated loss to assess the validity of simulated ground motions;
- Utilize a larger variety of MDOF models, such as wooden or concrete structures and buckling brace frames；
- Since simulation methods are still being updated, future work will also involve using this framework to validate future simulation methods.

Appendix A

For the building-code validation in chapter 4, 72 scenarios with 6 variables are considered. And all of the result are summarized in this appendix. Validation Variables include:

1) Three Broadband Platform simulation methods: GP, CSM and SDSU;
2) Five earthquake events: Northridge, Loma Prieta, Landers, North Palm Spring and Whittier;
3) Three structures: 4-story, 8-story and 20-story steel moment frames;
4) Two target spectra: Uniform Hazard Spectrum and Conditional Mean Spectrum
5) Two hazard levels: Design Basis Earthquake and Maximum Considered Earthquake
6) Two number of ground motions in each set: 7 and 40

Results are consistent with the discovery in chapter 4. In short structures, structural behavior resulting from recorded ground motions and simulated ground motions are different. The difference stems from the fact that simulated motions are mostly pulse like motions. Whereas in high structures, the large natural period bring about long GMSM selecting range (0.2T to 1.5T), the pulse-like ground motions are efficiently eliminating with the long selecting range. And results of simulated and recorded motion are in agreement.

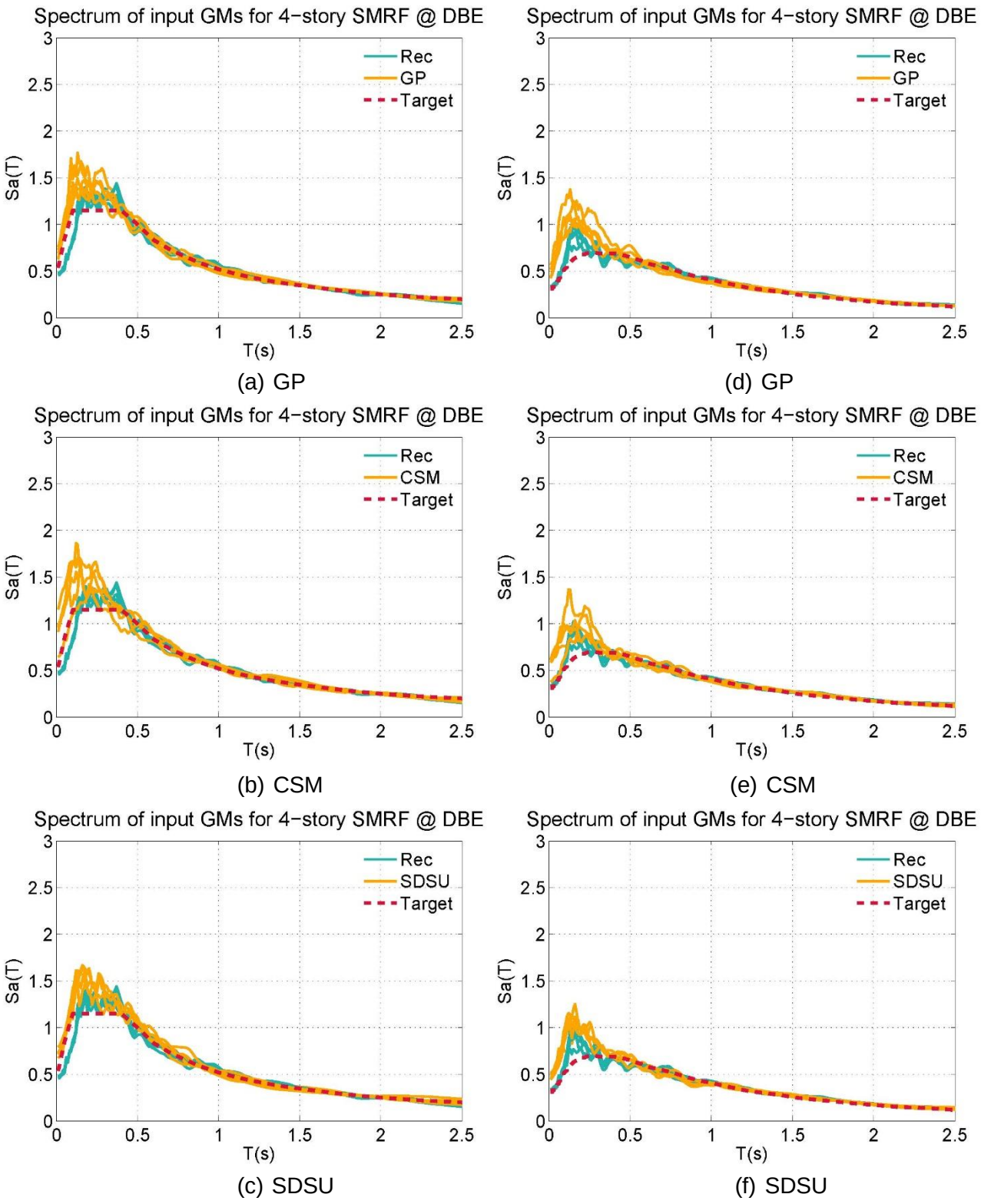

Figure A.1 Average spectra of selected and scaled ground motion sets, 7 per set, to the DBE with UHS (a, b, c) and CMS (e, d, f) target spectrum for the 4-story SMRF

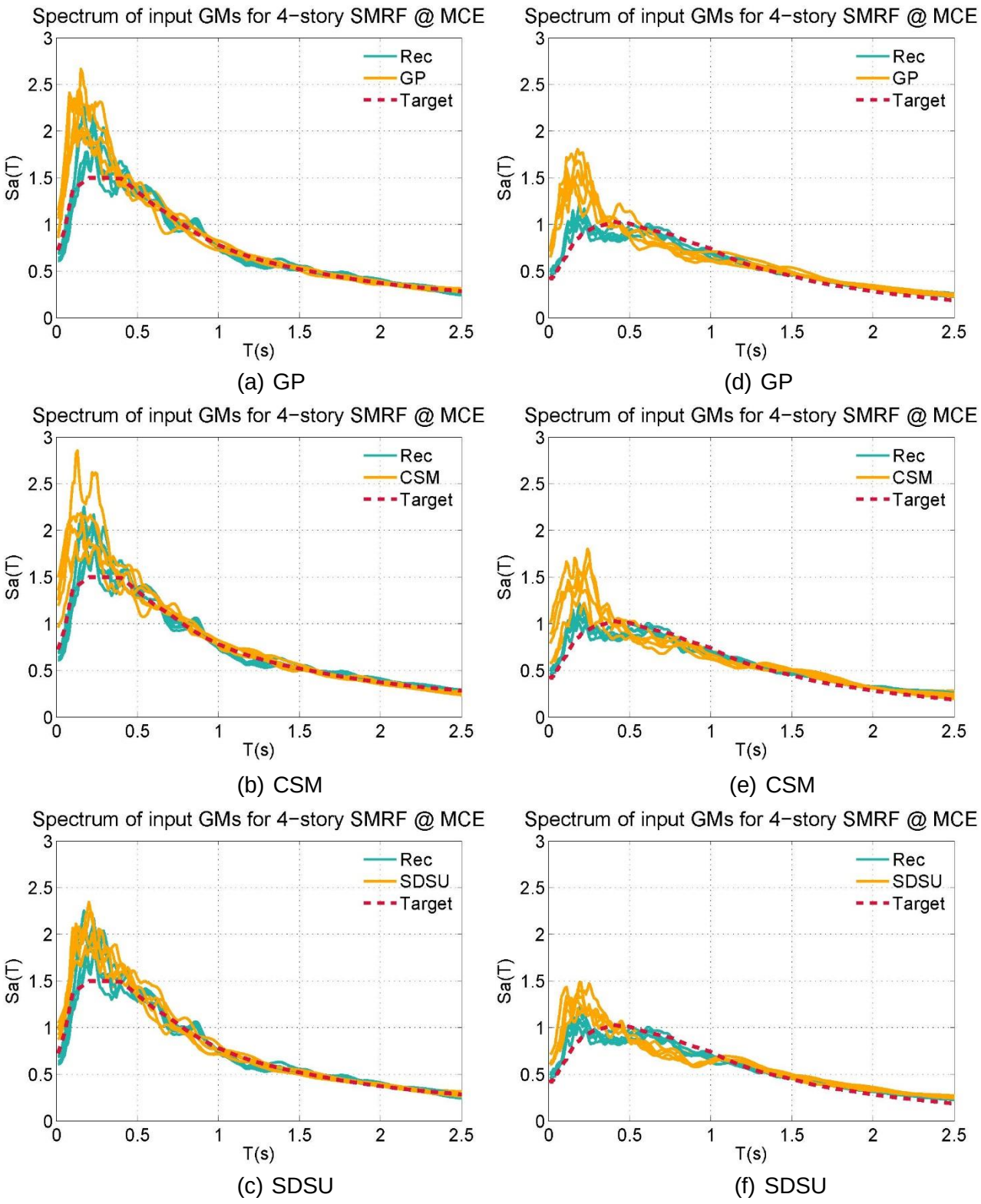

Figure A.2 Average spectra of selected and scaled ground motion sets, 7 per set, to the MCE with UHS (a, b ,c) and CMS (e, d ,f) target spectrum for the 4-story SMRF

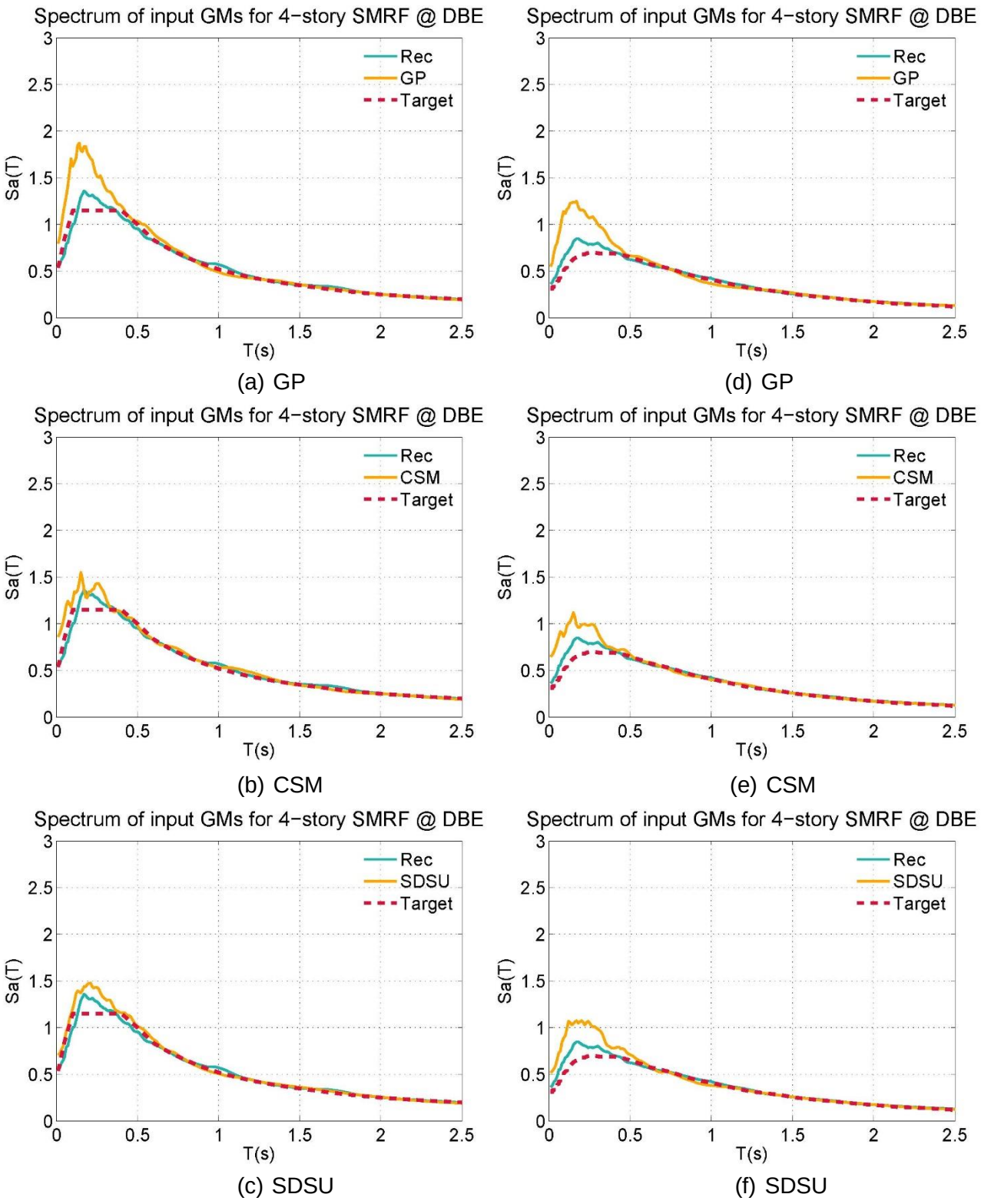

Figure A.3 Average spectra of selected and scaled ground motion sets, 40 per set, to the DBE with UHS (a, b, c) and CMS (e, d, f) target spectrum for the 4-story SMRF

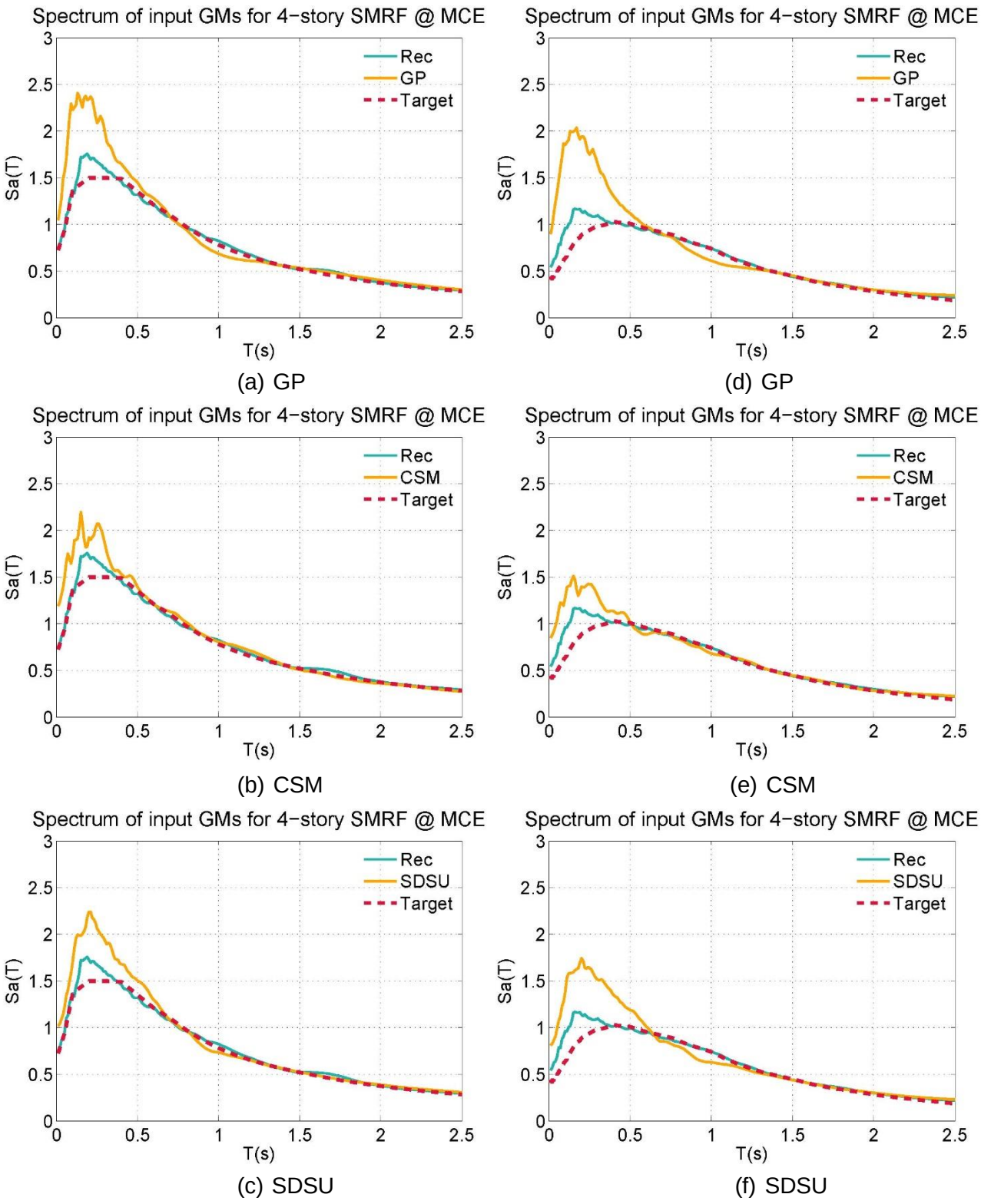

Figure A.4 Average spectra of selected and scaled ground motion sets, 40 per set, to the MCE with UHS (a, b ,c) and CMS (e, d ,f) target spectrum for the 4-story SMRF

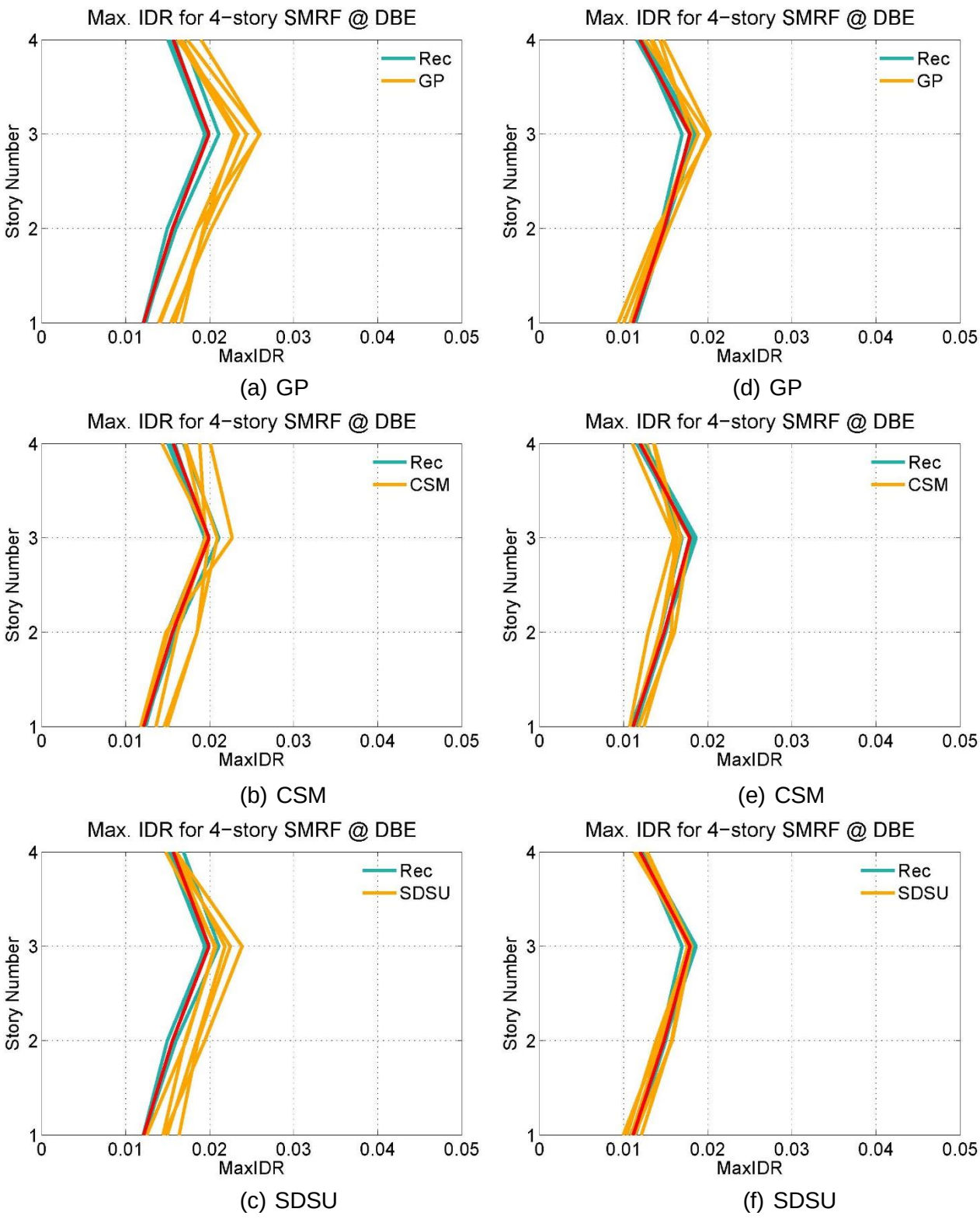

Figure A.5 Average maximum interstory drift ratio of the 4-story SMRF (DBE with UHS (a, b ,c) and CMS (e, d ,f), 5 sets of 7)

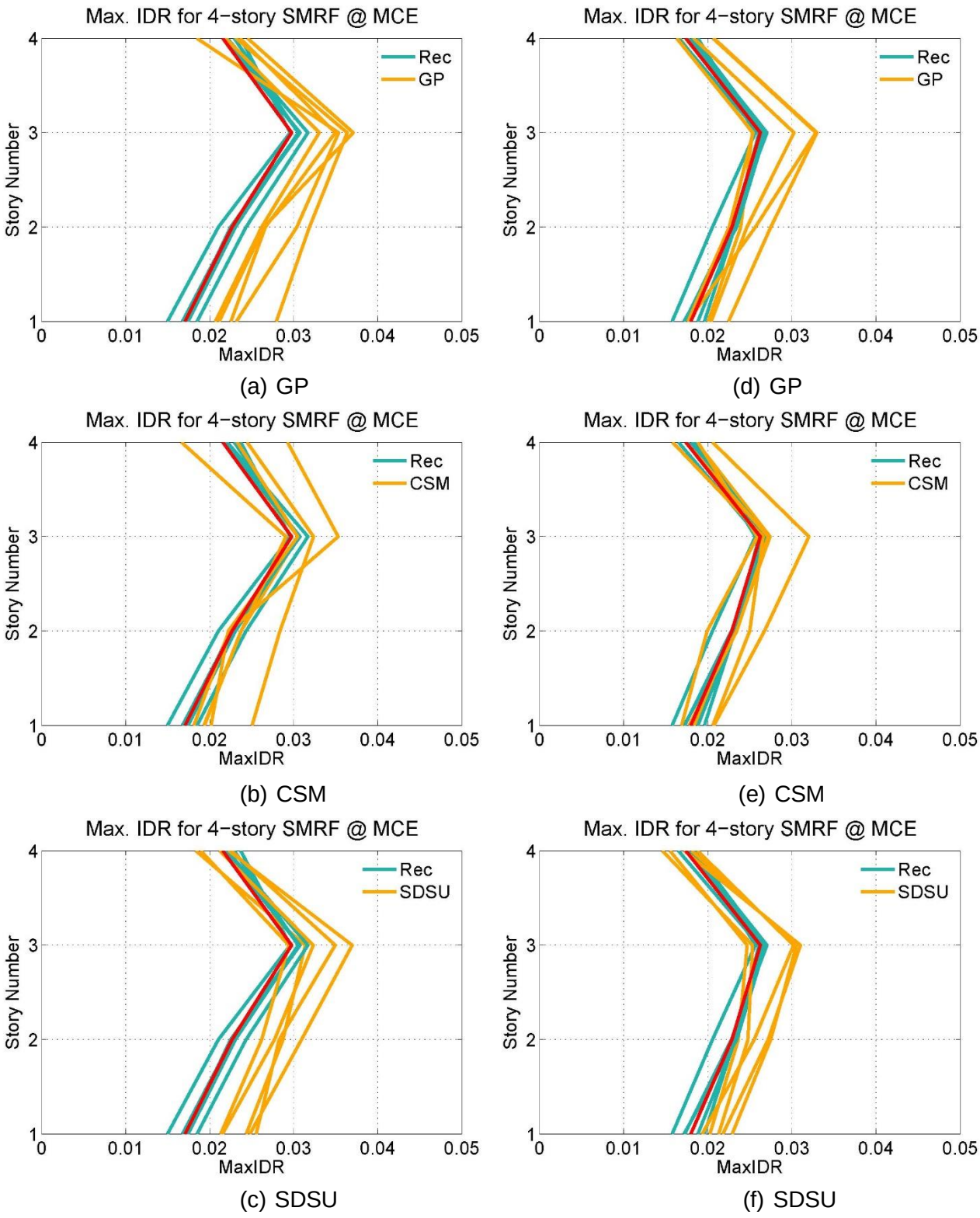

Figure A.6 Average maximum interstory drift ratio of the 4-story SMRF (MCE with UHS (a, b ,c) and CMS (e, d ,f), 5 sets of 7)

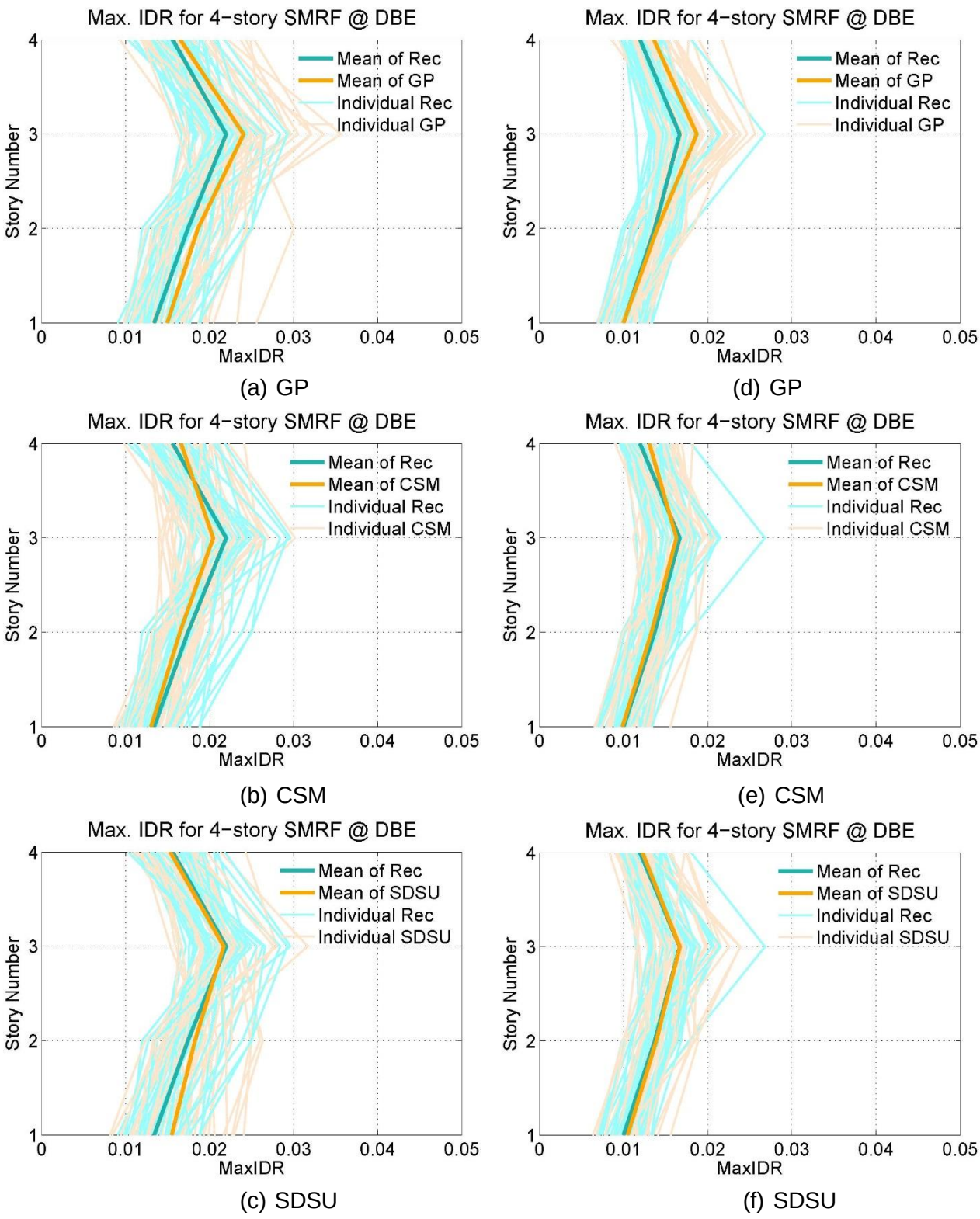

Figure A.7 Average maximum interstory drift ratio of the 4-story SMRF (DBE with UHS (a, b ,c) and CMS (e, d ,f), 1 sets of 40)

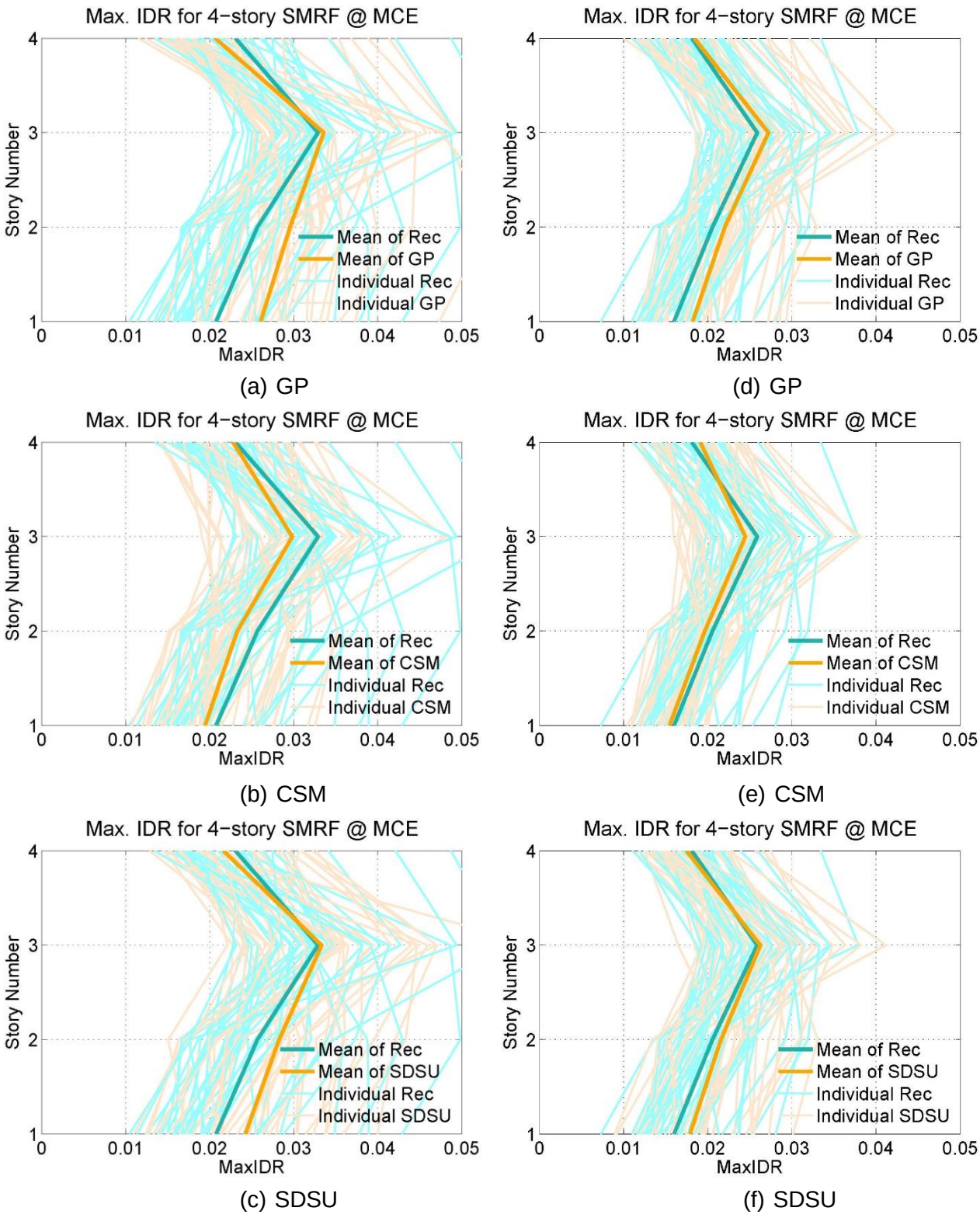

Figure A.8 Average maximum interstory drift ratio of the 4-story SMRF (MCE with UHS (a, b, c) and CMS (e, d, f), 1 sets of 40)

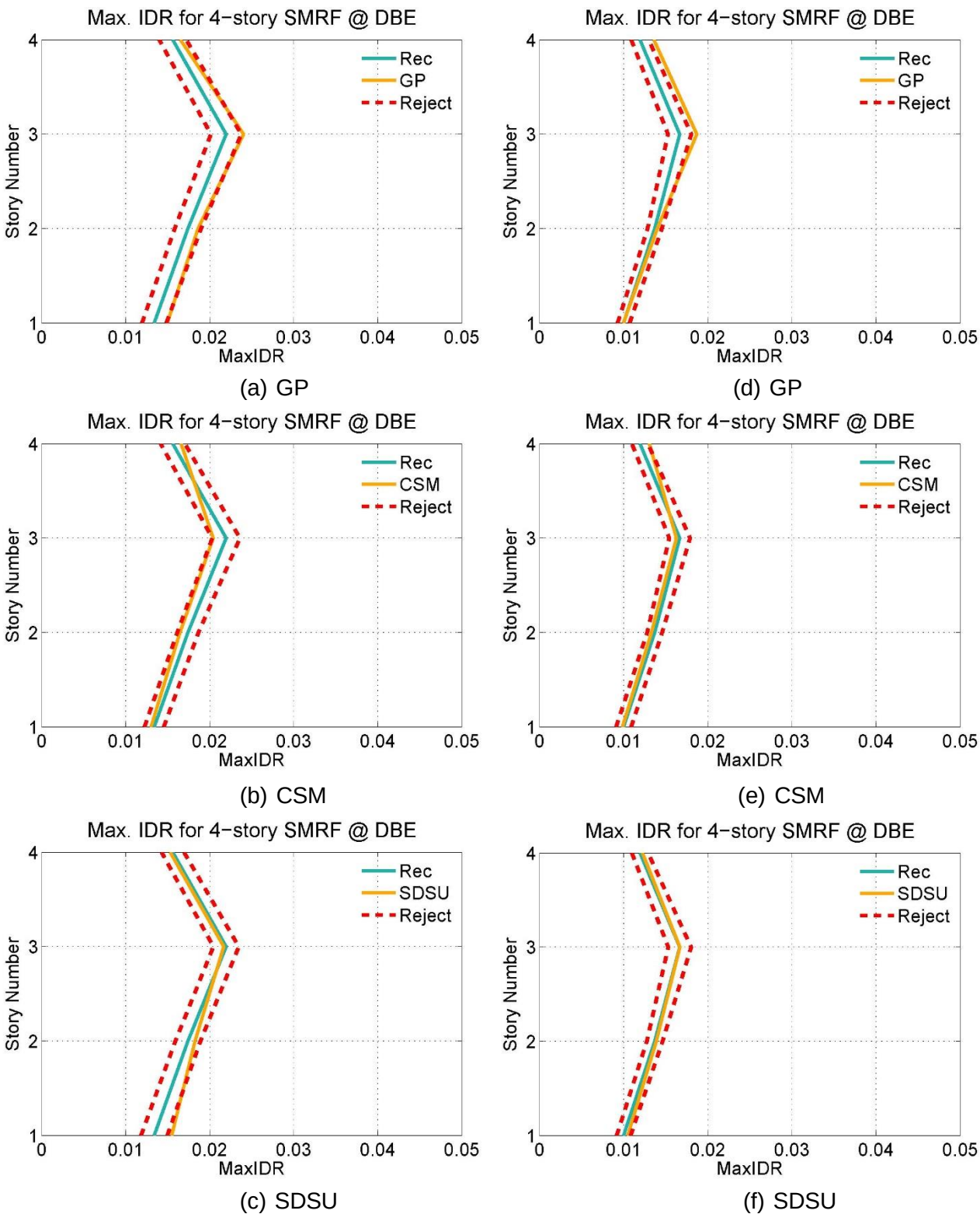

Figure A.9 Average maximum interstory drift ratio of the 4-story SMRF with statistical significant difference boundary (DBE with UHS (a, b, c) and CMS (e, d, f), 1 sets of 40)

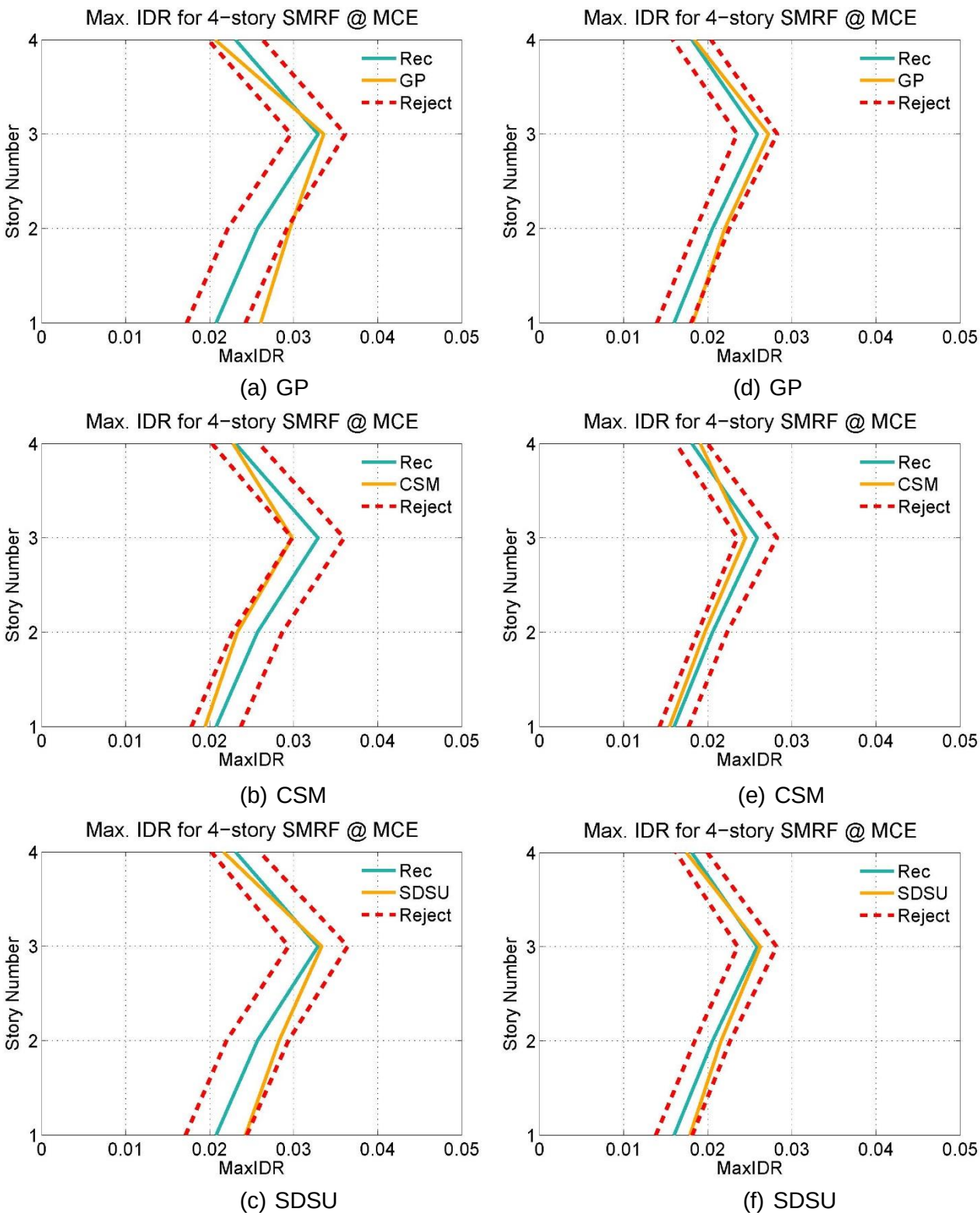

Figure A.10 Average maximum interstory drift ratio of the 4-story SMRF with statistical significant difference boundary (MCE with UHS (a, b, c) and CMS (e, d, f), 1 sets of 40)

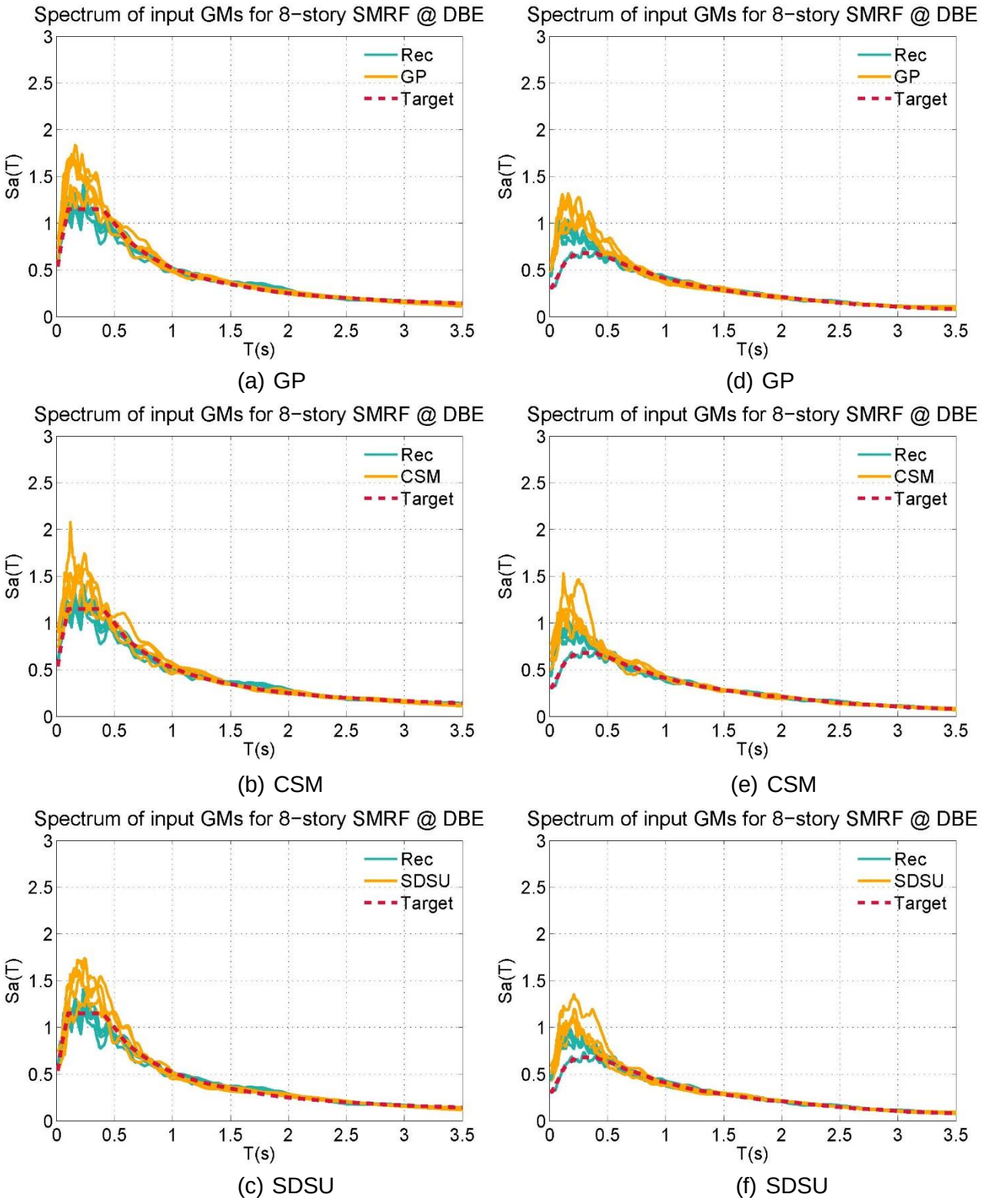

Figure A.11 Average spectra of selected and scaled ground motion sets, 7 per set, to the DBE with UHS (a, b ,c) and CMS (e, d ,f) target spectrum for the 8-story SMRF

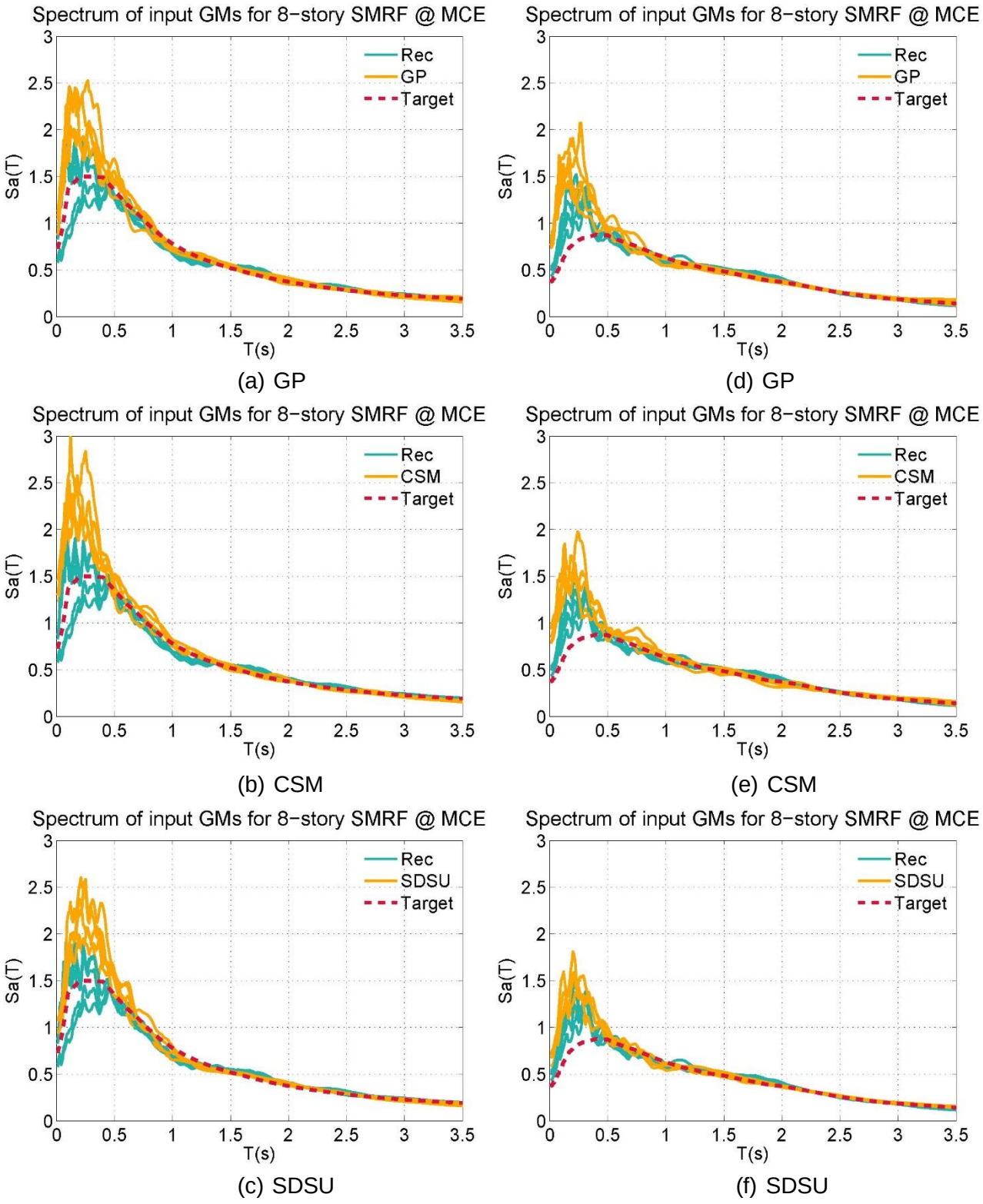

Figure A.12 Average spectra of selected and scaled ground motion sets, 7 per set, to the MCE with UHS (a, b ,c) and CMS (e, d ,f) target spectrum for the 8-story SMRF

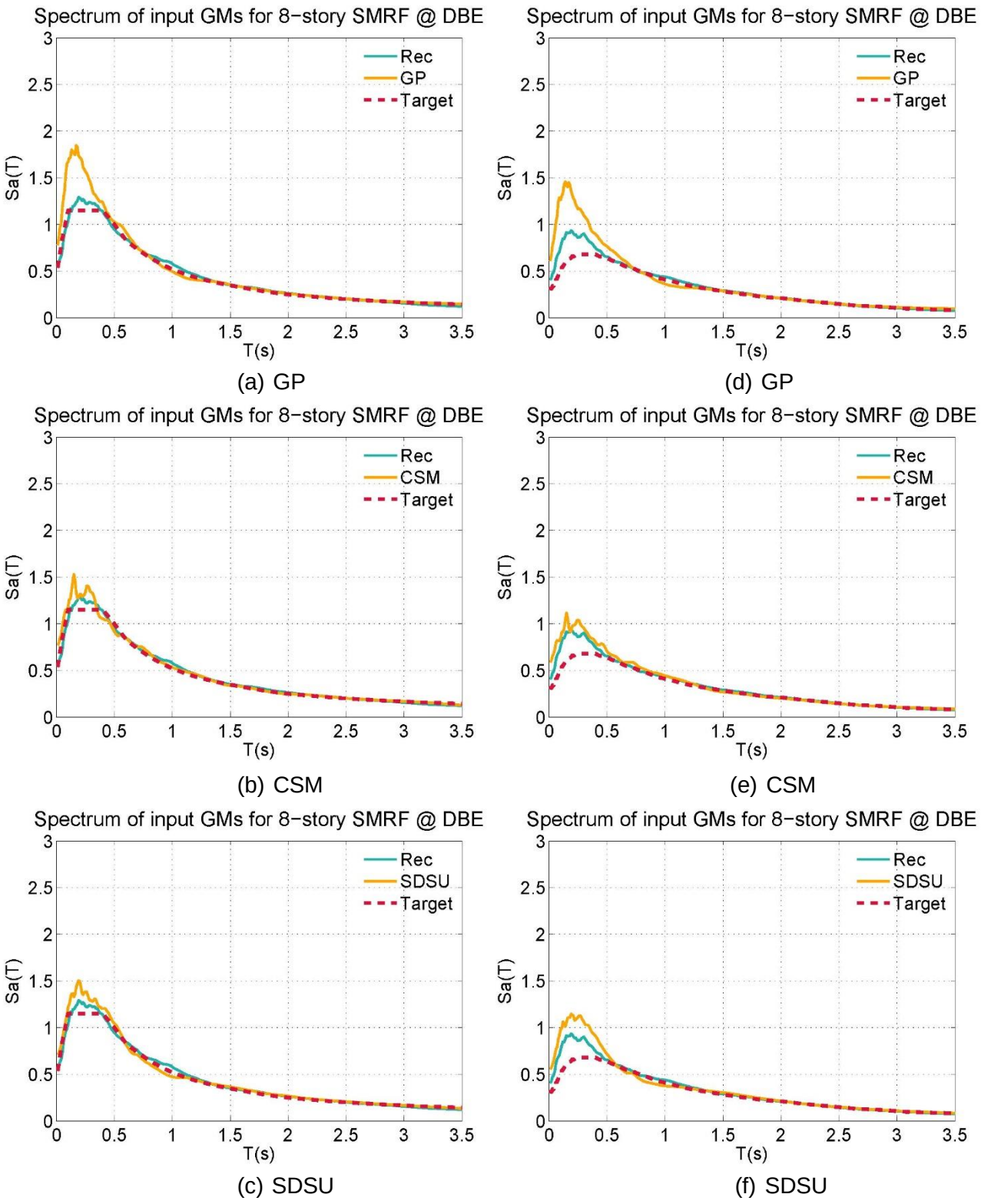

Figure A.13 Average spectra of selected and scaled ground motion sets, 40 per set, to the DBE with UHS (a, b, c) and CMS (e, d, f) target spectrum for the 8-story SMRF

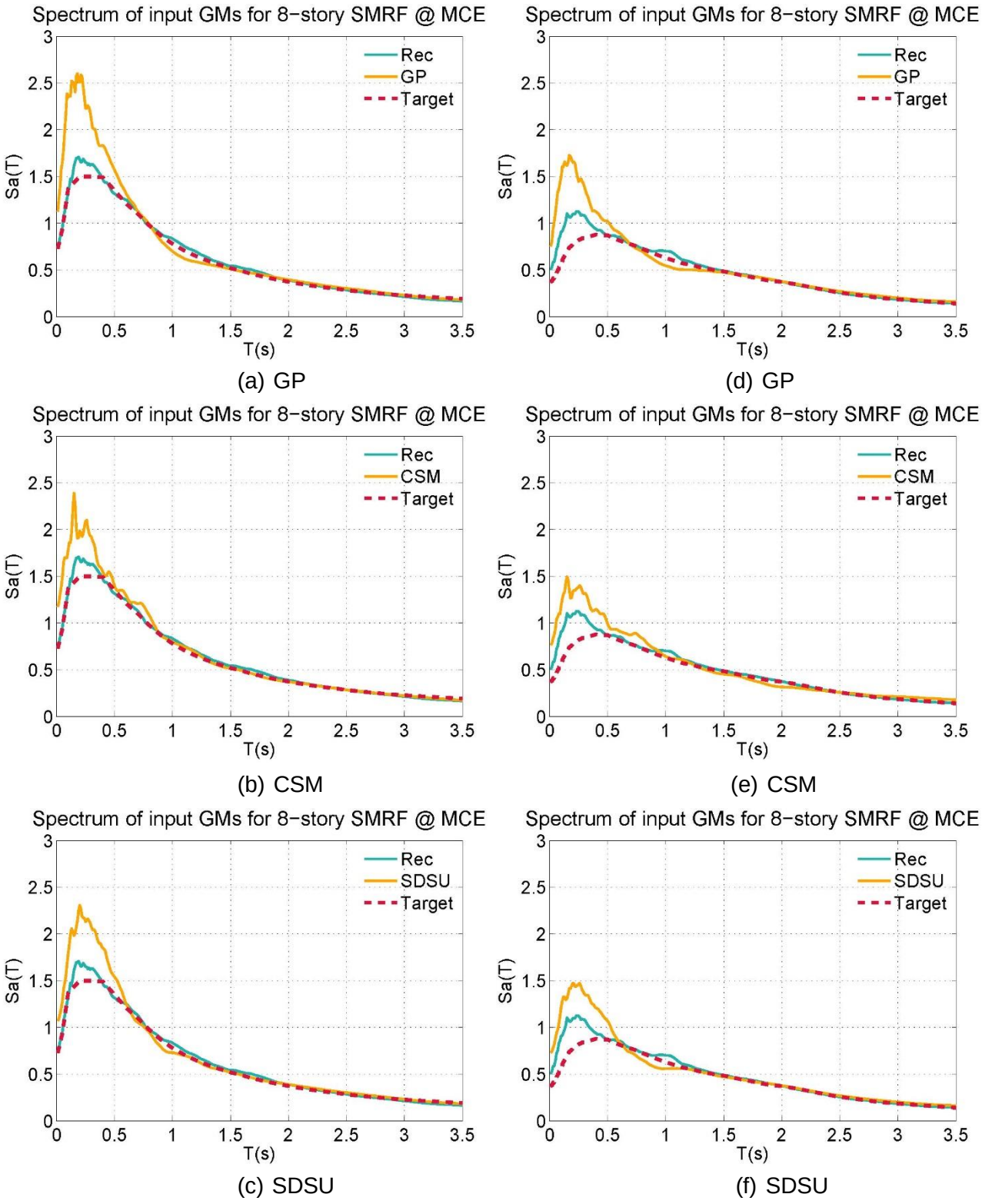

Figure A.14 Average spectra of selected and scaled ground motion sets, 40 per set, to the MCE with UHS (a, b, c) and CMS (e, d, f) target spectrum for the 8-story SMRF

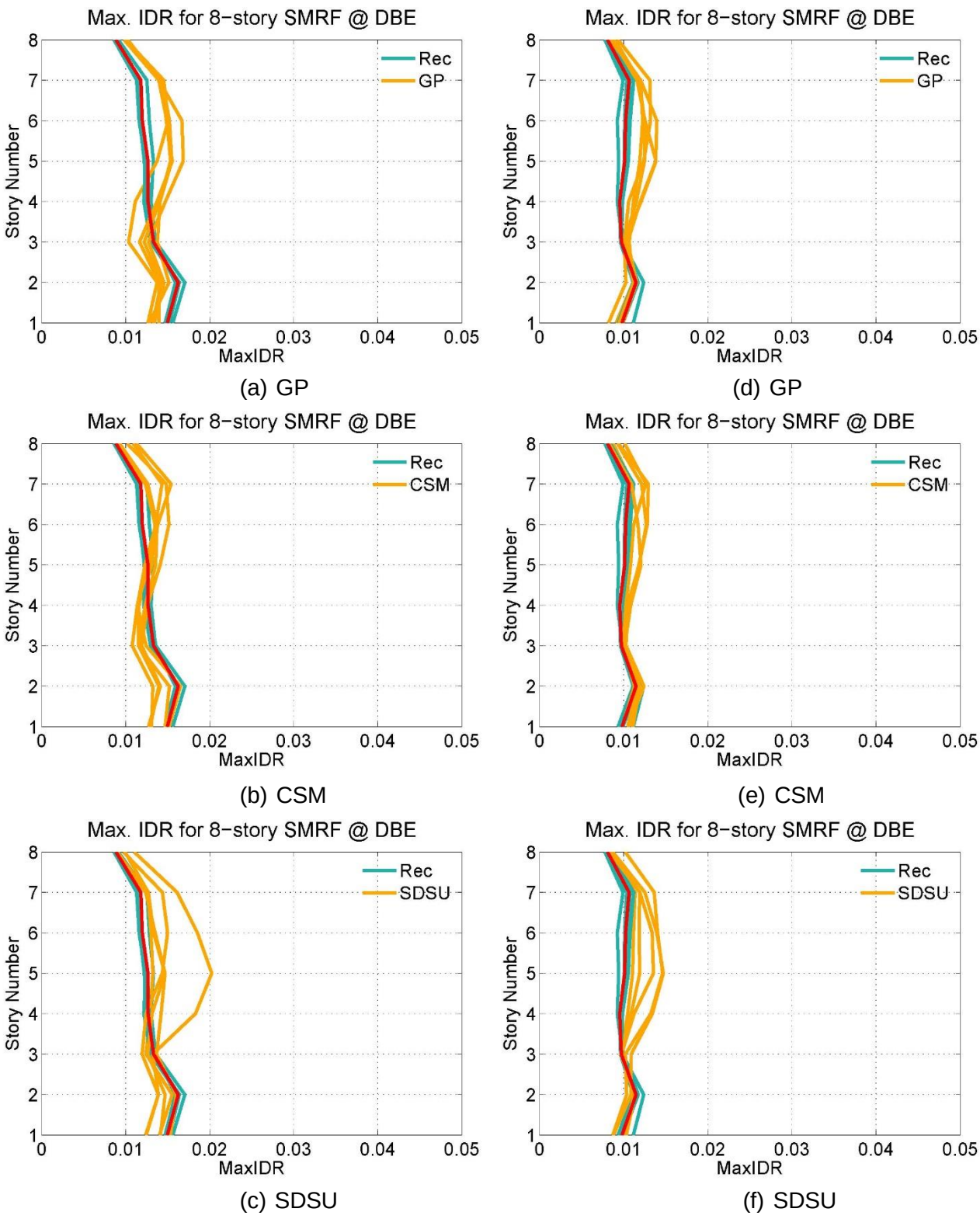

Figure A.15 Average maximum interstory drift ratio of the 8-story SMRF (DBE with UHS (a, b, c) and CMS (e, d ,f), 5 sets of 7)

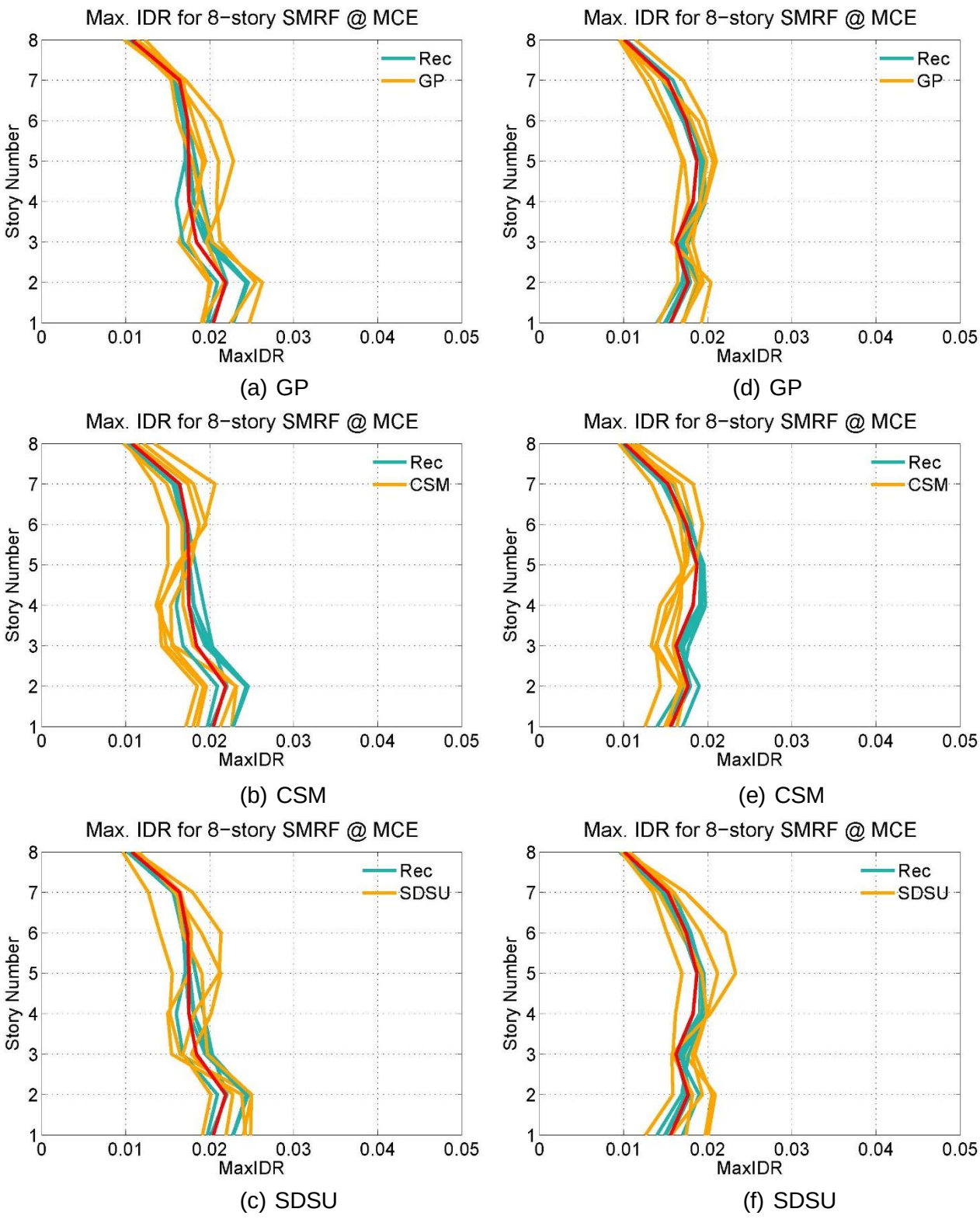

Figure A.16 Average maximum interstory drift ratio of the 8-story SMRF (MCE with UHS (a, b, c) and CMS (e, d, f), 5 sets of 7)

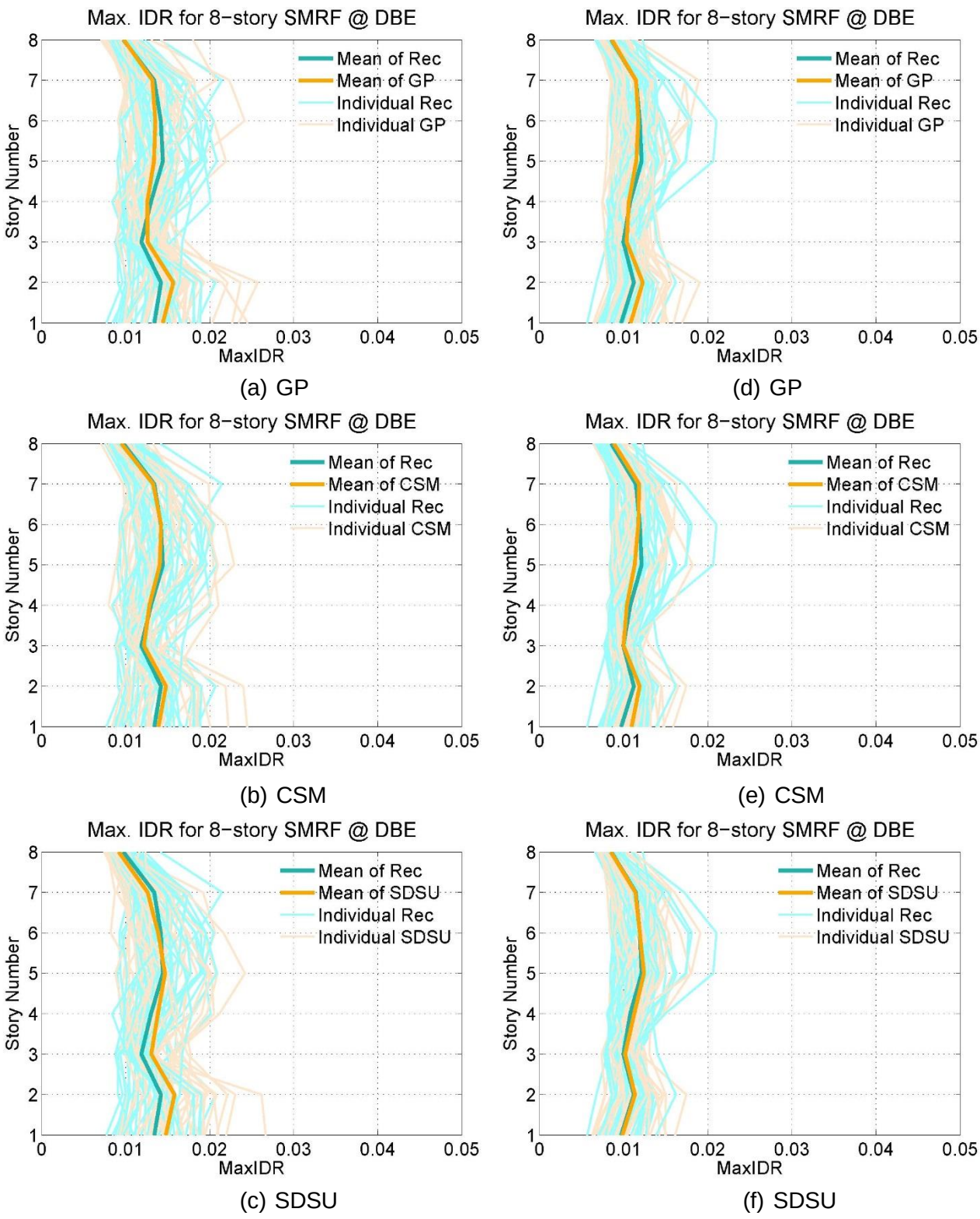

Figure A.17 Average maximum interstory drift ratio of the 8-story SMRF (DBE with UHS (a, b, c) and CMS (e, d, f), 1 sets of 40)

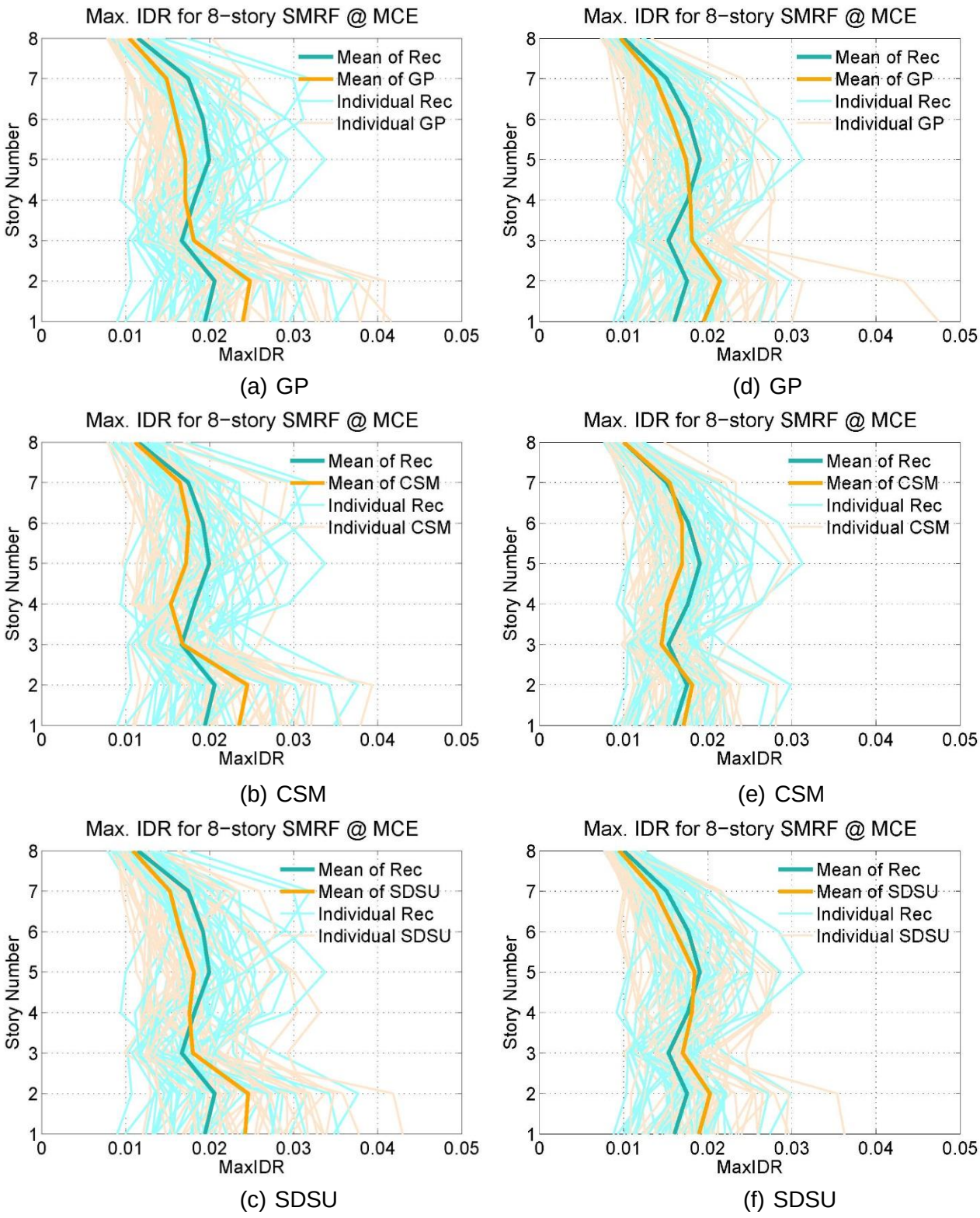

Figure A.18 Average maximum interstory drift ratio of the 8-story SMRF (MCE with UHS (a, b, c) and CMS (e, d, f), 1 sets of 40)

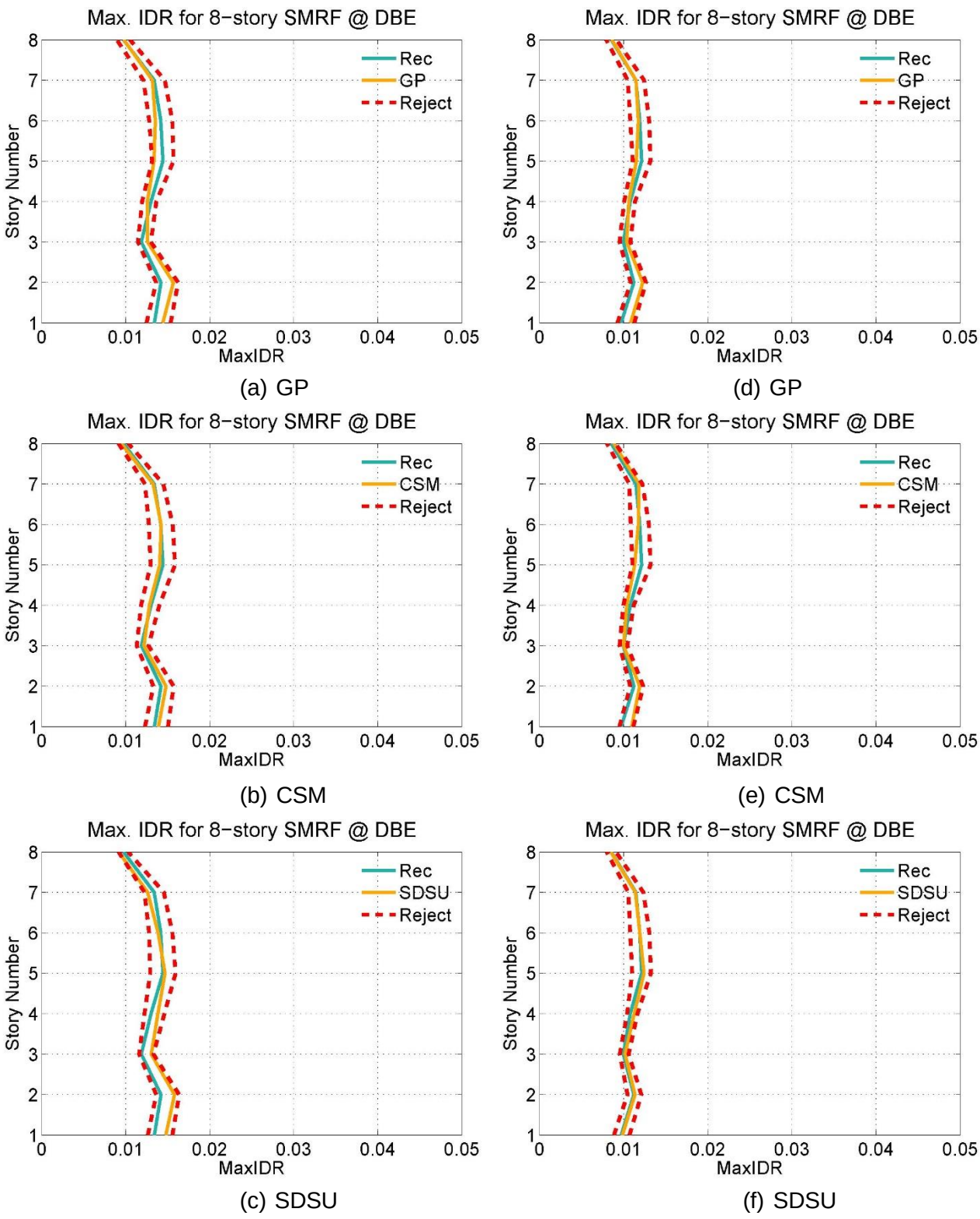

Figure A.19 Average maximum interstory drift ratio of the 8-story SMRF with statistical significant difference boundary (DBE with UHS (a, b, c) and CMS (e, d, f), 1 sets of 40)

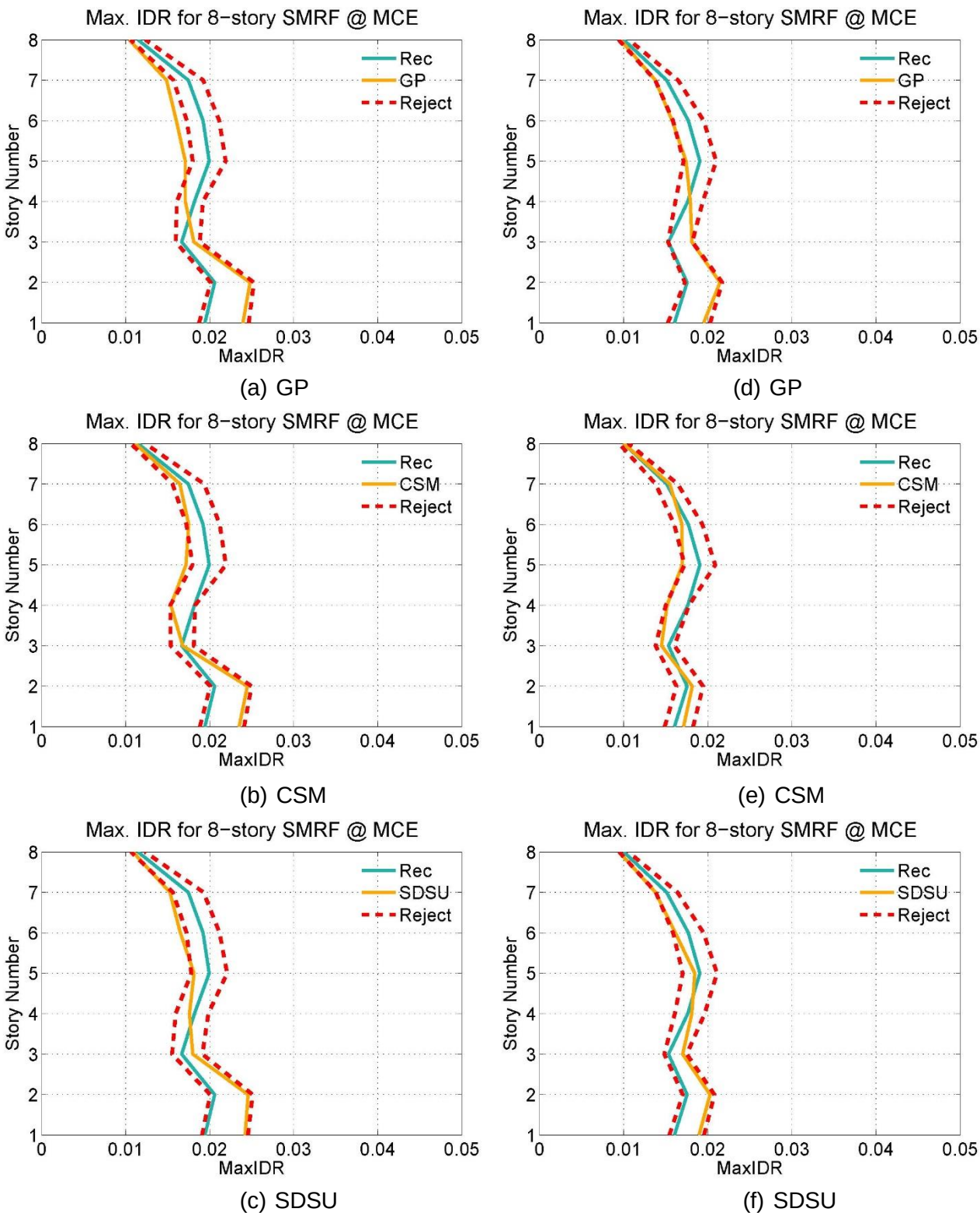

Figure A.20 Average maximum interstory drift ratio of the 8-story SMRF with statistical significant difference boundary (MCE with UHS (a, b, c) and CMS (e, d, f), 1 sets of 40)

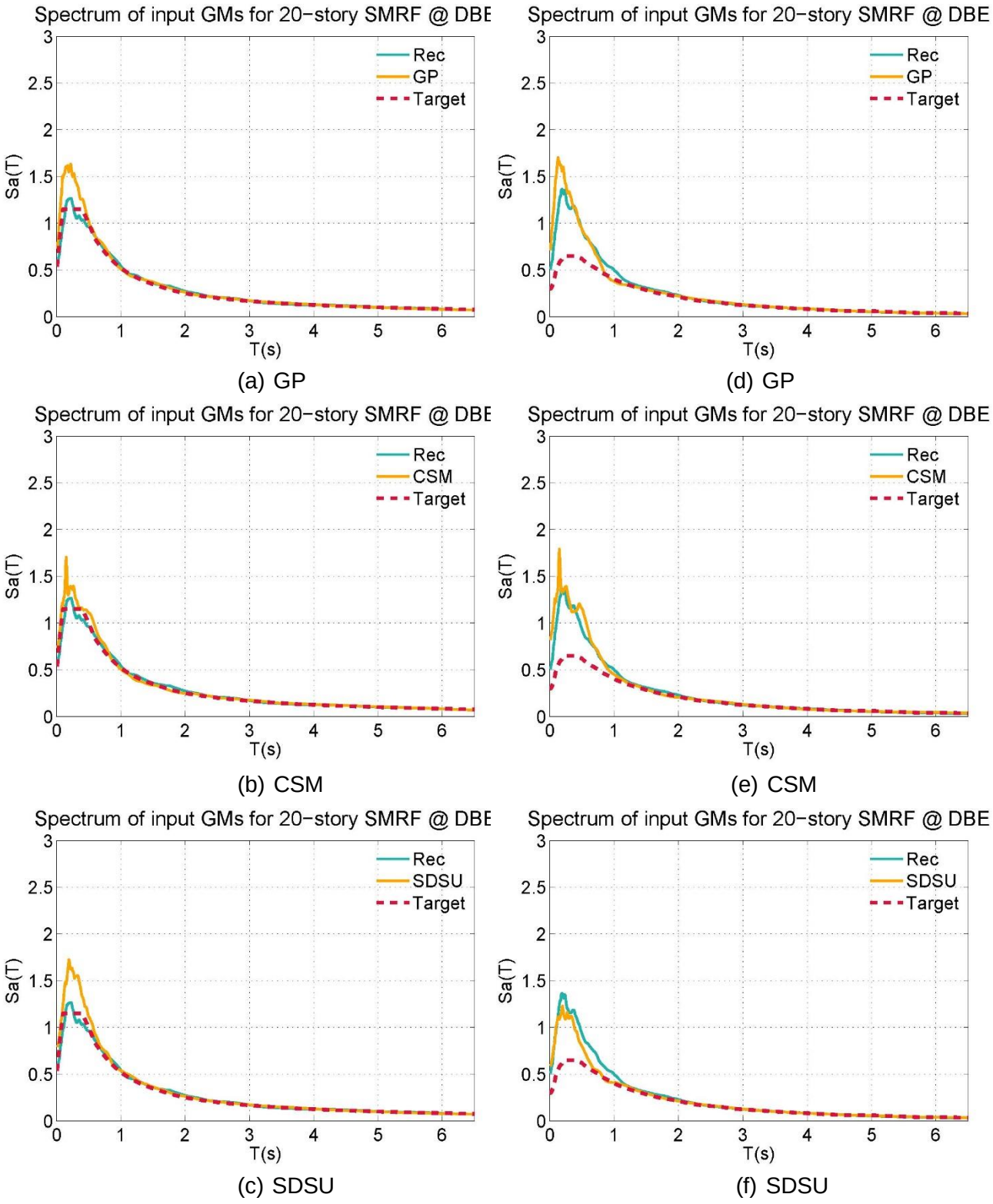

Figure A.21 Average spectra of selected and scaled ground motion sets, 40 per set, to the DBE with UHS (a, b, c) and CMS (e, d, f) target spectrum for the 20-story SMRF

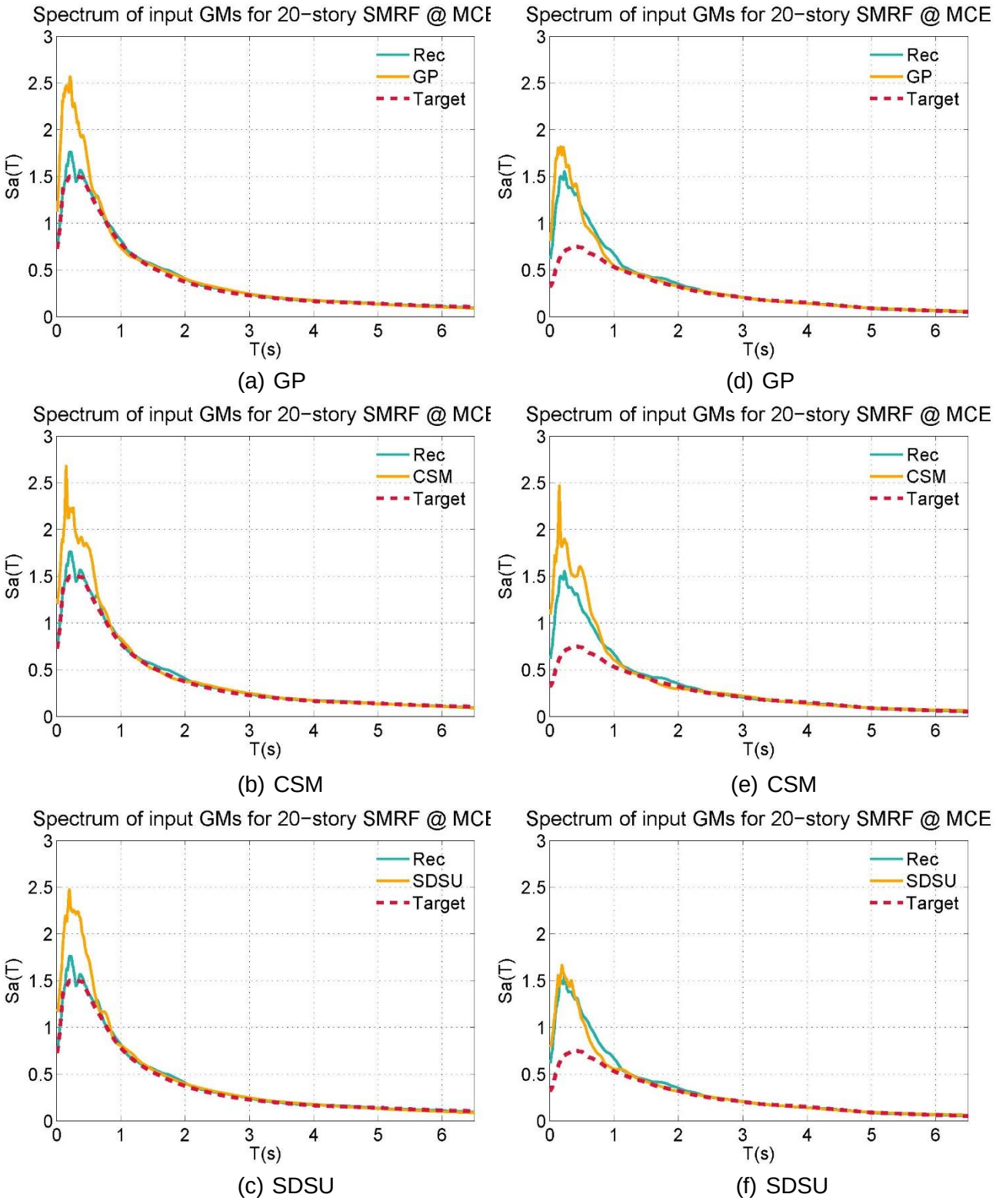

Figure A.22 Average spectra of selected and scaled ground motion sets, 40 per set, to the MCE with UHS (a, b, c) and CMS (e, d, f) target spectrum for the 20-story SMRF

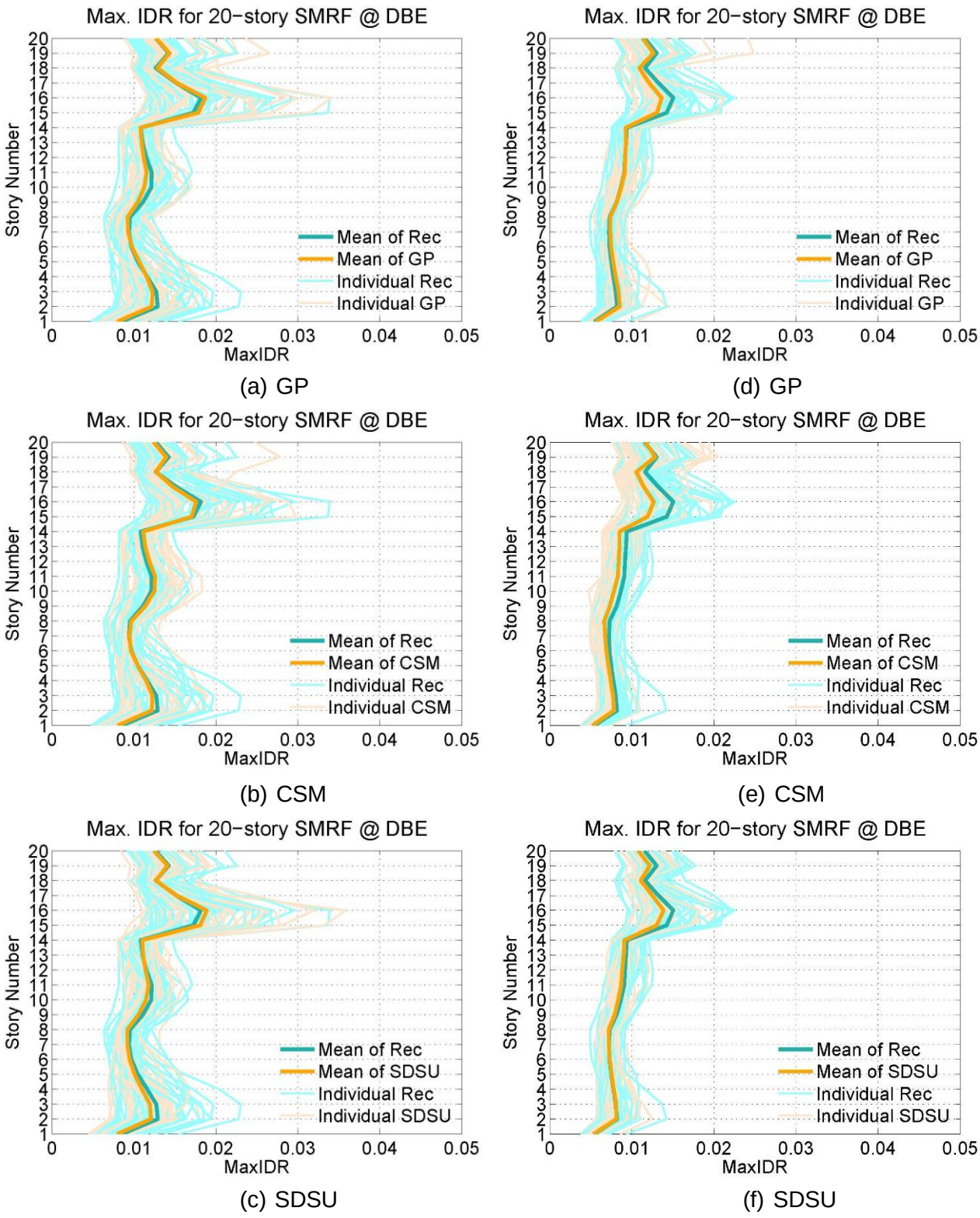

Figure A.23 Average maximum interstory drift ratio of the 20-story SMRF (DBE with UHS (a, b, c) and CMS (e, d, f), 1 sets of 40)

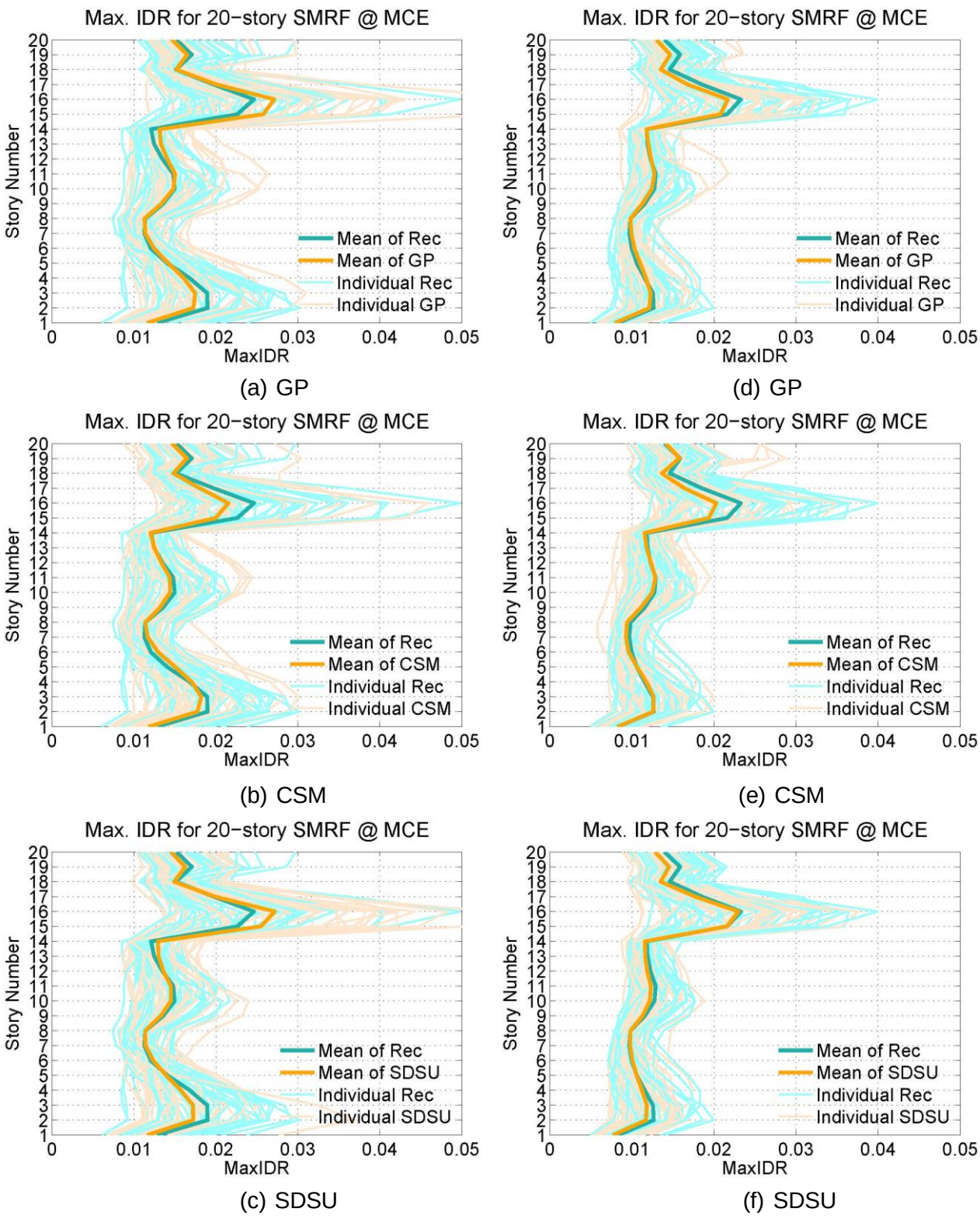

Figure A.24 Average maximum interstory drift ratio of the 20-story SMRF (MCE with UHS (a, b, c) and CMS (e, d, f), 1 sets of 40)

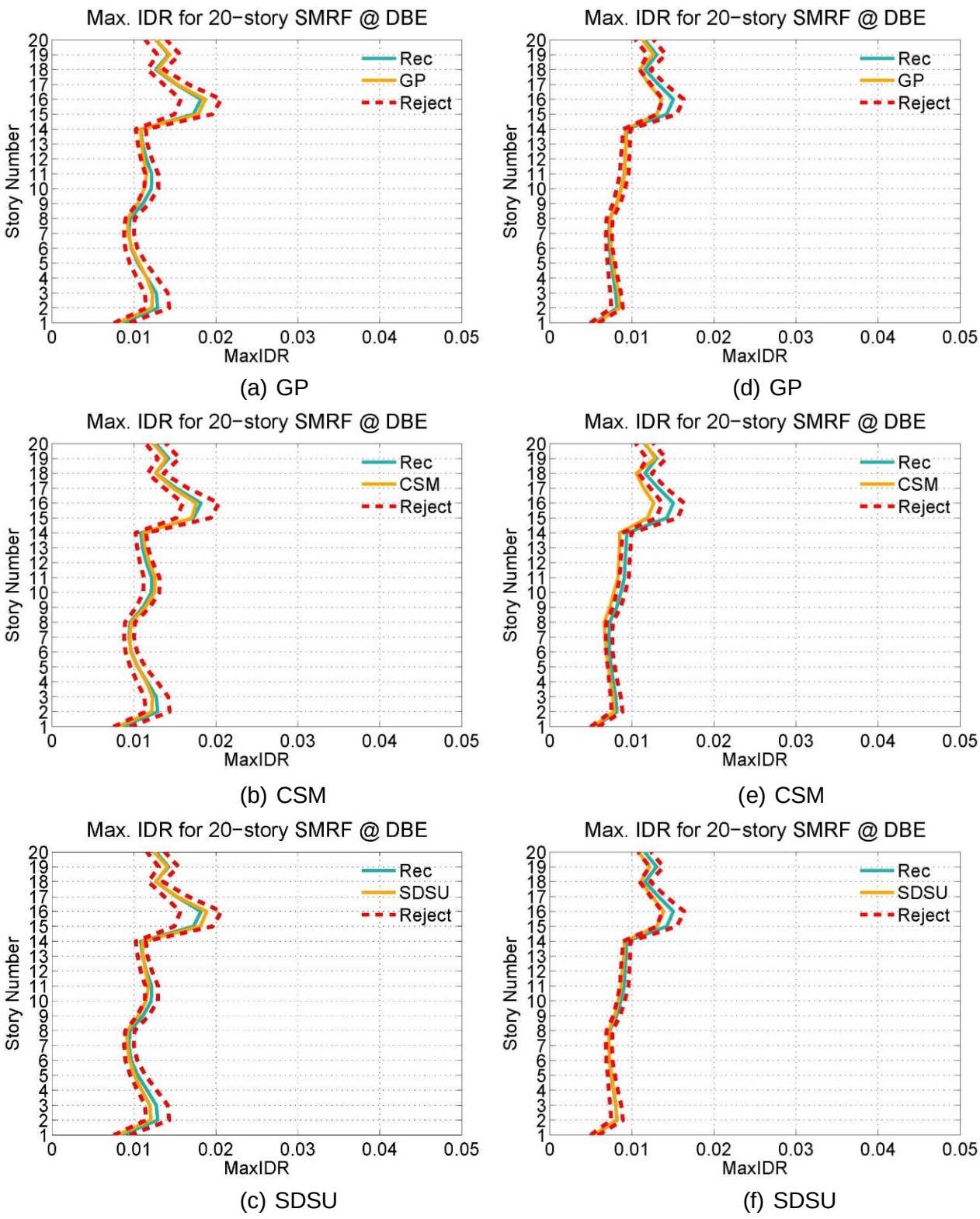

Figure A.25 Average maximum interstory drift ratio of the 20-story SMRF with statistical significant difference boundary (DBE with UHS (a, b, c) and CMS (e, d, f), 1 sets of 40)

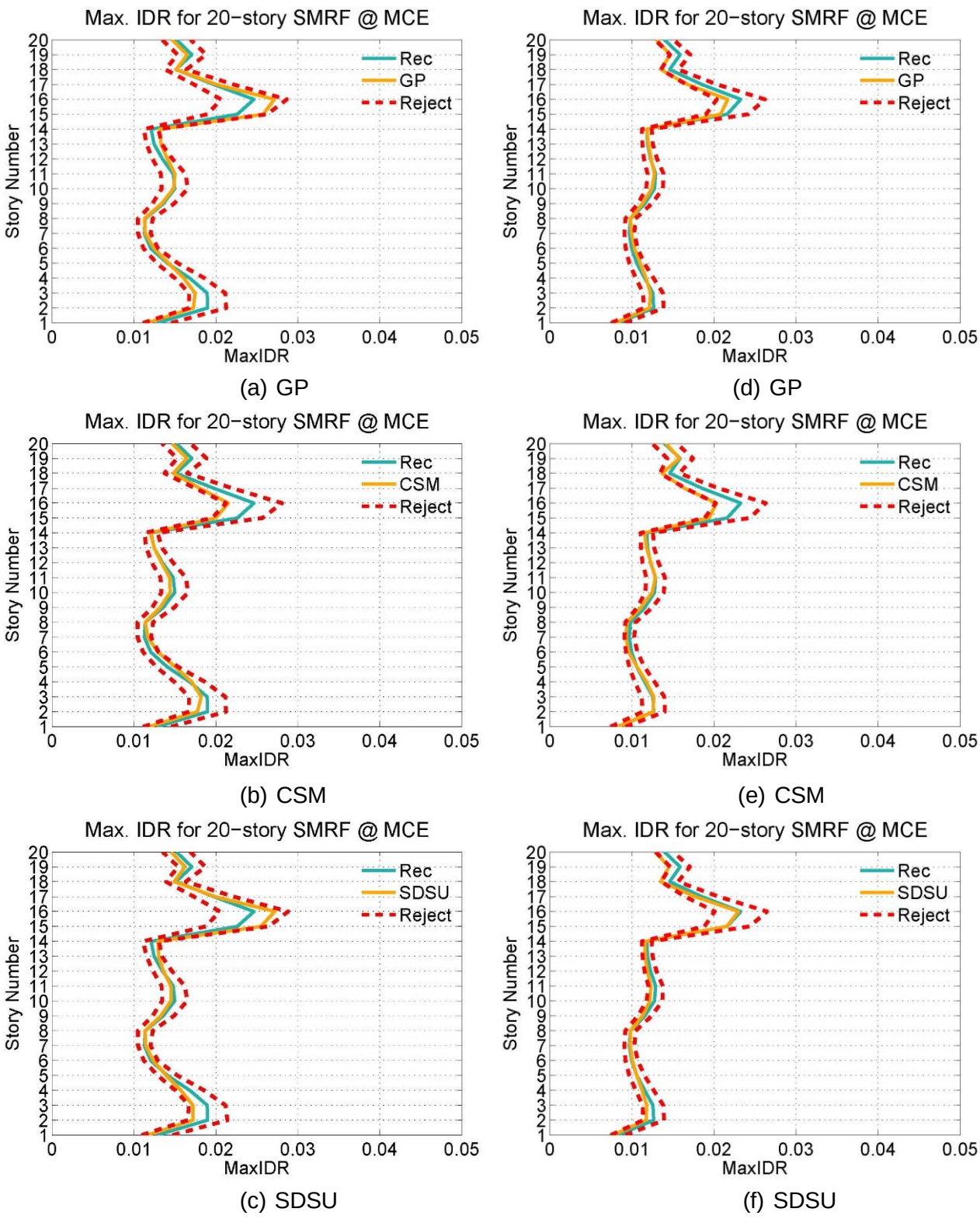

Figure A.26 Average maximum interstory drift ratio of the 20-story SMRF with statistical significant difference boundary (MCE with UHS (a, b, c) and CMS (e, d, f), 1 sets of 40)

Appendix B

A sensitivity study on finding the effect of scalar parameters on engineering demand parameters is conducted. In order to make result convincing, a wide variety of structures are implemented, including seventy-seven SDOF systems and four inelastic MDOF systems. Chapter 5 only presents SDOF systems in one elastic case and one inelastic case with R=2 (strength reduction factors) and non-deterioration as well as one MDOF systems, 20-story steel moment frame. The appendix B includes the rest of scenarios:

1) case of non-deterioration and R=4;
2) case of non-deterioration and R=6;
3) case of deterioration and R=2;
4) case of deterioration and R=4;
5) case of deterioration and R=6;
6) case of inelastic 4-story steel moment frame;
7) case of inelastic 8-story steel moment frame;
8) case of inelastic 12-story steel moment frame;

In general, results are consistent with the discovery in chapter 5. The main observation is that building response is highly sensitive to Arias Intensity. The effect of the ω_{mid} on the EDP is observable in nonlinear structures. Duration and rate of change of frequency have little impact on the EDP.

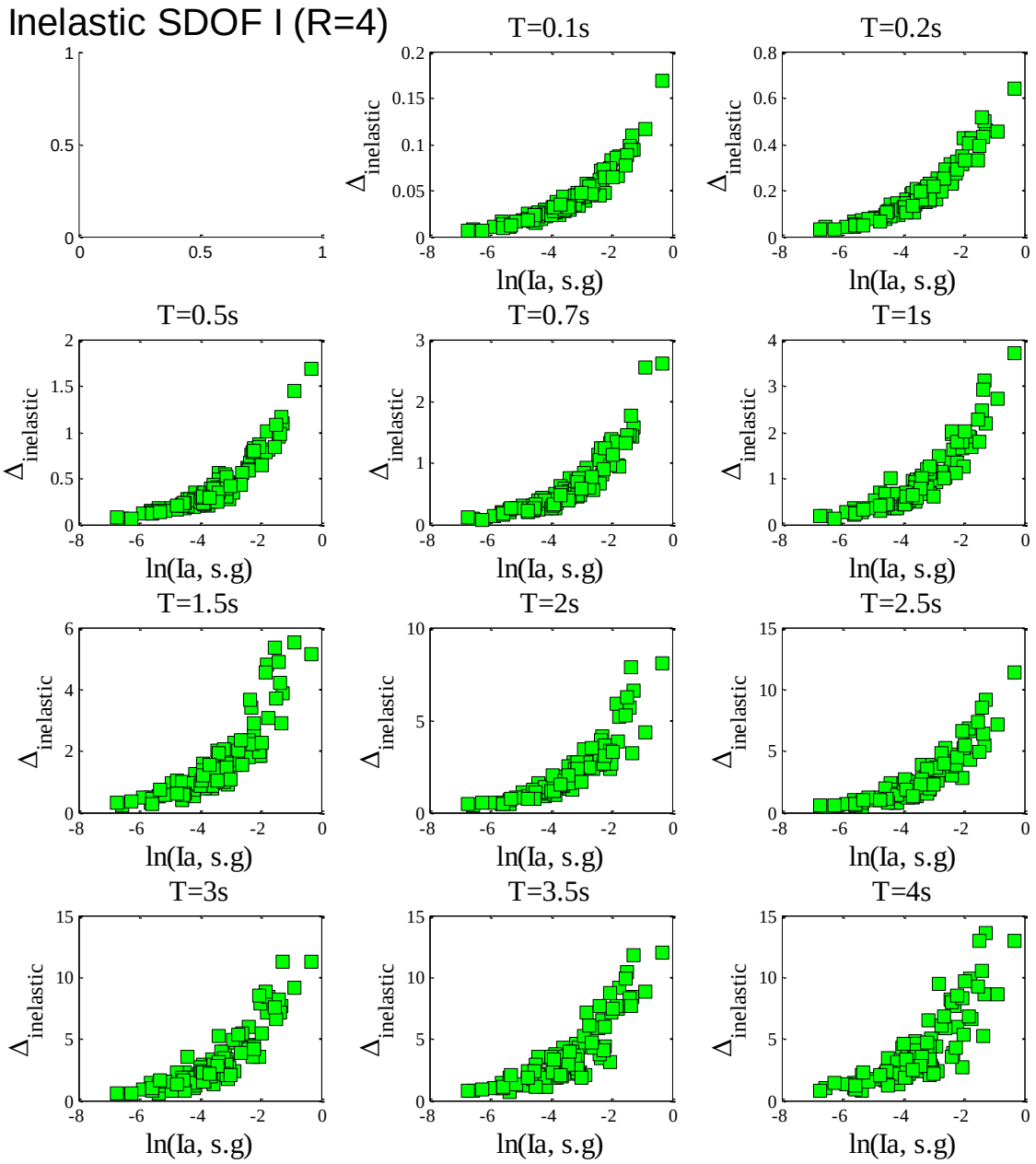

Figure B.1. Effect of arias intensity on engineering demand parameter in term of maximum inelastic displacement for non-deterioration inelastic SDOF, period from 0.1s to 4s with strength reduction factor, R=4, and positive strain-hardening, α=0.10.

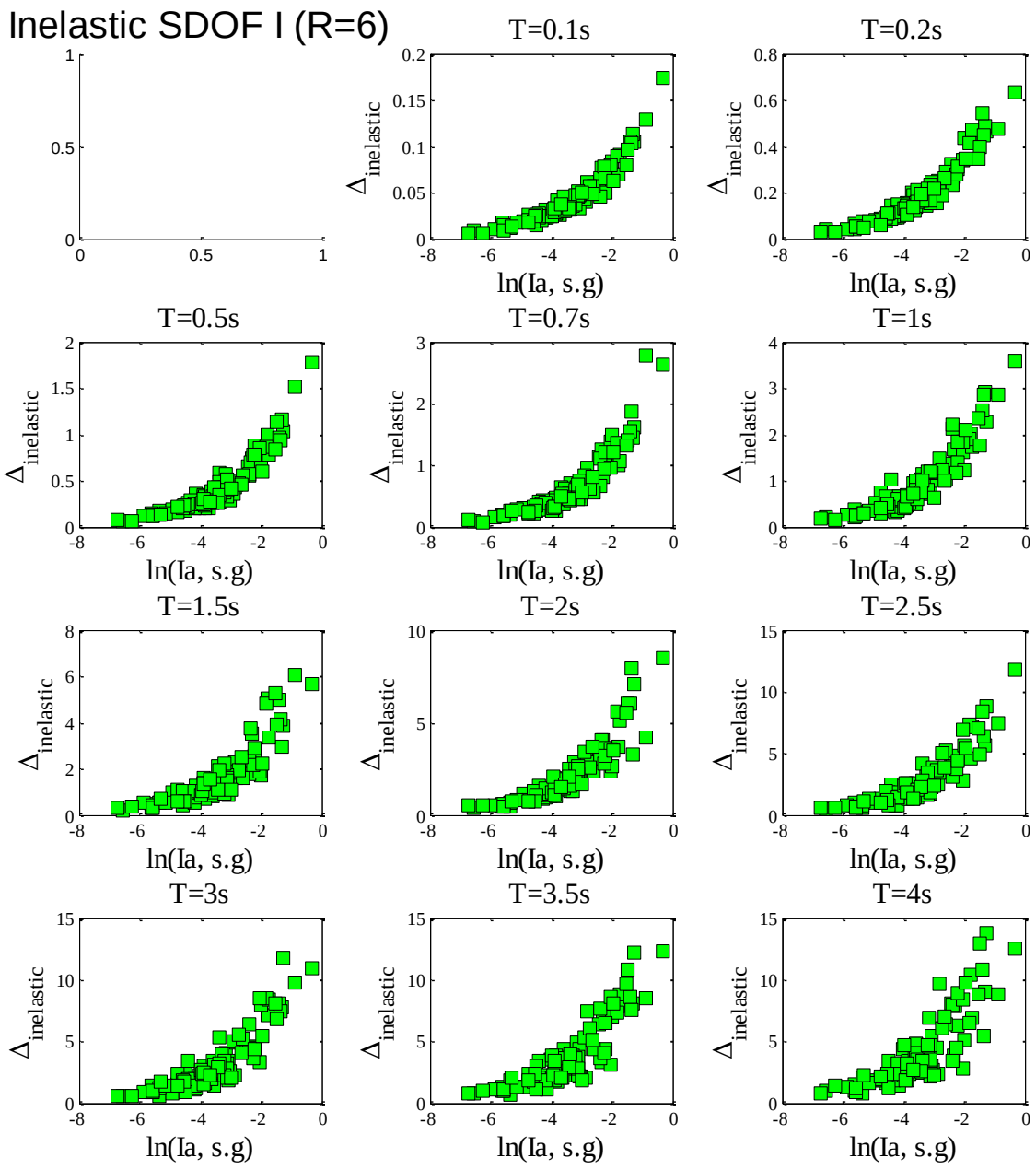

Figure B.2. Effect of arias intensity on engineering demand parameter in term of maximum inelastic displacement for non-deterioration inelastic SDOF, period from 0.1s to 4s with strength reduction factor, R=6, and positive strain-hardening, α=0.10.

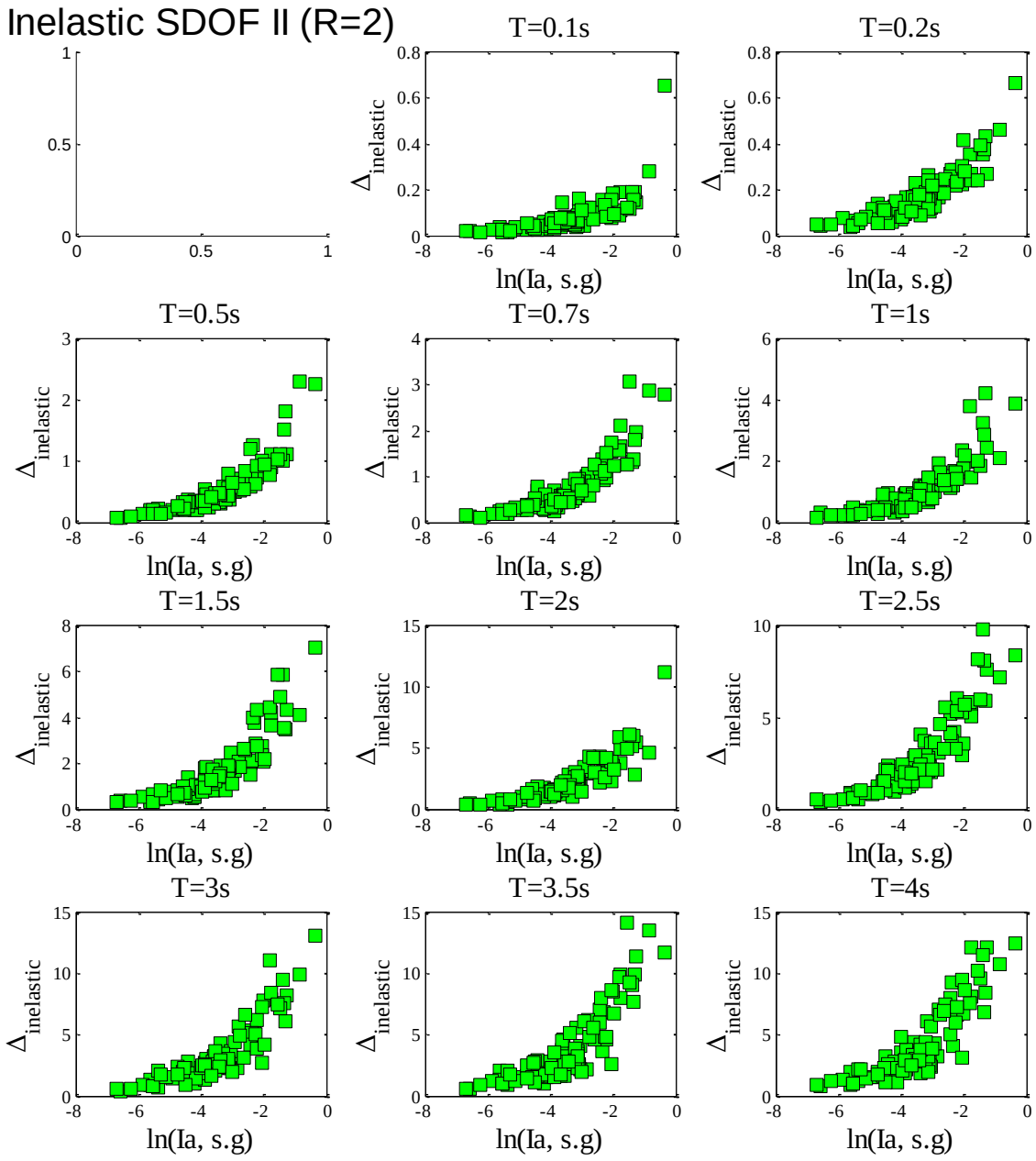

Figure B.3. Effect of arias intensity on engineering demand parameter in term of maximum inelastic displacement for deterioration inelastic SDOF, period from 0.1s to 4s with strength reduction factor, R=2, and negative strain-hardening, α= ─ 0.10.

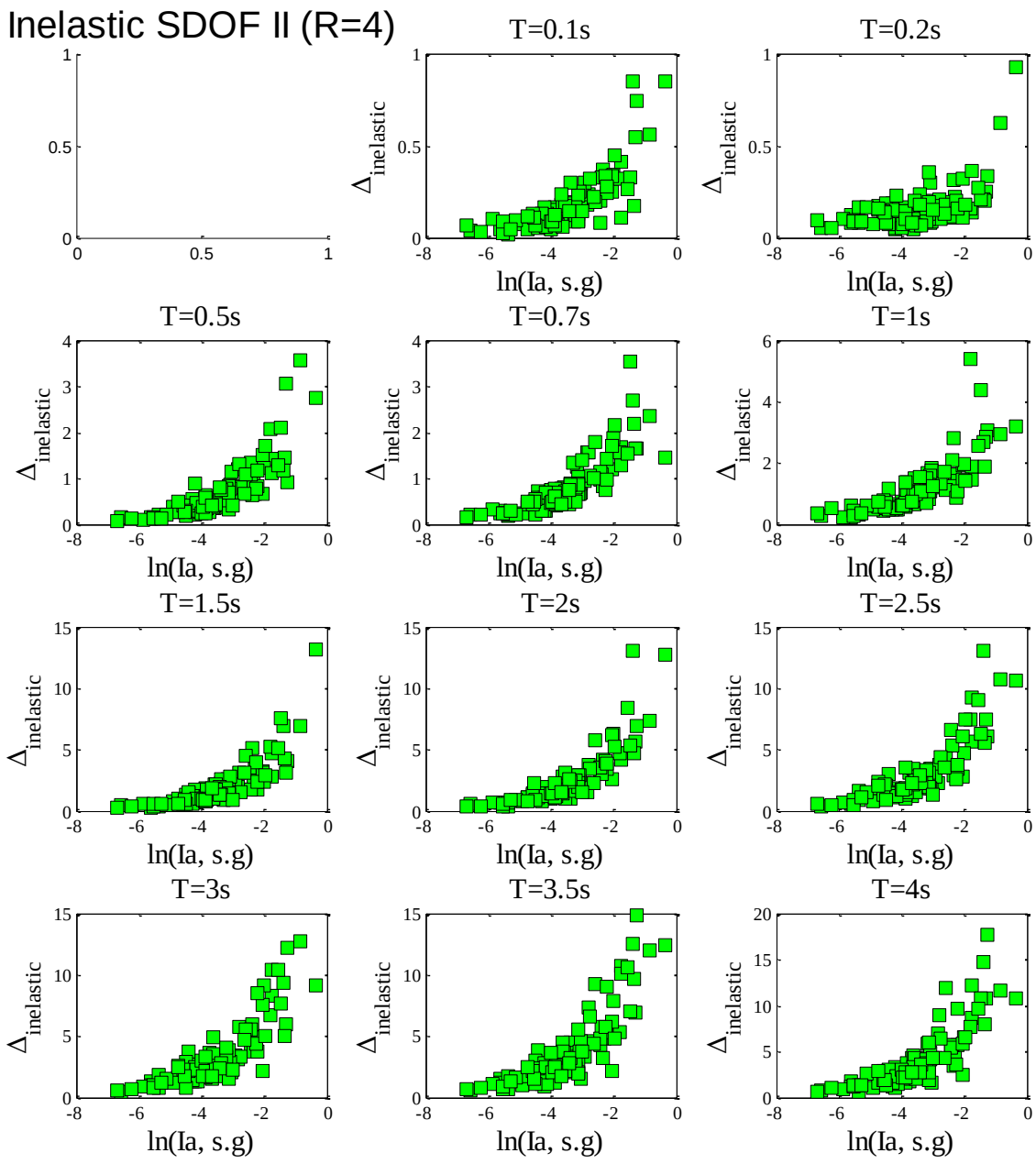

Figure B.4. Effect of arias intensity on engineering demand parameter in term of maximum inelastic displacement for deterioration inelastic SDOF, period from 0.1s to 4s with strength reduction factor, R=4, and negative strain-hardening, α= ─ 0.10.

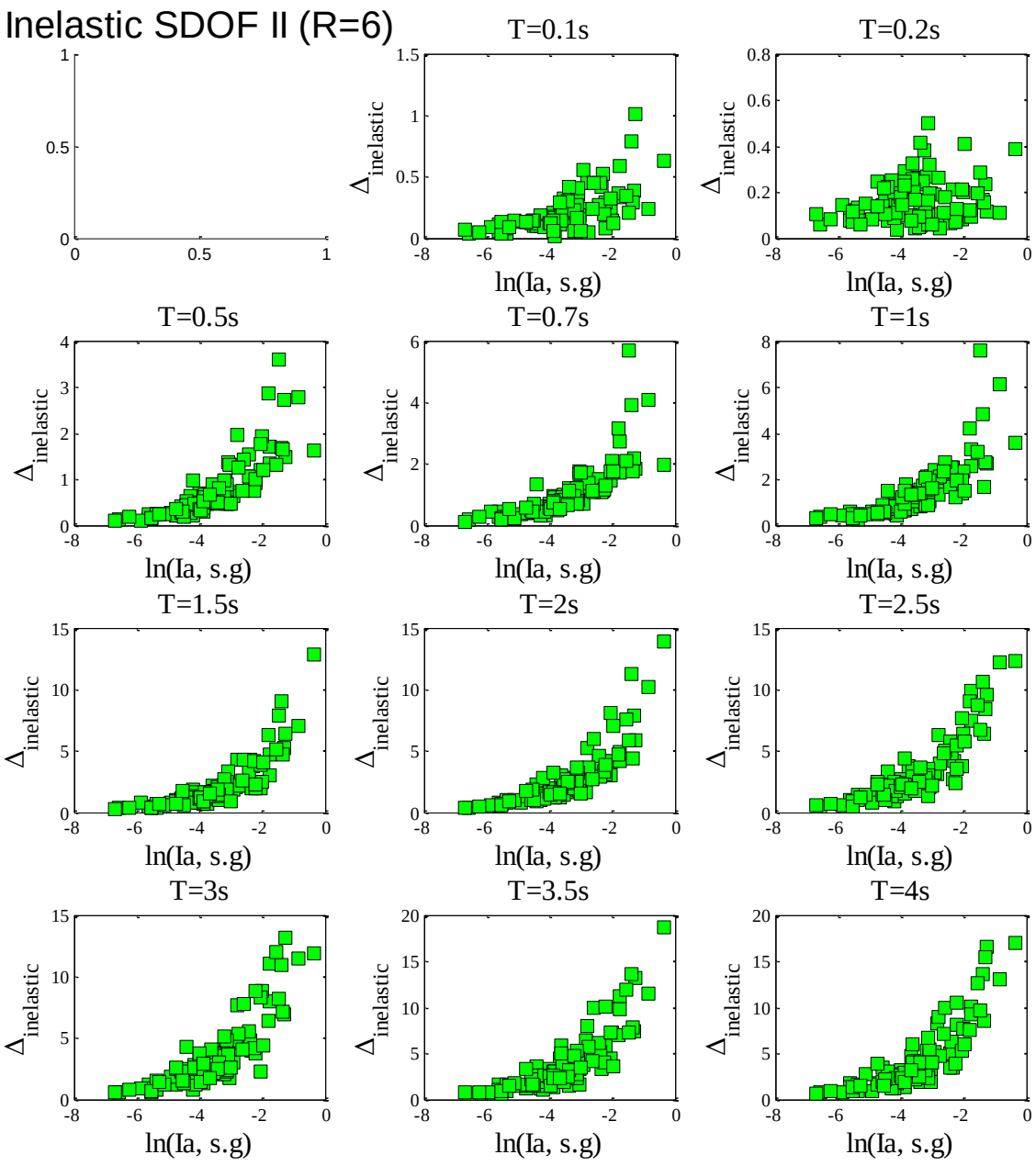

Figure B.5. Effect of arias intensity on engineering demand parameter in term of maximum inelastic displacement for deterioration inelastic SDOF, period from 0.1s to 4s with strength reduction factor, R=6, and negative strain-hardening, α= ─ 0.10.

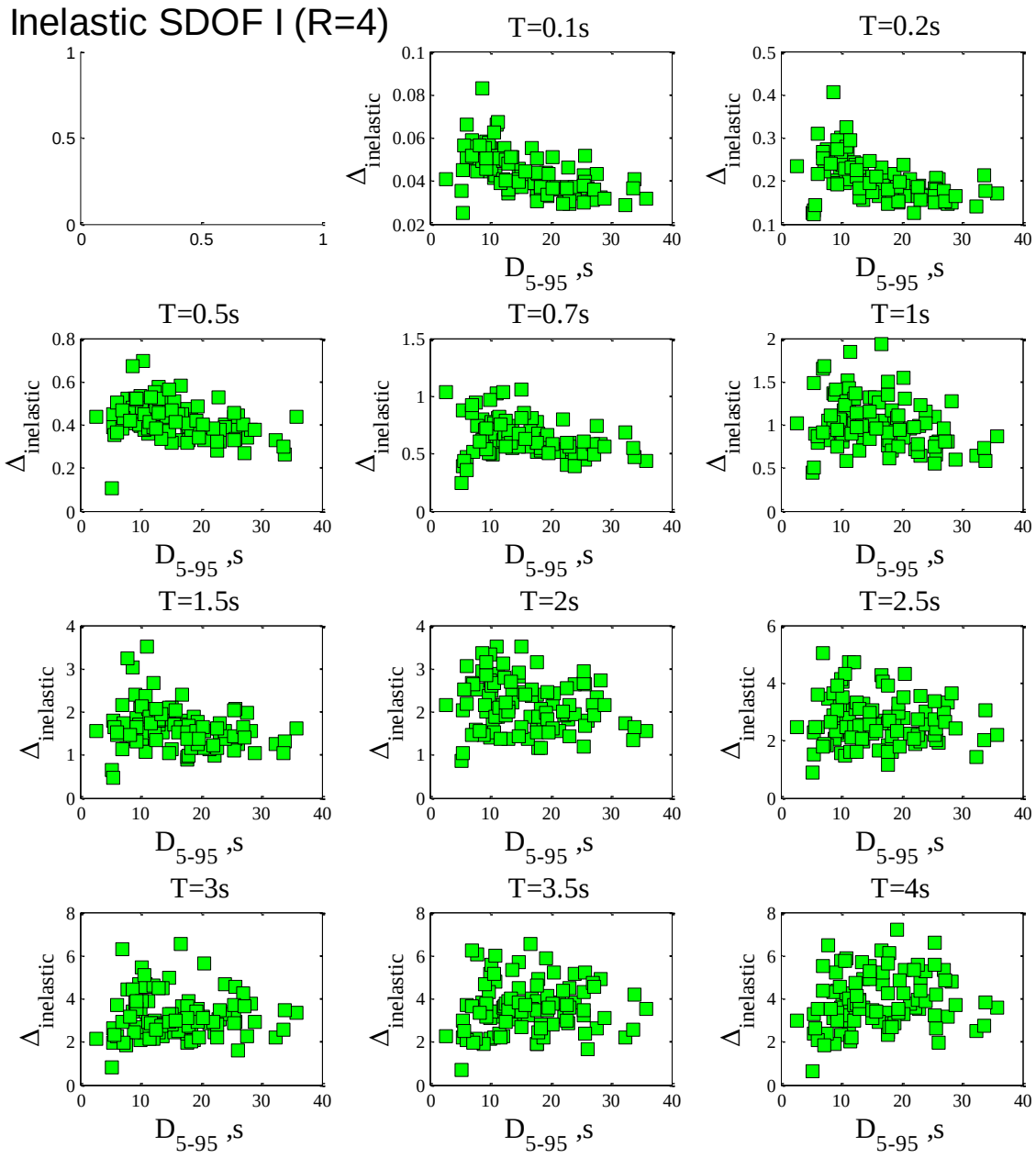

Figure B.6. Effect of duration on engineering demand parameter in term of maximum inelastic displacement for non-deterioration inelastic SDOF, period from 0.1s to 4s with strength reduction factor, R=4, and positive strain-hardening, α=0.10.

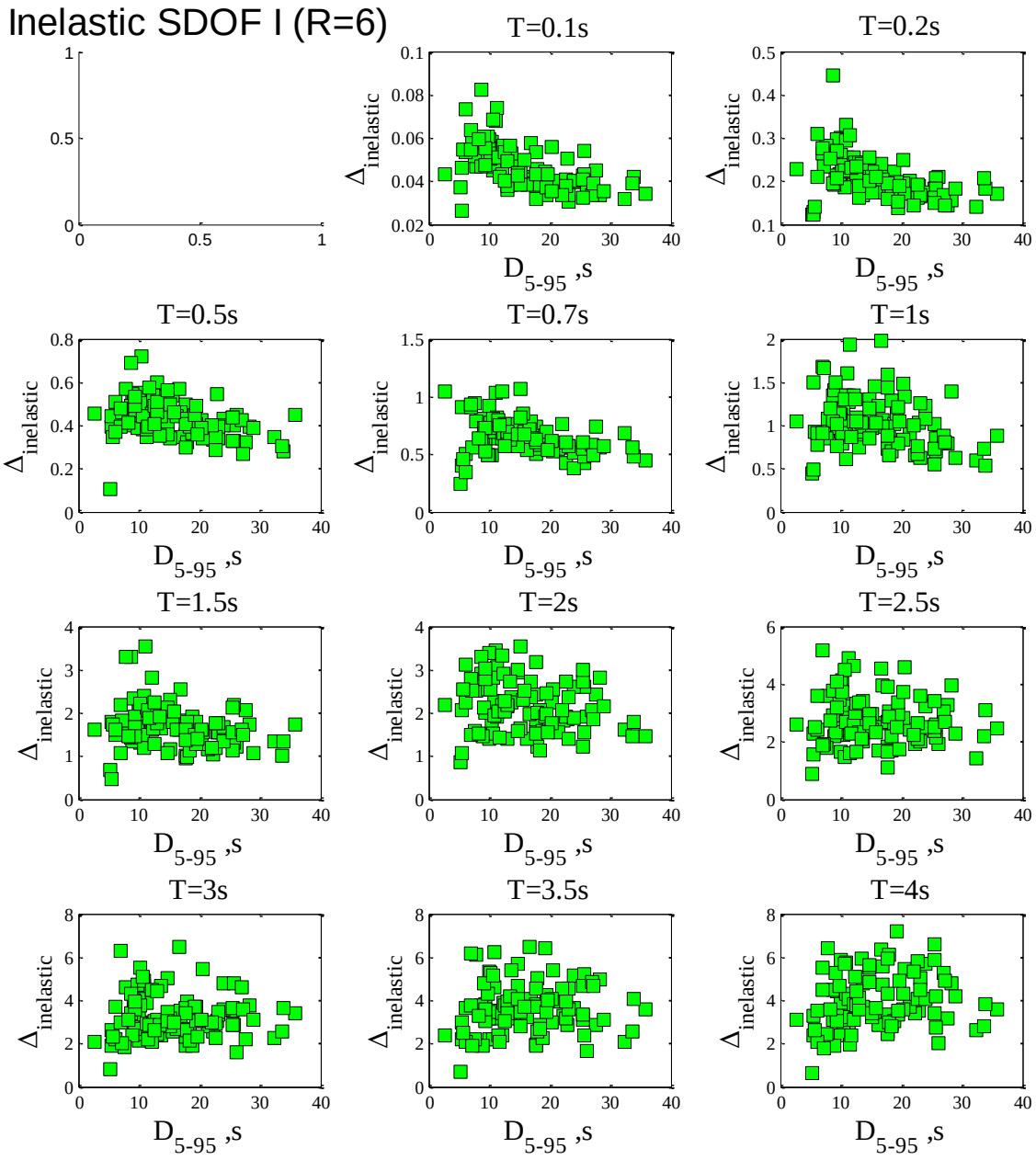

Figure B.7. Effect of duration on engineering demand parameter in term of maximum inelastic displacement for non-deterioration inelastic SDOF, period from 0.1s to 4s with strength reduction factor, R=4, and positive strain-hardening, α=0.10.

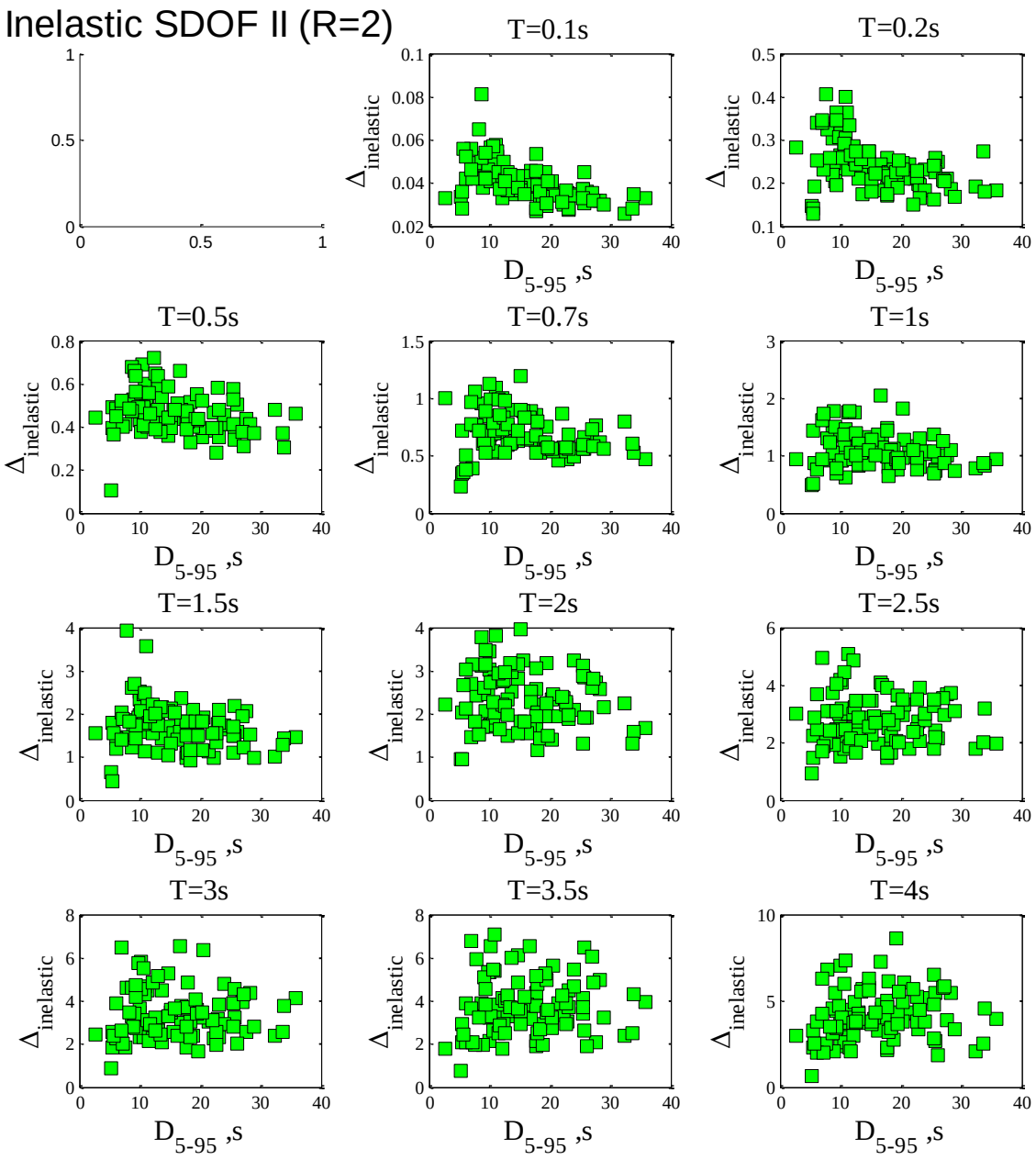

Figure B.8. Effect of duration on engineering demand parameter in term of maximum inelastic displacement for deterioration inelastic SDOF, period from 0.1s to 4s with strength reduction factor, R=2, and negative strain-hardening, $\alpha = -0.10$.

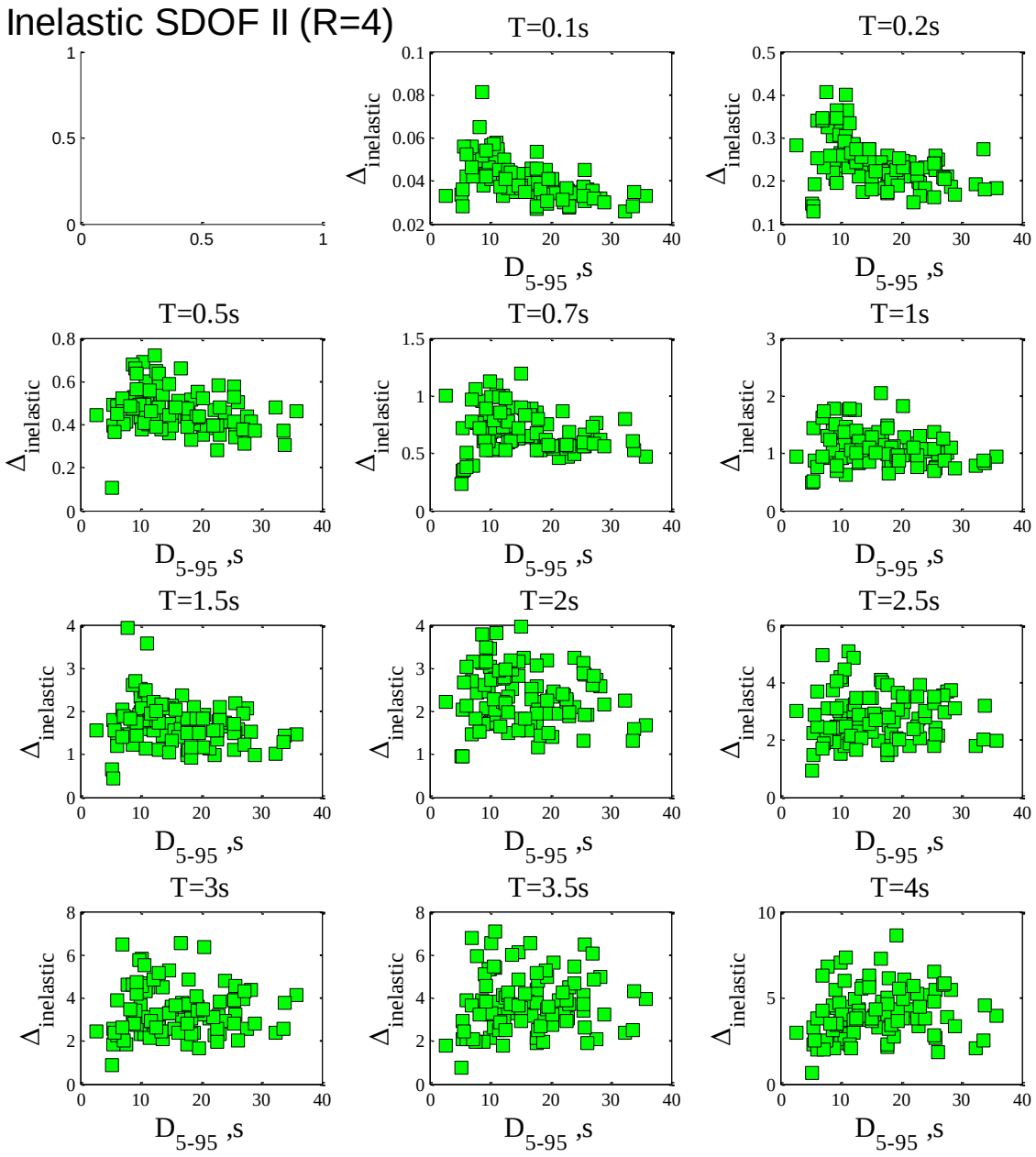

Figure B.9. Effect of duration on engineering demand parameter in term of maximum inelastic displacement for deterioration inelastic SDOF, period from 0.1s to 4s with strength reduction factor, R=4, and negative strain-hardening, $\alpha = -0.10$.

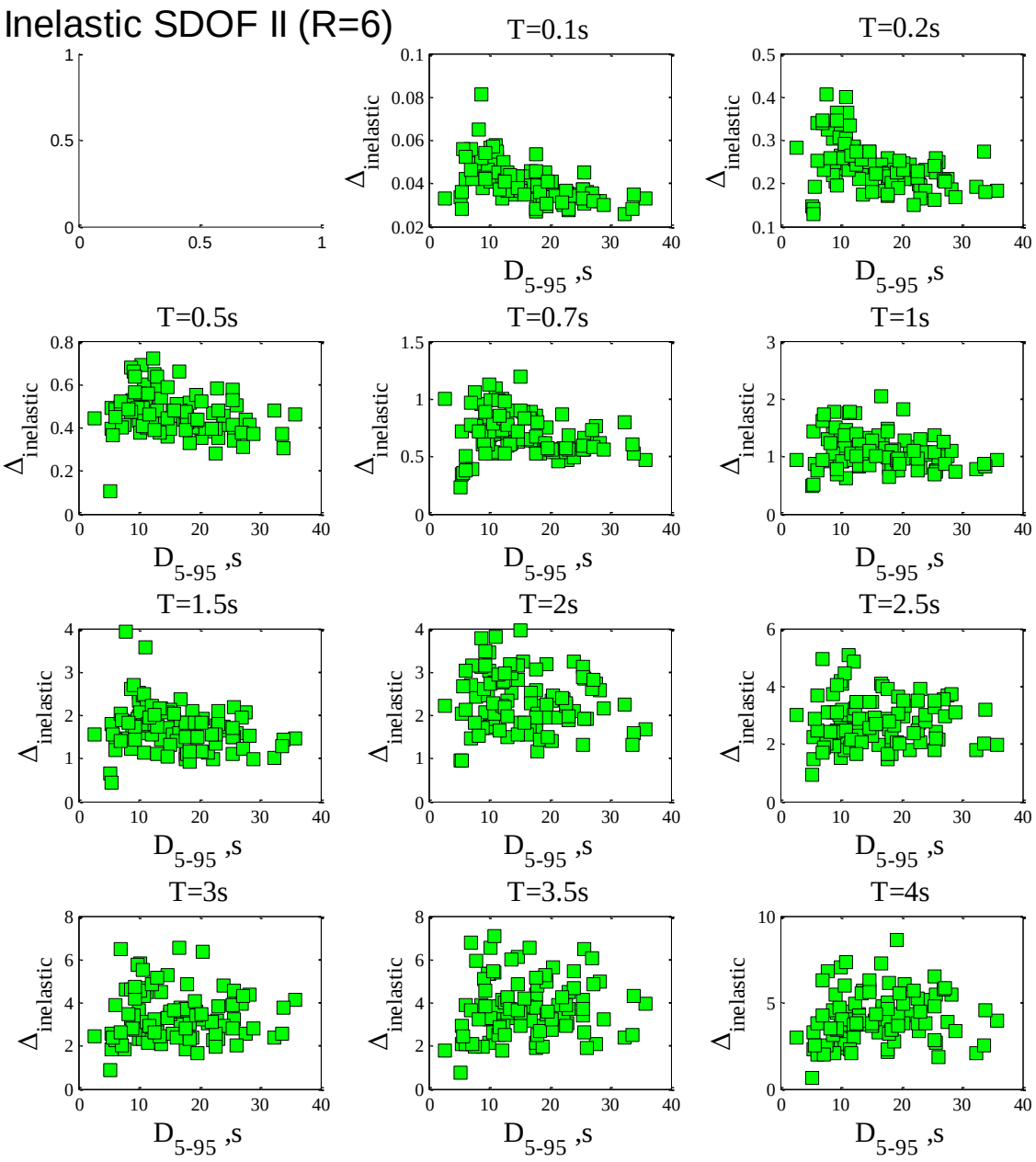

Figure B.10. Effect of duration on engineering demand parameter in term of maximum inelastic displacement for deterioration inelastic SDOF, period from 0.1s to 4s with strength reduction factor, R=6, and negative strain-hardening, α= ─ 0.10.

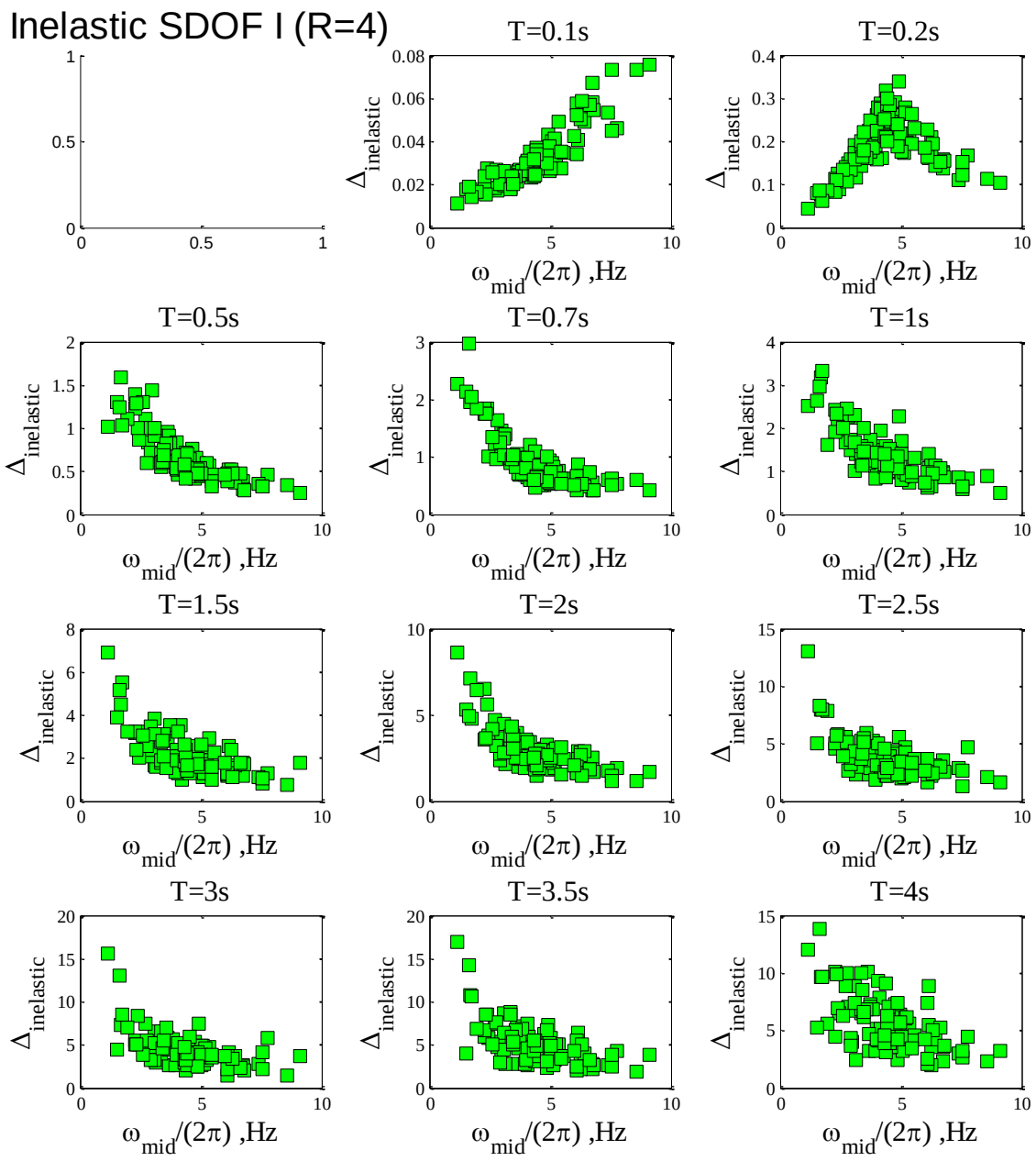

Figure B.11. Effect of dominant frequency on engineering demand parameter in term of maximum inelastic displacement for non-deterioration inelastic SDOF, period from 0.1s to 4s with strength reduction factor, R=4, and positive strain-hardening, α=0.10.

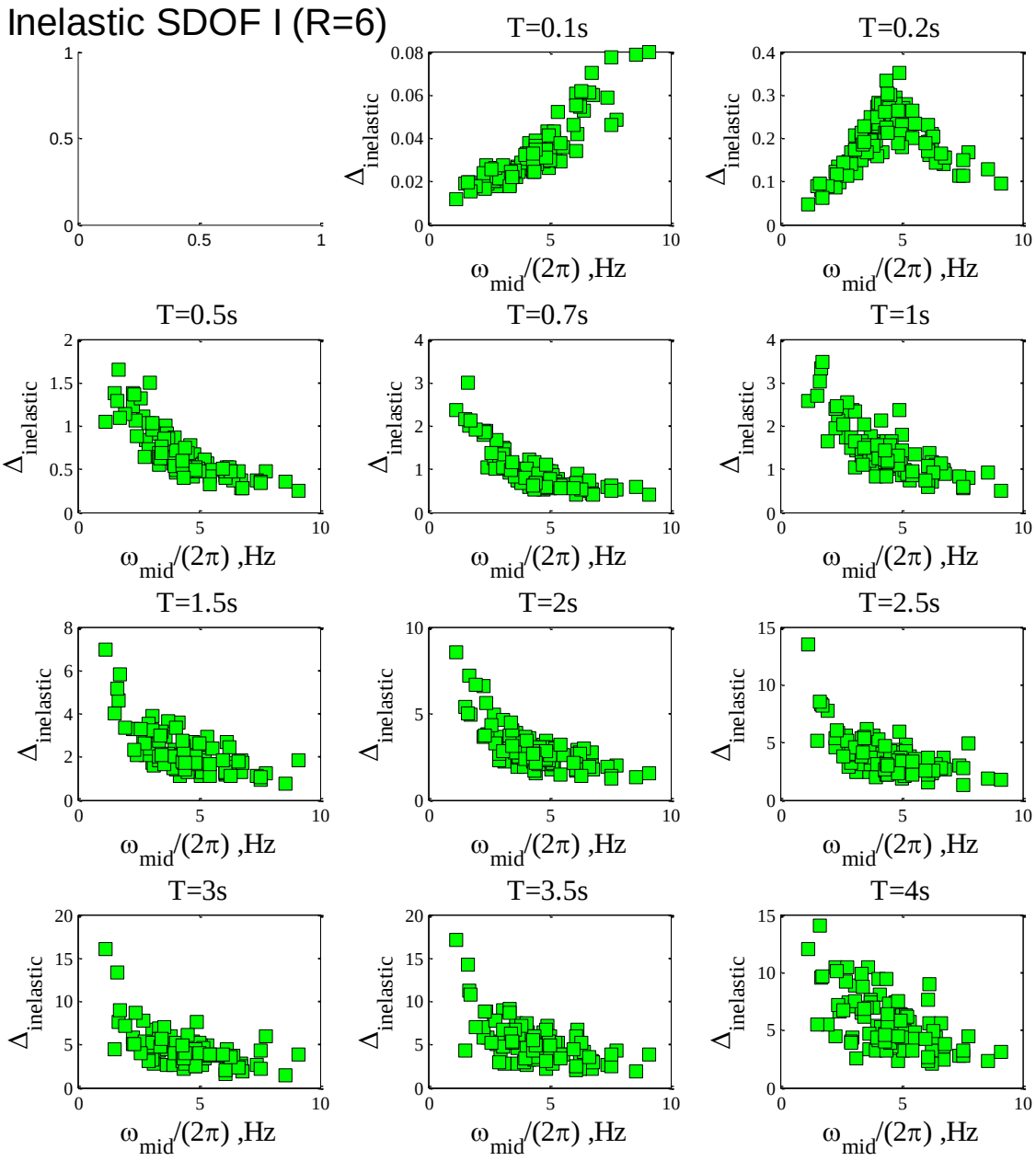

Figure B.12. Effect of dominant frequency on engineering demand parameter in term of maximum inelastic displacement for non-deterioration inelastic SDOF, period from 0.1s to 4s with strength reduction factor, R=6, and positive strain-hardening, α=0.10.

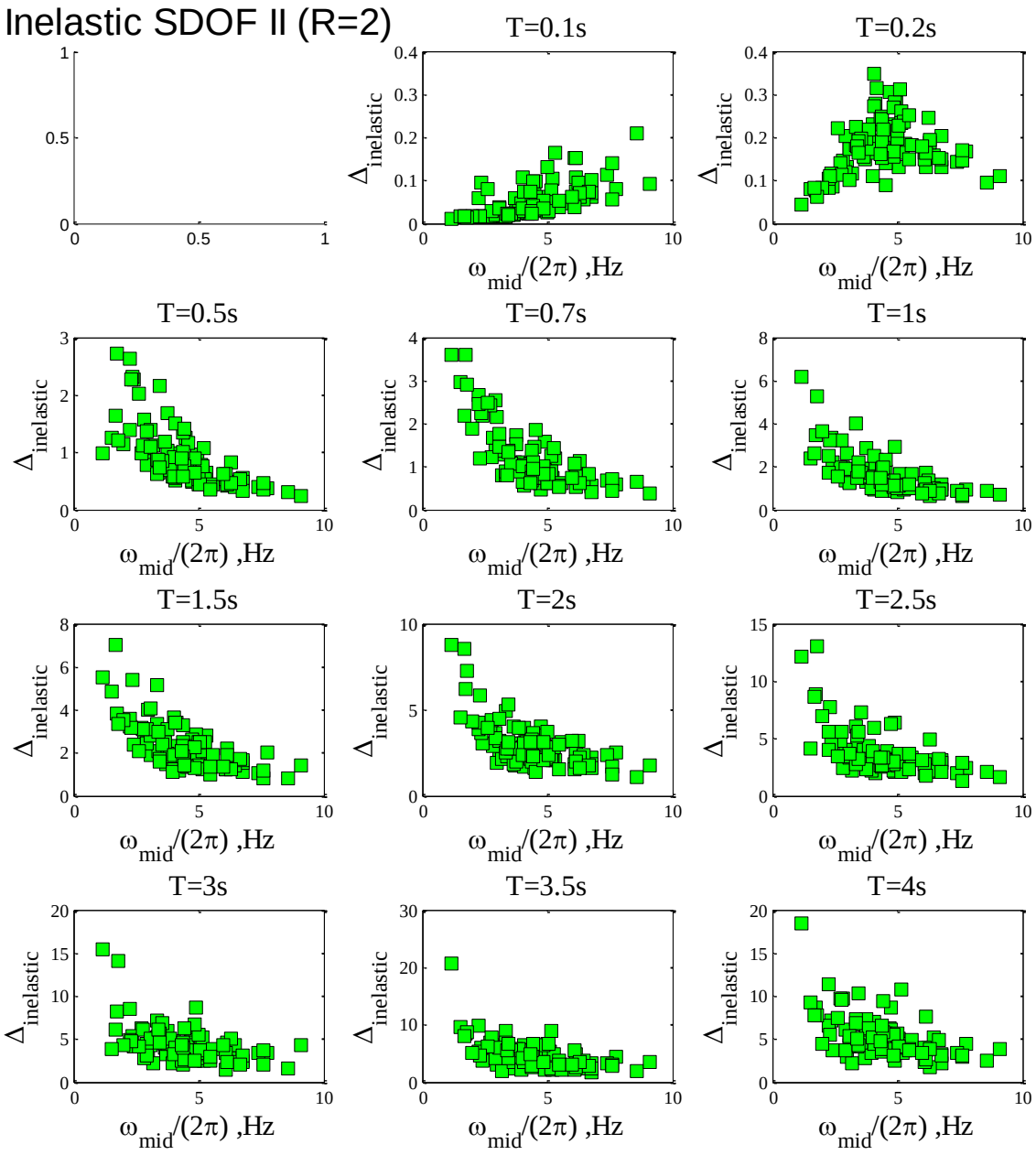

Figure B.13. Effect of dominant frequency on engineering demand parameter in term of maximum inelastic displacement for deterioration inelastic SDOF, period from 0.1s to 4s with strength reduction factor, R=2, and negative strain-hardening, $\alpha = -0.10$.

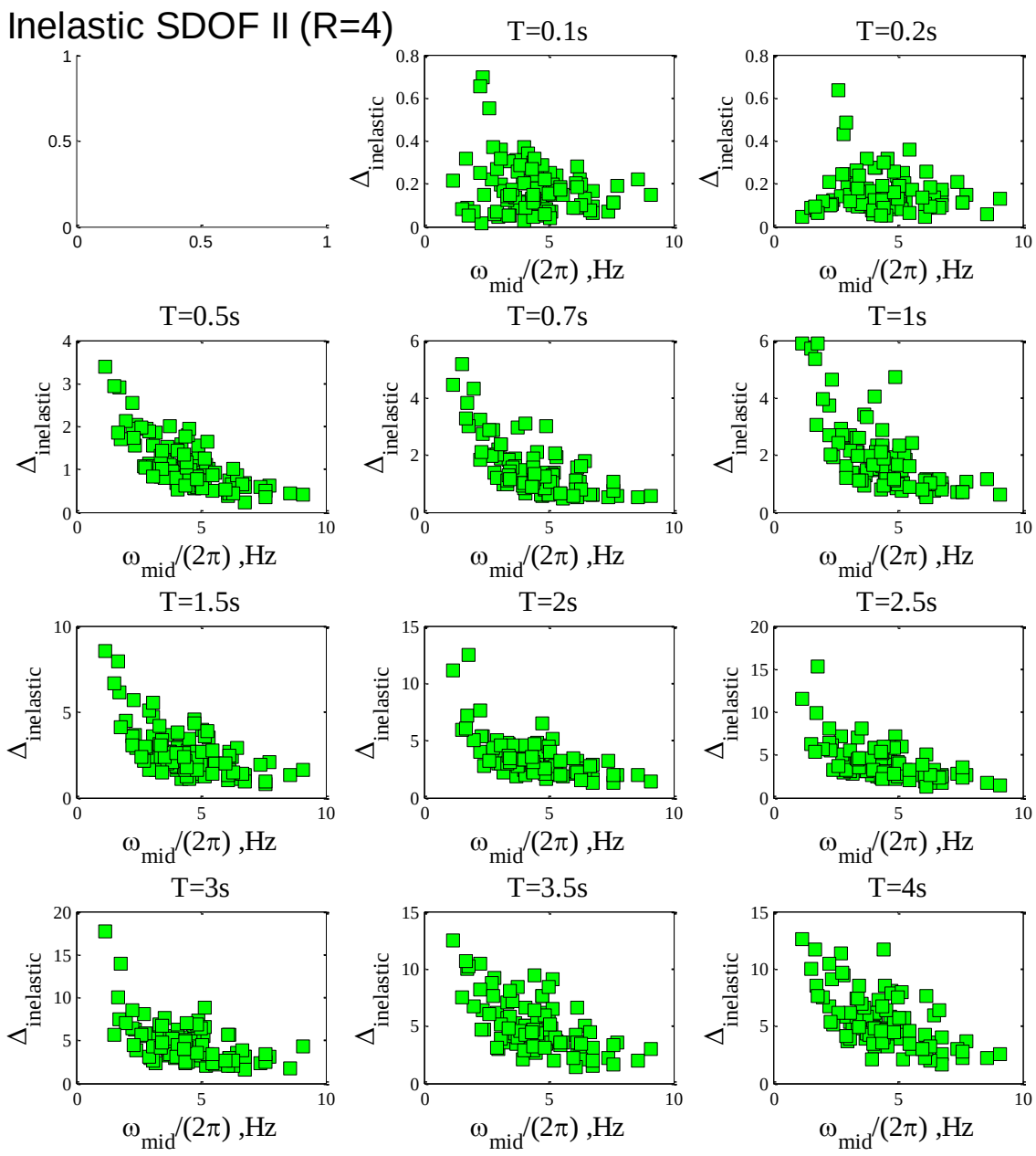

Figure B.14. Effect of dominant frequency on engineering demand parameter in term of maximum inelastic displacement for deterioration inelastic SDOF, period from 0.1s to 4s with strength reduction factor, R=4, and negative strain-hardening, α= ─ 0.10

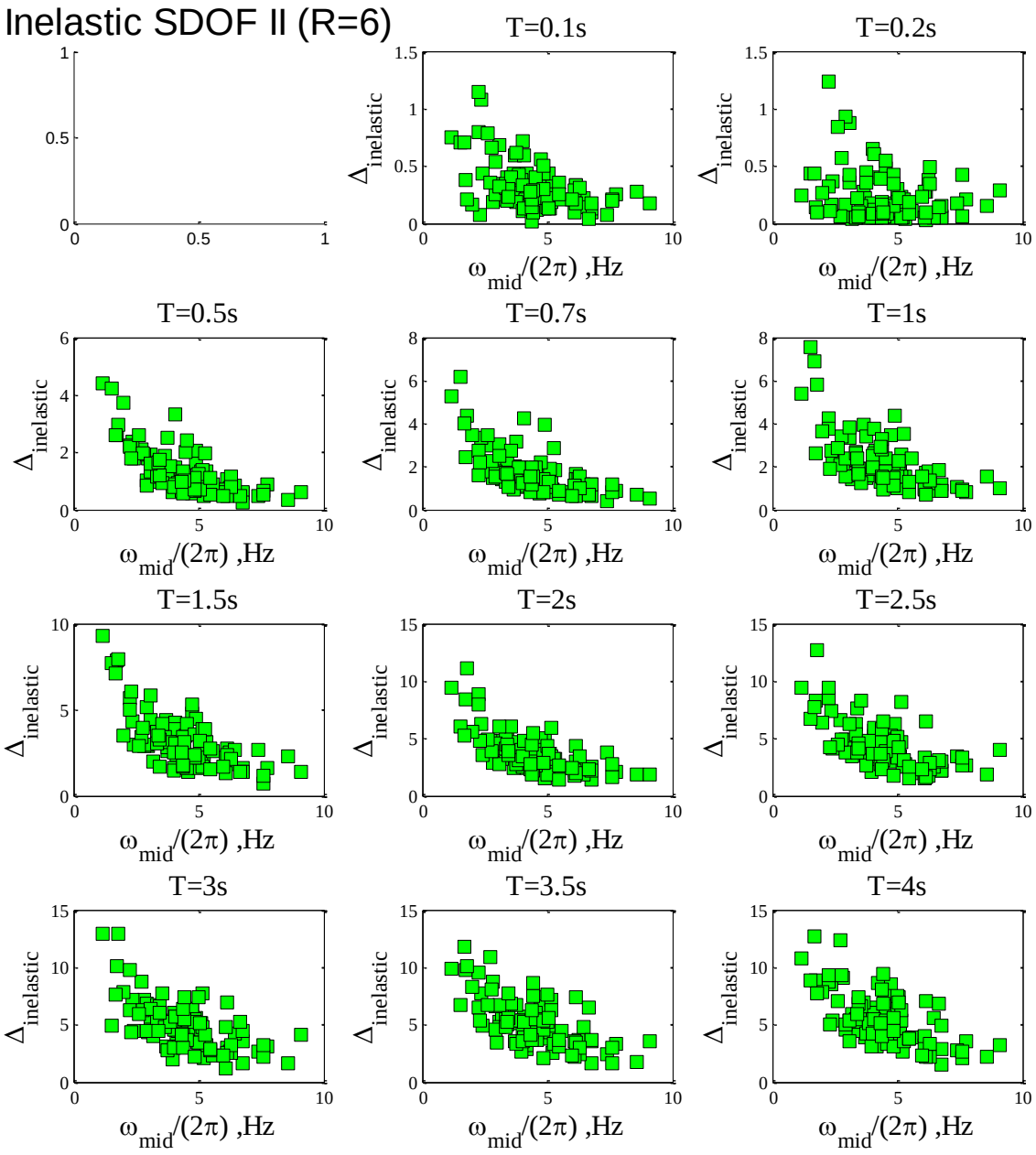

Figure B.15. Effect of dominant frequency on engineering demand parameter in term of maximum inelastic displacement for deterioration inelastic SDOF, period from 0.1s to 4s with strength reduction factor, R=6, and negative strain-hardening, $\alpha = -0.10$

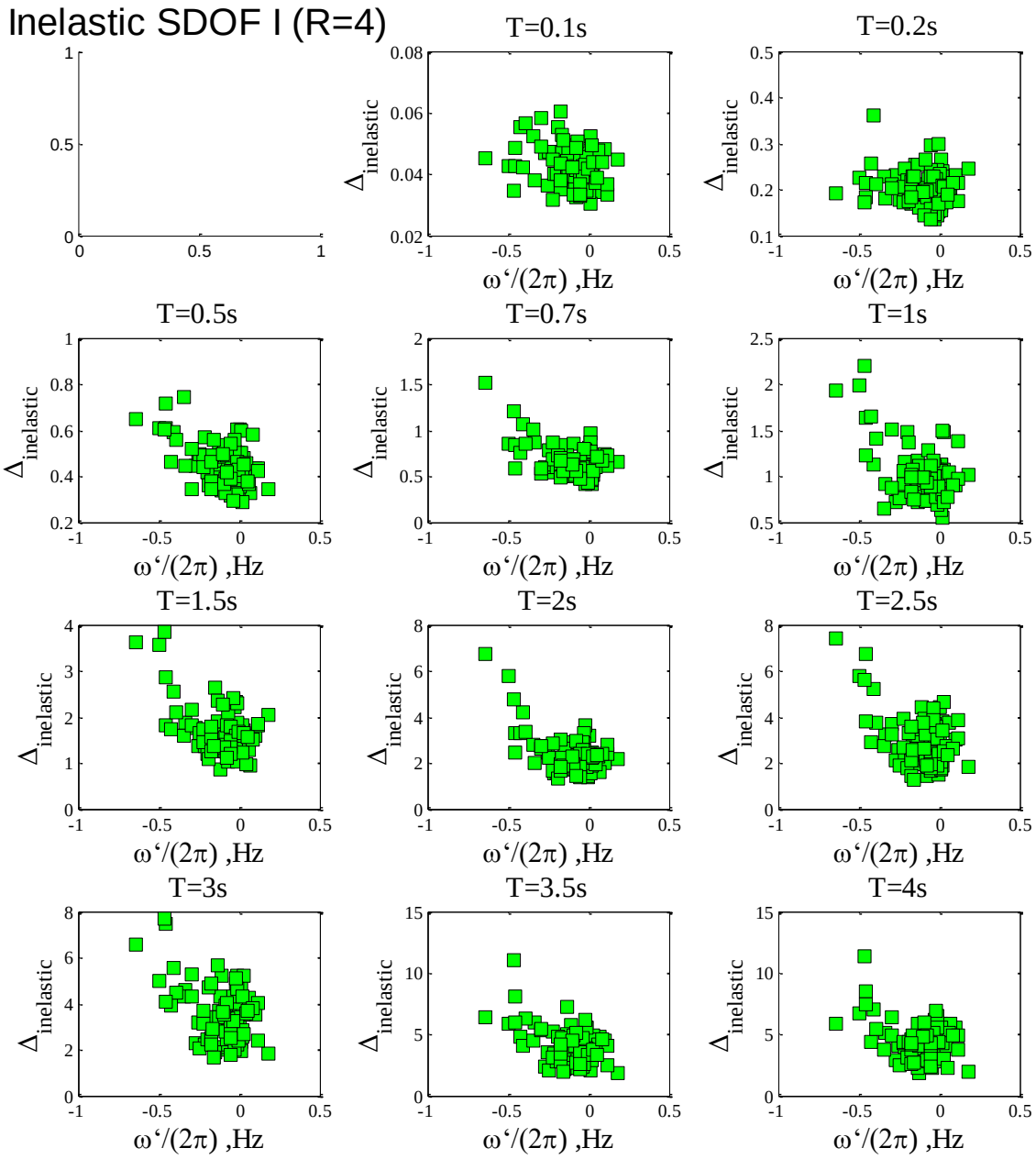

Figure B.16. Effect of slope of frequency on engineering demand parameter in term of maximum inelastic displacement for non-deterioration inelastic SDOF, period from 0.1s to 4s with strength reduction factor, R=4, and positive strain-hardening, α=0.10.

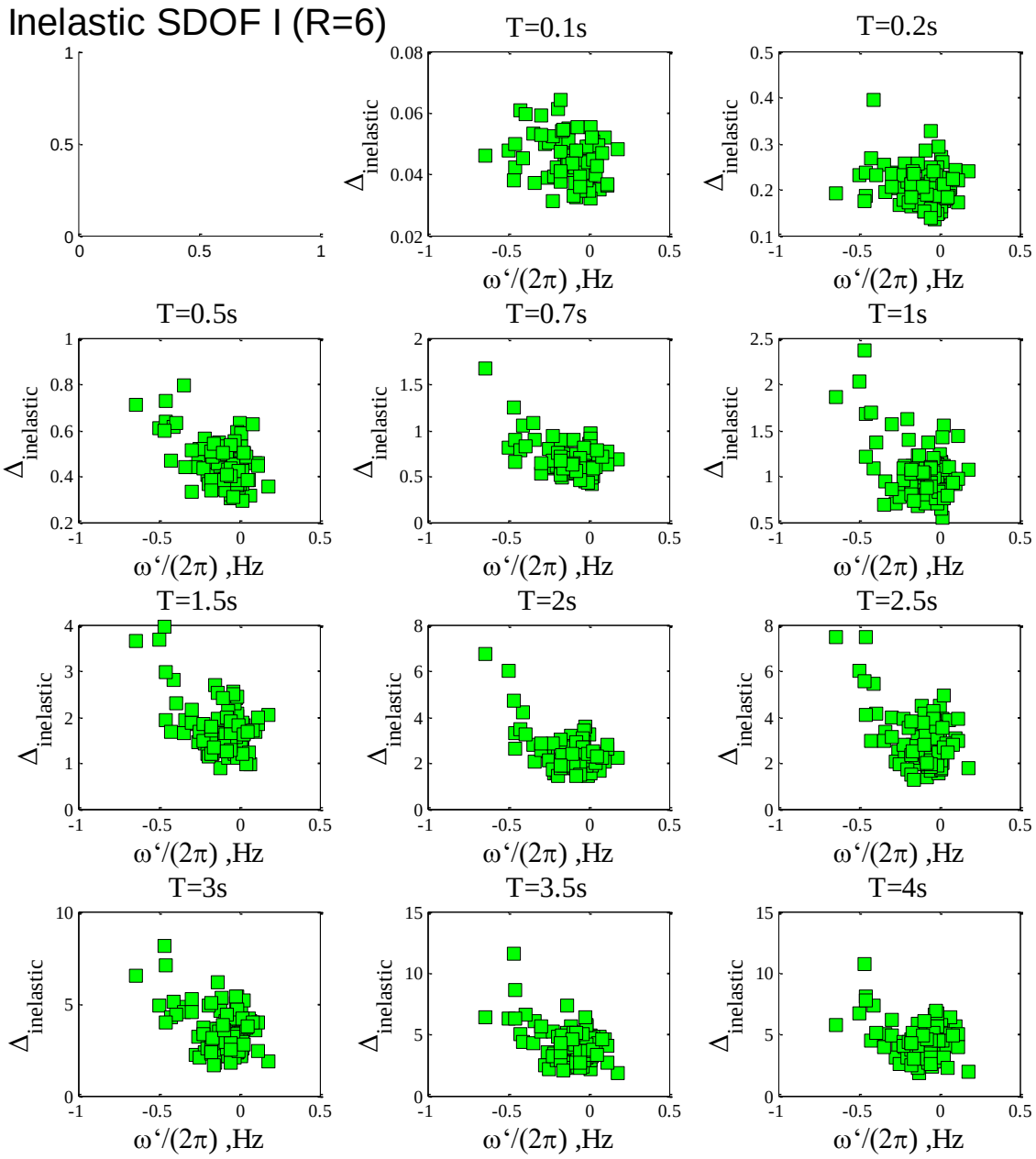

Figure B.17. Effect of slope of frequency on engineering demand parameter in term of maximum inelastic displacement for non-deterioration inelastic SDOF, period from 0.1s to 4s with strength reduction factor, R=6, and positive strain-hardening, α=0.10.

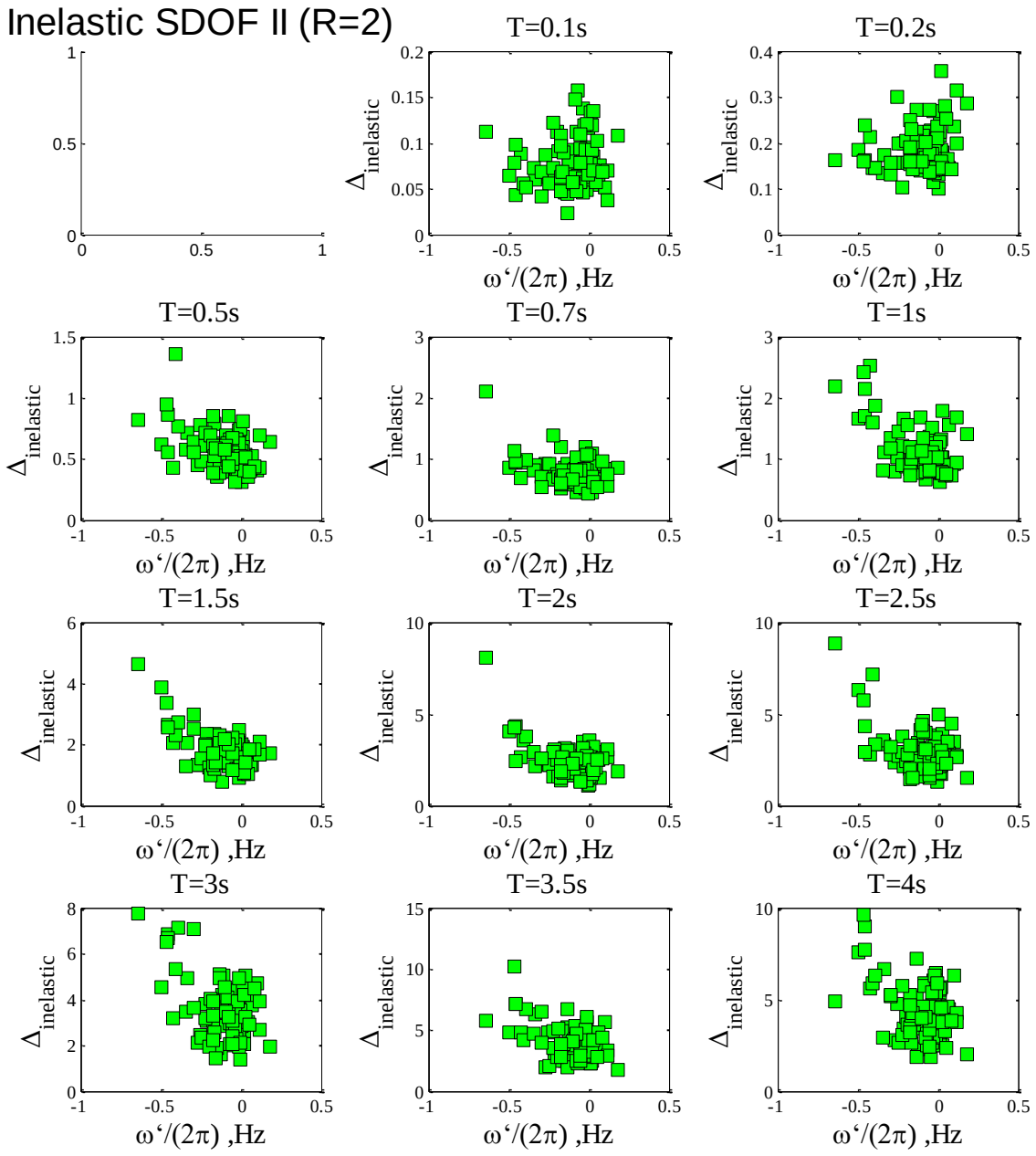

Figure B.18. Effect of slope of frequency on engineering demand parameter in term of maximum inelastic displacement for deterioration inelastic SDOF, period from 0.1s to 4s with strength reduction factor, R=2, and negative strain-hardening, α= ─ 0.10.

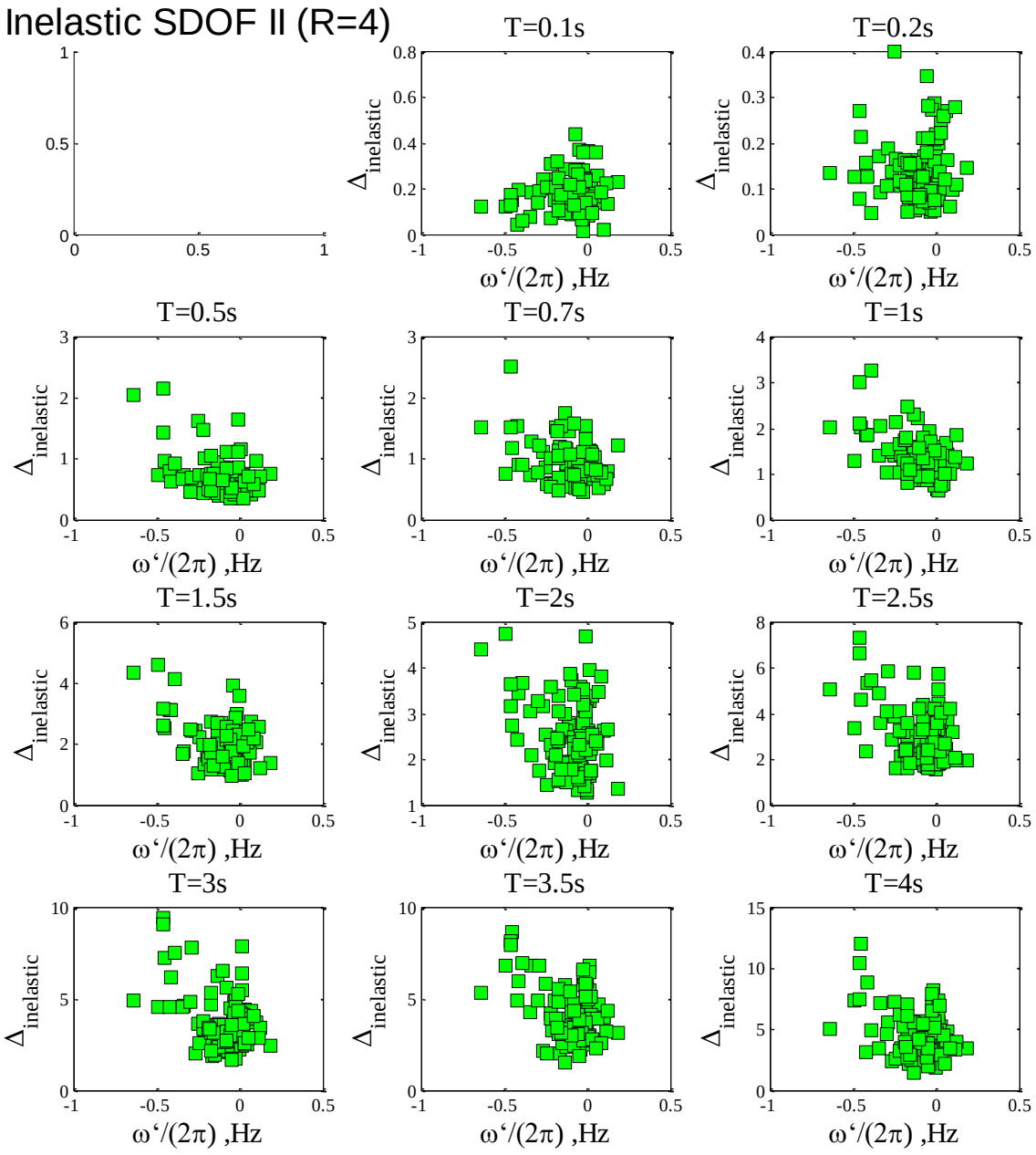

Figure B.19. Effect of slope of frequency on engineering demand parameter in term of maximum inelastic displacement for deterioration inelastic SDOF, period from 0.1s to 4s with strength reduction factor, R=4, and negative strain-hardening, α= ─ 0.10.

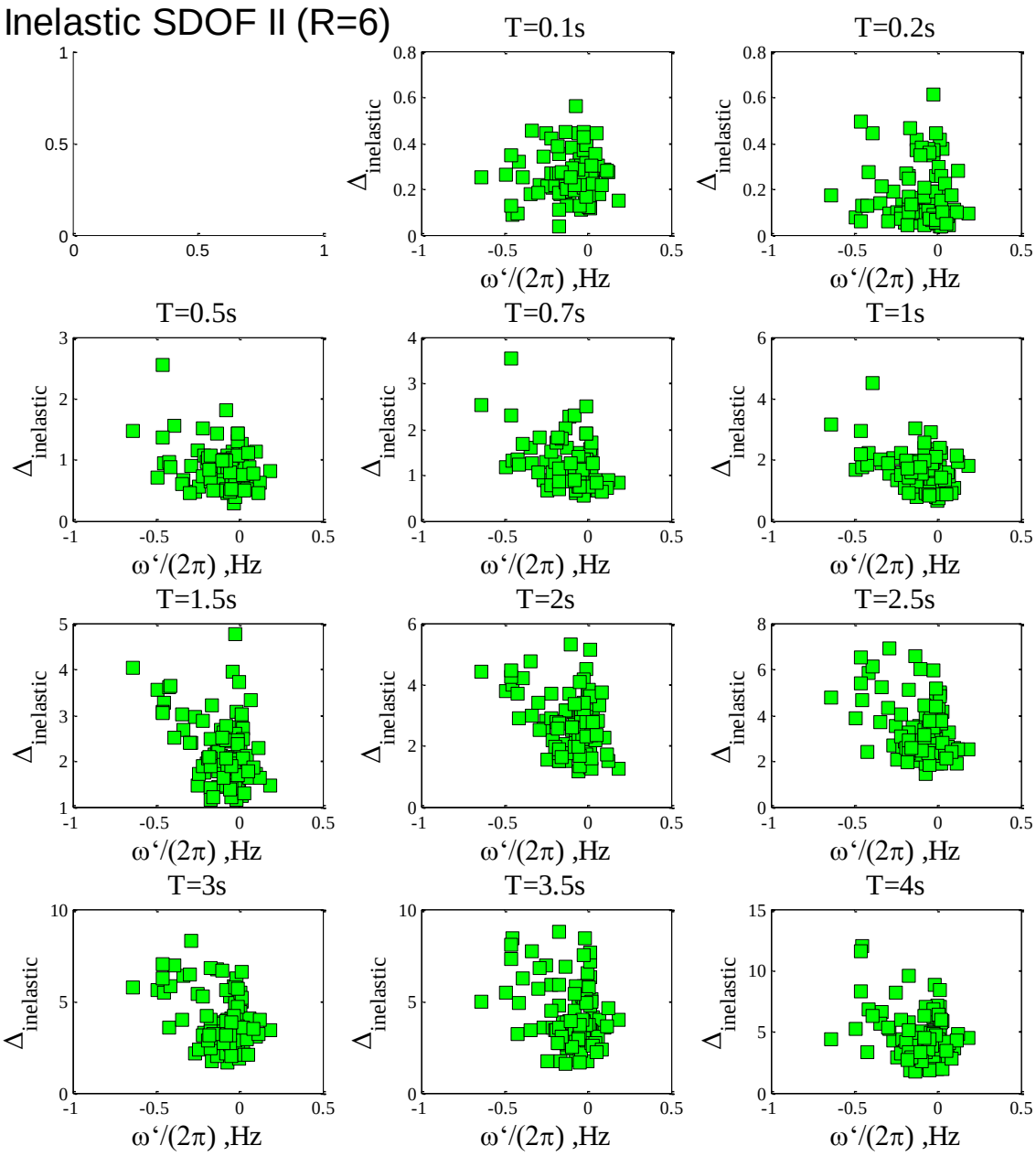

Figure B.20. Effect of slope of frequency on engineering demand parameter in term of maximum inelastic displacement for deterioration inelastic SDOF, period from 0.1s to 4s with strength reduction factor, R=6, and negative strain-hardening, α= ─ 0.10.

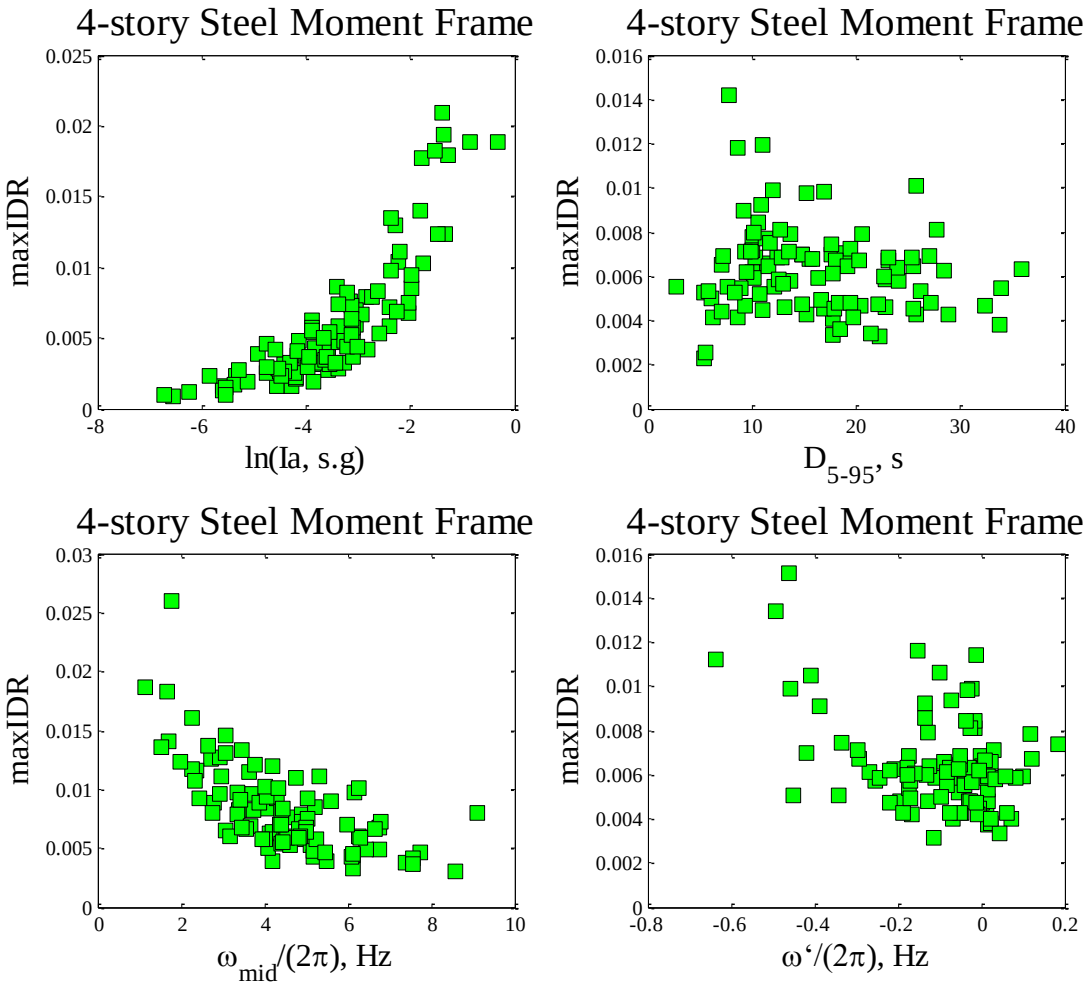

Figure B.21. Effect of arias intensity, duration, mid-frequency and slope of frequency on engineering demand parameter in term of maximum interstory drift ratio for 4-story steel moment frame

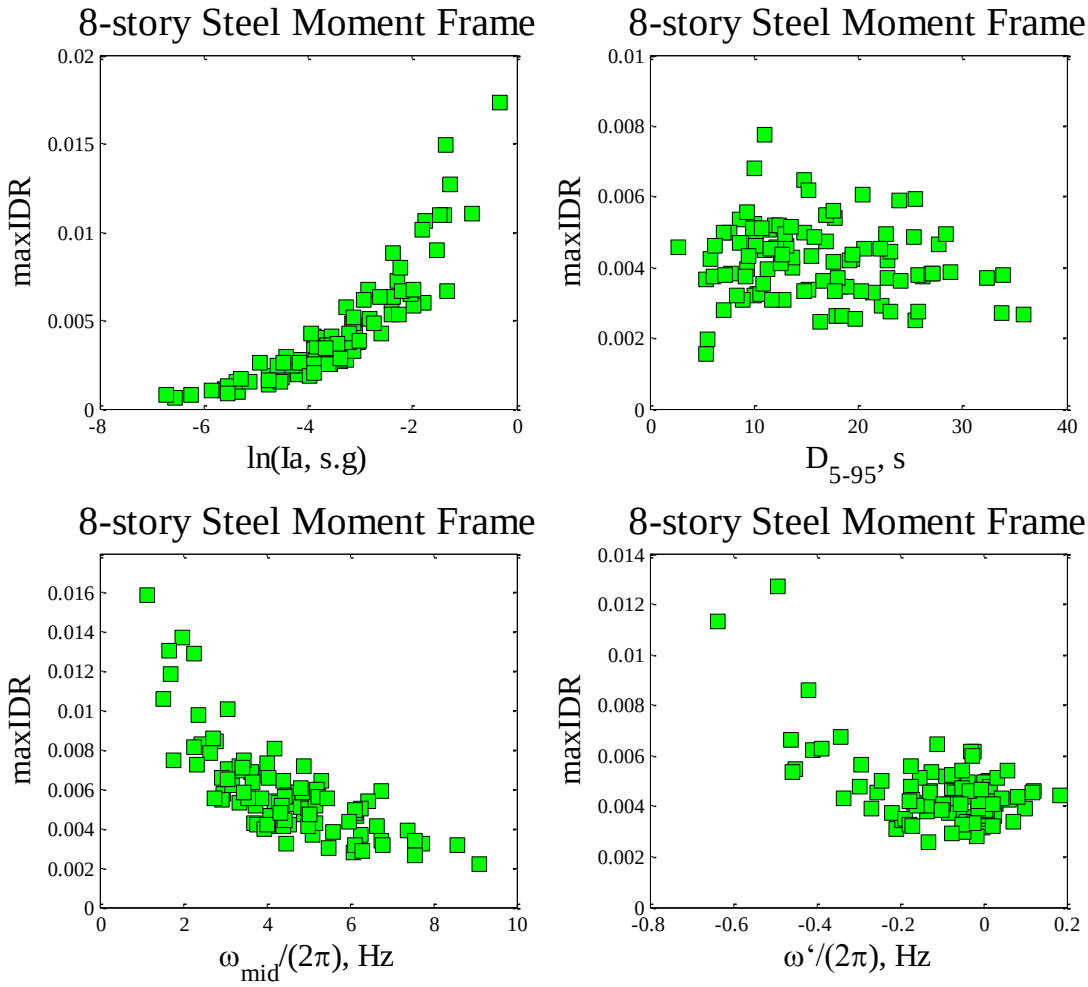

Figure B.22. Effect of arias intensity, duration, mid-frequency and slope of frequency on engineering demand parameter in term of maximum interstory drift ratio for 8-story steel moment frame

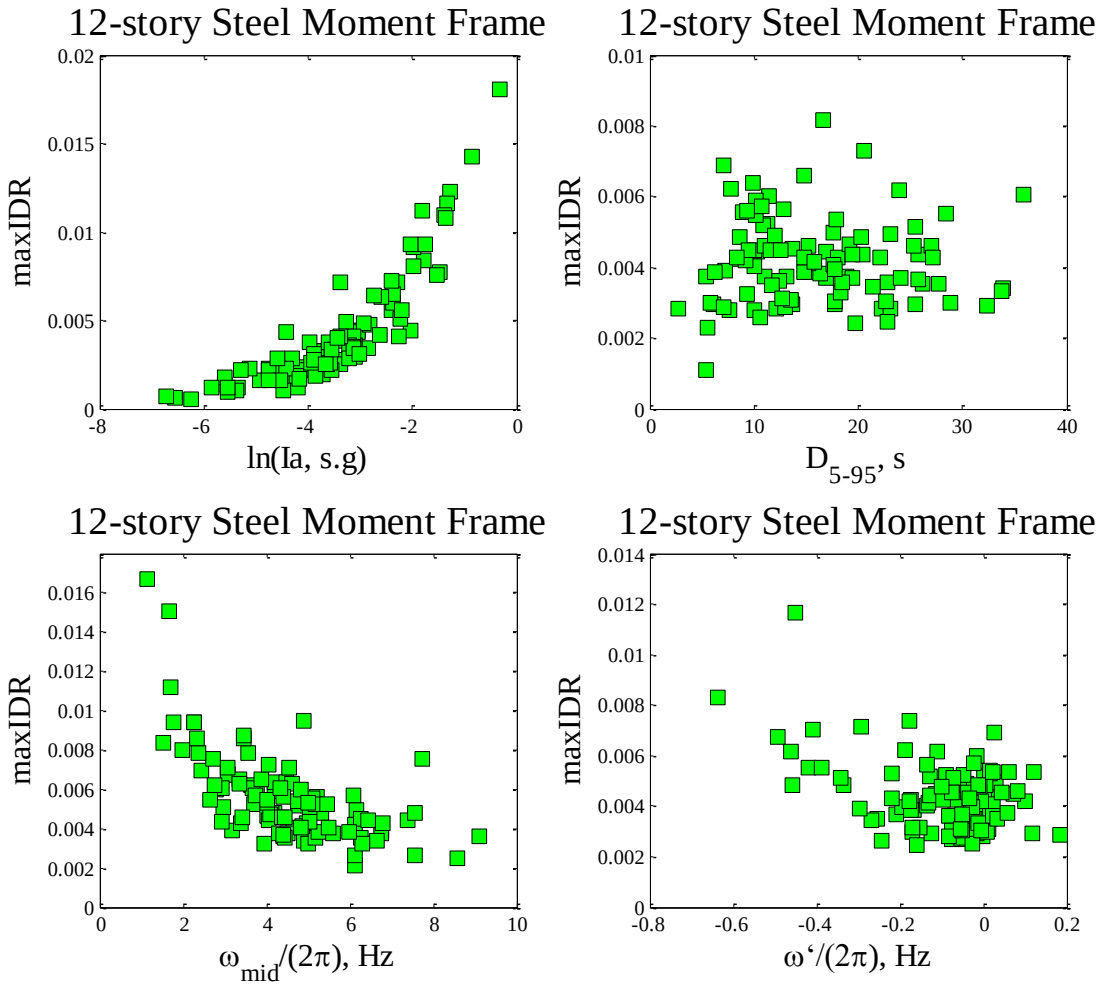

Figure B.23. Effect of arias intensity, duration, mid-frequency and slope of frequency on engineering demand parameter in term of maximum interstory drift ratio for 12-story steel moment frame

REFERENCES

Afshari, K., Stewart, JP., 2016. Physically Parameterized Prediction Equations for Significant Duration in Active Crustal Regions, Earthquake Spectra. Doi: 10.1193/063015EQS106M

AISC., 2005. Specification for Structural Steel Buildings. Chicago, IL: American Institute of Steel Construction, ansi/aisc 341-05 ed.

AISC., 2005 Seismic provisions for structural steel buildings. Chicago, IL: American Institute of Steel Construction, ansi/aisc 341-05 ed.

AISC., 2005. Prequalified Connections for Special and Intermediate Steel Moment Frames for Seismic Applications. Chicago, IL: American Institute of Steel Construction, ansi/aisc 341-05 ed.

Anderson.G,J. 2004. Quantitative measure of the goodness of fit of synthetic seismograms, 13th World Conference on Earthquake Engineering 2004: Paper NO. 243

Anderson, J. G. 2015. The Composite Source Model for Broadband Simulations of Strong Ground Motions, Seismological Research Letters, January/February 2015, v. 86, p. 68-74, doi:10.1785/0220140098

ASCE, American Society of Civil Engineering, 2005. Minimum Design Loads for Buildings and Other Structures (7-02), Standards ASCE/SEI 7-02.

ASCE, American Society of Civil Engineering, 2006. Minimum Design Loads for Buildings and Other Structures (7-05), Standards ASCE/SEI 7-05.

ASCE, American Society of Civil Engineering, 2010. Minimum Design Loads for Buildings and Other Structures (7-10), Standards ASCE/SEI 7-10.

Atkinson, G.M., and Goda, K., 2010. Inelastic seismic demand of real versus simulated ground motion records for the Cascadia subduction earthquakes. Bulletin of the Seismological Society of America, 100(1), 102-115.

Baker, J.W., Cornell, C.A., 2006. Spectral shape, epsilon and record selection. Earthquake Engineering & Structural Dynamics; 35(9):1077–95.

Baker, J.W., 2007. Quantitative classification of near-fault ground motions using wavelet analysis, Bulletin of the Seismological Society of America, vol. 97, no. 5, pp. 1486 – 1501.

Baker. J. W., 2008. Identification of near-fault velocity pulses and prediction of resulting response spectra, Geotechnical Earthquake Engineering and Structural Dynamics IV, May 18-22, 2008, Sacramento, CA

Baker, J.W., 2011. Conditional mean spectrum: Tool for ground-motion selection, Journal of Structural Engineering, vol. 137, no. 3, pp. 322–331,

Bazzurro, P., and Luco, N., 2006. Do scaled and spectrum-matched near-source records produce biased nonlinear structural responses? Proceeding of the 8th National Conference on Earthquake Engineering, San Francisco, California, 18–22 April 2006, 10 pp.

Bolt, B.A., 1969. Duration of strong motions. Proceedings of the 4th World Conference on Earthquake Engineering, Santiago, Chile, pp.1304-1315

Bommer, JJ, Acevedo, AB. The use of real earthquake accelerograms as input to dynamic analysis, Journal of Earthquake Engineering 2004; 8: S1, 43–91.

Boore, D. M. (1983). Stochastic simulation of high-frequency ground motions based on seismological models of the radiated spectra, Bull. Seismol. Soc. Am. 73, 1865–1894.

Burks, L., and Baker, J., 2014. Validation of ground motion simulations through simple proxies for the response of engineered systems. Bulletin of the Seismological Society of America, 104(4), pp. 1930–1946, August 2014, doi: 10.1785/0120130276

Haselton, C. B., 2009. "Evaluation of ground motion selection and modification methods: Predicting median interstory drift response of buildings," PEER Report 2009/01.

Campbell, K.W. and Bozorgnia, Y., 2008. NGA ground motion model for the geometric mean horizontal component of PGA, PGV, PGD and 5% damped linear elastic response spectra for periods ranging from 0.01 to 10 s. Earthquake Spectra, 24, 139–171.

Dashti, S., Bray, J. D., Pestana, J., Riemer, M. R., Wilson, D., 2010. Centrifuge testing to evaluate and mitigate liquefaction-induced building settlement mechanisms, J. Geotechnical and Geoenvironmental Engineering ASCE 136, pp.918–929.

Eaton, Morris L., 1983. Multivariate Statistics: a Vector Space Approach. John Wiley and Sons. pp. 116–117. ISBN 0-471-02776-6.

Frankel, A., 1995. Simulating strong motions of large earthquakes using recordings of small earthquakes: the Loma Prieta mainshock as a test case. Bulletin of the Seismological Society of America, 85(4), pp.1144-1160.

Galasso, C, Zareian, F, Iervolino, I, Graves, R.W., 2012. Validation of ground motion simulations for historical events using SDOF systems. Bulletin of the Seismological Society of America, 102(6): 2727–2740.

Gallaso, C., Zhong, P., Zareian, F., Iervolino, I., Graves, R. W., 2013. Validation of ground-motion simulations for historical events using MDOF systems. Earthquake Engineering Structural Dynamics, 42(9), 1395-1412.

Graves, R.W. and Aagaard B.T., 2011. Testing long-period ground-motion simulations of scenario earthquakes using the M w 7.2 El Mayor-Cucapah mainshock; evaluation of finite-fault rupture characterization and 3D seismic velocity models, Bulletin of the Seismological Society of America, 101(2):895-907.

Graves, RW, Pitarka A., 2010. Broadband ground-motion simulation using a hybrid approach. Bulletin of the Seismological Society of America. 100(5A): 2095–2123.

Graves, RW, Pitarka A., 2015. Refinements to the Graves and Pitarka (2010) broadband ground-motion simulation method. Seismological Research Letters 2015. Vol 86, no 1, pp 75-80.

Graves, R. W., Pitarka, A., Mai, P.M., Imperatori, W., Olsen, K.B., Schmedes, J., Archuleta, R. J. and Lavallée, D., 2011. Broadband Platform (BBP). Southern California Earthquake Center.

Hall JF. 1997. Seismic response of steel frame buildings to near-source ground motions. Technical Report EERL 97-05, California Institute of Technology, Pasadena, CA.

Hancock, J., Watson-Lamprey, J., Abrahamson, N., Bommer, J., Markatis, A., McCoy, E., and Mendis, R., 2006. An improved method of matching response spectra of recorded earthquake ground motion using wavelets. Journal of Earthquake Engineering, 10(1), 67-89.

Hartzell, S., 1978. Earthquake aftershocks as Green's functions, Geophysics Research Letter 5, 1–4.

Hatzell, S., Frankel, A., Liu, P., Zeng, Y., and Rahman, S., 2011. Model and parametric uncertainty in source-based kinematic models of earthquake ground motion. Bulletin of the Seismological Society of America, 101(5), 2431-2452.

Hartzell, S., Harmsen, S., Frankel, A., Larsen, S., 1994. Calculation of broadband time histories of ground motion: Comparison of methods and validation using strong-ground motion from the 1994 Northridge earthquake. Bulletin of the Seismological Society of America, 89(6), pp. 1484-1504.

Iervolino I., De Luca F., Cosenza E., 2010 Spectral shape-based assessment of SDOF nonlinear response to real, adjusted and artificial accelerograms. Engineering Structures. 32(9), 2776-279.

Iervolino, I., Galasso, C., Paolucci, R., Pacor, F., 2011. Engineering ground motion record selection in the ITalian ACcelerometric Archive. Bulletin of Earthquake Engineering, 9, 1761-1778.

Iervolino I., Maddaloni G., Cosenza E., 2008 Eurocode 8 compliant real record sets for seismic analysis of structures. Journal of Earthquake Engineering, 12(1):54-60.

Jones, P. and Zareian, F., 2009. Relative safety of high-rise and low-rise steel moment-resisting frames in Los Angeles. The Structural Design of Tall and Special Buildings. 19. pp.183–196. doi: 10.1002/tal.559.

Jones, P., Zareian, F., 2013. Seismic response of a forty-story buckling restrained braced frame designed for the Los Angeles region. The Structural Design of Tall and Special Buildings 22(3). Doi: 10.1002/tal.687

Jordan, T. H., Maechling, P., 2003. The SCEC community modeling environment—an

information infrastructure for system-level earthquake science, Seismology Research Letter. 74, pp. 324–328.

Kramer, S. L., 1996. Geotechnical earthquake engineering. Upper Saddle River, N.J., U.S.A.: Prentice Hall.

Krawinkler, H., Alavi, B., and Zareian, F., 2005. Impact of Near-Fault Pulses on Engineering Design, Earth and Environmental Sciences, 58, 2005, pp 83-106

Kottke, A., Rathje, E., 2008. A semi-automated procedure for selecting and scaling recorded earthquake motions for dynamic analysis. Earthquake Spectra, 24(4), 911-932.

Lin, T., Harmsen, S. C., Baker, J. W., and Luco, N., 2013. Conditional spectrum computation incorporating multiple causal earthquakes and ground motion prediction models. Bulletin of the Seismological Society of America, 103(2A), 1103-1116.

Liu, P.C., Archuleta, R.J., Hartzell, S., 2006. Prediction of broadband ground-motion time histories: hybrid low/high frequency method with correlated random source parameters. Bulletin of the Seismological Society of America, 96(6), pp. 2118-2130. doi: 10.1785/0120060036

Lutes, L. D., and Sarkani, S., 2004. Random Vibrations: Analysis of Structural and Mechanical Systems, Elsevier Butterworth-Heinemann, Burlington, Massachusetts.

Mai, P. M., W. Imperatori, and K. B. Olsen., 2010. Hybrid broadband ground-motion simulations: combining long-period synthetics with high-frequency multiple s-to-s backscattering, Bulletin of the Seismological Society of America,. 100(5A), pp. 2124–2142

Miranda, E., 1999. Approximate seismic lateral deformation demands in multistory buildings. Journal of Structural Engineering, ASCE, 125(4), 417–425.

Miranda, E. and Akkar, S., 2006. Generalized interstory drift demand spectrum. Journal of Structural Engineering, ASCE, 132(6), 840-852.

Miranda, E. and Reyes, C.J., 2002. Approximate lateral drift demands in multi-story buildings with nonuniform stiffness. Journal of Structural Engineering, ASCE, 128(7), 840–849.

Miranda, E. and Taghavi, S., 2005. Approximate floor acceleration demands in multistory Building. I: formulation. Journal of Structural Engineering, ASCE, 131(2), 203–211.

Kristekova´, M., Kristek, J., Moczo, P., Day, S, M., 2006. Misfit Criteria for Quantitative Comparison of Seismograms, Bulletin of the Seismological Society of America, 96(5), pp. 1836–1850

McKenna, F., Fenves, G. L., Scott, M. H., and Jeremic, B., (2000). Open System for Earthquake Engineering Simulation (OpenSees). Pacific Earthquake Engineering Research Center, University of California, Berkeley, CA.

Mood, M.A., Graybill F.A., Boes D.C., 1974. Introduction to the Theory of Statistics (3rd

edition). McGraw-Hill Companies, New York.

Naeim, F., Alimoradi, A., Pezeshk, S., 2004. Selection and Scaling of Ground Motion Time Histories for Structural Design Using Genetic Algorithms. Earthquake Spectra, 20(2), 413-426.

Naeim, F., Graves, RW., 2006. The case for seismic superiority of well-engineered tall buildings. The Structural Design of Tall and Special Buildings. 14(5), 401–416.

Newmark, N.M., 1973. A study of vertical and horizontal earthquake spectra. N.W. Newmark Consulting Engineering Services, Directorate of Licensing, U.S. Atomic Energy Commission, Washington, D.C.

NIST, 2010. "Evaluation of the FEMA p-695 methodology for quantification of building seismic performance factors," Tech. Rep. PEER/ATC 82, NEHRP Consultants Joint Venture, Redwood City, CA.

Olsen, K.B., Mayhew, J.E., 2010. Goodness-of-fit Criteria for Broadband Synthetic Seismograms, with Application to the 2008 Mw 5.4 Chino Hills, California, Earthquake. Seismological Research Letters, 81, 715-723.

Reinoso, E. and Miranda, E., 2005. Estimation of floor acceleration demands in high-rise buildings during earthquakes. The Structural Design of Tall and Special Buildings, 14, 107–130.

Rezaeian, S., Der Kiureghian, A., 2010. Stochastic Modeling and Simulation of Ground Motions for Performance-Based Earthquake. Pacific Earthquake Engineering Research Center Report, College of Engineering, University of California, Berkeley

Rezaeian, S., Der Kiureghian, A., 2011. Simulation of orthogonal horizontal ground motion components for specified earthquake and site characteristics. Earthquake Engineering and Structural Dynamics, 41(2), 335-353.

Rezaeian, S., Zhong, P., Zareian, F., and Hartzell, S 2014 Validation of simulated earthquake ground motions based on evolution of intensity and frequency content. Bulletin of the Seismological Society of America, 105(6), Doi: 10.1785/0120140210

Satterthwaite, F E., 1941. Synthesis of variance. Psychometrika, 6, 309-316.

Schmedes, J., Archuleta, R.J., Lavalle, D., 2010. Correlation of earthquake source parameters inferred from dynamic rupture simulations, J. Geophysics Research. 115, doi 10.1029/2009JB006689.

Shapiro, S.S., and Wilk, M.B., 1965. An analysis of variance test for normality (complete samples). Biometrika, 52, 591-611.

Shome, N., Cornell, C.A., Bazzurro, P., Carballo, J.E., 1998. Earthquakes, Records, and Nonlinear Responses. Earthquake Spectra, 14(3), 469-500.

Seyhan, E., Stewart, J.P., Graves, R.W., 2012. Calibration of a semi stochastic procedure for simulating high frequency ground motions. Earthquake Spectra 2012

Somerville, P.G., 2005. Engineering characterization of near fault ground motions. 2005 New Zealand Society for Earthquake Engineering Conference

Star, L., Stewart, J.P., Graves, R.W., 2011. Comparison of Ground Motions from Hybrid Simulations to NGA Prediction Equations. Earthquake Spectra, 27, 331-350.

Tothong, P., Luco, N., 2007. Probabilistic seismic demand analysis using advanced ground motion intensity measures. Earthquake Engineering & Structural Dynamics, 36 (13), 1837-1860.

Vanmarcke, E.H., Fenton, G.A., Heredia-Zavoni, E., 1997. SIMQKE-II, Conditioned Earthquake Ground Motion Simulator: User's Manual, Version 2. Princeton University, 25 pp

Welch, BL., 1938. The significance of the difference between two means when the population variances are unequal. Biometrika, 29, 350-362.

Yeh, C. H., Wen, Y. K., 1990. Modeling of nonstationary ground motion and analysis of inelastic structural response, Structural Safety 8, 281–298.

Zareian, F., Kanvinde., 2012. Effect of Column-Base Flexibility on the Seismic Response and Safety of Steel Moment-Resisting Frames. Earthquake Spectra 2012.

Zareian, F. and Krawinkler, H., 2012, Conceptual performance-based seismic design using building-level and story-level decision support system. Earthquake Engineering & Structural. Dynamics. doi: 10.1002/eqe.2218.

Zareian, F., Rahnama, M., 1997. ارزیابی نیازهای لرزه ای سازه ها.MS Dissertation. Sharif Institute of Technology.

Zeng, Y., J. G. Anderson., G. Yu., 1994. A composite source model for computing realistic synthetic strong ground motions, Geophysics. Research Letter. 21, 725–728.

Zeng, Y., Anderson, J. G., 1996. A composite source model for computing realistic synthetic strong ground motions, Bulletin of the Seismological Society of America, 86(1B), pp. S71-S83

Zhong P., 2012. Sensitivity of building response to variation in integration time step of response history analysis, Master's thesis, ProQuest Dissertations and Theses, ISBN: 9781124558400.